Molecular Characterisation of CD4$^+$ T Cell Responses to Tumour Antigens

Bruce MacLachlan

A thesis submitted to Cardiff University in candidature for the degree of Doctor of Philosophy

School of Medicine
Cardiff University

2016

"For noncrystallographers, it is important to appreciate that, with this type of work, you really have nothing in your hands, despite years of effort, until there are crystals that diffract to a sufficient resolution."

(Kai Wucherpfennig, 2010)

ACKNOWLEDGEMENTS

DECLARATION

This work has not been submitted in substance for any other degree or award at this or any other university or place of learning, nor is being submitted concurrently in candidature for any degree or other award.

Signed ………………………………………… (candidate) Date …………………………

STATEMENT 1

This thesis is being submitted in partial fulfilment of the requirements for the degree of PhD

Signed ………………………………………… (candidate) Date …………………………

STATEMENT 2

This thesis is the result of my own independent work/investigation, except where otherwise   stated.
Other sources are acknowledged by explicit references. The views expressed are my own.

Signed ………………………………………… (candidate) Date …………………………

STATEMENT 3

I hereby give consent for my thesis, if accepted, to be available for photocopying and for inter-library loan, and for the title and summary to be made available to outside organisations.

Signed ………………………………………… (candidate) Date …………………………

SUMMARY

Background – Colorectal cancer (CRC) is the second most common cause of cancer death. CD4$^+$ T cells play an important role in anti-tumour immunity by promoting immune processes that can mediate tumour inhibition. CD4$^+$ immunity to tumours, however, is not able to prevent tumour outgrowth. It is hypothesised that tumour outgrowth can occur due to weak recognition of tumour-derived epitopes by tumour-reactive T cell receptors (TCRs) and due to negative regulation by inhibitory T cell molecules. In this study, CD4$^+$ T cell responses to the oncofoetal antigen 5T4 are studied at the molecular level. The function of the co-inhibitory molecule LAG-3 is described biophysically and monoclonal antibodies which recognise LAG-3 were developed.

Results – Three 5T4-reactive CD4$^+$ T cell clones were shown to recognise 5T4-derived peptides restricted to HLA-DR1. Each clone was sensitive to antigen and produced T$_H$1 cytokines despite exhibiting weak recognition of cognate antigen. Subsequently, the structural characteristics of a 5T4-derived peptide epitope was described through x-ray crystallography which revealed insights into MHC-II presentation of peptides. Cell expressed LAG-3 was shown to interact with MHC-II at the cell surface and was characterised at the protein level using surface plasmon resonance (SPR) where LAG-3 bound MHC-II via an intermediate affinity interaction. Thirdly, through the immunisation of mice, anti-LAG-3 antibodies were cloned and characterised in terms of their specificity and function.

Conclusions – These studies demonstrate how tumour-specific CD4$^+$ T cells can produce immune-stimulatory molecules *in vitro* yet exhibit weak engagement of cognate antigen. It is shown that peptide flanking residues of HLA-DR1 presented epitopes can contribute to peptide anchoring as well as form structural features that may influence TCR binding. It is shown that LAG-3 binds MHC-II at higher affinity than CD4 with implications in its inhibitory function. Finally, specific antibodies that bind LAG-3 have been characterised with potential for therapeutic development.

TABLE OF CONTENTS

LIST OF FIGURES

LIST OF TABLES

LIST OF ABBREVIATIONS

aa	amino acid
ADCC	Antibody-dependent cellular cytotoxicity
ADCP	Antibody-dependent cellular phagocytosis
APC	Antigen presenting cell
APC-**gene**	*Adenomatous polyposis coli*
APCy	Allophycocyanin
APL	Altered peptide ligands
BCR	B cell receptor
CCD	Charge-coupled device
CD	Cluster of differentiation
CDC	Complement-dependent cytotoxicity
CDR	Complementarity determining region
CEA	Carcinoembryonic antigen
CHO	Chinese hamster ovary
CLIP	Class II-associated invariant chain peptide
CLP	Common lymphoid progenitor
CRC	Colorectal cancer
CTLA-4	Cytotoxic T-lymphocyte-associated protein 4
CXCL	Chemokine (C-X-C motif) ligand
DAMP	Damage-associated molecular pattern
DLS	Diamond Light Source
DN	Double negative
DNA	Deoxyribonucleic acid
DP	Double positive
EC$_{50}$	Half maximal effective concentration
ELISA	Enzyme-linked immunosorbent assay
ELISpot	Enzyme-Linked ImmunoSpot
EM	Electron microscopy
FACS	Fluorescence activated cell sorting
Fc	Fragment crystallisable
FITC	Fluorescein isothiocyanate
FMO	Fluorescence minus one
FoxP3	Forkheadbox P3
FPLC	Fast protein liquid chromatography
FSC	Fourier shell correlation
gMFI	Geometric Mean fluorescence intensity
GMP	Good manufacturing practices

HCC	Hepatocellular carcinoma
HIV	Human immunodeficiency virus
HL	Hodgkin lymphoma
HLA	Human leukocyte antigen
HSC	Hematopoietic stem cell
hTERT	human Telomerase reverse transcriptase
IB	Inclusion body
IFNγ	Interferon γ
IFNγR	Interferon γ receptor
Ig	Immunoglobulin
IL	Interleukin
ILT2	Immunoglobulin-like transcript 2
IMGT	International ImMunoGeneTics information system
ITAM	Immunoreceptor tyrosine-based activation motif
JRT	Jurkat cell line
K_A	Equilibrium association affinity constant
K_D	Equilibrium dissociation affinity constant
K_{DV}	Equilibrium dissociation avidity constant
KLH	Keyhole limpet hemocyanin
LAG-3	Lymphocyte activation gene-3
LAG-3:Fc	LAG-3: IgG Fc fusion protein
LAP	latency-associated peptide
LCL	Lymphoblastoid cell line
LPS	Lipopolysaccharide
mAb	monoclonal Antibody
MAC	Membrane attack complex
MCA	Methylcholanthrene
MHC	Major histocompatibility complex
MHC-I	Major histocompatibility complex class I
MHC-II	Major histocompatibility complex class II
MIP-1β	Macrophage inflammatory protein-1β
mRNA	messenger Ribonucleic Acid
MVA	Modified Vaccinia Ankara virus
NK	Natural killer
PAMP	Pathogen-associated molecular pattern
PB	Pacific blue
PBMC	Peripheral blood mononuclear cell
PD-1	Programmed cell death protein 1

PDB	Protein databank
pDC	plasmacytoid dendritic cell
PE	Phycoerythrin
PFR	Peptide flanking residues
PHA	Phytohemagglutinin
pHLA	peptide-HLA
pMHC	peptide major histocompatibility complex
PPD	Purified protein derivative
PRR	Pattern recognition receptor
pTα	pre-TCR alpha chain
pT$_{reg}$	peripherally-derived regulatory T cell
RAG	Recombination activating gene
RMSD	Root mean square deviation
RU	Resonse units
sf9	*Spodoptera frugiperda* clonal isolate 9
sfcs	spot forming cells
sLAG-3	soluble lymphocyte activation gene-3
SPR	Surface plasmon resonance
TAA	Tumour associated antigen
TCR	T cell receptor
TEM	Transmission electron microscopy
T$_{FH}$	T folicular helper
TGF-β	Transforming growth factor β
T$_H$	T helper cell
TIL	Tumour infiltrating lymphocyte
TNF	Tumour necrosis factor
TOPS	TCR/pMHC Optimized Protein crystallisation Screen
Tr1	Type 1 regulatory
T$_{reg}$	Regulatory T cell
TSA	Tissue specific antigen
tT$_{reg}$	thymically-derived regulatory T cell
vdW	van der Waals
VH	Variable heavy domain
VL	Variable light domain
WT	Wild type

1   Chapter 1: Introduction

1.1   Tumourigenesis and colorectal cancer

Cancer is a highly heterogeneous disease characterised by aberrant cell growth and evasion of the immune system (Hanahan & Weinberg 2011). According to statistics collated by Cancer Research UK, in the UK in 2014, combined cancer related deaths were estimated at ~163,000 with a reported incidence of ~352,000 new cancer cases reported the previous year (Cancer Research UK 2016). In 2011 in England & Wales the combined 10-year survival for all cancers was ~50 % with marginally higher survival in women compared to men. Different cancer types, however, exhibit a wide range in survival; cancer of the testis resulted in a ~98 % 10-year survival compared to ~1 % in pancreatic cancer. As a result, a better understanding of how tumours are shaped by the immune system and how the immune system can be modulated through therapy is required.

1.1.1   Colorectal cancer epidemiology

Colorectal cancer (CRC) is the formation of primary cancer of the lower gastrointestinal tract from the large bowel to the anus. CRC is the second most common cause of cancer death worldwide. In the UK in 2014, there was over ~16,000 deaths as a result of CRC with a reported incidence of ~41,000 new cases in the previous year (Cancer Research UK 2016). Incidence rates are more common in men that in women and increase with age, highlighted by 58 % of all cases diagnosed in people aged 70 or over (2011-2013). In 2011 in England & Wales, 10-year survival was ~57 % and thus higher than the combined overall 10-year survival rate for all cancers. Disease occurrence varies worldwide with higher prevalence in the developed world (particularly Europe, North America & Oceania) likely due to environmental and lifestyle factors including diet; with incidences in developing countries on the rise (Haggar & Boushey 2009). Such increases have been attributed to changes towards a more 'Westernised" lifestyle in developing areas (Center et al. 2009). Risk factors of disease are a combination of both environmental/lifestyle factors – such as consumption of red and processed meat, smoking and excessive alcohol intake – as well as disease/genetic factors such as family history, inflammatory bowel disease, diabetes and obesity (Brenner et al. 2014).

1.1.2   Formation of CRC tumours

CRC is a heterogenous disease that can develop over long time periods (>10 years) and can arise through multiple driving pathways. The majority of CRC pathology manifests as cellular disorder of the mucosa resulting in dysplastic adenomas. Uncontrolled proliferation of epithelial cell

division at intestinal crypts most commonly results in the formation of adenomatous polyps which can progress to malignant adenocarcinomas (Ponz de Leon & Di Gregorio 2001). Such dysplasia is driven by the gradual acquirement of mutations within mucosal epithelial cells. Commonly acquired mutations occur in the *Adenomatous polyposis coli* gene (*APC*-gene), for example, which is a tumour suppressor gene pivotal in WNT signaling and thus maintaining cellular proliferation (Powell et al. 1992). Tumourigensis, however, can occur through a plethora of mutations in cellular maintenance signaling pathways including WNT, MAPK, PI3K, TGF-β, p53 pathways as well as DNA mismatch-repair mechanisms (Fearon 2011). Whole genome sequencing and large-scale analysis of genomic organization has shown that hypermutated tumours driven by errors in DNA repair, termed microsatellite instable tumours, are molecularly distinct from non-hypermutated tumours which are driven by chromosomal instability (The Cancer Gene Atlas et al. 2012).

1.2   T cells as part of the immune system

The first line of defence between a multi-cellular organism and the surrounding environment are the physical barriers that encapsulate it. In order to survive, however, organisms must interact and exchange material from this environment – whether oxygen through the respiratory system or water, food and therefore energy through the digestive system. Moreover, physical barriers cannot prevent pathology derived from the cells from within the organism, such as the case of cancer. As a result, the organism utilises a complex network of cells and soluble factors, known as the immune system, to mediate protection of the host from undesired entities. This network can be broadly categorised into two components: innate immunity and adaptive immunity.

1.2.1   Innate immunity

Innate immunity incorporates the physical barriers against pathogens as well as a number of cellular and molecular factors that make up the immediate response against pathogenic entities. These innate immune processes can be triggered by common hallmarks of pathogens or injury (Janeway & Medzhitov 2002). For example, innate cells such as macrophages, neutrophils and dendritic cells, express pattern recognition receptors (PRRs) which can recognise molecular signals termed pathogen-associated molecular patterns (PAMPs) or damage-associated molecular patterns (DAMPs). In response to their activation through PPRs, innate cells can engulf cells and cellular debris through phagocytosis and signal to other arms of the immune system by the release of soluble molecules – cytokines, chemokines and small molecule inflammatory mediators – to trigger a response against the insult or pathogen. Such a response can be broadly described as acute inflammation, whereby blood vessels dilate and increase permeability, local temperature is increased and cellular and soluble immune mediators are delivered to the area. Innate immunity is characterised by its limited ability to adapt to damage or pathogens over time. This property is as a result of innate receptors, such as PRRs, being germline encoded.

1.2.2   Adaptive immunity

The adaptive immunity arm of the immune system is characterised by its ability to alter over time as a result of adapting to encountered pathogens or immunogens throughout the lifetime of the organism. This functionality is required by higher organisms due to the vast array of potential aggressors exhibiting large variability and faster evolutionary time scales. Moreover, adaptive immunity mediates the process of immunological memory and is thus the target of vaccination.

Adaptation is achieved through the specific recognition of pathogenic material using receptors that, unlike innate receptors, are highly variable. This is achieved via somatic gene

processes. The pathogenic material recognised by these receptors are termed antigens and can be in the form of proteins, short peptides, carbohydrates, lipids or small molecules. The highly variable receptors that recognise antigens are the B-cell receptor (or antibodies in its soluble form) or the T cell receptor (TCR). These receptors are expressed on B and T cells, respectively, which are generated and developed in the primary lymphoid organs.

Whilst innate immunity does not adapt over time, innate immune processes are essential for the initiation and function of an adaptive immune response. Complement, for example, is recruited to opsonised antibody targets on cellular material and is able to lyse cells through the formation of the membrane attack complex (MAC) which perforates cellular membranes (Tegla et al. 2011). Crucially, for this thesis, the communication between innate cells performing as professional antigen presenting cells (APCs) are essential in triggering the T cell response against antigens.

1.2.3   T cells

T cells are a lymphocytic cell type that are defined by their maturation in the thymus and their expression of the highly variable antigen receptor: the T cell receptor (TCR). This TCR is variable between different T cells and is thus clonotypic. As a result, clonotypic T cells possess unique TCR gene sequences and therefore a unique receptor with a unique specificity. Due to this highly variable receptor, T cells are able to bind to and respond to pathogens or tumours via the specific recognition of a vast array of antigenic markers.

1.2.4   Generation of the αβT cell repertoire

T cells are a highly heterogeneous cell population. As a result of the processes described herein, a pool of clonotypic T cells, defined by their TCR sequence (T cell clonotype) is generated and trained to distinguish pathogenic 'foreign' molecular antigens from molecular antigens derived from the host (self-antigens). To achieve this function, T cells undergo TCR gene assembly, T cell development and thymic selection. The result of which is a vast population of T cell clonotypes termed the T cell repertoire. An overview of the processes involved in generating the T cell repertoire described in this section are illustrated in *Figure 1.1*.

1.2.4.1   TCR generation

The generation of T cells bearing diverse TCR sequences occurs via the somatic recombination of *TCR* genes during the development of T cells in the thymus. This process allows the *theoretical* generation of 10^{18} unique αβ TCRs from the *TCR* loci from a genome that encodes

Bone marrow

HSC

Migration to thymus

Thymic
Outer cortex

CLP

Thymocyte commitment

DN
thymocyte

TCRγ
TCRδ

TCRβ & TCRγδ rearrangement
See Figure 1.2a

γδ
Committed
thymocyte

Pre-TCR⁺
DN
thymocyte

pTα
TCRβ

Co-receptor acquisition

CD4⁺

CD8⁺

Pre-TCR⁺
DP
thymocyte

pTα
TCRβ

TCRα rearrangement
See Figure 1.2b

CD4⁺

CD8⁺

TCR⁺
DP
thymocyte

TCRα
TCRβ

Positive selection

Thymic
Inner cortex

CD4⁺
TCRα
TCRβ
CD8⁺

CD4
dependent
TCR⁺ DP

CD8
dependent
TCR⁺ DP

CD4⁺
TCRα
TCRβ
CD8⁺

Death by neglect

Thymic
Medulla

Negative selection

TCRα
TCRβ
CD4⁺

CD4⁺
precursor

TCRα
TCRβ
CD8⁺

CD8⁺
T
precursor

Death by apoptotic signalling

(Figure legend overleaf)

- 5 -

Figure 1.1 – Overview of TCR generation, T cell development and thymic selection:
Haematopoietic stem cells (HSC) migrate via blood from bone marrow to thymus and differentiate into the common lymphoid progenitor (CLP) before committing to the T cell lineage to form double negative (DN) thymocytes. Within the thymic outer cortex, simultaneous rearrangement of TCRβ,γ & δ chains occurs and upon which a successful rearrangement of TCRβ chain commits thymocytes to the TCRαβ lineage. Arranged TCRβ chain associates with the pre-T cell receptor alpha (pTα) chain to form the pre-TCR on surface of thymocytes before acquisition of both CD4 and CD8 co-receptors to form pre-TCR$^+$ double positive (DP) thymocytes. Consequent rearrangement of the TCRα chain is triggered allowing the formation of TCRα chain pairing to form TCRαβ$^+$ DP thymocytes which travel through to the thymic inner cortex where they undergo positive selection against self-MHC molecules expressed by the thymic cortical epithelial cells. TCRαβ rearrangements which do not signal through the TCR due to insufficient binding to self-MHC are subjected to death by neglect due to programmed cell death. DP thymocytes which pass positive selection migrate to the thymic medulla where they undergo negative selection. Based on negative selection against tissue specific antigens (TSAs) presented on APCs within the medulla, candidate thymocytes are deleted by apoptotic signalling or licensed for the periphery as naïve CD4$^+$ T$_H$ precursors or CD8$^+$ T cell precursors – depending on TCR engagement with MHC TSAs and consequent signal strength.

approximately 3×10^4 genes in order to bind near infinite possible antigenic sequences (Davis & Bjorkman 1988).

During the formation of αβ T cells, thymocytes which commit to the T cell lineage from common lymphoid progenitor (CLP) cells, upon entry into the thymus, undergo the process of TCR gene assembly, firstly via somatic recombination at the TCRβ locus (Hedrick et al. 1984). This process is termed V(D)J recombination. Within the human germline encoded TCRβ loci are a number of gene segments: two constant (C), two diversity (D), thirteen joining (J) and 52 variable (V) segments. Catalysis by the recombination activation genes-1 and -2 (RAG1 & RAG2) allow the recombination of one of each of the gene segments to form a candidate TCRβ chain sequence (*Figure 1.2a*) (Schatz & Swanson 2011). The resultant TCRβ chain is consequently transcribed, translated and transported to the cell surface where it associates with the pre-TCR α chain (pTα) and associates with CD3 component subunits (Fehling et al. 1995). The ability of the pre-TCRαβ/CD3 complex to successfully signal through the formed TCRβ represents the first positive selection step in TCR generation (von Boehmer 2005). Upon successful recombination to a TCRβ chain, TCRγ and TCRδ chain recombination is halted (which occurs simultaneously) and the thymocyte is committed to the αβ T cell lineage.

Following acquisition of both CD4 and CD8 co-receptors, rearrangement of the TCRα locus is triggered (*Figure 1.2b*). Arrangement of the TCRα is similar to the TCRβ locus except it differs in the constituent gene segments: one constant (C), 61 joining (J) and between 70 and 80 variable (V) segments. Crucially, the TCRα locus contains no diversity (D) gene segments, thus, TCRα chain diversity is generated through VJ recombination only (Schatz & Swanson 2011).

Whilst the selection of different combinations of V(D)J gene segments introduces diversity to the TCR repertoire, further variation is introduced during recombination through the process of junctional diversity. During recombination of both TCRα and TCRβ, double stranded breaks catalysed by RAG1/2 recombinases form hairpin loop coding ends of recombining gene segments. Consequently, the DNA repair enzyme Artemis cleaves these hairpin ends leaving single stranded palindromic nucleotide sequences (P nucleotides) (Ma et al. 2002). These single stranded extensions are consequently capped by random nucleotide addition by the enzyme terminal deoxynucleotidyl transferase (TdT), paired and ligated to complete the join between gene segments (Schatz & Swanson 2011). This process is error-prone and consequently adds non-germline encoded nucleotide sequences to the junctions between recombined gene segments. In arranged TCRα genes there is a single junction – between VJ segments – whereas in arranged TCRβ genes there are two junctions – between VD and DJ. As a result, the TCRβ chain exhibits a further level of diversity compared to the TCRα (Davis & Bjorkman 1988).
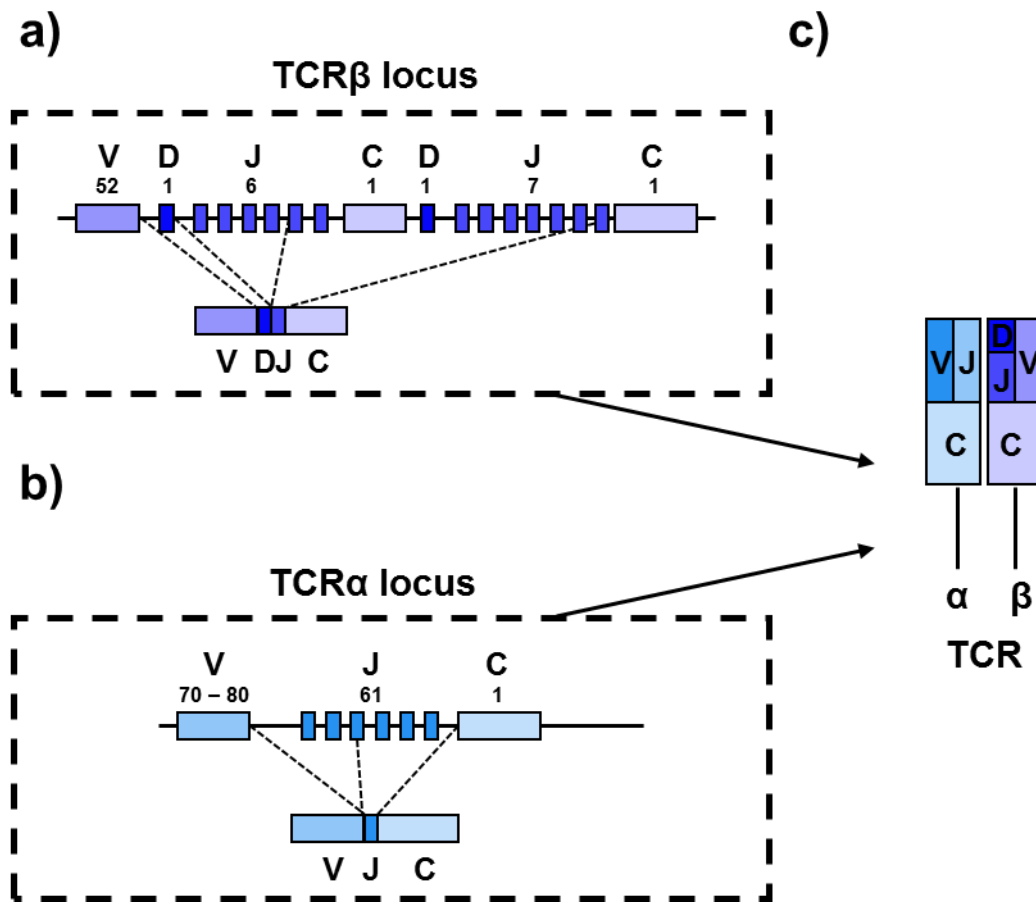
Figure 1.2 – TCR gene rearrangement to form the highly variable αβ TCR:

a) Organisation of the TCRβ locus containing variable (V), diversity (D), joining (J) and constant (C) gene segments (top). The number of gene segment introns within each cluster is defined as numbers below segment labels. Consequent somatic recombination between V,D,J and C segments results in the formation of an assembled TCR gene sequence (bottom).

b) Organisation of the TCRα locus containing variable (V), joining (J) and constant (C) gene segments (top) and assembled TCRα gene (bottom); labelled as in *a)*.

c) Contribution of gene segments to the expressed αβ TCR highlighting the additional presence of D-gene incorporation into the TCRβ chain; coloured and labelled as in *a)* and *b)*.

1.2.4.2   Shaping the T cell repertoire via positive and negative thymic selection

Having arranged TCRα and TCRβ genes and expressed the consequent αβ TCR at the cell surface of developing thymocytes (*Figure 1.2c*), generated TCRs are selected to be both functional and tolerant to self through the process of positive and negative selection. Together, these processes create an αβT cell repertoire that is restricted to antigens presented on MHC molecules (by positive selection) and with constraints on self-reactivity (by negative selection) which forms the basis of central T cell tolerance. Firstly, αβ TCRs, which have already undergone β selection with the pTα chain (described previously), undergo the process of positive selection (Hogquist et al. 1992) . Here, self-antigens bound to MHC molecules are presented by thymic cortical epithelial cells to developing αβ TCR bearing thymocytes which, at this stage, express both CD4 and CD8 co-receptors – termed double positive (DP) thymocytes. TCRs which are able to bind self-peptide-MHC molecules with sufficient affinity to induce T cell triggering receive consequent survival signals and are able to proceed to further development. T cells bearing αβ TCRs without sufficient binding capacity for MHC are deleted through the process of neglect over approximately 36 hours (in mice) (Stritesky et al. 2013).

Secondly, MHC binding-capable T cells migrate to the thymic medulla where they undergo negative selection against self-peptide MHC-molecules presented by medulla thymic epithelial cells (mTECs) and thymic dendritic cells (Gallegos & Bevan 2004). These cells present an array of tissue specific antigens (TSAs) to candidate αβ TCRs which, if very strongly engaged by the expressed TCR above a certain threshold, signal for deletion by apoptosis and are thus removed from the T cell repertoire (Kappler et al. 1987). αβ TCRs which engage MHC presented TSAs weakly are licensed for the periphery. A portion of MHC-II restricted αβ T cells which exhibit higher end of affinities to TSAs – but not so high as to be deleted – are differentiated to thymically-derived regulatory T (tT$_{reg}$) cells by expression of the FoxP3 transcription factor and consequent expression of CD25 (Hsieh et al. 2012) – the functional consequence of which will be described to follow.

Once they have undergone positive and negative selection, thymocytes leave the thymus as naïve T cells which survey and sample the periphery for cognate MHC presented antigens. The outcome of TCR generation, T cell development and thymic selection is a peripheral T cell repertoire of approximately 10^7 to 10^8 T cell clonotypes (Turner et al. 2006).

1.2.5   T cell types

T cells represent an immune cell that exhibits a high degree of functional, molecular and phenotypic variability. As a result, T cells can be categorised into a number of different types and

subsets based on the type of TCR they possess, the cell surface markers expressed on their surface and ultimately the function they perform as part of the immune system. An overview of the T cell types and subsets discussed in this section, with focus on those of the CD4$^+$ lineage, is outlined in *Figure 1.3*.

T cells are separated into two distinct cell types based on their TCR expression. γδ TCR expression defines the γδ T cell which seem to perform 'innate-like' function. The full extent of γδ T cell function is not fully understood, however, these T cells are able to recognise a large array of non-peptide ligands and are thought to be important in generating early responses to pathogens (Vantourout & Hayday 2013). αβ TCR expression defines the αβ T cell which make up the majority of T cells in the periphery and are the focus of this thesis. Unlike antibodies or B cell receptors, αβ TCRs do not directly recognise antigenic markers *in situ* i.e. directly as part of the antigenic protein or, for example, on the surface of an evading pathogen. Instead, most 'conventional' αβ TCRs bind to peptide derivatives of antigenic proteins presented by (APCs) on the antigen presentation family of proteins called major histocompatibility complex (MHC). 'Conventional' T cells therefore survey the periphery for antigens presented on MHC molecules bearing peptide ligands for which their expressed TCR can bind.

In contrast, a portion of αβ T cells such as invariant natural killer T cells (iNKT), mucosal-associated invariant T (MAIT) and germline-encoded mycolyl-reactive (GEM) T cells make up the 'unconventional' T cell fraction which do not bind MHC presented peptide ligands (Godfrey et al. 2015). Nevertheless, upon binding of ligand all T cells can undergo the process of T cell triggering, consequent activation and clonal expansion. The functional consequence of such activated T cells is diverse – from direct lysis of ligand bearing cells, to the release of immune stimulatory cytokines or immune regulatory factors.

The functional fate of T cell triggering is dependent on the T cell phenotype, driven by a number of different surface and transcriptional factors. In conventional αβ T cells, there are two major types: CD4$^+$ T cells and CD8$^+$ T cells defined by their expression of respective namesake co-receptors. Commitment to either lineage occurs during thymocyte development - based on the restriction of the αβ TCR recombined – resulting in two functionally distinct T cell types. Commitment to either lineage occurs prior to negative selection and is thought to be driven by a number of different models including (a) CD4/CD8 specific signalling instruction, (b) TCR signal strength or (c) stochastic binding of CD4 or CD8 during positive selection (Germain 2002).
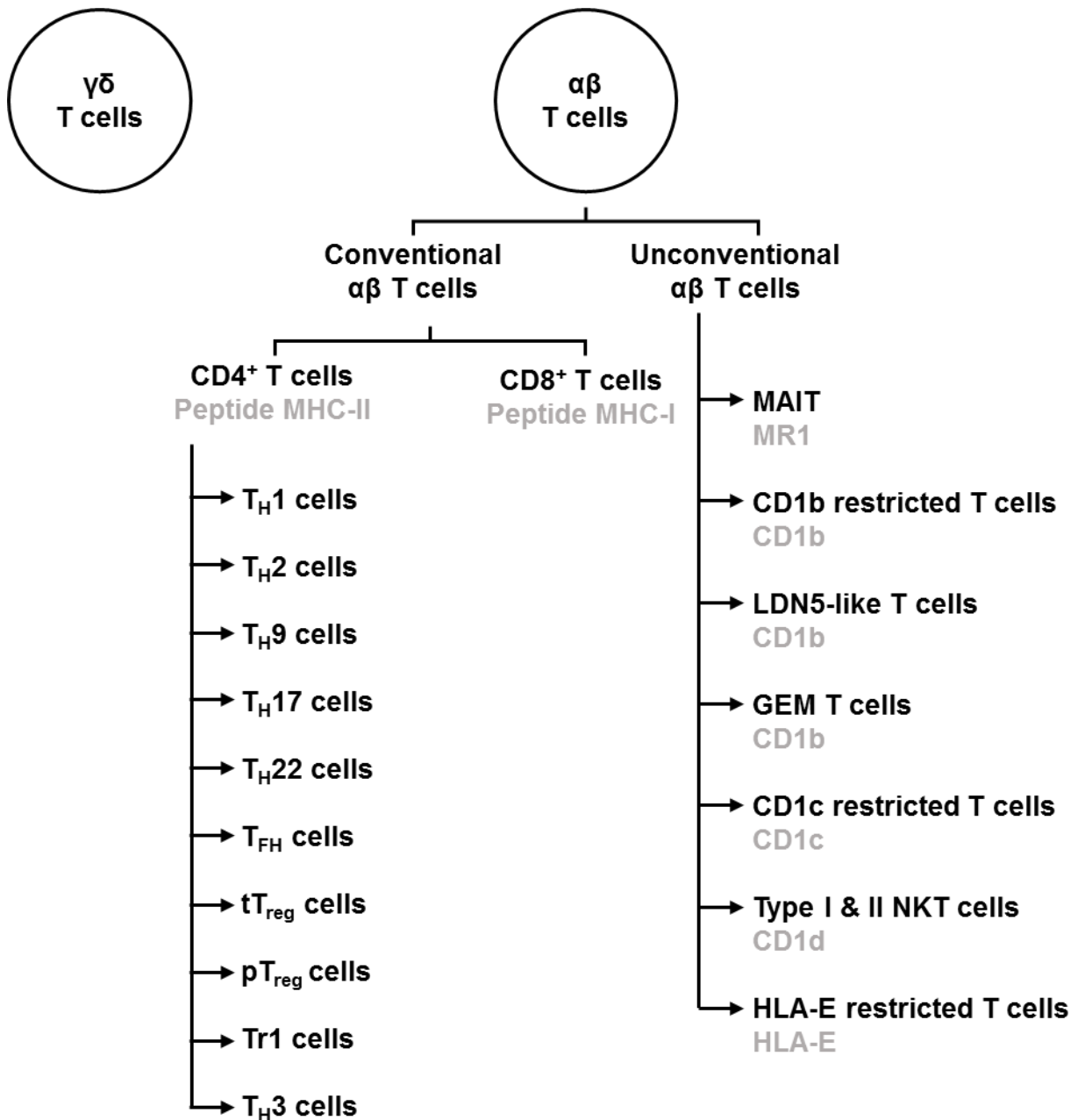
Figure 1.3 – Overview of αβ T cell lineage subsets:

Schematic overview of the lineage of various, but not all, αβ T cell subsets. T cell (black) and corresponding restriction ligand (grey) is shown. Collated from (Dong & Martinez 2010; Godfrey et al. 2015).

T_H = T helper, T_{FH} = T follicular helper, Tr1 = type 1 regulatory T cells, T_{reg} = regulatory T cells, tT_{reg} = thymus-derived T_{reg}, pT_{reg} = peripherally-derived T_{reg}, MAIT = Mucosal-associated invariant T cells, GEM = germline-encoded mycolyl-reactive, CD1b/c/d = cluster of differentiation 1b/c/d, NKT = Natural killer T cells, HLA-E = Human Leukocyte Antigen-E.

The primary difference is their restricting ligands: CD8$^+$ T cells express TCRs which bind peptides presented on MHC class I (MHC-I) molecules the result of which is generally to lyse ligand bearing presenting cells. CD4$^+$ T cells, on the other hand, express TCRs that bind peptides presented on MHC class II molecules; the functional consequence of which is far more diverse – from enhancing to regulating adaptive and innate immune responses.

1.2.6   CD4$^+$ T cell subsets

The range of effector functions performed by CD4$^+$ T cells is mediated by a further differentiation in the periphery of antigen unexperienced (naïve) CD4$^+$ T cells, upon antigen stimulation, into various subsets defined by their function. CD4$^+$ T cells can be categorised into two seemingly opposite functional phenotypes: those that undertake 'helper' or effector function and those that perform 'regulatory' or homeostatic function. This subset definition is generally assigned due to the expression of signature cytokine molecules and lineage-defining transcription factors.

1.2.6.1   T helper cells

T helper (T$_H$) cells are generally described functionally as promoting immunity through a number of different mechanisms, including the release of inflammatory cytokines resulting in consequences on the activity of innate and adaptive immune responses. The exact pathways by which T$_H$ cells enhance immune networks is dependent on the functional differentiation of naïve T cells during the processes of T cell priming, described in more detail in section 1.3.4. Here, activation of naïve T cells in the presence of T cell 'polarising' cytokines within the microenvironment results in the differentiation to effector CD4$^+$ T$_H$ cell subsets. Each subset can therefore be defined by the polarisation cytokine which signals their differentiation, the consequent transcription factors which initiate this differentiation of phenotype and the characteristic 'signature' cytokine profile of the T$_H$ cell subset.

The T helper 1 (T$_H$1) subset, for example, is polarised by IFNγ and IL-12 signalling, differentiated through expression of the lineage-specific transcription factors STAT4 and T-bet and characterised by the expression of the inflammatory cytokine IFNγ (Kaiko et al. 2008). The function of activated T$_H$1 cells, through release of IFNγ and other cytokines (such as IL-2, IL-12, TNFα & TNFβ), involves the provocation of cell-mediated immunity, for example, through stimulation of antigen presentation by triggering assembly of the immunoproteasome (Griffin et al. 1998) and the activation of macrophages (Nathan et al. 1983). A further description of T$_H$1 function, with a focus on T$_H$1 responses to tumours, will be described to follow.

In contrast, the T_H2 subset of cells, polarised by IL-4, is characterised by the lineage-specific transcription factors STAT6 and GATA-3 and production of cytokines such as IL-4, IL-5, IL-9, IL-10 and IL-13 (Mosmann & Coffman 1989). T_H2 effector functions include stimulating B cells and class switching to IgE antibodies (Shimoda et al. 1996), with consequent influence on mast cells and eosinophil activation (Amin 2012; Deo et al. 2010).

T_H17 cells, polarised under a microenvironment of IL-6 and TGFβ and absence of IL-4 and IL-12 are driven to differentiate by the RORγT transcription factor and are characterised by the expression of the signature IL-17 cytokine (Kaiko et al. 2008). IL-17 expressing T_H17 cells have implications in neutrophil recruitment to sites of inflammation (Miyamoto et al. 2003). In a study of 125 colorectal tumour patients, an elevated T_H17 gene expression signature by tumour infiltrating lymphocytes correlated with poorer patient prognosis (Tosolini et al. 2011).

Finally, IL-6 and IL-21 cytokines are able to polarise and differentiate T follicular helper (T_{FH}) cells through expression of the Bcl6 transcription factor which, in turn, produce further IL-6 and IL-21 (Eto et al. 2011). These cells enhance the formation of germinal centres in secondary lymphoid organs and thus shape adaptive B cell immunity. A summary of other T_H cell subsets is presented in *Figure 1.3*.

1.2.6.2 T cells with regulatory function

$CD4^+$ T cells possessing regulatory function are defined by their ability to suppress immunity and are essential in maintaining self-tolerance. The most characterised T cell with regulatory function is termed the regulatory T (T_{reg}) cell, which are characterised, in humans, by CD25 surface marker expression and the transcription factor FoxP3 (Sakaguchi 2005). Differentiation of T_{reg} cells can occur under TGFβ polarising signalling where differentiation towards a regulatory phenotype is induced by FoxP3 expression through SMAD2/SMAD4 signalling molecules (Pollizzi & Powell 2014).

T_{reg} cells, in response to antigen encounter, release cytokines which possess suppressive capacity such as IL-10, TGF-β and IL-35 (Sakaguchi et al. 2009). Additionally, T_{reg} cells suppress effector T cells through cell-contact mechanisms. For example, T_{reg} cells can effect antigen presentation through competitive blockade of APCs and consequent prevention of effector T cell access (Onishi et al. 2008). Moreover, T_{reg} cells can modulate APC expression of CD80 and CD86 co-signalling molecules through trogocytotic ligand ripping by the suppressive molecule CTLA-4 (Qureshi et al. 2011). In addition, T_{reg} cells are able to modulate local T cell immunity by 'mopping' of the T cell growth cytokine IL-2 through their high affinity IL-2 receptor α chain (CD25) thus resulting in effector T cell deprivation (Pandiyan et al. 2007). Additionally, through

an unknown mechanism, expression of the co-inhibitory molecule LAG-3 by T_{reg} cells is required for optimal T_{reg} function (Huang et al. 2004).

As well as 'classical' FoxP3$^+$ T_{reg} cells, other T cell subsets with regulatory function have been described, however, lack of subset specific cell surface markers have limited their characterisation and functional distinction from other subsets with regulatory function. T_H3 cells have been shown to be distinct regulatory subset induced from naïve T_H cells that are characterised by high expression of TGF-β with implications in antibody class switching to IgA (Fukaura et al. 1996). It has been postulated, however, that observed T_H3 cell function, is an extension of peripherally induced T_{reg} cells due to contradicting evidence of FoxP3 expression by the potential subset (Gol-Ara et al. 2012).

One distinct T cell subset with regulatory function is the Type 1 regulatory (Tr1) cell subset which is characterised by the expression of cell surface CD49b and LAG-3 (Gagliani et al. 2013). Tr1 cells express high levels of the immunosuppressive cytokines IL-10 and TGF-β but also low levels of IFN-γ, IL-2 and IL-5 whilst lacking IL-4 expression (Willimsky & Blankenstein 2005). Tr1 cells are able to modulate the presentation of antigens by the direct killing of myeloid derived APCs through the release of granzyme B and perforin (Magnani et al. 2011). Despite a highly suppressive function, Tr1 cells do not express FoxP3 and thus are considered a phenotypically distinct regulatory T cell subset (Vieira et al. 2004).

1.2.6.3 T cell plasticity

Despite classification of T_H subsets, T_H cells exhibit plasticity and can therefore be influenced into shifting functionality or phenotypic conversion (Hirahara et al. 2013). IFNγ signalling, for example, can interconvert T_H2 cells to T_H1 cell function by inducing T-bet expression, highlighting a capacity for plasticity in T_H cell subsets (Hegazy et al. 2010). Moreover, plasticity between T_H and T_{reg} subsets also occurs. Whilst the T_{reg} lineage can be determined in thymocyte development – characteristic of thymically derived T_{reg} cells (tT_{reg} cells) – regulatory function can also be induced peripherally by the interconversion of T_H cells to T_{reg} cells. T cells with this induced regulatory function are termed peripherally-derived T_{reg} cells (pT_{reg}). Such interconversion can occur when naïve T_H cells encounter pMHC antigen under sub-immunogenic conditions and consequently induce T_{reg} function (Apostolou & von Boehmer 2004).

1.3 Antigen specific activation of CD4^{+} T cells

Within the periphery, circulating CD4^{+} T cells sample antigen presenting cells via their TCR and, upon binding cognate MHC-II presented antigen, initiate TCR triggering, consequent T cell signalling and activation. The ability of CD4^{+} T cells to mount a response to tumour antigens is dependent on the immune microenvironment and the molecular interactions that occur at the interface between CD4^{+} T cells and antigen presenting cells. This interface is termed the immunological synapse, within which, the TCR-pMHC interaction is key to initiating an antigen specific functional response. Upon activation, T cells proliferate through clonal expansion, differentiate and perform subset specific functions which modulate immunity.

1.3.1 Structural features of the T cell receptor

An αβ TCR is a heterodimeric protein comprised of TCRα and TCRβ chains generated by somatic recombination as described previously. The structure of an assembled human TCR was first described in 1996 (Garcia et al. 1996). The TCR is formed by covalent linkage of the TCRα and TCRβ chains via a membrane proximal disulphide bridge (Claverie et al. 1989). Each TCR chain forms two Ig-like domains: a membrane proximal constant domain (C) and membrane distal variable (V) domain (*Figure 1.4a*). These domains are encoded by corresponding C- and V(D)J-gene segments as described in section 1.2.4 whereby the Vα domain is constructed from V- and J-gene segments, whilst Vβ is constructed from V-, D- & J-gene segments (*Figure 1.4b*). Association of the Vα and Vβ domains results in the highly variable membrane distal antigen binding site of the αβ TCR (Chothia et al. 1988).

The surface of the antigen binding site is constructed from six variable loops which mediate binding – termed complementarity determining regions (CDR) loops; numbered CDR1α -2α -3α and CDR1β -2β and -3β (Davis & Bjorkman 1988). The variability within these loops are generated during TCR gene arrangement. In both the Vα and Vβ domain, CDR1α, CD2α, CDR1β and CDR2β are encoded within the V-gene segments and thus variability is induced by variable (V) domain selection only – known as combinatorial diversity. Thus CDR1 and CDR2 represent the germline encoded segments of the antigen binding surface. Contrastingly the CDR3 loops exhibit higher variability as they are encoded by the junctions between recombined V(D)J-segments and are thus non-germline encoded. The Vα CDR3α loop sequence is derived from the V-J junction about which junctional diversity occurs as well as combinatorial diversity. Furthermore, the Vβ CDR3β loop is encoded by two junctions via incorporation of the D-gene segment at the TCRβ locus. As a result, the CDR3β loop is also non-germline encoded and exhibits increased variability compared to CDR3α due to junctional diversity introduced at both V-D and D-J junctions.
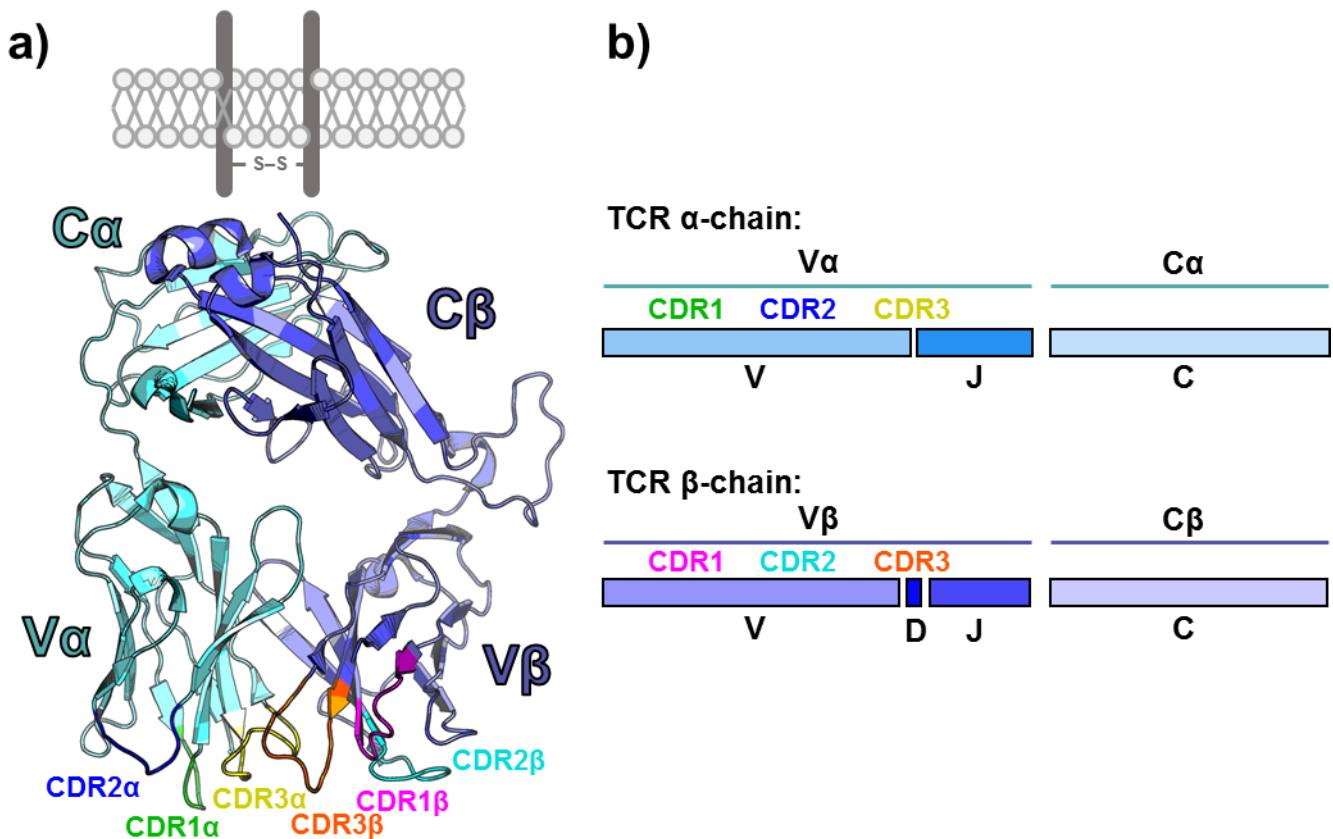
Figure 1.4 –The αβ T cell receptor (TCR) and its highly variable antigen receptor:

a) Cartoon representation of the structure of the extracellular domain of a TCR. TCRα chains and TCRβ chains associate and are covalently linked via a disulphide bridge (S – S) at the membrane proximal region of the TCR. The heterodimeric TCR contains four Ig-like domains classified as Cα, Vα, Cβ and Cβ. At the membrane distal edge, the six complementarity determining region (CDR) loops (coloured and labelled accordingly) make up the antigen binding site. Images generated from PDB: 4GKZ (Holland et al. 2012).

b) Contribution of the assembled TCRα and TCRβ genes to the formation of the highly variable antigen binding site as a result of somatic recombination. Variable domains Vα and Vβ are encoded by TCRα VJ and TCRβ VDJ gene segments, respectively. Constant domains Cα and Cβ are encoded by the TCRα C- and TCRβ C-gene segments, respectively. CDR1 and CDR2 loops of both TCR chains are encoded by respective V-gene segments. CDR3α is encoded by the TCRα VJ junction. CDR3β is encoded by the TCRβ V-D-J junction.

1.3.2   Presentation of antigens by MHC-II molecules

Unlike antibodies, TCRs do not bind to native immunogenic molecules in solution or directly on pathogenic entities. Instead, αβ TCRs bind antigens presented on MHC molecules to the T cell repertoire. Due to positive selection during TCR rearrangement and a preselection bias in the germline TCRα and TCRβ genes, the T cell repertoire is shaped to recognise peptide antigens presented on MHC molecules and thus TCRs are 'hardwired' for binding MHC (Garcia et al. 2009; Dai et al. 2008). As a result, TCRs are 'restricted' to MHC engagement. This system of antigen presentation and recognition allows exchange of antigenic material from innate immunity to adaptive immunity. Moreover, presentation of antigens on the surface of cells allows the detection of intracellular antigens which are inaccessible to antibodies.

1.3.2.1   MHC-II molecules and their role in presenting to CD4^{+} T cells

As previously eluded to, classical MHC molecules are divided into two classes: MHC class I molecules (MHC-I) and MHC class II molecules (MHC-II). In humans, the MHC family of proteins are encoded by the *human leukocyte activation* (*HLA*) complex of genes which contains over 200 individual genes. The studies described in this thesis involve presentation of peptide antigens by MHC-II molecules and, thus, will be the focus of this section.

In humans, MHC-II presenting molecules are encoded by the HLA- DR, -DP and -DQ loci. Whilst each MHC-II molecule is structurally related and functionally similar, subtle differences between different MHC molecules exist, particularly at the peptide binding region (discussed to follow). For example, there are almost 2000 known alleles of the HLA-DRB1 gene which defines the MHC-II molecule HLA-DR1 according to the IPD and IMGT/HLA database (Robinson et al. 2015). Ultimately, the variations between MHC-II genes and alleles possessed by a single individual allows the presentation of different peptide sequences by different MHC-II molecules, thus, increasing the number of potential presentable peptide chemistries– termed the ligandome (Rammensee 1995). The genes encoded by MHC loci are highly polymorphic and thus variable between individuals. Indeed the MHC gene complex is the most polymorphic region within the human genome (Potts & Slev 1995). For MHC-II molecules, these genes are generally expressed on cells with professional APC function.

In the periphery, professional APC function is typically performed by multiple immune cell types including: B cells, dendritic cells and macrophages (Kambayashi & Laufer 2014). MHC-II expression, however, can be induced in non 'professional' APCs (Kambayashi & Laufer 2014) such as mast cells and eosinophils, but also on non-haematopoietic cells such as mucosal epithelial cells (Shiao et al. 2007). Professional APCs, however, expressing MHC-II molecules, survey the body via constant uptake of soluble antigens, degraded cellular material – or whole

cells through phagocytosis pathways – and present peptide derivatives on MHC-II molecules at their surface. Upon activation by innate process such as PPR signalling in dendritic cells and macrophages or by B cells in response to antigen specific activation through the B cell receptor, professional APCs can enter the lymphatic system where they present antigens to naïve CD4^{+} T cells in secondary lymphoid organs (Itano & Jenkins 2003).

1.3.2.2 Processing of antigens onto MHC-II molecules

Presentation of peptide epitopes on MHC-II molecules classically occurs through the processing of extracellular antigens through the endocytic pathway. By this pathway, exogenous antigens are internalised by professional APCs, processed to peptide derivatives and presented to the T cell repertoire on MHC-II molecules (Watts 1997). Antigen uptake can occur through a number of different processes and is cell type dependent. Macrophages, for example, can phagocytose whole cells through phagosomes resulting in MHC-II antigen presentation within 20 minutes *in vitro* (Harding & Geuze 1992). B cells can specifically internalise antigens by receptor mediated endocytosis through the B cell receptor (BCR) (Lanzavecchia 1990).

Acquired antigens are compartmentalised into low pH endocytic vesicles which degrade whole proteins through lysosomal proteolysis by peptidases such as the cathepsin family (Watts 1997). Endocytic vesicles fuse with precursor invariant chain (I_i)-associated MHC-II molecule containing vesicles to form the MHC-II compartment. Consequent cleavage of the I_i chain results in MHC-II molecules bound with the class II-associated invariant-chain peptide (CLIP) which prevents early exchange of peptides into the presenting molecule. Through the action of the MHC-II molecules HLA-DM, CLIP removal is catalysed allowing for the exchange of peptides capable of binding MHC-II at a higher affinity (Denzin & Cresswell 1995). Consequently, peptide loaded MHC-II molecules are transported to the cell surface via exosomes to the cell surface in order to present to the T cell repertoire.

1.3.2.3 Characteristics of peptide presentation on MHC-II molecules

MHC-II molecules are approximately 60 kDa heterodimeric glycoproteins consisting of an α and β chain each anchored to the plasma membrane via a transmembrane domain (Brown et al. 1993). Each chain organises as two Ig-like domains resulting in a four domain extracellular portion with domains noted α1, α2, β1 & β2 (*Figure 1.5a*). The membrane proximal α2 and β2
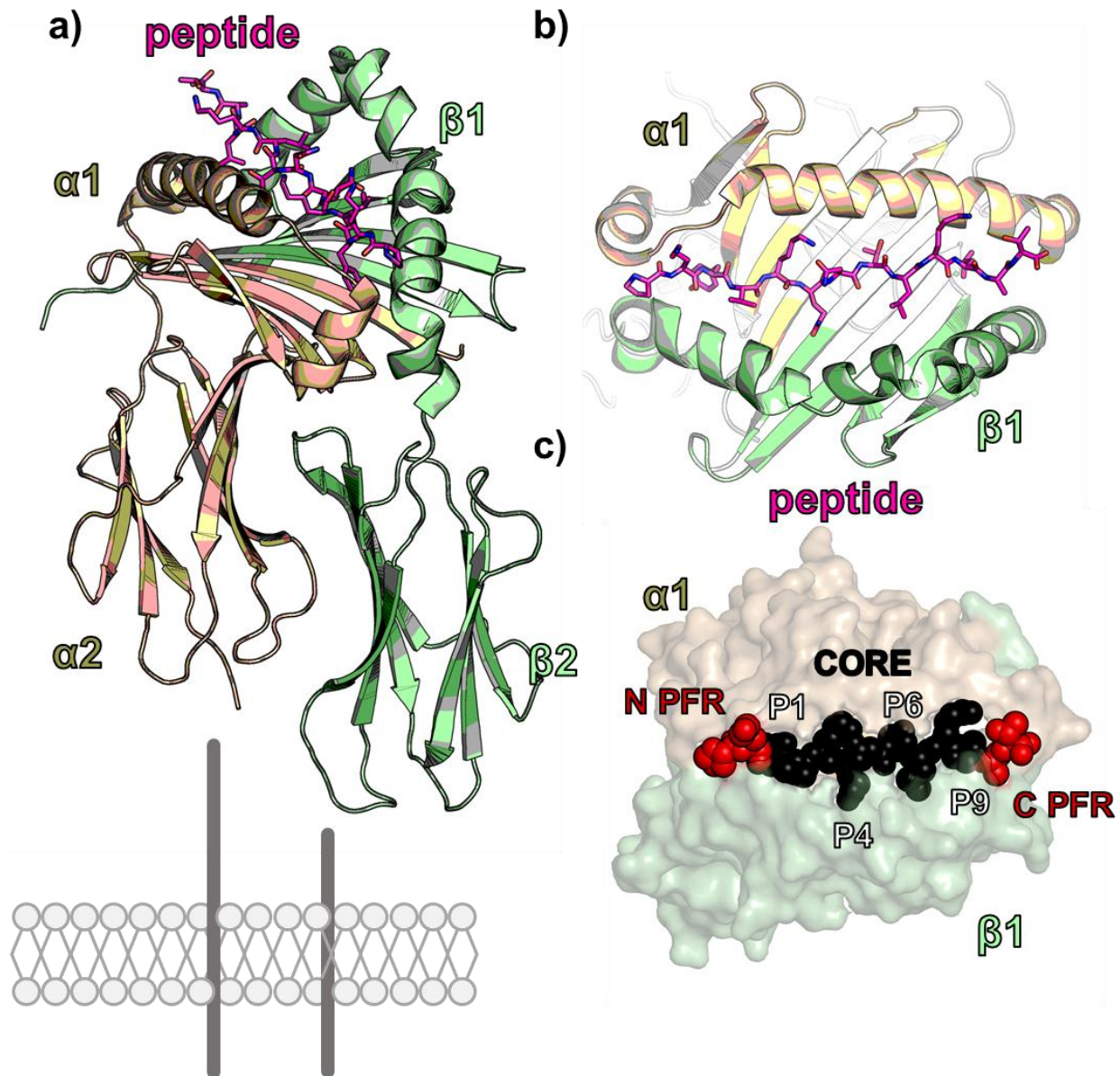
Figure 1.5 – Structural features of peptides presented on MHC-II molecules:

a) Cartoon and stick representation of the structure of an influenza-derived peptide (magenta) presented on the MHC-II molecule HLA-DR1. The assembled HLA-DR1 structure, comprised of α chain (pale pink) and β chain (pale green) form four Ig-like domains: α1, α2, β1 and β2. The peptide is presented at the membrane distal end of the protein.

b) Top down view of peptide binding into the open ended peptide binding groove of HLA-DR1. The peptide lies above a bed of eight anti-parallel β sheets, walled by α chain and β chain helices. Coloured as in *a)*.

c) Top down view of the MHC (surface) binding the 13mer influenza-derived peptide (spheres). Peptide core residues (black) are bound into the P1, P4, P6 and P9 binding pockets resulting in a two amino acid N-terminal peptide flanking residues (N PFR) and two amino acid C-terminal peptide flanking residues (C PFR).

All images generated from PDB: 1FYT (Garboczi et al. 1996)

domains exhibit less variation and are involved in the binding of the CD4 co-receptor (Yin et al. 2012). At the membrane distal end of the associated MHC-II molecule, however, the α1 and β1 domains combine to form a peptide binding groove upon which the peptide antigens presented to TCRs are loaded. In MHC-II molecules, the peptide binding groove is constructed from both α and β chains of the MHC. The resulting binding groove consists of a base of eight anti-parallel β sheets that form the 'floor' of the peptide binding groove (Brown et al. 1993). The concaved nature of the groove is constructed from two helical portions that span the length of the molecule in anti-parallel orientation forming the 'walls' to the binding groove (*Figure 1.5b*). The helical portion that lines the α domain side of the groove is discontinuous and is comprised of a 3_{10} helix followed by an α-helix structure, linked by a flexible loop. Contrasting to MHC-I molecules, the sides of the peptide binding groove are in an open conformation which has implications in the binding of MHC-II restricted peptides (Holland et al. 2013).

1.3.2.4   Binding of the core peptide epitope to MHC-II molecules

Through elution of peptides from MHC molecules, it was revealed that different MHC molecules bound different peptide sequences which were characterised by allele-specific peptide motifs (Falk et al. 1991). Elucidation of the first high-resolution structure of an MHC-II molecule (HLA-DR1) highlighted that the polymorphic residues of MHC-II molecules were focused on the areas of the α1β1 peptide binding groove (Stern et al. 1994). As a result, each MHC-II molecule has a motif of preferential peptide 'anchoring' residues which orientate into the MHC molecule in the direction of the membrane (Rammensee et al. 1995). Together, these studies showed that peptides are bound into a series of peptide binding pockets, lined by polymorphic residues, which determine allele-specific peptide motifs. The MHC-II molecule HLA-DR1, for example, is described to have four binding pockets, designated: P1, P4, P6 and P9 (Jones et al. 2006). These concaved pockets make extensive contacts with the peptide and generally facilitate the largest binding energy of peptide to MHC-II stability. Due to the formation of four anchoring points to the peptide, MHC-II bind peptides deeply into the groove in a flat extended conformation (Stern & Wiley 1994). Due to the open-ended conformation of MHC-II peptide binding grooves, MHC-II molecules are able to bind peptides of varying length – typically between 12-20 amino acids (Holland et al. 2013). MHC-II molecules, however, maintain a nine amino acid binding 'core' which facilitates the majority of binding between peptide and MHC-II (*Figure 1.5c*). For HLA-DR1, the nonamer binding core residues of a peptide are fixed by the P1, P4, P6 and P9 pockets which anchor the peptide (Stern & Wiley 1994; Jones et al. 2006).

1.3.2.5 Influence of peptide flanking residues on MHC-II peptide presentation

The ability to facilitate longer peptides is enabled by the extension of peptide residues outwards and beyond the peptide groove. This property is unique to MHC-II molecules and is not generally observed in MHC-I molecules which have a fixed width within the groove – and extension of peptide length results in 'bulging' out of the centre of the groove and a consequent increase in peptide height (Holland et al. 2013). These residues which extend out of the peptide binding core, in MHC-II systems, are termed the peptide flanking residues (PFRs).

The role of PFRs on peptide to MHC-II binding and consequent TCR activation is yet to be fully elucidated. Analysis of a murine I-A^K restricted hen egg white lysozyme epitope revealed that naturally processed antigen, by B-cell lymphoma cell lines, showed an increased relative abundance of presented peptides with extended PFRs compared to the core nine amino acid binding core (Nelson et al. 1992). Such higher abundance was later attributed to an increased pMHC half-life by PFR containing peptides at the surface of APCs *in vitro* (Nelson et al. 1994). Subsequently, this increased pMHC stability was shown to influence T cell activation in a murine I-A^b presented self-peptide system where the length of both N-terminal and C-terminal PFRs impacted the ability to activate a cognate CD4$^+$ T cell clone *in vitro* (Sant'Angelo et al. 2002). Here, *Sant'Angelo et al.* showed, via pMHC stability assays, that increasing PFR length at both termini allowed increased MHC-II peptide stability – whilst mutation of these residues did not impact clone activation. Together, these observations suggested that, in the system studied, both N- and C-terminal PFRs primarily promote enhanced T cell activation through enhanced peptide presentation. Such findings have been supported by computational modelling where increased N- and C-terminal flanks were predicted to enhance peptide to MHC-II binding affinity and a predicted optimal length of 18-20 was calculated (O'Brien et al. 2008).

1.3.3 Structural and biophysical characteristics of MHC-II engagement by TCRs

Understanding of how TCRs bind to cognate pMHC molecules has been driven by the study of soluble TCR and MHC molecules using biophysical and structural techniques (Bridgeman et al. 2012). Such techniques have been applied to numerous different TCR-pMHC systems: from the study of viral antigen-specific TCRs binding cognate peptides, to tumour-specific TCRs binding tumour-derived presented antigens (Hennecke & Wiley 2002; Deng et al. 2007). Analysis of different TCR-pMHC systems has revealed a number of different patterns and molecular rules that generally define TCR engagement of pMHC molecules and, thus, provide a snapshot of the rules governing binding by the TCR repertoire as a whole (Rudolph et al. 2006). Data describing TCR engagement to MHC-I restricted antigens, however, far outweighs that of MHC-II restricted counterparts. As a result, less is known about how CD4$^+$ T cells engage their ligand.

Despite parallels in structural organisation and generation, MHC-II engagement by TCRs occurs at a comparatively weak affinity compared the binding of antigen by antibodies (Bridgeman et al. 2012). This low affinity is attributed to slow association rates (K_{on}) followed by fast dissociation rates (K_{off}) (Boniface et al. 1999). The affinity at which TCRs bind cognate pMHC antigens is governed by the MHC restriction; whereby TCRs restricted to MHC class I molecules bind at higher affinity than MHC class II counterparts (Cole et al. 2007). Moreover, the affinity of TCR engagement is also dependent on the chemistry of the presented peptides and the TCR's antigen binding site constructed from the CDR loops (Peled et al. 2008). As a result, variation in binding strength is observed by different TCRs binding to different peptide epitopes on the same MHC molecule (D. Cole et al. 2007). The origin of the peptide antigen also appears to influence the affinity of cognate TCR engagement to pMHC. Viral-derived peptide antigens, for example, have been shown to be bound by TCRs at higher affinity that those derived from either self or tumour-derived antigens (Aleksic et al. 2012). For TCRs restricted to MHC-II molecules, this exact affinity range is unknown as TCRs have been shown to bind to cognate pMHC-II at unmeasurably low affinities. However, such binding can be confirmed via experimental multimersation effects (Li et al. 2005; Deng et al. 2007). An estimate of the potential affinity range between TCRs and pMHC-II molecules is between $5 - 500$ µM (K_D) (Bridgeman et al. 2012).

The mode of binding between TCRs and pMHC occurs via the antigen binding site located on the membrane distal surface of the TCR Vα & Vβ domains which is comprised of the six CDR loops, described previously. All TCRs described structurally, except one, bind atop pMHC-II ligands with a fixed polarity whereby the TCRα chain interacts largely with the MHC β chain and the TCRβ chain interacts primarily with the MHC α chain (Rossjohn et al. 2015). This polarity is also replicated in MHC-I restricted TCR engagement. As a result of this polarity, MHC-II engagement is not parallel to the long axis of the peptide. Instead TCRs bind diagonally across the peptide at an angle termed the 'crossing angle' or 'docking angle'. The docking angle of TCR engagement of MHC-II, according to a meta-analysis of available structure data, is on average 76 ° within a range of 44 – 115 ° (Rossjohn et al. 2015). The exception to this standard geometry is a HLA-DR4 restricted TCR, expressed from an *in vitro* induced T_{reg} clone which bound its cognate self-peptide HLA-DR4 with a reversed polarity and at a considerable tilt (Beringer et al. 2015). The result of this abnormal binding mode was that the T_{reg} derived TCR engaged the pHLA-DR4 molecule using the TCRα chain only.

Analysis of the CDR loop contribution to binding of pMHC has shown that, similarly, TCRs exhibit commonality in binding. MHC-II restricted TCRs generally bind the MHC portion using the germline encoded CDR1 and CDR2 loops whilst the non-germline encoded CDR3 loops are

located centrally to the antigen binding site and bind primarily the peptide (Feng et al. 2007). This observation led to the hypothesis that TCRs are hardwired to bind MHC-II molecules first via CDR1 and CDR2 'codons' allowing for CDR3 loop 'scanning' for peptide specificity (Garcia et al. 2009). These rules, however, appear flexible as shown by the binding of a single TCR to two peptides bound to the same MHC-II molecule – which exhibited a differential foot-print of ligand engagement (Mazza et al. 2007).

TCRs have been shown to exhibit a high degree of cross-reactivity resulting in the ability of single TCRs can bind more than a million different peptides (Wooldridge et al. 2012). The nature of the CDRs suggests that the surface interface, which make up the antigen binding site of the TCR, may exhibit inherent plasticity which enables such cross-reactivity (Garcia & Wilson 1999). Structural studies of TCRs and pMHC-II molecules in ligated and unligated states, however, have shown that, in contrast, minimal CDR loop movements can occur to mediate binding and that loop flexibility is not required to bind to the same peptide epitope presented on two different MHC-II molecules (Holland et al. 2012).
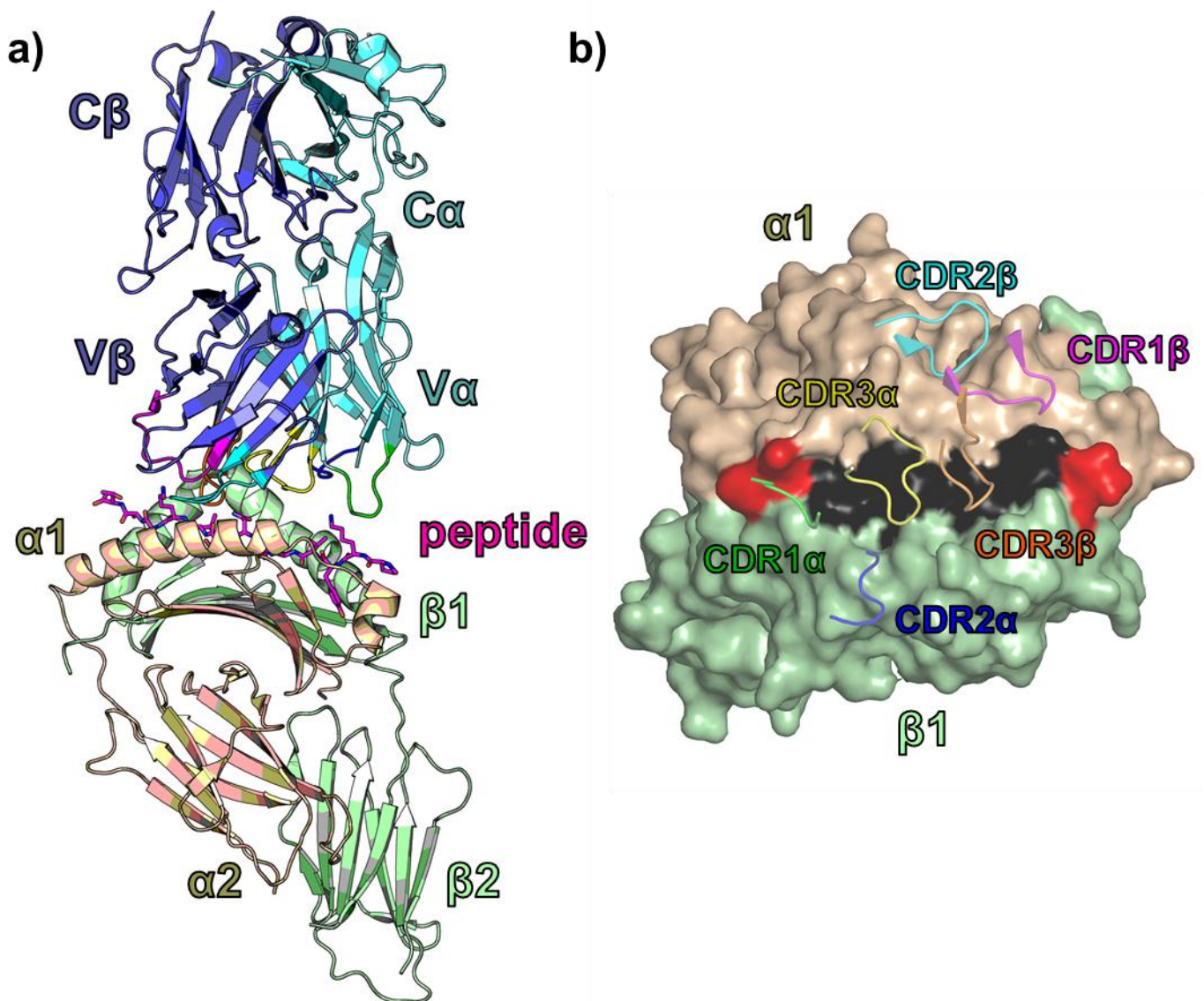
Figure 1.6 – Engagement of pMHC-II by a TCR:

a) Cartoon and stick representation of an influenza-reactive TCR (cartoon; blue:aqua) binding to an influenza-derived peptide (sticks; pink) presented on the MHC-II molecule HLA-DR1 (cartoon; pale pink/pale green). TCR engagement occurs via a generally conserved polarity: Vβ over α1 and Vα over β1.

b) Top down view of CDR loop binding over the pMHC-II surface volume. CDR1α and CDR2α primarily bind the β1 domain of MHC-II whilst CDR1β and CDR2β primarily bind the α1 domain. CDR3α and CDR3β interact primarily with the bound peptide core (black). In this influenza model, only the CDR1α binds over the peptide flanking residues (red) at the N-terminus. CDR loops coloured according to inset labels.

All images generated from PDB: 1FYT (Jens Hennecke et al. 2000)

1.3.3.1   Influence of PFRs on TCR engagement of MHC-II presented peptides

As well as enhancing pMHC-II stability, described previously, PFRs have also been implicated in pMHC-II engagement. Such an interaction was evidenced by structural data describing the influenza-reactive HA1.7 TCR in complex with the hemagglutinin derived $HA_{306-318}$ peptide presented by HLA-DR1, where a direct electrostatic interaction between the TCR and the N-terminal flanking P-1 lysine residue was observed (J Hennecke et al. 2000). Moreover, mutation of the P-1 residue of this peptide epitope to an alanine resulted in decreased HA1.7 clone proliferation (Alexander et al. 1993). Together, these data provide evidence of N-terminal PFRs influencing TCR engagement and thus T cell functionality.

Similarly, analysis of the contribution of PFRs to engagement by TCRs has shown that C-terminal PFRs are able to modulate binding, in particular, through large positively charged residues that elevate the peptide height of the C-terminal PFR (Godkin et al. 2001). Indeed, disruption of the C-terminal PFR of an HIV-derived peptide, which protruded out of the MHC binding groove, abrogated the ability to activate a cognate TCR clone (Zavala-Ruiz et al. 2004). In addition, modification of a residue in the C-terminal flank to introduce large positively charged arginine residues both increases TCR affinity and TCR repertoire selection in a HLA-DR1 restricted influenza model (Cole et al. 2012; Holland et al. 2013). These data provide further evidence of TCR engagement with the PFRs and a potential capacity for enhancement of TCR binding through introduction of basic residues within the C-terminal PFR.

1.3.4   T cell activation and priming through T cell signalling processes

Engagement of TCR molecules with sufficient capacity to bind pMHC molecules can result in the activation of T cells through the process of T cell signalling. The affinity of TCR binding to pMHC correlates with the degree of T cell activation (Corse et al. 2011). The way in which the TCR transduces this ligand discrimination and receptor sensitivity to trigger T cell signalling is currently disputed; with evidence for a number of different TCR triggering models such as the kinetic segregation model (James & Vale 2012), serial triggering (Valitutti et al. 1995) and conformational/mechanistic models, amongst others (van der Merwe & Dushek 2011). Nevertheless, the functional consequence of TCR binding cognate MHC is the initiation of a signalling cascade about the TCR/CD3 complex which can ultimately lead to T cell activation.

The process by which antigen inexperienced T cells encounter antigen and are activated for the first time is termed T cell priming. T cell activation in naïve T cells cannot occur via stimulation through the TCR alone (Pollizzi & Powell 2014). It is understood that T cell activation requires, firstly, the presence of the CD4 co-receptor which localises the phosphokinase Lck to the TCR/CD3 complex which, upon TCR triggering, results in a phosphorylation of the CD3ζ

chain ITAMs. This signal is cascaded through consequent recruitment of the ZAP70 kinase to the TCR/CD3 complex. Consequent signal transduction results in the eventual dephosphorylation and consequent nuclear translocation of NFAT – a transcription factor with immune target genes. This process is defined as the 'signal 1' of T cell signalling. The consequence of signal 1 transduction alone due to TCR triggering, however, leads to induction of T cell anergy through the induction of suppressive gene targets (Appleman & Boussiotis 2003).

Instead, induction of activation requires a second signalling cascade, 'signal 2' which is provided by the co-stimulatory molecule CD28 (Pollizzi & Powell 2014). CD28 localisation to the immune synapse is enabled by the expression of its ligands CD80/CD86 on the surface of APCs. Upon CD28 recruitment to the immune synapse, signal transduction results in the nuclear translocation of the immune master transcription factor NF-κB. Moreover, through phosphorylation of RAS by CD28 and the 'signal 1' signalling molecule DAG, both signal 1 and 2 are integrated to allow the activation of AP-1 – a third transcription factor. As a result of both signal 1 and 2 transduction and consequent localisation of the three canonical transcription factors, NF-κB, AP-1 and NFAT, naïve T cells are licensed for activation.

As a result of the requirement for signal 2 in the activation of naïve T cells, APCs are able to modulate the priming of the T cell response to presented antigens by regulation of the CD28 ligands CD80/CD86 expression during antigen presentation (Hertz et al. 2001). Indeed, CD80/CD86 are only expressed on activated dendritic cells and, as a result, require their activation through innate signalling processes before licensing naïve T cell priming.

As mentioned previously, a number of different CD4$^+$ T cell subsets exist. The functional fate of naïve T cells, upon priming by APCs, is determined by a third signal: the T cell polarisation signal (Kaiko et al. 2008). Upon priming of naïve T cells through both signal 1 and 2, cytokines within the microenvironment influence the functional outcome of naïve T cell differentiation. This process forms the basis of CD4$^+$ T cell subset generation as described previously in section 1.2.6.

Antigen experienced memory T cells, however, have altered requirements of T cell signalling to induce activation (London et al. 2000). In such cells, a lower threshold of signalling is required for activation, although a degree of co-stimulatory signalling is still required for memory T cell activation (Boesteanu & Katsikis 2009).

1.4 5T4 as a model of αβ T cell immunity to tumours

Strong evidence of a role of the immune system and CD4$^+$ T cells in suppressing tumours was shown by a number of studies of tumour models in mice in the late 20th and early 21st Century. In 1994, a role for the inflammatory cytokine IFNγ was implicated in tumour progression using the Meth A mouse fibrosarcoma tumour model (Dighe et al. 1994). Here, dominant negative IFNγ receptor (IFNγR^{DN}) tumours exhibited enhanced tumour growth in tumour implanted BALB/c mice. This enhanced growth, induced by loss of IFNγ signalling function, was shown to render IFNγR^{DN} tumours insensitive to LPS-induced tumour rejection.

In 2001, evidence of a role for adaptive immunity in tumour rejection was revealed by the generation of the RAG2$^{-/-}$ knock out mouse (Shankaran et al. 2001). In these studies, RAG2$^{-/-}$ mice, which effectively have no functional T or B cell repertoire, exhibited increased tumour rates using the methylcholanthrene- (MCA)-induced tumour model providing evidence of lymphocyte involvement in limiting tumour growth in wild type RAG2 sufficient mice. Moreover, the tumour limiting capacity by the immune system was shown to be dependent once more on IFNγ.

In 2005, a direct role of CD4$^+$ T cells and professional APCs presenting tumour-derived antigens was revealed using a transgenic mouse system and the MOPC315 mouse myeloma tumour model (Corthay et al. 2005). Here, mice bearing a monoclonal TCR repertoire specific for a tumour-antigen expressed by implanted myeloma tumours (via transgenic TCR expression on a SCID mutated background) were resistant to tumour formation; whilst non-transgenic mice exhibited higher tumour burden. It was shown that tumour implantation resulted in the recruitment of macrophages to the tumour site, consequent presentation of tumour-derived peptides on MHC-II molecules, subsequent activation of tumour-specific CD4$^+$ T cells in the lymph nodes and subsequent release of effector cytokines. These studies therefore highlighted a role of macrophages presenting tumour-derived antigens to tumour-specific CD4$^+$ T cells in the observed ability to suppress tumour formation.

1.4.1 The tumour immunoediting hypothesis

Postulation as to why the immune system is able to recognise tumours through immunosurveillance, yet immunocompetent individuals still develop tumours, led to the formulation of the tumour immunoediting hypothesis (Dunn et al. 2002). It was hypothesised that the immune system shapes tumours by adding a selection pressure to tumour formation by which a selective advantage to the tumour is to survive in an anti-tumour-competent environment. This hypothesis

was evidenced by the transplant of tumours developed in either immunocompetent or immuno-deficient environments. Tumours grown in RAG2$^{-/-}$ mice and transplanted into RAG2^{+} WT mice were suppressed at a higher rate than tumours grown in RAG2^{+} immunocompetent WT mice and transplanted into RAG2^{+} immunocompetent WT mice (Shankaran et al. 2001). This observation suggested that tumours grown in immunodeficient mice were more immunogenic than tumours grown in the absence of anti-tumour immunity. It was consequently reasoned that tumours grown in an immunocompetent environment were 'imprinted' by anti-tumour immunity and that those grown in the absence of an immunocompetence were yet to be shaped or 'edited' into a tumour variant which had evolved to avoid anti-tumour immunity. Thus in the presence of immunocompetence, highly immunogenic tumour variants are eliminated whilst those which exhibit low immunogenicity have a selective advantage. At this stage, the tumour is said to be in a state of equilibrium with the immune system. Outgrowth of such cells eventually occurs due to the escape of tumours from anti-tumour immunity. This led to the formulation of three stages on cancer immunoediting, known as the three Es of cancer immunoediting: Elimination, Equilibrium and Escape.

1.4.2 T$_H$1 responses to tumours

As described previously, T$_H$1 cell differentiation is achieved by the stimulation of primed CD4^{+} T cells by professional APCs under IL-12 polarising signal conditions (Kaiko et al. 2008). The consequence of T$_H$1 cell polarisation is the release of an inflammatory cytokine profile including IFN-γ, TNFα, TNFβ as well as autologous T$_H$1 promoting IL-2 and IL-12.

Analysis of the genetic profile of immune cell infiltrate into tumours in a large cohort of patients revealed that expression of T$_H$1 immunity associated genes such as those that encode IFNγ, Granzyme-B and CD3ζ negatively correlated with tumour recurrence and thus suggests that T$_H$1 immunity is an overall correlate of better clinical outcome (Galon et al. 2006). Much of the anti-tumour function by tumour specific T$_H$1 cells is attributed to IFNγ. As described previously, removal of IFNγR function on tumour mouse models suggested a direct role for IFNγ on tumours (Dighe et al. 1994). Synergistically, IFNγ and TNFα are able to induce tumour cell senescence and thus arrest tumour cell cycle through the release of reactive oxygen species and NADPH oxidases (Hubackova et al. 2015). IFNγ induces MHC-I upregulation on tumour cells and thus may contribute to the increased tumour burden in IFNγR^{DN} mice through removal of cytotoxic T cell elimination of tumour cells (Propper et al. 2003). Moreover, IFNγ has been shown to induce MHC-II expression on tumour cells and thus may themselves be able to present antigens to CD4^{+} T cells as a result of IFNγR signalling (Thibodeau et al. 2012). IFNγR signalling also induces the production of CXCL10 which possesses anti-angiogenic properties

(Angiolillo et al. 1995) as well as serves as a chemoattractant for various immune cells (Liu et al. 2011).

As well as having a direct effect on tumour cells expressing IFNγR, release of IFNγ has a broader effect on anti-tumour immunity. As eluded to previously, IFNγ has been shown to induce macrophage activation at tumour sites which, as a result, present tumour-derived antigens to CD4$^+$ T cells (Corthay et al. 2005). Moreover, such macrophage activation results in the release of anti-tumour factors such as reactive oxygen species (Mantovani et al. 2004).

1.4.3 Regulatory responses to tumours

As a result of thymic selection against self-presented antigens, TCR clonotypes with an increased affinity to self-antigens can enter the periphery as thymic-derived T$_{reg}$ (tT$_{reg}$) cells through acquired expression of the FoxP3 transcription factor (Maloy & Powrie 2001). Due to the self-derived nature of tumour antigens, with the exception of neo-antigens, the generation of tumour-specific tT$_{reg}$ cells as a consequence of central tolerance is a barrier to immunity to tumours. Moreover, antigen stimulation of naïve CD4$^+$ T cells in the absence of co-stimulation can lead to T cell anergy and T cell priming in the presence of TGFβ can lead to the induction of T$_{reg}$ function and the differentiation to peripherally-derived (pT$_{reg}$) cells (Pollizzi & Powell 2014). Indeed, human breast tumours have been shown to express TGFβ and thus may directly alter naïve T cell polarisation (Relf et al. 1997). In contrast, however, analysis of the infiltrating T cell repertoire of FoxP3$^-$ cells compared to FoxP3$^+$ T$_{reg}$ in the MCA induced tumour model revealed little overlap in the repertoires of effector and regulatory T cell populations suggesting that T$_{reg}$ conversion does not significantly contribute to the population of T$_{reg}$ cells residing in tumours (Hindley et al. 2011).

Many studies have focused on the frequency of T$_{reg}$ cells in cancer patients and their potential impact on tumour progression. For example, the degree of infiltrate of FoxP3$^+$ T$_{reg}$ cells into ovarian tumours has been shown to correlate with poorer disease prognosis (Curiel et al. 2004). In a cohort of 42 patients with epithelial malignancies, the frequency of T$_{reg}$ cells, identified as CD4$^+$ CD25$^+$ T cells, were shown to be elevated in the peripheral blood compared to that of healthy controls (Wolf et al. 2003). In addition, T$_{reg}$ cells, identified as CD4$^+$CD25$^+$FoxP3$^+$ cells have been shown to be increased in both the peripheral blood and mesenteric lymph nodes of patients with CRC (Clarke et al. 2006). Removal of such regulatory cells was shown to unmask tumour-antigen-specific CD4$^+$ T cell responses *in vitro*.

Infiltration of other suppressive T cell subsets such as Tr1 cells have also been implicated in generating regulatory responses to tumours. Tr1 cells are thought to be a subset of induced cells with regulatory function as a result of chronic antigen stimulation and priming in the presence

of IL-10 (Vieira et al. 2004). Tr1 cells have been shown to be enriched at the sites of human hepatocellular carcinomas (Pedroza-Gonzalez et al. 2015) as well as in peripheral blood of head and neck squamous cell carcinoma patients (Mandapathil et al. 2009). Moreover, enrichment of a highly suppressive T cell subset infiltrating in colorectal tumours, characterised by the expression of the latency associated peptide (LAP) and LAG-3, have also been identified by our group in Cardiff and implicated in possessing potent immunosuppressive capacity (M Scurr et al. 2013). It is possible that these detected cells are also Tr1 or Tr1-like cells. Identification of LAG-3 and CD49b as surface co-markers for Tr1 cells will likely aid the further characterisation of Tr1 cells and their role in tumours by allowing methodologies for their identification from other T cells with regulatory function *in vivo* (Gagliani et al. 2013).

Nevertheless, these cells with regulatory phenotype are characterised by expression of high levels of IL-10 which suppresses dendritic cell and macrophage maturation causing down-regulation of MHC and co-stimulatory molecules as well as the inhibition of T_H1 cytokines by $CD4^+$ T cells (Sato et al. 2011). As a result, levels of IL-10 in the serum correlate positively with melanoma disease progression suggesting a role of IL-10 producing regulatory T cell subsets in allowing tumour progression (Itakura et al. 2011).

1.4.4   5T4 is a cancer antigen expressed on solid tumours

5T4, also known as Trophoblast glycoprotein or Wnt-Activated Inhibitory Factor 1 (WAIF1) is a tumour associated antigen (TAA) expressed on a number of different tumours including bladder, breast, cervix, endometrium, lung, oesophagus, ovary, pancreas, stomach and testicular tumours – as shown by immunohistological staining (Southall et al. 1990). Immunohistological staining of non-transformed tissue, however, is limited to human placental tissue as well as some detected staining in oral sites; particularly in the presence of inflammation (Ali et al. 2001) . As a result of this restricted expression, 5T4 has been highlighted as a target antigen for immunological therapy. Due to its expression in placental tissue and the foetal trophoblast, 5T4 is classified as an oncofoetal antigen.

5T4 is a single pass transmembrane glycoprotein consisting of a 42 kDa protein component and average glycosylated molecular weight of 72 kDa (Hole & Stern 1990). 5T4 functions as a modulator of WNT signalling by inhibiting canonical β-catenin signalling and promoting non-canonical WNT pathways (Kagermeier-Schenk et al. 2011). It's function is likely to be dependent on the short intracellular domain as transfection of cytoplasmic domain deficient 5T4 into epithelial cells was not able to induce enhanced mobility observed by *in vitro* delivery of wild type 5T4 (Carsberg et al. 1996). The high resolution structure of 5T4 revealed the extracellular domain of 5T4 as a twisted solenoid made up of eight leucine rich repeat units (Zhao et

al. 2014). Whilst potential ligand hotspots required for WNT signalling function have been described, no ligand or signalling partner molecules of 5T4 have identified, thus, the mechanisms by which 5T4 modulates WNT signalling are not fully understood. Nevertheless, due to its role in WNT signalling, aberrant expression of 5T4 in humans has potential implications in cellular migration and therefore metastatic capacity. Indeed, murine fibroblast cells transfected with 5T4 exhibit increased motility and dispersion as well as altered morphology *in vitro* (Woods et al. 2002)

Expression of 5T4 is observed at high frequency in human colorectal tumours. In a cohort of 72 colorectal cancer patients, 85 % exhibited $5T4^+$ tumours as shown by immunohistological staining (Starzynska et al. 1992). In the same cohort, presence of 5T4 expressing tumours was a correlate of poor-prognosis with a five year survival rate of 22 % in patients histologically determined as $5T4^+$ compared to 75 % in $5T4^-$ tumour patients (Starzynska et al. 1994).

1.4.5 Immune responses to 5T4

Knowledge of the immune response to 5T4 in either healthy individuals or cancer patients was limited pre-2000. Despite this, development of a cancer vaccine with the aim of boosting immune responses to 5T4 antigen was developed (Mulryan et al. 2002).

In healthy individuals, 5T4-reactive $CD8^+$ T cells have been detected in the peripheral blood of a healthy donor (Redchenko et al. 2006). Such responses were observed *ex vivo* in one of 30 tested donors from which cultured T cell lines were grown from the single responding donor. Consequent analysis of 5T4-derived peptides revealed an epitope restricted to the HLA-C molecule Cw7 from the donor. Subsequent cultured T cell lines and clones were shown to lyse 5T4 expressing autologous presenting cells.

Similarly, *ex vivo* IFNγ response rates to 5T4 whole protein was detected at a rate of 1/14 CRC patient blood samples, however, depletion of T_{reg} cells unmasked a response in a further 5/14 patients (Clarke et al. 2006). In a study of 5T4 responses in pre-operative CRC patients, 7/19 patients were classified as 5T4 responders by IFNγ ELISpot assays whilst post-surgery responses were increased to 14/19 patients (Betts et al. 2012). This increase in responders could be attributed to the decrease in T_{reg} suppression post-operation due to fewer 5T4 responders requiring T_{reg} removal to unmask 5T4 responses which correlated with increased T_{reg} numbers in pre-operative patients compared to post-operative patients and healthy controls. Moreover, *in vitro* cultured IFNγ responses to an overlapping peptide library of 5T4 revealed that 5T4 responses were detected in 100 % of healthy donors and correlated, along with T_{reg} numbers, with disease progression in CRC patients (Scurr et al. 2013). Presence of a detectable $5T4^+$ T cell response pre-operatively, however, did not influence 5-year tumour recurrence rates but did not

negatively correlate with tumour recurrence – as exhibited by a different tumour antigen: carcinoembryonic antigen (CEA) (Scurr et al. 2015)

Few studies have begun to identify T cell epitopes of 5T4 in order to describe the observed response to 5T4 in healthy donors and tumour patients at the antigenic level. Assaying the potential for MHC-I presentation revealed peptide epitopes of 5T4 initially identified *in vitro* and later characterised *ex vivo* in vaccinated CRC patients (Shingler et al. 2008). As a result, three further epitopes of 5T4 have been identified which were restricted to HLA-A1 and -A2 molecules – as shown by *ex vivo* responses in individual HLA-A1^{+} and -A2^{+} colorectal patients. Subsequent detection of CD8^{+} T cells specific to two of these epitopes (restricted to HLA-A2) using 5T4-derived MHC-I multimer staining was achieved in *in vitro* cultured T cell lines from multiple (healthy and renal cell carcinoma) donors (Tykodi et al. 2012). Moreover, one of these epitopes $5T4_{17-25}$ was shown to be naturally processed on renal cell carcinoma cells and a cytotoxic T cell clone grown against this epitope was able to directly lyse a 5T4 expressing renal cell carcinoma cell line.

A study into the potential recognition of 5T4 by CD4^{+} T cells highlighted that indeed CD4^{+} T cells were detectable in *in vitro* cultured T cell lines from healthy donors (Elkord et al. 2008). Such responses, however, were enhanced upon removal of CD25^{+} cells suggesting once more that T_{reg} cells may play a role in dampening immune responses to 5T4. Nevertheless, a CD4^{+} T cell epitope of 5T4 ($5T4_{222-236}$) restricted to HLA-DR4 was identified. IFNγ producing CD4^{+} T cells were detectable in T cell lines cultured from 4 out of 9 HLA-DR4^{+} healthy donors. Consequently, 5T4 responses were shown to deteriorate with tumour stage.

From studies in mice, it has been hypothesised that for a successful anti-5T4 and consequent anti-tumour T cell response, central tolerance must be broken. mRNA transcripts for 5T4 have been detected in the thymus suggesting that, at least in mice, 5T4 is likely presented as a TSA by thymic antigen presenting cells during negative selection (Castro et al. 2012). Indeed, knock out of 5T4 in mice was shown to enable enhanced antibody and IFNγ mediated CD8^{+} T cell responses as a result of 5T4 vaccination compared to 5T4 replete wild type C57BL/6 mice. Moreover, modulation of T_{reg} cells via antibody depletion enhances CD8^{+} T cell responses after vaccination in wild type 5T4 replete mice to levels observed in 5T4 knock out mice. It has therefore been hypothesised that removal of 5T4 expression from the thymus enables a T cell repertoire more receptive to 5T4 recognition and effector function. Clearance of implanted 5T4[+] B16 tumours in such mice, however, was not halted in 5T4^{-/-} mice unless immunity was boosted via 5T4 vaccination, thus, suggesting a role for induced tolerance to 5T4 in the periphery. These data highlight how the induction of tolerance to tumour vaccine targets, such as 5T4, is a challenge of cancer vaccination efficacy (Zhou et al. 2006).

1.4.6 Potential therapeutic enhancement of immunity to 5T4

Immunity to 5T4 antigens in both humans and mice appears to be masked by regulatory T cell mechanisms. Consequently, a highly attenuated, non-replicating modified vaccinia virus Ankara (MVA) vaccine encoding 5T4 (MVA-5T4/Trovax®) has been developed in efforts to enhance immunity in cancer patients. This vaccine showed promise in pre-clinical models where tumour burden is reduced in the $5T4^+$ CT26 murine tumour model and where a prolonged immunity to tumour was maintained six months post treatment (Mulryan et al. 2002). This prolonged immunity in vaccinated mice was consequently shown to be dependent on $CD4^+$ T cell and antibody mediated immunity (Harrop, Ryan, et al. 2006).

Vaccination of 22 metastatic colorectal patients with MVA-5T4/Trovax® in a phase I/II trial showed that the vaccine is generally well tolerated and is able to boost 5T4-specific neutralizing antibodies (Harrop, Connolly, et al. 2006). Furthermore, combination treatment of MVA-5T4/Trovax® in conjunction with 5-fluorouracil, folinic acid, and oxaliplatin chemotherapeutic agents in a phase II trial of seventeen metastatic colorectal cancer patients resulted in enhancement of IFNγ mediated T cell immunity in cultured T cell lines from vaccinated patients (Harrop et al. 2007). In both these trials, presence of anti-5T4 immunological responses retrospectively correlated with survival and over half of patients exhibited stable disease or clinical response as classified by radiological computed tomography (CT) of tumour burden.

Despite some promising detection of enhanced immunity in colorectal patients treated with MVA-5T4/Trovax® these CRC patients do not clear their tumours (Harrop, Connolly, et al. 2006; Harrop et al. 2007). As a result, further knowledge of natural and induced immune responses to 5T4 is required in order to design better vaccines which would promote a more robust cell mediated responses including both $CD8^+$ T cell immunity enabled through $CD4^+$ T_H1 type immunity.

1.5 LAG-3 as a modulator of immunity

Lymphocyte activation gene-3 (LAG-3), also known as cluster of differentiation 223 (CD223), is an immune checkpoint receptor which has implications in the modulation of immunity. Due to its perceived role in suppressing immune responses – particularly T cell responses – LAG-3 has recently been branded as a promising therapeutic target molecule for modulation of immunity in cancer (Sierro et al. 2011). Despite this interest, the function of LAG-3, particularly at the molecular level, is not fully understood.

1.5.1 The *LAG3* gene and protein sequence

The LAG3 gene was first isolated and characterised in 1990 from cDNA of an activated IL-2 dependent NK cell line termed F5 (Triebel et al. 1990). It was defined as possessing eight exons spanning ~7 kbp at the DNA level which was transcribed as a ~2 kbp mRNA transcript. This mRNA transcript was not detectable in resting T cell blasts but was detected in T cell blasts activated with PHA, hence its lymphocyte activation gene etymology. Analysis of the sequenced gene revealed a domain organisation containing four extracellular Ig-like domains, a single transmembrane domain sequence and a short cytoplasmic tail (*Figure 1.7a*). The four extracellular domains were designated D1 to D4, in the membrane distal to proximal direction, and were characteristic of a V-type Ig-like (D1) followed by three C2-type Ig-like domains (D2 – D4). Within the V-type D1 domain, a novel sequence feature in the V-type Ig-like predicted arrangement was observed: an addition 30 amino acid insertion between the predicted C and C' β-strands (*Figure 1.7b*).

1.5.1.1 Similarities to the CD4 co-receptor

Although the protein sequence homology between LAG-3 and CD4 is barely above background levels (~20 % protein sequence identity) upon examination of the *LAG3* gene, a number of factors highlighted LAG-3 as a structural homologue of the CD4 co-receptor. Firstly, the *LAG3* gene was located to chromosome 12 (12p13) and is thus located adjacent to *CD4* (Triebel et al. 1990; Isobe et al. 1986). Secondly, both *CD4* and *LAG3* exhibit similar intron/exon gene organisation (Triebel et al. 1990). Furthermore, it was observed that CD4 also consists of four Ig-like domains within its extracellular portion. These four domains exhibit structural homology between D1 and D3 as well as between D2 and D4 – a property exhibited by both LAG-3 and CD4 – suggesting that both molecules evolved through duplication of a two domain precursor.

The biggest similarity between LAG-3 and CD4 was shown by evidence of the functional binding of MHC-II molecules by LAG-3 – of which CD4 is also a ligand. A comprehensive
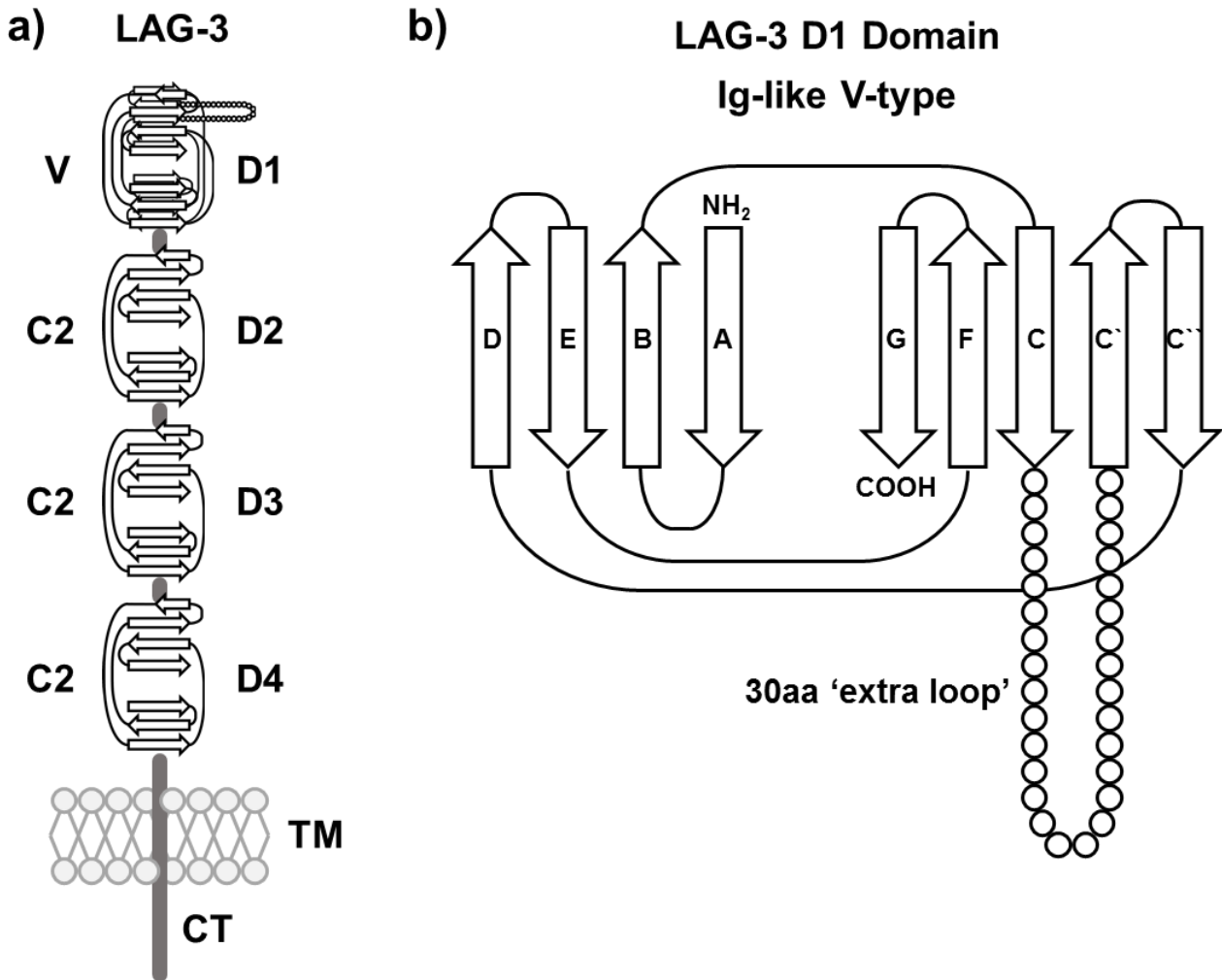
Figure 1.7 – Overview of the sequence inferred LAG-3 domain arrangement:

a) Domain arrangement as inferred from the LAG-3 protein sequence. Sequence analysis suggests LAG-3 possesses four extracellular Ig-like domains (D1-D4), a single transmembrane domain (TM) and a short cytoplasmic tail (CT). D1 domain contains a V-type Ig-like domain (V) whilst D2 to D4 contains C2-type Ig-like domains (Triebel et al. 1990).

b) 2D schematic representation of LAG-3 D1 domain Ig-like sequence inferred domain organisation as demonstrated in (Triebel et al. 1990). The V-type domain contains an additional 30 amino acid (aa) 'extra loop' sequence between C and C`β-strands not characteristic of V-type Ig-like domains. NH_2 = N-terminus, COOH = C-terminus.

overview of the current evidence of a LAG-3-MHC-II interaction is described to follow in Chapter 4.

1.5.2 Expression of LAG-3 by immune cells

LAG-3 is expressed on a number of different cell types confined to immune cells. LAG-3 is expressed on activated but not resting $CD4^+$ and $CD8^+$ T cells (Huard et al. 1994). Expression of LAG-3 by human PBMCs stimulated *in vitro* by PHA stimulation results in detectable LAG-3 expression after two days, maximal at day eight and trends towards baseline by day twelve. LAG-3 expression kinetics by ($CD4^+$ & $CD8^+$ co-purified) T cells in mice *in vitro* via CD3/CD28 bead activation are slightly altered: LAG-3 is detectable 24 hours after stimulation, maximal at 48 hours and returns to baseline after 96 hours (Sega et al. 2014). LAG-3 expression at the transcription level is detected in mouse $TCR\gamma\delta^+$ intraepithelial lymphocytes (Shires et al. 2001), as well as at the protein level on $TCR\gamma\delta^+$ splenocytes of C57BL/6 mice (C. J. Workman et al. 2002). Similarly, LAG-3 expression is detected on $2B4^+$ mouse splenocyte derived NK cells. Indeed, expression of LAG-3 on both $TCR\gamma\delta^+$ and NK cells was significantly higher compared to both $CD4^+$ and $CD8^+$ T cells.

LAG-3 is expressed on human $LAG-3^+$ $CD49b^+$ Tr1 cells extracted directly from peripheral blood without the requirement of *in vitro* stimulation (Gagliani et al. 2013). Similarly, LAG-3 expression is detectable on a subset of $CD4^+CD25^+FoxP3^+$ T cells in peripheral blood, however, this subset of cells are functionally active and may represent LAG-3 upregulation as a consequence of T_{reg} activation (Camisaschi et al. 2010). LAG-3 expressing Tr1 cells, *in vivo*, can be generated by the treatment of mice with MHC-II coated nanoparticles and thus may present a methodological way of generating $LAG-3^+$ cells *in vitro* (Clemente-Casares et al. 2016).

LAG-3 is also expressed on activated ($CD19^+$) B cells during *in vitro* stimulation of PBMC cultures (Kisielow et al. 2005). The kinetics of LAG-3 expression by B cells is concurrent with that of LAG-3 expression on T cells, albeit at lower levels. LAG-3 expression on activated B cells was only observed in the presence of co-culture with activated T cells and was shown to be endogenously produced. LAG-3, therefore, may be a surface marker of B cell activation mediated by T cells.

Finally, LAG-3 is expressed at high levels by $CD11c^{low}$ $B220^+$ $PDCA-1^+$ plasmacytoid dendritic cells (pDCs) in mice (Workman et al. 2009). Interestingly, expression of LAG-3 by these immune cells is detected both as a membrane bound protein (after activation with CpG) and as a secreted form of LAG-3, termed soluble LAG-3 (sLAG-3). Consequently, sLAG-3 is detectable in mouse and human serum of which pDCs are thought to be the main producers with contribution by $CD4^+$ T cells (Workman et al. 2009; Triebel et al. 2006; Annunziato et al. 1996).

pDC expression of LAG-3 has been shown to have both a cell intrinsic role in mediating pDC homeostasis as well as having an influence on T cell expansion.

1.5.3 Inhibition of T cell activation through LAG-3

Given the evidence of binding between LAG-3 and MHC-II, much of the functional studies into LAG-3 have focused on the role of LAG-3 in CD4$^+$ T cells. First insights into a role for LAG-3 in the suppression of T cell responses was revealed by the influence of LAG-3 function upon antigen specific activation of human CD4$^+$ T cell clones (Huard et al. 1994). Incubation of an anti-LAG-3 antibody in T cell activation assays resulted in the increased production of IFNγ. This process was shown to be antigen specific as anti-LAG-3 antibody blockade had no effect on mitomycin or IL-2 stimulation of CD4$^+$ T cell clones. Similar experiments using LAG-3 fusion proteins highlighted that LAG-3 binding to MHC-II expressing T cells resulted in inhibition of T cell activation and thus suggests LAG-3 may function to limit T cell to T cell mediated presentation and activation in humans (Huard et al. 1996). Having observed that LAG-3 function causes the downregulation of T cell activation in an antigen-specific manner, it was hypothesised that LAG-3 may interrupt TCR/CD3 signalling (Hannier et al. 1998). Crosslinking of LAG-3 proteins on the surface of MHC-II expressing cells resulted in the downregulation of TCR and CD3 expression as shown by flow cytometry and consequent inhibition of Ca^{2+} influx leading to the reasoning that LAG-3 associated with the TCR/CD3 complex.

After review of the experiments described in humans, it was hypothesised that the main mechanism of LAG-3 suppression of CD4$^+$ T cell activation may be through the competitive binding for MHC-II with the CD4 co-receptor (Huard et al. 1995). Following on from these studies in humans, however, LAG-3 functionality was shown to be dependent on the cytoplasmic domain of LAG-3 which consequently suggested that blockade of CD4 engagement by LAG-3 may not be the only mechanism of LAG-3 mediated T cell inhibition (Workman et al. 2002). Transduction of wild type LAG-3 into a T cell hybridoma clone (3A9) abrogated peptide specific clone activation, however, this effect was only exhibited in a CD4 replete variant of the 3A9 clone and not a CD4 deplete variant. These data suggested that the negative regulatory function of LAG-3 was dependent on CD4 expression. Similar experiments were performed by transduction of a truncated LAG-3 construct deficient in the cytoplasmic tail of LAG-3 which resulted in the loss of T cell regulation in response to antigen. Furthermore, mutation of the unique cytoplasmic KIEELE motif abrogated function. Similar functionality was later shown *in vivo* by restoring LAG-3 expression in LAG-3$^{-/-}$ knock out mice (Workman & Vignali 2003). Here, using the OT-II transgenic mouse model, LAG-3 restoration resulted in reduced antigen specific release of IL-2 and IFNγ cytokines. The mechanisms by which LAG-3 mediates an

inhibitory signal into the T cell is currently unknown. Recruitment of an accessory protein to the intracellular domain via a unique EP repeat motif in the LAG-3 has been documented (Iouzalen et al. 2001). This protein, termed LAG-3-associated protein is a 45 kDa protein with no obvious homologues.

Biochemical analysis of the protein constituents of LAG-3 on expressing cells revealed the presence of oligomeric association of truncated LAG-3 products at the cell surface (Li et al. 2004). A 54 kDa fragment which corresponded to the extracellular portion of LAG-3 was shown to associate with full length LAG-3 at the cell surface. A comprehensive overview of the evidence of LAG-3 oligermisation is described in Chapter 4. The formation of soluble truncation products, however, raises implications in the function of LAG-3 mediated suppression of T cell activation. Through the use of CD4-LAG-3 fusion constructs, the cleavage of LAG-3 to form sLAG-3 was shown to be dependent on the membrane proximal D4 domain of LAG-3 (Li et al. 2004). Moreover, this cleavage was shown to be performed by the metalloproteases ADAM10 and ADAM17 which act as a regulatory mechanism to LAG-3 function by cleavage and consequent release of LAG-3 from the T cell surface (Li et al. 2007). Indeed, formation of LAG-3 cleavage-resistant mutants rendered cells unable to proliferate and produce cytokines.

LAG-3 function through an interaction with MHC-II can be rationalised for CD4^{+} T cell inhibition, however, LAG-3, as described previously, is expressed on a number of different immune cell types including CD8^{+} T cells (Huard et al. 1994). A role of LAG-3 in inhibiting T cell activation in CD8^{+} T cells is less obvious. Nevertheless, transduction of LAG-3 into primary CD8^{+} T cells *in vitro* reduced the release of IFNγ in response to cognate antigen stimulation which was also shown to be dependent on the cytoplasmic tail of LAG-3 (Tian et al. 2015). Initial studies have identified a second potential ligand for LAG-3: the adhesion molecule LSECtin/CLEC4G which is expressed on endothelial cells (Xu et al. 2014). Such binding may explain how CD8^{+} T cells are modulated by LAG-3 expression.

1.5.4 Effect of LAG-3 engagement on dendritic cells

As well as mediating a cell intrinsic effect on T cells, LAG-3 also exhibits a cell extrinsic modulatory effect on interacting APCs. LAG-3 engagement of a soluble form of LAG-3, the LAG-3:Fc fusion protein, exhibits an immunostimulatory effect on human monocyte-derived dendritic cells (Andreae et al. 2002). LAG-3:Fc was shown, firstly, to bind to mature but not immature MHC-II expressing dendritic cells – an observation attributed to the requirement of MHC-II molecules to clustered in organised lipid rafts. Nevertheless, LAG-3:Fc was able to induce morphological changes and phenotypic maturation of dendritic cells resulting in the up-regulation of CD80/CD86, CD40 and CD83 in a similar capacity to the innate stimulatory

molecule LPS. The consequent outcome was that LAG-3:Fc matured dendritic cells captured less antigen and instead shifted function towards presentation to T cells as shown by increased proliferation of CD4+ T cells in a mixed lymphocyte reaction co-cultured in the presence of LAG-3:Fc matured dendritic cells. These data suggested that LAG-3 – at least in the form of a soluble fusion protein – is able to stimulate dendritic cells and consequently CD4+ T cell immunity in a similar capacity to that of LPS.

In a wider study, the effects of LAG-3:Fc binding to whole PBMC populations was studied and it was shown that LAG-3:Fc could only bind to 10 % of all MHC-II positive cells (Brignone et al. 2007). These cells were attributed to myeloid-derived dendritic cells, once again, and a small number of monocytes. Binding to these cells, however, resulted in the production of IFNα and CCL4 (MIP-1β) and consequent activation of CD8$^+$ effector memory T cells through the promotion of T_H1 immunity. This activation of CD8$^+$ T cells as a consequence of LAG-3:Fc treatment of PBMCs was show to be cell contact dependent.

In apparent contrast to the previous described studies, LAG-3 expressed on the surface of T_{reg} cells was shown to instead inhibit dendritic cell activation through an interaction with MHC-II expressing cells. This effect was shown in mice whereby T_{reg}-dendritic cell interactions were required to inhibit dendritic cell activation in a T cell antigen specific manner (Liang et al. 2008). Upon engagement of MHC-II expressing dendritic cells in the presence of cognate peptide, LAG-3 expressing OT-II transgenic T_{reg} cells were able to inhibit maturation of dendritic cells as indicated by decreased expression of CD86. Such an effect was not observed in either OT-II T_{reg} cells deplete of LAG-3, conventional OT-II T cells or in the absence of peptide. Truncation of the cytoplasmic tail of LAG-3 had no effect on the ability to inhibit dendritic cell maturation and required cell-cell contact. These data suggest that dendritic cell inhibition was as a result of a direct mechanism mediated by LAG-3 interacting with MHC-II expressing cells and not by signalling through the T cell.

These studies therefore present contrasting roles of an extrinsic function of LAG-3 on dendritic cell function. Importantly, these studies vary in the formulation of LAG-3 by which these experiments are constructed. Observed activation of dendritic cells occurs via LAG-3 in a soluble form whereas inhibition of dendritic cells was demonstrated in a membrane bound setting with the addition of peptide specificity. One model which may explain this observed difference is that soluble release of LAG-3, through cleavage, can promote distal antigen non-specific promotion of dendritic cell maturation whilst allowing antigen specific downregulation of dendritic cells presenting exhausted/regulatory antigens – mediated by surface bound LAG-3. Alternatively, discordance may be observed due to differences in mouse and human immunology or artefactual effects of LAG-3 dimerisation by the LAG-3:Fc molecule.

1.6 LAG-3 and cancer: a potential therapeutic target

1.6.1 Immune checkpoint inhibitor therapies

Immune checkpoint therapies are a class of therapeutics which aim to enhance immunity to tumours by modulation of regulatory signals and pathways (Sharma & Allison 2015). Through central and peripheral tolerance mechanisms, described previously, immunity is poised between reactivity to non-self whilst preventing reactivity to self (Houghton & Guevara-Patiño 2004). This balance in self / non-self discrimination is tuned by the activating and regulatory networks that govern immunity. Modulation of regulatory signals within this network which tip the balance towards reactivity to self may facilitate enhanced immune activity. As a result, the aim of checkpoint inhibitor therapies are to enhance immunity to self and thus increase the selection pressure on tumours (Sharma & Allison 2015). Such modulation, however, comes at a cost as tuning the immune system towards self renders individuals at risk to the symptoms of autoimmunity.

Ipilimumab, for example, targets CTLA-4, a co-inhibitory molecule which is expressed at low levels on naïve effector T cells but is upregulated upon T cell activation and maintained in intracellular stores of memory cells (Jago et al. 2004). CTLA-4 expressed at the cell surface competes with CD28 for binding of CD80/CD86, thus preventing signal 2 of T cell activation and instead promoting T cell inhibition (Boesteanu & Katsikis 2009). Consequently, ipilimumab binds and blocks CTLA-4 function allowing the continuation of CD28 based signal 2 activation. Moreover, CTLA-4 is expressed on T_{reg} cells and is required for maximal function (Read et al. 2000). Ipilimumab is designed such that binding to CTLA-4 can mediate immune cell depletion of ipilimumab opsonised cells, a concept discussed in Chapter 5, and has therefore been shown *ex vivo* to promote cytotoxicity of T_{reg} cells in melanoma patients (Romano et al. 2015).

Currently, two immune checkpoint therapies have approval for use in England and Wales by the National Institute for Health and Care Excellence (NICE) for the treatment of unresectable or metastatic melanoma. These two therapeutic agents, ipilimumab (Yervoy®) and nivolumab (Opdivo®) are monoclonal antibodies that target the immune checkpoint molecules CTLA-4 and PD-1, respectively (Hodi et al. 2010; Topalian et al. 2014). Both agents have shown clinical efficacy in the treatment of metastatic melanoma in phase III clinical trials both as individual and combined therapies where treatment of a combined therapy group exhibited a progression free survival of 11.5 months compared to ipilimumab alone (2.9 months) and nivolumab alone (6.9 months) (Larkin et al. 2015). Despite clinical success in patients with melanoma, clinical benefit of current checkpoint inhibitors have shown underwhelming response rates in colorectal

cancer (Singh et al. 2015). However, trials are currently underway to assess nivolumab and ipilimumab combined therapy in metastatic CRC (ClinicalTrials.gov Identifier: NCT02060188)

1.6.2   Implications of LAG-3 expression in human tumour progression

Exhibiting parallels with CTLA-4, LAG-3 function is required for optimal T_{reg} suppressive functionality (Huang et al. 2004). As a result of T cells with regulatory function being involved in suppressing anti-tumour immunity, it has been hypothesised that LAG-3 contributes to immune escape by tumours (Goldberg & Drake 2011).

Indeed, in a study of 45 patients with Hodgkin lymphoma (HL), LAG-3 expression was detected on lymphocytes infiltrating into areas of malignant Hodgkin Reed-Sternberg (HRS) cells via immunohistochemistry (Gandhi et al. 2006) Moreover, LAG-3^{+} T cells were detected at higher frequencies in the peripheral blood of HL patients who were yet to undergo chemotherapy compared to patients in remission and healthy controls – suggesting that LAG-3 expression may correlate with disease state severity.

In the described studies of HL patients, LAG-3 expression was not confined to co-expression of FoxP3 and thus suggested LAG-3 expression was distinct from classical FoxP3^{+} T_{reg} cells (Gandhi et al. 2006). In contrast, enrichment of LAG-3^{+} T cells into both melanoma and colorectal tumour sites were restricted mainly to LAG-3^{+} FoxP3^{+} CD4^{+} CD25^{+} T cells where this subset of cells were increased in peripheral blood, tumour bearing lymph nodes and tumour sites (Camisaschi et al. 2010). This subset of cells exhibited an effector memory phenotype whilst producing the immunosuppressive cytokines IL-10 and TGFβ. Functional analysis of LAG-3^{hi} and LAG-3^{low} T cells from PBMC of healthy donors revealed that LAG-3^{hi} cells exhibited suppressive capacity to inhibit T cell proliferation which required cell-cell contact. As a result, these data show that this subset of LAG-3^{+} FoxP3^{+} CD4^{+} CD25^{+} T cells are residing in tumours as well as peripheral blood and have a direct suppressive capacity on other T cells.

Similar observations have been made in non-small-cell lung cancer patients (Wei et al. 2015). In a study of 53 patients, increased numbers of FoxP3^{+} CD4^{+} CD25^{+} T cells were detected and found to express high levels of several inhibitory molecules such as LAG-3 but also CTLA-4 and PD-1. The phenotypic consequence of this was, once again, associated with IL-10 and TGFβ release. Also in non-small-cell lung cancer patients, infiltrated CD8^{+} T cells were found to express the same inhibitory molecules but also Tim-3 and BTLA (Thommen et al. 2015). A role for reduced anti-viral clearance in viral induced hepatocellular carcinoma (HCC) by LAG-3 has also been observed (Li et al. 2013). Expression of LAG-3 on Hepatitis B virus (HBV)-specific CD8^{+} T cells within the tumour sites of HCC patients revealed upregulation compared to matched peripheral blood and, once again, impaired function.

Together, these data highlight how T cells with inhibitory and regulatory phenotype in a tumour context express multiple inhibitory molecules and thus use multiple seemingly redundant pathways to mediate T cell suppression. This regulatory phenotype is possessed by a variation of LAG-3 expressing T cell subsets. As a result, successful targeting of such cells may require the combinational targeting of multiple suppressive pathways concurrently.

1.6.3   Implications of LAG-3 expression in human colorectal cancer

Expression patterns of LAG-3 exhibited by T cells in tumours, in general, are replicated in colorectal cancer, however, preferential detection of T cells with regulatory function that display Tr1 or Tr1-like function has been observed.

Analysis of $CD4^+$ T cells extracted from matched tumour, healthy colon and peripheral blood of CRC patients revealed the presence of a population of $FoxP3^-$ cells that were characterised by the surface expression of LAP, CD39, CTLA-4 along with LAG-3 which were specific to tumour alone (Scurr et al. 2013). These cells, isolated from CRC tumours, exhibited a Tr1-like phenotype characterised by high expression of IL-10. Consequent isolation of $CD4^+$ LAP^+ cells via fluorescence-activated cell sorting (FACS) enabled the assaying of the suppressive capacity of this population. Using *in vitro* suppression assays, $CD4^+$ LAP^+ cells exhibit an approximate 50-fold suppressive capacity compared to $FoxP3^+$ T_{reg} cells.

Definition of Tr1 cells as expressing LAG-3 and CD49b concurrently has since allowed the study of Tr1 cell infiltrate into CRC tumours (Gagliani et al. 2013). Analysis of T cell infiltrate in 108 matched CRC tumour and peritumoural samples revealed the enrichment of a diverse range of T cells infiltrated into tumours (Chen & Chen 2014). In these patients, high frequency of $FoxP3^+$ T_{reg} cells were detected but also high frequency of $LAG-3^+$ cells including those that co-expressed CD49b (Tr1 cells) as well as a subset of $LAG-3^+$ $CD49b^-$ cells.

1.6.4   LAG-3 blockade and depletion in animal disease models

There is currently no published data on the efficacy of LAG-3 blockade or depletion in humans. However, there are ongoing clinical trials assessing the safety and efficacy of anti-LAG-3 antibodies in cancer patients. An overview of current anti-LAG-3 antibodies are presented in Chapter 5. Nevertheless, rationale for the development of therapeutics modulating LAG-3 function has been displayed in animal models of disease.

Evidence for LAG-3 as a therapeutic intervention target in cancers has been demonstrated in both the Sa1N fibrosarcoma and MC38 colon adenocarcinoma murine tumour model whereby blockade of PD-1 and LAG-3, through a combined intervention regime administered after detection of palpable tumours, resulted in tumour clearance in mice (Woo et al. 2012). In the MC38

CRC tumour model, all tumour bearing mice in the untreated control group developed tumours (0 of 10 mice tumour free after day 50). In anti-PD-1 treated mice, 4 out of 10 mice remained tumour free after 50 days. Interestingly, anti-LAG-3 treated mice exhibited decreased tumour rate, however, all mice still developed tumours (0 of 10 mice tumour free after day 50). Combination treatment of anti-LAG-3 and anti-PD-1 resulted in reduced tumour burden compared to both control, LAG-3 mono-treament and PD-1 mono-treatment (8 of 10 mice tumour free after day 50). Analysis of treated mice revealed that dual blockade of PD-1 and LAG-3 induced increased numbers of CD8$^+$ IFNγ expressing T cells in the tumour draining inguinal (DLN) and non-draining brachial and axillary lymph nodes (NDLN).

Interestingly, a second study analysing the therapeutic modulation of LAG-3 expressing cells in autoimmunity demonstrates a seemingly opposite rationale for anti-LAG-3 therapy (Poirier et al. 2011). In this study, it was hypothesised that depletion of LAG-3 expressing cells – therefore depleting activated cells – would deplete disease-mediating T cells in a T cell driven autoimmune disorder. This was despite the effects LAG-3 depletion may have on the targeting of LAG-3 expressing T cells with regulatory function – which have anti-autoimmune potential (Okazaki et al. 2011).

Nevertheless, non-human primates were challenged with tuberculin-purified protein derivative (PPD), a model of delayed-type hypersensitivity, after administration of an anti-LAG-3 antibody designed to deplete LAG-3 expressing cells (Poirier et al. 2011). Treatment of animals with anti-LAG-3 before challenge indeed resulted in reduced disease severity compared to PPD administration without anti-LAG-3 therapy. This protection prevented symptoms completely in animals challenged two days after treatment with anti-LAG-3 but also exhibited reduction in symptoms during re-challenge six weeks after anti-LAG-3 intervention. This time period suggests that treatment was able to have a persisting effect over the period of weeks.

Together, these two studies show that current development of LAG-3 therapeutics, in phase I/II clinical trials, have contrasting hypothesised outcomes. An implication of these two preclinical studies is that targeting of LAG-3 as a mechanism for shifting self / non-self discrimination in favour of enhanced tumour immunity requires better understanding of LAG-3 biology.

1.7 Aims of Thesis

The overall aim of this thesis is to study the efficiency of the CD4$^+$ T cell immune response to tumours through molecular studies of the TCR-pMHC-II interaction in the context of colorectal cancer and its impediment by the co-inhibitor molecule LAG-3. My overall hypothesis is that effector anti-cancer CD4$^+$ T cell responses are suboptimal due to multiple causes that include key cell intrinsic mechanisms including (i) weak recognition of tumour antigens through TCR-pMHC interactions, and (ii) negative regulation by the cell surface CD4 homologue molecule LAG-3.

To explore this hypothesis further, I had three overall key objectives:

- To measure TCR binding of tumour-antigen derived pMHC at the cellular/molecular level to explore whether anti-cancer TCRs were engaged weakly

- To study and measure LAG3-pMHC binding at the cellular, biophysical and structural level

- To develop anti-LAG-3 monoclonal antibodies for the study and targeting of LAG-3.

This would be achieved firstly through the study of CD4$^+$ T cell responses to the oncofoetal antigen 5T4 by molecular analyses of the presentation of 5T4-derived peptide epitopes and consequent recognition by 5T4-reactive CD4$^+$ T cell clones derived from healthy donors. The outcomes of these molecular studies are described in **Chapter 3.** Secondly, the efficiency of CD4$^+$ T cell immunity to tumours would be analysed through understanding of the function of the co-inhibitory molecule LAG-3 which has been implicated in the functional efficiency of CD4$^+$ T cells infiltrated into colorectal and other tumours. It was hypothesised that LAG-3 may bind to MHC-II molecules using a higher affinity interaction than that of CD4 engagement and, thus, has potential to impede T cell activation within a tumour context. The outcomes of these functional analyses are detailed in **Chapter 4.** Finally, the generation of anti-LAG-3 antibodies would be performed through the generation and functional characterisation of monoclonal antibodies against human LAG-3 protein generated through the immunisation of mice. The generation of anti-LAG-3 antibodies should aid future studies of LAG-3 structure-function and may possess future therapeutic potential in the depletion and/or blockade of LAG-3 expressing cells in the tumour context. The progress of this translational project is detailed in **Chapter 5.**

2   Chapter 2: Materials and Methods

NB. A full list of reagents used is available in Appendix 1.

2.1   Generation and characterisation of 5T4-reactive T cell clones

2.1.1   List of materials

2.1.1.1   Antibodies

αLAG-3-FITC: Fluorescein isothiocyanate (FITC)-conjugated anti-human LAG-3 clone 17B4 – Enzo Life Sciences

αCD4-APCy: Allophycocyanin (APCy)-conjugated anti-human CD4 clone – Miltenyi Biotec

αCD14-PB: Pacific Blue™ anti-human CD16 Antibody clone 3G8 - BioLegend

αTCR-FITC: FITC-conjugated anti-human αβ TCR clone IP26 – BioLegend

αPE: Unconjugated anti-phycoerythrin (PE) clone PE001 - BioLegend

2.1.1.2   Buffers

Phosphate Buffered Saline Dulbecco 'A' (PBS) – Oxoid: 8 g/L Sodium chloride, 0.2 g/L Potassium chloride, 1.15 g/L Disodium hydrogen phosphate & 0.2 g/L Potassium dihydrogen phosphate, pH 7.3

PBS-T: PBS, 0.05 % Tween 20

Dextramer buffer: 0.05 M Tris-HCl, 15 mM Sodium azide, 1 % BSA, pH 7.2

Mammalian Cell Freezing Buffer: 90 % FCS & 10 % DMSO

2.1.1.3   Culture media

R0: RPMI 1640 media, 2mM L-Glutamine, 100 IU/mL Penicillin & 100 μg/mL Streptomycin.

R5: RPMI 1640 media, 5 % FCS, 2mM L-Glutamine, 100 IU/mL Penicillin & 100 μg/mL Streptomycin.

R10: RPMI 1640 media, 10 % FCS, 2mM L-Glutamine, 100 IU/mL Penicillin & 100 μg/mL Streptomycin.

CD4$^+$ T cell media (TCM): RPMI 1640 media, 10 % FCS, 2mM L-Glutamine, 100 IU/mL Penicillin & 100 μg/mL Streptomycin, 0.02M HEPES, 1mM Non-essential amino acids, 1mM Sodium pyruvate, 200IU/mL human recombinant IL-2 (Proleukin®)

2.1.1.4   Peptides

5T4p2: AGDGRLRLARLALVLLGWVS

5T4p12: FARRPPLAELAALNLSGSRL

5T4p38: LLVLYLNRKGIKKWMHNIRD

All peptides synthesised at 90 % purity solubilised in DMSO by Peptide Protein Research
        Ltd. (Hampshire, UK).

2.1.2   Culture of cells

T2 (174 x CEM.T2) (ATCC® CRL-1992™) cells (henceforth T2) and T2 cells stably expressing
surface expressed HLA-DR1 through lentiviral gene delivery (henceforth T2-DR1) were ob-
tained from and produced by Alexander Greenshields Watson (Cardiff University). Autologous
BLCL cells were generated by Dr Chris Holland (previously Cardiff University). Autologous
BLCL, T2 and T2-DR1 cells were cultured at 37 ˚C, 5 % CO_2 in R10 media. All APCs were
cultured in suspension by renewing culture media three times per week, maintaining cells at a
density of 3 x 10^5 and 1 x 10^6 cells/mL.

5T4-reactive T cell clones were maintained by culturing at 3 x10^6 cells/mL in 24-well plates,
replacing half the culture volume three times per week with fresh CD4$^+$ TCM without homoge-
nous dispersion of the cells in the well. Every 2-4 weeks, T cell clones were expanded in
conjunction with Dr Garry Dolton (Cardiff University) using irradiated (3100 Gy) allogeneic
PBMC feeder cells from three separate healthy donors and 1 µg/mL phytohemagglutinin (PHA)
performed.

2.1.3   Generation of 5T4-reactive T cell clones

Three CD4+ T cell clones specific for three distinct 20mer amino acid peptides (5T4p2, 5T4p12
& 5T4p38) derived from the full length 5T4 protein were produced by Dr. Garry Dolton (Cardiff
University) using the T cell library cloning methodology as outlined previously (Theaker et al.
2016). In brief, PBMCs were isolated from a HLA-DR1$^+$ donor using density gradient centrifu-
gation by extraction of the buffy coat layer formed from Lymphoprep™ (Axis-Shield)
centrifugation. CD4$^+$ T cells were enriched from PBMCs by magnetic separation using anti-
CD4$^+$ microbeads (Miltenyi Biotec) and consequently plated at approximately 1x10^4 cells per
well of a 96-well U-bottom plate. Plated cells were expanded using human T-Activator
CD3/CD28 Dynabeads® (Life Technologies) at a cell to bead ratio of 1:2 in CD4$^+$ TCM. After
14 days culture, individual wells of the expanded cell library were screened for reactivity to the
pool of three 5T4 derived peptides (1x10^{-5} M) in the presence of T2-DR1 cells as antigen pre-
senting cells. Reactivity to peptide was determined by the release of IFNγ using enzyme linked
immunospot assay (ELISpot) according to manufacturer's instructions (Mabtech). Library wells
positive for IFNγ expression in the presence of 5T4 peptides by ELISpot were pooled and ex-
panded by culturing pooled cells with 1x10^{-5} M individual peptide for 4 hours. Activated cells

were consequently enriched by IFNγ capture isolation (Miltenyi Biotec). The subsequent enriched line was tested for individual reactivity to 5T4 peptides in the presence of T2-DR1 cells as APCs via IFNγ ELISpot as described previously. The enriched 5T4-reactive T cell line was cloned by single cell serial dilution cloning and resulting clones validated for reactivity to the individual 5T4-derived peptides as described to follow.

2.1.4 Peptide sensitivity cytokine/chemokine release ELISA

T cell peptide stimulation assays were performed by co-culturing individual 5T4-reactive T cell clones with T2-DR1 as antigen presenting cells (APCs) with or without the presence of cognate 5T4 derived peptides. One day prior to the assay, T cell clones were rested in R5 media overnight. The following day, T cell clones were counted via haemocytometer, washed with 10 mL PBS and resuspended in R5 media at 4.44×10^5 cells/mL. Similarly, T2-DR1 cells were counted, washed with 10 mL PBS and resuspended in R5 media at 8.88×10^5 cells/mL.

T cells were peptide specifically stimulated by combining 45 µL of T2-DR1 with 45 uL of T cells resulting in 4×10^4 and 2×10^4 APCs and T cells per well, respectively. Serial dilutions of cognate peptide were prepared in R0 media at a concentration range of 10^{-3} to 10^{-9} M. 10 µL of peptide at each concentration was added to the T cell-APC culture to form a final volume of 100 µL, thus resulting in a final peptide concentration range of 10^{-4} to 10^{-10} M. In addition, negative control wells were incubated with no peptide and positive control wells incubated with 10µg polyhydroxyalkanoates (PHA; Alere). All conditions were performed in at least duplicate. Cells were cultured overnight at 37 ˚C, 5 % CO_2.

The following day, cells were spun at 1500 rpm for 5 min and supernatants harvested for analysis of their release of human IFNγ, TNFα and MIP-1β due to exposure of T cell clone's cognate peptide. ELISA assays were performed using sandwich ELISA kits according to manufacturer's protocol (R&D Systems). In brief, half-area 96 well plates were coated overnight at room temperature with relevant capture antibody and later blocked with 1 % BSA. Supernatants and serial diluted protein standards were incubated on coated plates for 1 hour 15 min at room temperature before incubation with detect antibody (1 hour 15 min, room temperature), followed by streptavidin-horseradish peroxidase (HRP; 20 min, room temperature). Between each incubation step, wells were washed three times with 150 µL PBS-T. Lastly, ELISA plates were developed using HRP substrate colour reagents and stop solution (R&D Systems) and absorbance at 450 nm measured on a microplate absorbance reader (Bio-rad).

2.1.5   IFNγ release ELISpot assays

T cell activation assays were performed by co-culturing peptide-pulsed T2, T2-DR1 or autologous BLCL cells as APCs and consequent level of T cell activation determined by IFNγ release Enzyme-Linked ImmunoSpot (ELISpot) kit assays (Mabtech). One day prior to the assay, T cell clones were rested in R5 media overnight.

Firstly, 96-well ELISpot plates (Millipore) were incubated with 70 % ethanol for 30 seconds, washed three times with PBS and coated with anti-human IFNγ capture antibody overnight at 4 ˚C. Prior to use, unbound capture antibody was removed from wells and washed three times with PBS and consequently blocked with 150 µL of R5 media.

In order to prepare APCs, cells were first counted via haemocytometer, washed with 15 mL PBS, resuspended in R5 and plated into wells of a separate 96-well plate at 1.8×10^5 cells per well at a volume of 180 µL per well. Peptide was prepared by 10 times serial dilution of 5T4 derived peptides from 10^{-3} to 10^{-7} M concentration in R0 media. 20 µL of prepared peptide at various concentrations was added to the APC culture to form a final volume of 200 µL, thus resulting in a final peptide concentration range of 10^{-4} to 10^{-8} M. APCs were cultured at 37 ˚C, 5 % CO_2 for 2-3 hours after which cells were washed twice with 150 µL of PBS to remove unbound peptide. After washing, anti-DR blocking wells were incubated with 10 µg/mL L243 clone antibody for 1 hr at 37 ˚C. Cells were next washed and resuspended in R5 media at a concentration of 1×10^6 cells/mL and plated (50 µL; 5×10^4 cells per well) onto the blocked ELISpot plate. 5T4-reactive T cell clones were counted and serial diluted such that 300 T cell clones (50 µL) were added to each well of their cognate peptide-pulsed APCs. Positive control wells were incubated with co-cultured T cells and peptide-pulsed APCs were incubated overnight at 37 ˚C, 5 % CO_2.

The following day, cultured cells were removed from ELISpot plates and washed four times with PBS, incubated with IFNγ detection antibody (1 hour, 37 ˚C), washed four times with PBS and incubated with streptavidin-alkaline phosphatase conjugate (Strep-ALP) for 1 hour at room temperature in the absence of light. ELISpot plates were subjected to a final wash four times with PBS before being developed using a colorimetric alkaline phosphatase substrate reagent kit (Bio-rad). Once spots had developed, the colorimetric reaction was stopped by washing the wells of the plate with tap water. The developed plate was left to dry before being imaged and analysed using an immunospot analyser (Cellular Technology Limited).

2.1.6   MHC-II Multimer staining of 5T4-reactive T cell clones

MHC-II multimers, were assembled within 24 hours before the day of use by combining 2 μL of Phycoerythrin (PE)-labelled dextramer backbone (Immudex) with 0.5 μg of refolded and biotinylated peptide-HLA-DR1 monomers per stain. Biotinylated peptide-HLA-DR1 molecules were produced as described in section 2.2.

T cell clones were counted via haemocytometer allowing the transfer of $1x10^5$ cells per stain to FACS tubes for analysis. T cells were washed with 4 mL of sterile PBS, cells pelleted by centrifugation at 1800 rpm for 5 minutes, resuspended via vortex and treated with 50 nM dasatanib for 30 minutes at 37 ˚C. MHC-II multimers were made up to a working volume of 10 μL per stain in dextramer buffer, centrifuged at 16.1k g for 1 minute and added directly to cognate T cell clones without washing after dasatinib treatment. T cell clones were incubated on ice for 30 minutes before washing with PBS. Stained cells were boosted using an anti-PE secondary antibody for 20 minutes before washing with PBS (Tungatt et al. 2015). Cells were then stained for viability using LIVE/DEAD® Fixable Violet Dead Cell Stain (Invitrogen) for 5 minutes at room temperature and then stained for surface markers (αCD4-APC, αLAG-3-FITC, αTCR-FITC) for 20 min on ice where appropriate. Stained cells were analysed on a FACS Canto II (BDBiosciences) correcting for compensation using Anti-Mouse Ig CompBeads (BDBiosciences) bound to corresponding conjugated antibodies used in the experiment. Viability stain was compensated using (αCD14-PB) bound compensation beads.

2.1.7   Biophysical analysis of TCR-MHC interactions

In brief, the *tcra* and *tcrb* gene sequences which encode the T cell receptor (TCR) of three 5T4-reactive T cell clones (D821, D104 & C112) were sequenced from cDNA by Dr. Meriem Attaf (Cardiff University). Constructs from sequencing data were designed *in silico* to include modifications to the TCRα and TCRβ extracellular domain sequences by addition of a non-native disulphide bridge between the refolded TCRα and TCRβ constant domains as previously published (Boulter et al. 2003). TCR-α and TCR-β chains of the three 5T4-reactive T cell clones (D821, D104 & C112) were cloned into the pGMT7 expression plasmid using restriction endonuclease cloning as outlined in section 2.4.4. TCRα and TCRβ chain inclusion bodies were processed from cell lysates and refolded by gradual denaturant dilution of combined TCRα and TCRβ chains through denaturant dialysis as previously published (Boulter et al. 2003).

SPR binding analysis was performed using a BIAcore T200 SPR instrument as described previously (Cole et al. 2012). In brief, BIAcore CM5 sensor chips (GE Healthcare Life Sciences) were immobilised with prepared biotinylated pMHC molecules by amine coupling of streptavidin to chip surfaces as described in section 2.5.4. Prepared biotinylated pMHC molecules were

immobilised to streptavidin coated CM5 sensor chips by injection of pMHC molecules to immobilise ~500 RU of ligand. pMHC-TCR binding was assayed using a dilution series kinetic equilibrium approach using immobilised pMHC molecules coated to sensor chips as experimental ligand and soluble TCR as experimental analyte.

2.1.8 Cryopreservation of generated cell lines

Generated cell lines and clones were cryopreserved by freezing multiple aliquots of pre-confluent cells at a viability of more than 90 %. Cells to be frozen were harvested by centrifugation for 5 min at 1500 rpm and resuspended in mammalian cell freezing buffer. Cells were aliquoted into cryovials and cooled at a rate of -1°C/min to a final temperature of -80 °C using a Mr. Frosty™ Freezing Container (Thermo Scientific) after which cells were transferred to vapour phase liquid nitrogen storage until required.

2.2 Generation of MHC-II molecules

2.2.1 List of materials

2.2.1.1 Oligonucleotide reagents

pGMT7-DRα – Cloned by Dr Christopher Holland (Previously of Cardiff University)

pGMT7-DRα-bt – Cloned by Dr Christopher Holland

pGMT7-DR1β – Cloned by Dr Christopher Holland

2.2.1.2 Buffers

Bacterial Cell Lysis Buffer: 10 mM Tris, 10 mM $MgCl_2$, 150 mM NaCl, 10 % glycerol; pH 8.1

Inclusion Body Wash Buffer: 50 mM Tris, 0.5 % Triton X-100, 100 mM NaCl, 2 mM EDTA; pH 8.1

Inclusion Body Resuspension Buffer: 50 mM Tris, 100 mM NaCl, 2 mM EDTA; pH 8.1

Urea Buffer A: 8 M Urea, 20mM Tris pH 8.1 and 0.5mM EDTA; pH 8.1

Urea Buffer B: 8 M Urea, 1 M NaCl, 20mM Tris pH 8.1 and 0.5mM EDTA; pH 8.1

MHC-II refold buffer: 25 % glycerol, 20mM TRIS, 1 mM EDTA, 20 mM NaCl, 1.48 g/L (13 mM) cysteamine hydrochloride & 0.83 g/L (3.7 mM) cystamine hydrochloride.

CAPS elution buffer: 50 mM 3-(Cyclohexylamino)-1-propanesulfonic acid (CAPS); pH 11.5

Neutralisation buffer: 300 mM Sodium phosphate; pH 6

Biomix A – Avidity: 0.5M Bicine Buffer; pH8.3

Biomix B – Avidity: 100mM ATP, 100mM $MgO(Ac)_2$ & 500μM Biotin

d-Biotin Buffer – Avidity: 500 μM d-biotin

Sample loading buffer (4 X): 1 M Tris, 0.008 % Bromophenol blue, 10 % SDS, 40 % glycerol; pH 6.8

Reducing sample loading (4 X): 4M Dithiothreitol (DTT), 1 M Tris, 0.008 % Bromophenol blue, 10 % SDS, 40 % glycerol; pH 6.8

2.2.1.3 Culture media

TYP media: 16g/L Tryptone, 16g/L Yeast Extract, 5g/L Potassium Phosphate Dibasic & 5 g/L Sodium chloride.

2.2.1.4 Peptides

5T4p2: AGDGRLRLARLALVLLGWVS

5T4p12: FARRPPLAELAALNLSGSRL

5T4p38: LLVLYLNRKGIKKWMHNIRD

HA-PKY: PKYVKQNTLKLAT

All peptides synthesised at 90 % purity solubilised in DMSO at 20 mg/mL by Peptide
Protein Research Ltd. (Hampshire, UK).

2.2.2   Construction of HLA-DR1 bacterial expression plasmids

The expression plasmids for the production of HLA-DR1 molecules were designed and cloned
previously into the pGMT7 expression plasmid based on published methodoliges by Dr Chris-
topher Holland (Previously of Cardiff University) (Frayser et al. 1999). HLA-DRα constructs
consisted of the extracellular domain of HLA-DRA*0101 (Uniprot: P01903, residues [26-207]).
HLA-DR1β consisted of the extracellular domain of HLA-DRB1 (Uniprot: P04229, residues
[30-219]). For the production of biotinylated HLA-DR1 molecules, a third construct, denoted
HLA-DRα-biotin tag (-bt) was cloned previous to include a C-terminal biotinylation signal se-
quence (GLNDIFEAQKIEWHE; AviTag™) ligated to the HLA-DRA*0101 sequence
described, via a flexible linker (GSGG).

2.2.3   Production of HLA-DR1 inclusion bodies

2.2.3.1   Culturing of recombinant *E. coli* cells

pGMT7-DR1β and pGMT7-DRα or pGMT7-DRα-bt plasmids were transformed into Ro-
setta™(DE3) competent BL21 strain-derived *Escherichia coli* cells (Novagen) as described in
section 2.4.4.3. Three individual colonies were picked from transformed plates, transferred to
30 mL of TYP media supplemented with 50 μg/mL carbenicillin and cultured at 37 °C and
shaken at 220 rpm to an optical density at 600 nm (OD600) of between 0.4 and 0.6. Starter
cultures were consequently transferred to 1 L TYP media supplemented with 50 μg/mL carben-
icillin and cultured at 37 °C, 220 rpm. Expression of recombinant protein was induced by
addition of 0.5 mM Isopropyl β-D-thio-galactoside, (IPTG; Fisher Scientific) when cultures had
reached an OD600 of between 0.4. and 0.6 after which cultures were continued for 3 to 4 hours.
Bacterial cells were harvested by centrifugation at 4000 rpm for 20 mins, cell pellets were re-
suspended by vortex and homogenisation in bacterial cell lysis buffer and frozen at -20 °C.
Samples before and after IPTG induction were analysed via SDS-PAGE for confirmation of
protein expression.

2.2.3.2   Processing of HLA-DR1 inclusion bodies

Frozen cells were thawed at room temperature and subjected to sonication, on ice, using a
Sonopulse HD 2070 with MS73 probe (Bandelin) at 60 % output power for 20 minutes using a
one second on, one second off oscillation cycle. High yield cell cultures were subject to a second
iteration of freeze, thaw and sonication as described to ensure complete cell lysis. Lysed cells

were treated with 160 μg/mL deoxyribonuclease (DNAse) for 2 hours, shaken at 220 rpm at 37 °C. Lysed cell suspension was pelleted by high-speed centrifugation at 10,000 rpm for 20 mins and washed in 100 mL of inclusion body wash buffer by resuspension of the cell pellet by homogenisation. Lysed cell pellets were washed at least twice by successive centrifugation and resuspension in inclusion body wash buffer, as described, until pellets appeared clear of gelatinous material. Washed pellets were consequently resuspended by homogenisation in inclusion body resuspension buffer, pelleted by high-speed centrifugation at 10,000 rpm for 20 mins and resuspended in urea buffer A by homogenisation. Solubilised inclusion bodies were subjected to a final centrifugation at 10,000 rpm for 20 mins to remove impurities insoluble in urea buffer A by harvesting the supernatant fraction after centrifugation.

2.2.3.3   Purification of HLA-DR1 inclusion bodies

Unpure HLA-DR1 inclusion body preparations solubilised in urea buffer A were 0.45 μm filtered using vacuum filtration and purified by ion exchanged chromatography using 5 mL Hi-Trap Q Sepharose High Performace anion exchange columns (GE Healthcare Life Science) on an ÄKTA FPLC or ÄKTApure fast protein liquid chromatography (FPLC) system. Unpure protein was bound to ion exchange columns and eluted by ionic competition using a variable elution gradient of NaCl containing urea buffer B. Eluted protein was collected as 1 mL fractions and analysed for protein purity using SDS-PAGE. Fractions containing high purity HLA-DR chains were analysed for contamination by DNA using a NanoDrop ND100 (ThermoScientific) by analysing protein concentration (Absorbance at 280 nm) and nucleotide concentration (Absorbance at 260 nm). Fractions containing an A260/A280 ratio greater than 1 were discarded due to considerable contamination with DNA. Purified HLA-DR chains were stored at -20 °C until use.

2.2.4   Refolding of HLA-DR1 molecules from inclusion bodies

Refolding of heterodimeric HLA-DR1 molecules was achieved by instant denaturant dilution of HLA-DRα and HLA-DR1β chains in the presence of excess HLA-DR1 restricted peptide as previously published (Frayser et al. 1999). 5 mg/L of HLA-DRα or HLA-DRα-bt inclusion bodies and 5 mg/L of HLA-DR1β inclusion bodies were added to cold MHC-II refold buffer supplemented with 0.5 mg/L peptide. Refold mixture was stirred vigorously for 1 hour before being left to incubate for 72 – 96 hours at 4 °C. Refold mixture was then 0.45 μm filtered using vacuum filtration and concentrated to a volume of approximately 20 mL using a 10 kDa molecular weight cut-off (MWCO) Vivaflow® crossflow concentration cassette (Sartorius). Concentrated refold was then washed with 500 mL of PBS and further concentrated to a volume of approximately 2 mL using 10 kDa MWCO centrifugal filter units (Merck Millapore).

2.2.5   Purification of functional heterodimeric HLA-DR1 molecules

Concentrated refolds were purified using antibody affinity purification columns containing an immobilised α-HLA-DR antibody (L243 clone). α-HLA-DR affinity columns were produced using Pierce™ Protein A IgG Plus Orientation Kit (ThermoFisher Scientific) according to manufacturer's protocols by crosslinking 8 mg of L243 antibody (produced by Sian Llewelyn-Lacey, Cardiff University) per 1 mL of immobilised protein-A beads. Refolded protein was applied to affinity columns equilibrated in PBS by flowing protein sample through columns at least four times. Non-specific proteins were washed from the column using PBS before eluting L243 specific proteins using CAPS elution buffer. Eluted protein samples were pH neutralised using an equal volume of neutralisation buffer. Affinity purified HLA-DR1 protein samples were concentrated to a volume of 1 mL using 10 kDa MWCO spin filtration columns according to manufacturer's protocols (Millipore) and further purified by size exclusion chromatography (SEC) using Superdex 200HR gel SEC columns on an an ÄKTA FPLC or ÄKTApure FPLC system (all GE Healthcare Life Sciences). SEC columns were equilibrated with appropriate buffer such that HLA-DR1 molecules were filtrated into the appropriate buffer for downstream applications. Protein concentration was analysed using NanoDrop ND100 (ThermoScientific) measuring absorbance at 280 nm and calculated using extinction coefficients generated using the ExPASy ProtParam tool (SIB Swiss Institute of Bioinformatics).

2.2.6   Biotinylation of HLA-DR1 molecules

Between affinity and SEC purification steps as outlined in section 2.2.5, HLA-DR1 molecules refolded with HLA-DRα-bt inclusion bodies were biotinylated using a BirA biotinylation kit (Avidity). Affinity purified HLA-DR1-bt molecules were washed by dilution with 15 mL of crystallisation buffer and concentrated to 700 µL using a 10 kDa MWCO spin filtration column. HLA-DR1-bt samples were then supplemented with 100 µL Biomix A, 100 µL Biomix B, 100 µL d-Biotin 500 µM and 2 µL BirA enzyme (Avidity). Biotinylation reaction was incubated overnight at room temperature after which, excess biotin was washed by dilution with 15 mL of crystallisation buffer and concentrated to 1 mL for purification via SEC as outlined in section 2.2.5.

Biotinylated HLA-DR1-bt molecules were assayed for efficient biotinylation by streptavidin shift assay. 5 µg of biotinylated HLA-DR1-bt was incubated with 5 µg of streptavidin and analysed by SDS-PAGE for the formation of complexed HLA-DR1-streptavidin under non-reducing conditions.

2.2.7   Polyacrylamide gel electrophoresis

Produced protein sample was analysed for quality via sodium dodecyl sulfate polyacrylamide gel electrophoresis (SDS-PAGE). Approximately 5 µg of protein to be analysed was combined with sample loading buffer. Samples run in reducing conditions were combined with reducing sample loading buffer (containing 1 M DTT) and boiled at 95 °C for 5 min prior to SDS-PAGE analysis. Prepared samples were run on Bolt™ 4-12 % Bis-Tris Plus Gels using NuPAGE® MES SDS Running Buffer in a Bolt™ Mini Gel Tank (all ThermoFisher Scientific). Gels were run at 200 V for 25 min using a Bio-Rad Powerpac 200 power supply (Bio-rad Laboratories).

2.3 Structural analysis of MHC-II molecules by X-ray Crystallography

2.3.1 List of materials

2.3.1.1 Buffers

Crystal buffer: 10 mM Tris, 10 mM NaCl, pH8.1

2.3.2 Preparation of protein samples

Purified pMHC-II molecules produced as outlined in section 2.2 were filtrated into Crystal buffer during SEC purification and concentrated to approximately 1 - 5 mg/mL using spin filtration columns for crystallisation screening.

2.3.2.1 Vapour diffusion condition screening

pMHC-II samples were screened for crystal formation using sitting drop vapour diffusion screening plates set up using an Art-Robbins Gryphon robot (Art Robbins Instruments, LLC.). Crystallisation screens were performed using a customised protein crystallisation screen optimised for the formation of pMHC, TCR and pMHC-TCR complexed crystals termed **T**CR/pMHC **O**ptimized **P**rotein crystallization **S**creen (TOPS) (Bulek et al. 2012). Crystal formation was also screened using two commercial screens; PACT premier™ MD1-29 (Molecular Dimensions) and JBScreen PEG/Salt HTS CS-205L (Jena Bioscience GmbH). Crystallisation screens were set up in ARI INTELLI-PLATE 96-2 Low Volume Reservoir plates (Art Robbins Instruments, LLC.) by dispensing 60 µL and 200 nL of mother-liquor screen solution into plate reservoirs and sitting drop wells, respectively. 200 nL of pMHC prepared sample was next dispensed into sitting drop wells to form a final drop volume of 400 nL. Dispensed plates were sealed immediately using ClearVue™ Sealing Sheets (Molecular Dimensions) and imaged using a Formulatrix Rock Imager 2 (Formulatrix, Inc.) directly after applying plate seal. Plates were incubated at 18 °C, imaged and screened for crystal formation after day 1, 3 and 7 followed by irregular intervals thereafter.

2.3.2.2 Crystal microseed condition screening

pMHC-II molecules were also screened for crystal formation using hanging drop vapour diffusion with the inclusion of homologous or heterologous pMHC-II crystal microseeds. Crystal microseed stocks were prepared from successfully formed crystals of the same pMHC or similar pMHC using a MicroSeed Beads™ kit according to manufacturer's instructions (Hampton Research). Formed crystals were first crushed using a macro crystal crusher in sitting drop well screening plates. Crushed crystals were then diluted in the sitting drop well with 60 µL of

mother-liquor solution from screening plate reservoir and transferred to a seed bead tube. Seed bead tubes were vortexed vigorously for 30 sec, kept on ice and used within 1-2 hours and frozen at -80 °C after use. Microseed experiments were set up by hand using the hanging drop vapour diffusion method on EasyXtal X-Seal crystal supports and EasyXtal 15-well DG plates (Qaigen). Plate reservoirs were first filled with 500 µL of crystal screen buffer before hanging drops of 1 µL crystal screen buffer, 1.5 µL of target protein and 0.5 µL of microseed stock were prepared on crystal supports. Hanging drops were repeated using neat microseed stock and two serial dilutions of 1:10 and 1:100 within the cell well. Microseed stocks were diluted using the crystal seed stock solution from which they were grown. Plates were sealed by tightly screwing supports to wells, incubated at 18 °C and screened for crystal formation after day 1, 3 and 7 followed by irregular intervals thereafter using a Leica S4E light microscope (Leica Microsystems).

2.3.3   Crystal harvesting and data collection

Crystals were cryoprotected by addition of 0.5 µL of 20 % ethylene glycol diluted in appropriate crystal screen buffer. Cryo-protected crystals were picked from wells using 20 µm or 40 µm mounted loops (Molecular Dimensions). Picked crystals were immediately flash frozen in liquid nitrogen, transferred to Diamond Light Source (DLS) storage pucks and maintained in liquid nitrogen until completion of data collection. X-ray diffraction data was collected at Diamond Light Source (Didcot, United Kingdom) via a Beamline Allocation Grant (BAG) under the Principal Investigator applicant Dr Pierre Rizkallah (Cardiff University). Crystals suspended in a stream of liquid nitrogen were diffracted using a fixed wavelength of x-rays. 1000 diffraction images were collected by rotation of crystals through 200 ° at 0.2 sec exposures resulting in 0.2 ° of rotation per exposure. Reflected x-rays were detected using a Pilatus 2M detector.

2.3.4   Determination and analysis of crystal structures

Obtained diffraction images were processed using the DLS automated data processing pipeline. Phases were solved using molecular replacement in PHASER using solved pMHC-II as a model (McCoy 2006). Generated molecular models were analysed and refined through molecular manipulation in COOT (Emsley & Cowtan 2004) and computationally refined through iterative TLS refinement using REFMAC5 (Murshudov et al. 2011) until convergence of R_{work} and R_{free}. Computational analyses were performed using the stated software available through the CCP4 computational suite (Winn et al. 2011). Refined models were subjected to a final round of REFMAC5 refinement and visualised using PyMOL Molecular Graphics System (Schrödinger, LLC.). Contact tables were generated using NCONT (CCP4) using a custom python script to annotate contact type (available from: https://github.com/brucemaclachlan/annotcontacts).

2.4 Generation of a stably expressing LAG-3+ cell line

2.4.1 List of materials

2.4.1.1 Oligonucleotide reagents

LAG-3.pUC57 – Custom synthesis by Genewiz

P2A.rCD2.pELNsxv – Prof. James Riley, University of Pennsylvania

pMD2.G – Addgene plasmid #12259

pMDLg/pRRE – Addgene plasmid #12251

pRSV-Rev – Addgene Plasmid #12253

pELNsxv-for primer (GCTAGCTCTAGAGCCGCCACCATG) – Custom synthesis by Eurofins Genomics

pELNsxv-rev primer (GAGAAGTTGGTGGCACCGGAGCCGC) – Custom synthesis by Eurofins Genomics

2.4.1.2 Antibodies

rCD2-PE: Phycocyanin conjugated anti-rat CD2 Mouse IgG2a, κ antibody clone OX-34 – Biolegend

LAG-3-PE: Phycocyanin conjugated anti-human LAG-3 Goat polyclonal IgG antibody clone – R&D Systems

2.4.1.3 Buffers

Flow cytometry (FC) buffer: PBS & 2 % FCS

TE Buffer: 10 mM Tris, 1mM EDTA & pH 8.0 with HCl

HEPES buffered water: 2.5 mM HEPES, pH 7.3 with HCl

Calcium chloride (CaCl$_2$) solution: 2.5 M CaCl$_2 \cdot$2H$_2$O

HEPES buffered saline: 280 mM NaCl, 50 mM HEPES, 1.5 mM Na$_2$HPO$_4$ & pH 7.0 with NaOH

2.4.1.4 Culture media

R10 media: RPMI 1640 media, 10 % FCS, 2mM L-Glutamine, 100 IU/mL Penicillin & 100 µg/mL Streptomycin.

D10 media: Dulbecco's Modified Eagle Medium (DMEM), 10 % FCS, 2mM L-Glutamine, 100 IU/mL Penicillin & 100 µg/mL Streptomycin.

TYP-Agar media: 16g/L Tryptone, 16g/L Yeast Extract, 5g/L Potassium Phosphate Dibasic, 5 g/L Sodium chloride & 15 g/L Agar Bacteriological.

TYP media: 16g/L Tryptone, 16g/L Yeast Extract, 5g/L Potassium Phosphate Dibasic & 5 g/L Sodium chloride.

2.4.2   Cell lines and culture

The J.RT3-T3.5 Jurkat cell line (ATCC® TIB-153™) was obtained from Dr. John Bridgeman (Cardiff University) as a frozen stock in 90 % FCS 10 % DMSO. The Human Embryonic Kidney 293T (HEK 293T) cell line (ATCC® CRL-3216™) was obtained from Dr. Bruno Laugel (Cardiff University) as a frozen stock in 90 % FCS 10 % DMSO. Cells were initiated from frozen culture by rapidly thawing cells at 37 °C before washing in 10 mL of pre-warmed R10 media. Washed cells were centrifuged at 1500 rpm for 5 minutes and subsequent cell pellet resuspended in 5 mL of fresh pre-warmed R10 media. Cells were transferred to a T25 tissue culture flask. J.RT3-T3.5 Jurkat cells (henceforth Jurkat) and cell lines derived thereof were subsequently cultured at 37 ˚C, 5 % CO_2 in R10 media. Jurkat cells were cultured in suspension by renewing culture media three times per week, maintaining cells at a density of 1×10^5 and 1×10^6 cells/mL. HEK 293T cells were cultured at 37 ˚C, 5 % CO_2 in D10 media as an adherent monolayer culture by passaging at 80-90 % confluency.

2.4.3   Construction of a LAG-3 lentiviral delivery vector

An expression construct consisting of the full length sequence of human LAG-3 (Uniprot: P18627) flanked by a 5' XbaI restriction site (TCTAGA), Kozak sequence (GCCGCCACC) and start codon (ATG) and a 3' XhoI restriction site (CTCGAG) was codon optimised for human expression systems and chemically synthesised contained within the pUC57 vector (Genewiz).

2.4.4   Cloning of the LAG-3 lentiviral delivery vector

The synthesised full length LAG-3 construct (described in 2.1.3) was cloned into the pELNsxv third generation lentiviral transfer vector (kindly provided by Prof. James Riley, University of Pennsylvania) containing a self-cleaving P2A linked rat CD2 (rCD2) expression cassette within the multiple cloning site (P2A.rCD2.pELNsxv). The final constructed plasmid was designed such that full length human LAG-3 a P2A linker and rCD2 are expressed under the control of a single promoter in one continuous open reading frame.

2.4.4.1   Vector and insert digestion and purification

All restriction digests were performed according to manufacturer's protocols and in supplied FastDigest buffer. 1 μg of the synthesised LAG-3 construct (described in 2.4.3) supplied within a commercial pUC57 vector was double digested in a 20 μL XbaI and XhoI restriction endonuclease reaction for 30 minutes at 37 °C. Likewise, the P2A.rCD2.pELNsxv vector was double

digested in a 20 µL XbaI and XhoI restriction endonuclease reaction for 30 minutes at 37 °C. The resulting digestion products were analysed by 1 % agarose gel electrophoresis for digestion efficiency using an ultraviolet transilluminator. Digestion products of expected electrophoretic mobility for the digested insert and digested vector, as indicated by a molecular weight marker (Bioline), were excised from the agarose gel and purified using the QIAquick Gel Extraction Kit (Qiagen).

2.4.4.2   Insert ligation and transformation

Purified XbaI/XhoI digested LAG-3 insert and XbaI/XhoI digested P2A.rCD2.pELNsxv vector samples were analysed for absorbance at 260 nm using a nano spectrophotometer allowing measurement of DNA concentration. Ligation of insert into the carbenicillin resistant P2A.rCD2.pELNsxv vector was achieved by incubating 50 ng of vector with 18.5 µg of insert (a 1:2 molar ratio of vector:insert) with T4 DNA ligase and DNA ligase buffer (Life Technologies) overnight at room temperature. Ligation reactions were screened for successful construct formation by transforming 1 µL of the ligation mixture into XL10 Gold Ultracompetent *Escherichia. Coli (E. coli)* cells (Agilent Technologies) as described below.

2.4.4.3   Transformation of competent E*scherichia. Coli (E. coli)*

E. coli bacterial cells were transformed by thawing 25 µL of competent cells for 5 minutes on ice. Thawed cells were incubated with 1 µL of ligation reaction for 5 minutes, mixing frequently via agitation before incubating at 42 °C for 2 minutes. Cells were subsequently returned to ice for 5 minutes before being positively selected on TYP-agar media culture dishes containing 50 mg/L carbenicillin. Transformation plates were incubated over night at 37 °C and subsequently analysed for the growth of distinct bacterial colony formation.

2.4.4.4   Screening for successful construct formation

Plasmid DNA from bacterial colonies selected on carbenicillin TYP-agar plates were first prepared using a plasmid DNA mini-prep kit according to manufacturer's protocols (Zymo Research). Prepared plasmid DNA was analysed via restriction screening by digesting candidate DNA in a 20 µL XbaI and XhoI restriction endonuclease reaction for 30 minutes at 37 °C as described previously. Consequent digestion products were analysed by 1 % agarose gel electrophoresis for a digestion product of the molecular size of the desired LAG-3 insert. Positive colonies by restriction screening were subsequently analysed by DNA sequencing performed by Central Biotechnology Services (CBS; Cardiff University) using the *pELNsxv-for* and *pELNsxv-rev* primers described in section 2.4.1.1. DNA sequencing results were compared to the known

sequence of the desired construct by the multiple sequence alignment program Clustal Omega (EMBL European Bioinformatics Institute).

2.4.4.5 Production of the LAG-3.P2A.rCD2.pELNsxv transfer vector

A sequencing positive clone confirmed to carry the LAG-3.P2A.rCD2.pELNsxv lentiviral transfer vector was consequently inoculated in 400 mL of TYP media supplemented with 50 mg/L carbenicillin overnight at 37 °C, shaking at 220 rpm. Subsequent plasmid DNA was prepared from the culture using a PureLink® HiPure Plasmid Filter Maxiprep Kit according to manufacturer's protocols (Life Technologies).

2.4.5 Generation of a LAG-3 encoding lentivirus

LAG-3 encoding lentiviral particles were generated by calcium chloride transfection of the LAG-3.P2A.rCD2.pELNsxv transfer vector and the pMD2.G, pMDLg/pRRE, pRSV-Rev packaging vectors into HEK 293T cells (Dull et al. 1998). HEK293T cells were prepared at 80 % confluency by replenishing culture media with fresh D10 media 4 hours prior to transfection. DNA particulates were generated by firstly combining 1.1 mL of TE buffer pH 8.0, 15 μg pMD2.G, 15 μg pMDLg/pRRE, 15 μg pRSV-Rev and 583 μL of HEPES buffered water, in the order described, before briefly vortexing. Secondly, 18.75 μg of the LAG-3.P2A.rCD2.pELNsxv transfer vector and 190 μL $CaCl_2$ solution were added in the order described before briefly vortexing. Thirdly, whilst vortexing, 1.9 mL of HEPES buffered saline was added dropwise to the transfection mixture before incubating at room temperature for 18 min to allow DNA precipitates to form. The transfection mixture was then added dropwise into the culture media of HEK293T cells under gentle agitation and avoiding direct pipetting on the cell monolayer. Treated HEK293T cells were incubated overnight for 16 hours at 37 ˚C and 5 % CO_2 after which the transfection mixture was replaced with fresh D10 media. Packaged lentiviral particles were harvested after 24 hours and 48 hours of culture at 37 ˚C and 5 % CO_2, 0.45 μm filtered and concentrated by ultracentrifugation at 150,146 x g for 2 hours at 4°C. Concentrated virus was resuspended in 300 μL of R10 media and stored at -80 °C via flash freezing on dry ice.

2.4.6 Lentiviral transduction of Jurkat cells

Jurkat cells were transduced with the generated LAG-3.P2A.rCD2 lentivirus by incubating 2 x 10^5 cells seeded in a 48 well plate with increasing volumes of lentiviral preparation (50 μL, 100 μL and 150 μL) overnight at 37 ˚C and 5 % CO_2. Following overnight incubation, lentiviral containing media was diluted out using 1 mL fresh R10 media and cells were cultured for 10 days until cells reached maximum growth capacity.

2.4.7 Flow cytometric analysis of LAG-3 transduction efficiency

2.4.7.1 Fluorescence antibody staining of Jurkat cells

Transduced Jurkat cells were prepared for antibody staining by splitting the suspension culture by a ratio of 1:2 using fresh R10 media one day prior to analysis. Cells to be analysed were transferred to a 96 well plate and washed twice by successive centrifugation for 5 min at 1500 rpm and resuspension in 150 µL FC buffer. Washed cells were stained for rCD2 expression and LAG-3 expression in separate single stain experiments using rCD2-PE (1:1500 dilution) and LAG-3-PE (1:15 dilution) antibodies respectively for 30 min at 4 ˚C. Stained cells were washed twice in FC buffer as described previously, resuspending in 200 µL FC buffer for analysis.

2.4.7.2 Flow cytometric analysis of fluorescent antibody stained cells

Fluorescent antibody stained Jurkat cells transduced with the generated LAG-3.P2A.rCD2 lentivirus were analysed for rCD2 and LAG-3 expression a BD FACSCanto II flow cytometer. Consequent data was analysed using the FlowJo (Tree Star Inc.) software package.

2.4.8 Limit dilution cloning of transfected Jurkat lines

A single cell derived LAG-3+ T cell line was cloned by limit dilution of the Jurkat cell line transduced with 150 µL of LAG-3.P2A.rCD2 lentiviral preparation. The parent Jurkat cell line was counted three times using a haemocytometer and serially diluted in fresh R10 media such that 0.5 cells were seeded into all wells of a 96 well plate. Cloning plates were incubated at 37 ˚C and 5 % CO_2 and monitored regularly for cell growth and media consumption. Consequent wells containing multiplied cells were expanded into 48 well plates after 21 days of culture and into T25 tissue culture flasks after a further four days using fresh R10 media. Individual daughter clones were screened for LAG-3 expression using the protocol outlined in section 2.4.7.

2.5 Molecular and biophysical analysis of LAG-3-MHC-II binding

2.5.1 List of materials

2.5.1.1 Antibodies

αLAG-3-FITC: Fluorescein isothiocyanate (FITC)-conjugated anti-human LAG-3 clone 17B4 – Enzo Life Sciences

αCD4-APCy: Allophycocyanin (APCy)-conjugated anti-human CD4 clone – Miltenyi Biotec

αCD14-PB: Pacific Blue™ anti-human CD16 Antibody clone 3G8 - BioLegend

αTCR-FITC: FITC-conjugated anti-human αβ TCR clone IP26 – BioLegend

αPE: Unconjugated anti-phycoerythrin (PE) clone PE001 – BioLegend

α-LAG-3: Unconjugated anti-LAG-3 clone 17B4 – Kindly provided by Professor Frédéric Triebel (Prima BioMed, Sydney, Australia)

2.5.1.2 Buffers

TBSB buffer: 20 mM Sodium citrate, 86 mM Sodium chloride, 100 mM L-arginine, 0.02 % Tween-20, pH 7.4 with citric acid

2.5.2 Characterisation of cell lines

Multimer staining was performed on JRT LAG-3$^+$ C8 and JRT WT cells produced and cultured as described in section 2.4 and MOLT-3 cells provided by Angharad Lloyd (Cardiff University). MOLT-3 cells were cultured in suspension by renewing culture media two or three times per week, maintaining cells at a density of 1 x 10^5 and 2 x 10^6 cells/mL. TCR, LAG-3 and CD4 expression by each of the three described cell lines was characterised using the standard anti-body staining for flow cytometry protocol as outlined in section 2.4.7 using antibodies outlined in section 2.5.1.1. Antibody staining was performed as single stains and analysed of a FACS Canto II flow cytometer (BD Bioscience).

2.5.3 Multimer staining of LAG-3$^+$ cells

PE-conjugated MHC-II dextramers were assembled using HLA-DR1 HA$_{306-318}$ (PKY) mono-mers into multimers as described in section 2.1.6. Negative control multimers were assembled from HLA-A2 hTERT$_{540–548}$ (ILA) monomers kindly provided by Michael Crowther (Cardiff University). Cells were stained as described previously for cognate T cell clone staining and according to a protocol published previous (Tungatt et al. 2015) with the following additional steps. Cells were counted and 1x10^5 cells per stain transferred to FACS tubes for analysis. Cells were washed with 4 mL of PBS and treated with 50 nM dasatinib for 30 min at 37 ˚C. Cells were first blocked with unconjugated anti-LAG-3 (17B4 clone) or irrelevant antibody (anti-

CD4-APCy) or PBS for unblocked samples. After blockade for 1 hr on ice, cell samples were washed with PBS and incubated with MHC-II multimers for 30 min on ice. After incubation with multimers, stained cells were washed with PBS, boosted using an anti-PE secondary antibody for 20 min and stained for live/dead cells as described previously. Stained cells were analysed on a FACS Canto II flow cytometer (BD Bioscience) as described previously. HLA-DR1 HA$_{306-318}$ (PKY) multimer staining of the cognate T cell clone DCD10, provided by Andrea Schauenburg (Cardiff University), performed as described in section 2.1.6.

2.5.4 Analysis of LAG-3-MHC-II binding via surface plasmon resonance (SPR)

2.5.4.1 Preparation of protein samples

LAG-3:Fc protein was obtained through a collaboration with Professor Frédéric Triebel (Prima BioMed, Sydney, Australia) in the form of a GMP-grade sample expressed in glycosylation-sufficient *Chinese hamster ovary* (CHO) cells at 30 mg/mL as described previously (Huard et al. 1995). LAG-3:Fc sample was gel filtrated into fresh TBSB buffer the day of SPR experiments. Biotinylated MHC-II molecules were prepared as described previously (section 2.2). *Spodoptera frugiperda* (sf9) insect cell produced HLA-DR1 CLIP was kindly provided by Andrea Schauenburg. HLA-A2 hTERT$_{540-548}$ (ILA) monomers were kindly provided by Michael Crowther (Cardiff University) as a negative control.

2.5.4.2 Immobilisation of streptavidin

Analysis of LAG-3-MHC-II interactions were performed on a BIAcore T200 surface plasmon resonance (SPR) instrument (GE Healthcare Life Sciences). Firstly, sensor chips were activated by injection of 10mM N-(3-dimethylaminopropyl)-N3-ethylcarbodiimide (EDC) and 400mM N-hydroxysuccinimide (NHS) which was combined directly before use. Secondly, approximately 5000 response units (RU) of streptavidin was covalently linked to the activated sensor chip by injection of 200 μg/mL streptavidin solution in 10 mM acetate pH 4.5 (Sigma-Aldrich). Finally, the chip surface was deactivated by injection of 1 M ethanolamine (GE Healthcare Life Sciences).

2.5.4.3 Immobilisation of pMHC molecules

Prepared biotinylated pMHC molecules were immobilised to streptavidin coated CM5 sensor chips by injection of pMHC molecules at a flow rate of 10 μL/min in order to obtain an even distribution of pMHC molecules across each flow cell. pMHC molecules were injected until a desired ligand concentration was loaded onto sensor chips as indicated by increase in RU as a

result of ligand injection. Remaining free streptavidin sites were blocked using injection of free biotin.

2.5.4.4   Measurement of LAG-3:Fc-MHC-II binding by SPR

LAG-3-MHC-II binding was measured using immobilised pMHC coated sensor chips as experimental ligand and soluble LAG-3:Fc as experimental analyte. All experiments were performed at 25 °C. LAG-3:Fc molecules were serial diluted by half resulting in a dilution series of ten concentrations (typically 10 mg/mL to 10 µg/mL). Each dilution of LAG-3:Fc was sequentially injected at 30 µL/min for 30 sec over all four flow cells of the pMHC immobilised sensor chip followed by a dissociation period of 300 sec at 30 µL/min. Association and dissociation of analyte was recorded in real-time and RU curves were analysed in BIAevaluation v4.1 software (GE Healthcare Life Sciences). Response unit changes were analysed as background subtracted sensograms by subtraction of background bulk effect response unit changes observed in negative control flow cells from experimental MHC-II immobilised response unit changes. Kinetic analyses of LAG-3:Fc binding were performed in BIAevaluation v4.1 using the simultaneous ka/kd fitting function. Equilibrium analyses were performed using nonlinear regression least squares ordinary fit of the Michaelis-Menton kinetic equation in GraphPad Prism v5 (GraphPad Software, Inc). Applied analyses are detailed in Chapter 4. All sensograms presented were plotted using GraphPad Prism v5.

2.6 Analysis of LAG-3:Fc and MHC-II via negative stain electron microscopy

2.6.1 Sample preparation

LAG-3:Fc was provided by a collaboration with Professor Frederic Triebel (Prima Biomed, Sydney, Australia) after encouragement (Brains Brewery, Cardiff, UK). LAG-3:Fc was formulated as described previously (Huard et al. 1995) and provided at a concentration of 30 mg/mL in TBSB buffer. For negative stain microscopy, LAG-3:Fc was serially diluted to a concentration of 20 µg/ml in TBSB buffer.

pMHC-II was produced as described in section 2.2 by the refolding of HLA-DR1 with the 5T4p12 peptide (DR1-5T4$_{p12}$). DR1-5T4$_{p12}$ was serially diluted to a concentration of 20 µg/mL in TBSB buffer and combined at a 1:1 molar ratio with LAG-3:Fc prepared as described (henceforth LAG-3:Fc-DR1).

2.6.2 Preparation of grids

Negative stain electron microscopy grids were prepared according to an optimised protocol for the imaging of macromolecular complexes of low symmetry (Rames et al. 2014). Carbon film coated 400 mesh copper grids (Agar Scientific) were glow discharged using a SC7620 Mini Sputter Coater/Glow Discharge System (Quorum Technologies Ltd) for 30 seconds. 4 µL of prepared LAG-3:Fc or LAG-3:Fc-DR1 complex samples were pipetted onto grids suspended over ice at a 45 ° tilt angle for 60 seconds. Excess protein solution was removed via blotting using Whatman® No. 1 filter paper (GE Healthcare Life Sciences). Grids were then washed three times in 40 µL droplets of deionised water, removing excess water with filter paper between washes. Washed grids were next incubated in three droplets of 0.2 µm filtered 2 % uranyl acetate (Sigma-Aldrich) for 3 seconds, 10 seconds and 60 seconds, consecutively, removing excess stain with filter paper between incubations. Stained grids were left to dry for 30 minutes at room temperature before being stored until imaging.

2.6.3 Data collection

Negative stained grids were imaged at Research Complex at Harwell (Didcot, United Kingdom) with access through a visitor access grant. Data was collected on a JEM-2100 LaB6 transmission electron microscope (JOEL USA, inc) equipped with a Gatan US1000-1 2048 x 2048 charged-couple device (CCD) digital imaging camera. Micrographs were collected at 50,000 X magnification at an acceleration voltage of 200 kV, sampling rate of 2.1 Å/pixel and spherical

aberration C_s of 1.0mm. Grids were exposed to a maximum electron dosage of 25 e$^-$/Å^2. Micrographs were collected with a 0.5 second exposure time at defocus levels of between 0.1 and 1.5 µm.

2.6.4   Image processing

LAG-3:Fc or LAG-3:Fc-DR1 complex negative stain micrographs were analysed using the EMAN2.1 scientific image processing suite (Tang et al. 2007). Processing steps were performed through command-line based execution of EMAN2.1 programs in combination with the graphical user interface (GUI) project workflow program *e2projectmanager.py*.

2.6.4.1   Micrograph selection

Recorded micrographs were curated for quality by viewing images using *e2evalimage.py* and removing micrographs with poor contrast. Micrographs which contained excessive astigmatism and drift, as indicated by non-spherical or incomplete Thon rings, respectively, in generated 2D power spectrums, were also removed from consequent analyses.

2.6.4.2   Particle picking

Particles from raw collected micrographs were picked using *e2boxer.py* interactive boxing program. Single particles were picked manually with a box size of 196x196 pixels for LAG-3:Fc and 224x224 pixels for LAG-3:Fc-DR1. Picked particles were outputted with edge normalisation as particle stacks in .hdf format.

2.6.4.3   Particle pre-processing

Particle images were first contrast transfer function (CTF) corrected using *e2ctf.py* by automated estimation of defocus values in conjunction with observed defocus at micrograph collection. CTF parameters were refined by calculation of particle structure factors and an estimated amplitude contrast of 60 %. Particle images were corrected for CTF by the generation of phase flipped images.

Particle images were further pre-processed through filtering of high and low frequency noise, mask application and image normalisation using *e2proc2d.py*. High resolution noise was removed from particles using a Gaussian low pass filter with a cut-off wavelength of 10 Å. Similarly, low frequency noise was removed with a cut-off Gaussian high pass filter wavelength of 200 Å for LAG-3:Fc and 300 Å for LAG-3:Fc-DR1. Furthermore, a circular mask of radius 0.9 X the particle box size with a linear drop off of 4 pixels was applied. Finally, particle images

were normalised to bring mean pixel intensity across particles to a zerofloat, thus, normalising particle images across all image stacks.

2.6.5   2D class averaging

Pre-processed particle images were processed into representative 2D class averages via the reference free classification approach by *e2refine2d.py*. For LAG-3:Fc and LAG-3:Fc-DR1, the top 1000 particle images with best signal to noise ratio were classified into 24 classes through 15 iterations of refinement.

2.6.6   Initial model building

Initial models were built from class averages featuring unique particle views using *e2initialmodel.py*. Multiple initial models of LAG-3:Fc and LAG-3:Fc-DR1 were generated from between 5 – 15 of the highest quality class averages, with each initial model refined by at least 6 iterations of refinement. Generated initial models were curated by visualisation and analysis of quality score defined by the program.

2.6.7   3D refinement

Particle datasets and generated initial models were used to refine 3D single particle reconstructions of LAG-3:Fc and LAG-3:Fc-DR1 using *e2refine_easy.py*. Models were generated and refined via multiple rounds; first starting with particle images with the best signal to noise ratio and a low resolution target of 35 Å. Each refinement was performed with no symmetry restraint (C1 symmetry), through at least 8 refinement iterations using the highest precision parameter available (speed parameter value of 1). Generated refined models were visualised and used as a starting model for further refinement rounds with additional particle images and higher resolution targets. This iterative process was repeated until convergence of resolution and model quality. Model resolutions are calculated according to the 'gold standard' resolution criteria (Scheres & Chen 2012).

2.6.8   Visualisation of models

Single particle reconstructions of LAG-3:Fc were visualised using UCSF Chimera v1.1 (Pettersen et al. 2004). Surface volumes were rendered using a 0.5 σ cut-off value.

2.7 Generation of anti-LAG-3 antibodies

2.7.1 List of materials

2.7.1.1 Antibodies

αMouse-HRP: Horse Radish Peroxidase AffiniPure Goat Anti-Mouse IgG, F(ab')$_2$ Fragment Specific No. 315-035-047 – Jackson Immuno Research Laboratories Ltd.

αMouse-FITC: FITC Goat Anti-Mouse Ig Clone Polyclonal (RUO) No. 554001 – BD Biosciences

αLAG-3-FITC: Anti-human LAG-3 clone 17B4 – Enzo Life Sciences

2.7.1.2 Buffers

PBS-T: PBS, 0.05 % Tween 20

FC buffer: PBS, 2 % FCS

Red Blood Cell Lysis Buffer: 155 mM Ammonium chloride (NH$_4$Cl), 10 mM Potassium bicarbonate (KHCO$_3$), 0.1mM Ethylenediaminetetraacetic acid (EDTA), pH 7.2 with HCl

2.7.2 Cell lines and culture

Generated mouse B cell hybridoma cell lines were cultured at 37 ˚C, 5 % CO$_2$ in R10 media by maintaining cells as a suspension culture at density of between 5 x10^4 and 5 x10^5 cells/mL. Mouse B cell hybridomas cell lines were cryoprotected and initiated from frozen culture when required as described in section 2.4.2 and 2.1.8 respectively. Wild type Jurkat (WT-JRT) and LAG-3$^+$ Jurkat (LAG-3-JRT) cells were cultured as described in section 2.4.2.

2.7.3 Immunisation of mice

The generation, initial cloning and ELISA screening of mouse anti-human LAG-3 B cell hybridomas through the *in vivo* immunisation of mice was kindly performed by and in collaboration with Professor B. Paul Morgan (Cardiff University).

2.7.3.1 Preparation of antigen

Antigen was prepared by diluting 20 µg of human LAG-3:Fc fusion protein (AdipoGen) in 300 µL of phosphate buffered saline (PBS) and combined with 300 µL of either Freund's Complete Adjuvant (CFA) or in Freund's incomplete adjuvant (IFA) (Sigma-Aldrich). The antigen and adjuvant were mixed via vigorous vortex to form an emulsion.

2.7.3.2 Immunisation schedule

Four C57BL/6 mice were first immunised via subcutaneous injection with 20 μg of human LAG-3:Fc emulsified in CFA, as described. Mice were then consequently boosted with 20 μg of LAG-3:Fc emulsified in IFA, as described, at four weeks post-challenge followed by additional boosts at week five and week six post-challenge. Mouse sera was isolated from each mouse via tail bleed and screened for LAG-3:Fc specific antibody production by direct enzyme-linked immunosorbent assay (ELISA) as described to follow. The mouse with highest sera reactivity via ELISA was administered a final boost of 20 μg LAG-3:Fc, intravenously without adjuvant, two days before sacrifice and splenectomy.

2.7.4 Generation of a mouse B cell hybridoma line

Mouse splenocytes were isolated by forcing the harvested mouse spleen through a cell strainer using the plunger of a syringe and rinsed through with R10 media in order to form a cell suspension. Harvested splenocytes were centrifuged at 800 g, resuspended in 10 mL of red blood cell lysis buffer and incubated for 10 minutes at room temperature. Splenocytes were centrifuged at 800 g, resuspended in R10 media and cultured at 37 ˚C, 5 % CO_2 until fusion. Cultured splenocytes were fused to the BALB/c derived Sp2/0-Ag14 (ATCC® CRL-1581™) mouse myeloma cell line via polyethylene glycol cell fusion.

2.7.5 Single cell cloning of anti-LAG-3 hybridomas

The parent B cell hybridoma line was serially diluted across 96 well plates by successive dilutions by a dilution factor of two. Cloning plates were incubated at 37 ˚C, 5 % CO_2 and monitored regularly for cell growth and media consumption. Culture wells exhibiting growth, with preference for wells seeded at the highest dilution factor, were selected for further cloning and reactivity screening via ELISA and flow cytometry, as described to follow. This process was repeated as a second and third iteration of cloning. For the fourth and final iteration of cloning, B cell hybridomas were counted and serially diluted such 0.33 cells were plated into wells of a 96-well plate. Cell growth was monitored and final clones which had formed distinct single colonies of divided cells were selected for reactivity screening via ELISA and flow cytometry to ensure clonality. Consequent wells containing multiplied cells were expanded into 48 well plates after 21 days of culture and into T25 tissue culture flasks after a further four days using fresh R10 media.

2.7.6 LAG-3:Fc reactivity screening by ELISA

Specificity of antibody contained within B cell hybridoma supernatants or mouse sera for LAG-3:Fc was tested using a direct ELISA approach. Half-area 96 well plates were coated with 50 µL of 1 µg/mL human LAG-3:Fc protein in PBS for 1 hour at 37 ˚C. Plates were then blocked with 100 µL of 1 % BSA in PBS for 1 hour at 37 ˚C followed by washing three times with PBS-T. 50 µL of neat B cell hybridoma supernatants or serial diluted mouse sera were added to coated plates for 1 hour at 37 ˚C before washing three times with PBS-T. Plates were then incubated with an anti-Mouse-HRP secondary antibody (Jackson Immuno Research Laboratories Ltd.) diluted 1:2000 in PBS. Plates were washed three times with PBS-T and developed using HRP substrate colour reagents and stop solution (R&D Systems) and absorbance at 450 nm measured on a microplate absorbance reader (Bio-rad).

2.7.7 LAG-3 reactivity screening by flow cytometry

Specificity of antibody contained within B cell hybridoma supernatants or immunised mouse serum for LAG-3 was tested by flow cytometry analysis of stained wild type Jurkat (WT-JRT) and LAG-3$^+$ Jurkat (LAG-3-JRT) developed in section 2.4. WT-JRT and LAG-3-JRT cells were counted and 2 x10^5 cells plated into wells of a 96 well plate. Cells were washed twice with FC buffer by addition of 150 µL of FC buffer and pelleting of cells by centrifugation at 1500 rpm for 5 minutes. Cells were resuspended in 40 µL mouse serum (diluted 1:3), B cell hybridoma supernatant (neat), FC buffer (negative control) or commercial FITC-conjugated anti-LAG-3 (positive control; 17B4 clone; 1:200 dilution; Enzo Lifescience) on ice for 30 min. Cells were washed twice with FC buffer, as described previously, and then resuspended, where appropriate, in 30 µL anti-Mouse-FITC conjugate (1:50 dilution, BD Biosciences) on ice for 30 min in the absence of light. Stained cells were washed twice with FC buffer and resuspended in 200 µL for analysis on a FACSCanto II flow cytometer (BD Biosciences). Obtained data was analysed in Flow Jo v10 (FlowJo, LLC).

2.8 Production and characterisation of anti-LAG-3 antibodies

2.8.1 List of materials

2.8.1.1 Culture media

R10-Ig⁻ media: RPMI 1640 media, 10 % Ig⁻ FCS, 2mM L-Glutamine, 100 IU/mL Penicillin & 100 µg/mL Streptomycin.

2.8.1.2 Buffers

NaOH wash buffer: 0.5 M Sodium hydroxide

Glycine elution buffer: 0.1 M Glycine, pH 2.5 with Hydrogen chloride

Neutralisation buffer: 1 M Tris, pH 10.5 with Sodium hydroxide

Endotoxin low Phosphate Buffered Saline Dulbecco 'A' (PBS) – Invitrogen: 8 g/L Sodium chloride, 0.2 g/L Potassium chloride, 1.15 g/L Disodium hydrogen phosphate & 0.2 g/L Potassium dihydrogen phosphate, pH 7.3

PBS-T: PBS, 0.05 % Tween 20

Western blot lysis buffer: 150 mM Sodium chloride, 50 mM Tris, 2 % v/v Triton X-100

FC buffer: PBS, 2 % FCS

Sodium acetate pH 4.5 buffer: 10 mM sodium acetate pH 4.5 with Acetic acid

TBSB buffer - 20 mM Sodium citrate, 86 mM Sodium chloride, 100 mM L-arginine, 0.02 % Tween-20, pH 7.4 with citric acid

Glycine pH 1.5 buffer: 10 mM Glycine, pH 1.5 with HCl

2.8.1.3 Antibodies

anti-Mouse-HRP conjugate: F(ab')2-Goat anti-Mouse IgG (H+L) Secondary Antibody, HRP conjugate No. A24524 – ThermoFisher Scientific

αMouse-FITC: FITC Goat Anti-Mouse Ig Clone Polyclonal (RUO) No. 554001 – BD Biosciences

IgG2a isotype control: unconjugated mouse IgG2a, κ isotype control – BioLegend

IgG2b isotype control: unconjugated mouse IgG2b, κ isotype control – BioLegend

Anti-LAG-3 (17B4): Unconjugated anti-LAG-3 clone 17B4 – Kindly provided by Professor Frédéric Triebel (Prima BioMed, Sydney, Australia)

Anti-LAG-3 (13E2): Unconjugated anti-LAG-3 clone 13E2 – Kindly provided by Professor Frédéric Triebel (Prima BioMed, Sydney, Australia)

2.8.2 Production of purified anti-LAG-3 antibodies

2.8.2.1 Culturing of cells

Large scale culturing and purification of anti-LAG-3 antibodies was performed by and in collaboration with Dr Emma Jones (Cardiff University). Cloned hybridomas were cultured in R10-Ig⁻ media using INTEGRA CELLine flasks (INTEGRA Biosciences AG) according to manufacturer's protocols.

2.8.2.2 Purification of antibodies

Antibody samples were purified from culture supernatants using a Protein L affinity column in conjunction with an ÄKTA Prime FPLC system (GE Healthcare Life Sciences). Prior to purification, FPLC system was cleaned with NaOH wash buffer. Culture supernatants were loaded onto affinity columns equilibrated with PBS. Bound antibody was eluted by a single step equilibration of affinity columns with Glycine elution buffer. Eluted samples were collected in 2 ml fractions into tubes pre-filled with 50 µL Neutralisation buffer. Fractions containing protein, as indicated by A_{280} spectra, were concentrated and dialysed into endotoxin low PBS using 10 kDa MWCO centrifugal filter units (Merck Millapore). Purified antibody samples were analysed for protein concentration and stored in aliquots at 2 mg/mL.

2.8.3 Western blot characterisation of antibodies

The ability of generated anti-LAG-3 antibodies to detect whole protein by Western blot assay was performed against cell lysates of LAG-3-Jurkat cells and WT Jurkat cells, generated and cultured as described previously. To produce lysates, 5×10^6 cells were harvested from culture by centrifugation at 1500 rpm, washed with 10 mL of PBS and resuspended in 1 ml of cold Western blot lysis buffer. Cells were vortexed for 1 minute before centrifugation at 16,100 g for 5 min at 4 °C. The resulting supernatant was harvested and assayed for protein concentration using a NanoDrop ND100 (ThermoScientific). LAG-3-Jurkat and WT-Jurkat cell lysates were normalised to an equal protein concentration by dilution in Western blot lysis buffer.

LAG-3-Jurkat and WT-Jurkat cell lysates were separated by SDS-PAGE, as described previously, by loading equal volume of each cell lysate. Separated proteins were transferred to 0.45 µm polyvinylidene fluoride (PVDF) membranes using a Bolt® Mini blot transfer module (ThermoFisher Scientific). Invitrolon™ PVDF/Filter Paper Sandwich membranes (ThermoFisher Scientific) were pre-wet with 100 % isopropanol (Fisher Chemicals) for 30 sec before thorough washing in deionised water. PVDF membranes, filter papers and sponges were soaked in Bolt®

Transfer Buffer and assembled into transfer module according to manufacturer's instructions (ThermoFisher Scientific). Membrane transfer was performed at 20 V for 60 minutes.

Obtained blots were washed 3 times for 5 min under agitation in PBS-T and blocked for 1 hr in 5 % whole skimmed milk-PBS-T (Premier Foods Group Ltd). Blocked membranes were washed as above, cut and incubated separately with 5 ml of different anti-LAG-3 mAbs overnight at 4 °C. Primary anti-LAG-3 antibodies were prepared from purified antibody samples diluted to 2 µg/mL in 5 % whole skimmed milk-PBS-T. After primary incubation, membranes were washed and incubated with 5 mL of goat anti-Mouse IgG-HRP conjugated secondary antibody (ThermoFisher Scientific) diluted 1:5,000 in 5 % whole skimmed milk-PBS-T for 1 hr at room temperature. Probed membranes were washed and developed using Pierce™ ECL Plus Western Blotting Substrate (ThermoFisher Scientific) and blots imaged using a myECL™ Imager in chemiluminescent imaging mode (ThermoFisher Scientific). Optimal exposure time was determined by the myECL™ Imager software.

2.8.4 Flow cytometric characterisation of antibodies

The ability of generated anti-LAG-3 antibodies to bind surface expressed LAG-3 was assessed by staining LAG-3-Jurkat cells and analysed via flow cytometry. LAG-3-JRT cells were counted and plated at 1×10^5 cells into wells of a 96 well plate. Cells were washed twice with FC buffer by addition of 150 µL of FC buffer and pelleting of cells by centrifugation at 1500 rpm for 5 minutes. Antibodies were prepared at multiple concentrations by serial dilution of purified antibody samples of known concentration, determined as described previously, in PBS. Cells were resuspended in 50 µL of anti-LAG-3 on ice for 30 min. Cells were washed twice with FC buffer, as described previously, and then resuspended in 50 µL anti-Mouse-FITC conjugate at 2 µg/mL (BD Biosciences) on ice for 30 min in the absence of light. Stained cells were washed twice with FC buffer, resuspended in 200 µL FC buffer and transferred to tubes for analysis on a FACSCanto II flow cytometer (BD Biosciences). Obtained data was analysed using Flow Jo v10 (FlowJo, LLC) and GraphPad Prism 5 (GraphPad Software, Inc).

2.8.5 Antibody-antigen kinetic analysis by SPR

Characterisation of anti-LAG-3 antibody to LAG-3 antigen interactions were performed on a BIAcore T200 surface plasmon resonance (SPR) instrument (GE Healthcare Life Sciences) using a single injection kinetics approach. LAG-3:Fc was immobilised directly to CM5 sensor chip by EDC/NHS amine activation coupling as described in section 2.5.4.2. Approximately 1,500 response units of LAG-3:Fc was immobilised to flow cells 2 and 4 by injection of 50

µg/mL LAG-3:Fc diluted in sodium acetate pH 4.5 buffer. Purified anti-LAG-3 antibody samples were prepared by gel filtration into TBSB buffer and concentrated to 0.2 mg/mL. Kinetic measurements were made by injection of analyte antibodies at 30 µL/min for 200 seconds and consequent dissociation period of 1200 sec. Chip regeneration was performed by a 30 sec injection of glycine pH 1.5 buffer. Obtained association-dissociation sensograms were analysed for conformity to kinetic rate models using BIAevaluation v4.1 software (GE Healthcare Life Sciences) and plotted in GraphPad Prism 5 (GraphPad Software, Inc).

2.8.6   Antibody competition analysis by SPR

Analysis of competition for binding of anti-LAG-3 antibodies was performed on a BIAcore 3000 SPR instrument (GE Healthcare Life Sciences) using a sequential injection approach. LAG-3:Fc coated CM5 sensor chips and anti-LAG-3 antibodies were prepared as described in section 2.8.5. Experiments were performed at a flow rate of 30 µL/min. Ligand binding site saturation was first achieved by injection of an anti-LAG-3 antibody for 200 sec and consequent dissociation period of 300 sec before 80 sec injection of a second anti-LAG-3 antibody. Analysis of competition was performed by comparison of association profile of anti-LAG-3 antibodies with and without previous saturation by potential competitor anti-LAG-3 antibody. Chips were regenerated and data analysed as described previously.

2.8.7   Molecular blockade of LAG-3-MHC-II binding

Blockade of LAG-3:Fc-MHC-II interaction was performed using SPR as described in section 2.5.4 using MHC-II as immobilised ligand and LAG-3:Fc as analyte with the following alterations. Prior to SPR analysis 2 µM LAG-3:Fc analyte was incubated with 13.2 µM irrelevant (IgG2a isotype control) 17B4, 13E2 or 6F7 purified antibody samples. Combined LAG-3:Fc-antibody samples were co-injected over immobilised MHC-II and binding analysed as in section 2.5.4. Consequently, titrating concentrations of 6F7 (0.6 – 13.2 µM) were incubated with 2 µM LAG-3:Fc and co-injected as described. The ability for generated anti-LAG-3 antibodies to block MHC-II multimer binding to JRT LAG-3^{+} C8 cells was assayed as described in section 2.5.3.

3 Chapter 3: Molecular and cellular basis of CD4$^+$ T cell responses to 5T4

3.1 Abstract

Recognition of the oncofoetal tumour antigen 5T4 by CD4$^+$ T cells has been detected in both healthy donors and patients with colorectal cancer. Moreover, responses to 5T4 peptide antigens deteriorates with tumour stage due to increased regulation of adaptive immunity towards tumours. Consequently, characterisation of the CD4$^+$ T cell response to 5T4 antigens at the clonal and epitope level should aid understanding in the sub-optimal response to the self-derived 5T4 antigen. To this end, using T cell activation assays, three 5T4-reactive clones were shown to be sensitive to 5T4 peptide epitopes by producing T_H1 cytokines in response to antigen. However, using pMHC-II multimer staining and surface plasmon resonance, TCR engagement by cognate antigen was shown to be minimal to undetectable despite known antigen recognition in cell-based assays e.g. IFNγ-release. In order to gain insights into the structural characteristics of 5T4-peptide presentation to the TCR repertoire, the structure of a 5T4-derived peptide presented on HLA-DR1 was solved to 1.95 Å. This structure revealed a flat presented peptide binding core offering minimal high enthalpy contact points with the TCR. Structural order at the peptide flanking residues, including a C-terminal hairpin loop, however, showed projection of the peptide away from the peptide binding groove and thus available for TCR contact. These features, as well as a near-optimal HLA-DR1 binding motif, may contribute to 5T4-peptide immunogenicity. These studies therefore describe the immunogenicity of tumour-derived peptide antigens and reveal novel structural phenomena of MHC-II peptide presentation.

3.2 Introduction

CD4^{+} T cells can detect the occurrence of cancerous cells via the recognition of presented peptides from tumour-derived proteins. These tumour associated antigens (TAAs) can be processed by antigen presenting cells (APCs) into peptide fragments which are presented at the cell surface via major histocompatibility complex class II (MHC-II) molecules. Peptide bound MHC-II complexes (pMHC-II) are in turn recognised by CD4^{+} T cells via their antigen specific T cell receptor (TCR). The ability to sufficiently present TAA-derived peptides on MHC-II molecules, and consequently form this interaction between pMHC-II and cognate TCR, governs CD4^{+} T cell activation and the consequent immune response against TAAs expressed by cancer cells.

One such TAA recognised by CD4+ T cells is the oncofoetal antigen 5T4 (Trophoblast glycoprotein/Wnt-Activated Inhibitory Factor 1/WAIF1) which is expressed on most solid cancers whilst rarely expressed on healthy adult tissue (Elkord et al. 2008). Indeed, in a cohort of 72 colorectal patients, 85 % of patients were 5T4 tumour positive (Starzynska et al. 1992). These properties have highlighted 5T4 as a potential marker for immunotherapies which aim to target 5T4[+] tumours directly or through the enhancement of immune responses to TAA expressing cancer cells (Stern et al. 2014). Specifically, a modified vaccinia Ankara viral vaccine (MVA-5T4) termed Trovax® is currently under development and has undergone a phase I/II clinical trial in colorectal cancer patients (Harrop et al. 2006). In both pre-clinical models and small phase II studies, individuals vaccinated with MVA-5T4 generate a consistent antibody response against 5T4 (Harrop et al. 2013).

3.2.1 T cell clones as a model for studying the CD4^{+} T cell response to 5T4

Study of human T cell responses to antigens at the molecular, cellular, structural and biophysical level has been enabled by the generation of human T cell clones, their consequent maintenance in culture and their analysis at the protein level. Generation of T cell clones, and thus the TCR that defines their clonotype, provide a snapshot of the T cell repertoire against a chosen antigen, such as tumour antigens like 5T4. Characterisation of the function and phenotype of such clones might give an indication as to the immunology of the active response to a specific peptide antigen (Matsuzaki et al. 2015). The generation of T cell clones allows the study of clonal TCR heterodimer molecules. (Deng et al. 2007). Acquisition of tumour reactive T cell clones therefore provide a model for the study of tumour recognition through the TCR and the peptide ligands, presented by MHC molecules. Characterisation of T cell clones against tumour antigens, such as 5T4, therefore help validate the recognition of peptide epitopes and their potential immunogenicity.

3.2.2 Analysing T cell recognition through structural and biophysical techniques

Recognition of tumour-derived peptide antigens is dependent on TCR engagement to ligands presented on MHC molecules with sufficient affinity to initiate triggering of T cell activation. The degree of T cell activation is driven in part by the affinity at which its TCR binds cognate pMHC-II (Corse et al. 2011). Thus, quantification of the affinity of TCR engagement by a tumour reactive TCR is a direct measurement of the possible potency in the response to tumour via the recognition of 5T4-derived peptide antigen. Detection and measurement of this binding affinity has been performed mostly by surface plasmon resonance (SPR), in particular, using the BIAcore series of instruments (Bridgeman et al. 2012).

SPR instruments allow the label-less real-time measurement of the kinetics of protein-protein interactions. This is achieved through the detection of binding between an immobilised ligand attached to a glass surface chip layered with gold and an analyte in solution which is flowed over the surface chip via a microfluidics flow cell. Measurement of binding is facilitated by the change in refractive index of light at the angle of total internal reflection upon the surface of the glass chip as a consequence of the change in mass at the chip surface upon binding. As a result, real time binding of proteins is detected and represented as sensograms which plot response units (RU) – the measured SPR signal – as a function of time. From sensograms, the kinetics of an interaction can be elucidated and, thus, the affinity of the interaction calculated.

SPR experiments have been used extensively in the characterisation of TCR to pMHC interaction affinity where pMHC tagged with biotin are immobilised to SPR sensor chips via the high-affinity interaction between biotin and streptavidin. This coupling technique allows the MHC molecule to be immobilised in neutral buffer conditions as well as fixing the orientation of immobilised MHC. Consequently, TCR binding to pMHC is measured by flowing TCR over the chip surface. These standards in T cell biophysics allow the comparison of affinities obtained by SPR data in order to describe differences in binding affinity by TCRs specific to a variety of antigens (Bridgeman et al. 2012).

Such biophysical studies have shown that TCRs expressed by tumour-reactive T cell clones recognise their cognate tumour derived antigens using a sub-optimal weak interaction ($K_D > 100$ μM) in both the context of MHC-I and MHC-II presented antigens compared to that of presented pathogenic non-self-antigens (typical $K_D = 25$ μM - 40 μM) (D. Cole et al. 2007) Moreover, tumour reactive TCRs have been described structurally despite exhibiting an affinity for cognate pMHC-II below the detectable sensitivity of SPR instruments (Deng et al. 2007).

Understanding TCR engagement by SPR affinity measurements in conjunction with structural techniques has therefore enabled an understanding of the molecular characteristics of

epitopes recognised by TCRs at high affinity compared to low affinity. Acquisition of such data has therefore begun to describe pMHC surface volumes that elucidate a high affinity T cell response and residues within epitopes which contribute to such a response. Molecular understanding of MHC-II presented epitopes however is limited compared to MHC-I counterparts. In particular, the full extent of the contribution by peptide flanking residues of MHC-II epitopes to TCR binding is under-described (Holland et al. 2013). These peptide flanking region residues, which extend out of the core MHC-II binding region, have been shown to have mixed influence on TCR recognition of pMHC-II molecules (Sant'Angelo et al. 2002; Zavala-Ruiz et al. 2004) Thus, a comprehensive understanding of TCR engagement of MHC-II presented ligands is yet to be achieved.

Knowledge of what makes an immunogenic TCR epitope has led to the structure led design of altered peptide ligands (APLs) with the aim of improving TCR engagement to weak affinity pMHC ligands. Such modifications can be designed to enhance peptide binding to MHC-II in order to increase immunogenicity (Chen et al. 2013). Alternatively, modification of residues with the aim of enhancing pMHC-II engagement by TCRs have also been designed. Such modifications have been to exchange large positively charged residues into the flanking regions of MHC-II presented epitopes in order to optimise TCR binding and thus alter the TCR repertoire (Cole et al. 2012). Indeed, modification of peptide epitopes presented on MHC-I molecules have been incorporated into tumour vaccinations and shown to increase immunogenicity to tumour in the context of melanoma antigens (Parkhurst et al. 1996). Such alterations to MHC-II restricted epitopes not yet been successfully designed to enable enhancement of tumour-derived peptide epitope immunogenicity (Chen et al. 2013).

Together, SPR with x-ray crystallography techniques can be used to therefore describe the efficiency of the TCR/pMHC axis to present and recognise tumour antigens, such as 5T4, and therefore describe the effectiveness of the T cell immune response against cancer. Furthermore, structural and biophysical understanding of 5T4-derived peptide epitopes could be used to infer structure led design of enhanced antigens through the incorporation of APL sequences into tumour vaccines such as MVA-5T4.

3.2.3 Aims

CD4^{+} T cell responses to 5T4-derived peptide antigens presented on MHC-II molecules are detectable in healthy donor PBMCs as well as in patients with colorectal cancer. These responses, however, negatively correlated with progression of disease from stage I to stage III tumours (Martin Scurr et al. 2013). Analysis of the non-diseased human CD4^{+} response to 5T4 within the periphery therefore provides a good model of the effectiveness of the T_H cell response to 5T4 antigen. Such effectiveness is governed by the ability of MHC-II molecules to present 5T4-derived peptide epitopes and for such epitopes to be detected by 5T4-reactive TCRs.

As a result, the overall aim of this chapter was to analyse at the molecular, biophysical and structural level, the efficiency of the TCR/MHC-II recognition/presentation axis of 5T4 derived peptide antigens. Due to the commonality of the HLA-DRB1*0101 allele, as well as the availability of cellular and protein reagents, these studies focus around peptides presented on HLA-DR1. The overall aim of this chapter is divided into the following sub-aims:

(i) To review the current available data to determine candidate immunogenic 5T4-derived peptide antigens

(ii) To assess the MHC restriction of 5T4-reactive CD4^{+} T cell clones

(iii) To characterise the functional sensitivity of 5T4-reactive CD4^{+} T cell clones to peptide antigen

(iv) To assess the ability of 5T4-reactive T cell clones to bind their cognate pMHC-II

(v) To gain structural insights into the molecular presentation of 5T4-peptide antigens on MHC-II molecules.

3.3 Selection of 5T4 epitopes and generation of 5T4-reactive clones

Prior to this project, current data on peptide epitopes of 5T4 presented on MHC-II molecules was reviewed. 5T4-derived peptide epitopes that were known to elicit a CD4⁺ T cell response were consequently chosen for screening and selection of CD4⁺ T cell clones specific to 5T4 peptide antigens.

3.3.1 Immunogenic epitopes of 5T4

Previous studies within our group in Cardiff have highlighted immunogenicity to 5T4 exhibited within the periphery of both a cohort of healthy donors and colorectal cancer patients (detailed in the thesis of Dr. Matthieu Besneux 2015). Such studies characterised a number of peptide epitopes presented on MHC-II alleles to CD4⁺ T cells cultured *in vitro*. Mapping of CD4⁺ T cell epitopes within 5T4 was achieved by culture of CD4⁺ enriched T cell lines to individual peptides and consequent determination of 5T4-peptide-specific responses within cultured lines to peptide via IFNγ ELISpot indicated T cell activation. Here, sixteen candidate peptides, which had previously been identified as immunogenic using pooled peptide screening, were tested for responding cells in a number of individuals of diverse HLA type. These studies highlighted 5T4 epitopes for which there was a presence of tumour-peptide specific T cell populations that exhibited activation in response to stimulation in both healthy donors and colorectal cancer donors (*Figure 3.1; all data and figures adapted from Besneux M., Thesis 2015*).

In general, responses to the candidate 5T4 peptides were higher in healthy individuals compared to patients as signified by an elevated average percentage of positive responders across all peptides (*Figure 3.1a&b*). Despite exhibiting strong frequent responses in healthy donors, responses to immunogenic peptides in healthy donors were decreased amongst the patient cohort. In individuals that did respond to each peptide, however, the magnitude of the response was greater compared to healthy controls (*Figure 3.1c&d*). For example, 5T4 p12 response rates in patients was less than 20 % (~80 % in healthy controls), however, the mean IFNγ response (measured by ELISpot) in those responders was increased more than three-fold to ~250 mean spot forming cells (sfcs)/10^5 cultured cells (75 mean sfcs/10^5 cells in healthy donors). Our group has shown this loss of 5T4 recognition correlates with colorectal tumour progression and is thought to be the result of immune regulation through expansion of CD4⁺ regulatory T cell subsets in advanced disease (Scurr et al. 2013).

In healthy donors, peptide specific CD4⁺ T cells were observed in 50 % or more of tested individuals against five peptides: 5T4p2, p12, p20, p26 & p38; listed in *Table 3.1*. As well as showing a consistent response across donors, these five peptides exhibited a strong response to

peptide as quantified by the mean IFNγ sfcs/10^5 cells in ELISpot assays. As a result of the described data, it was reasoned that study of the 5T4 CD4$^+$ T cell response to these peptides in healthy donors would provide an understanding of how surveillance of tumour antigens such as 5T4 is mediated in individuals without disease and is therefore a model of potential reactive response against 5T4 antigen.
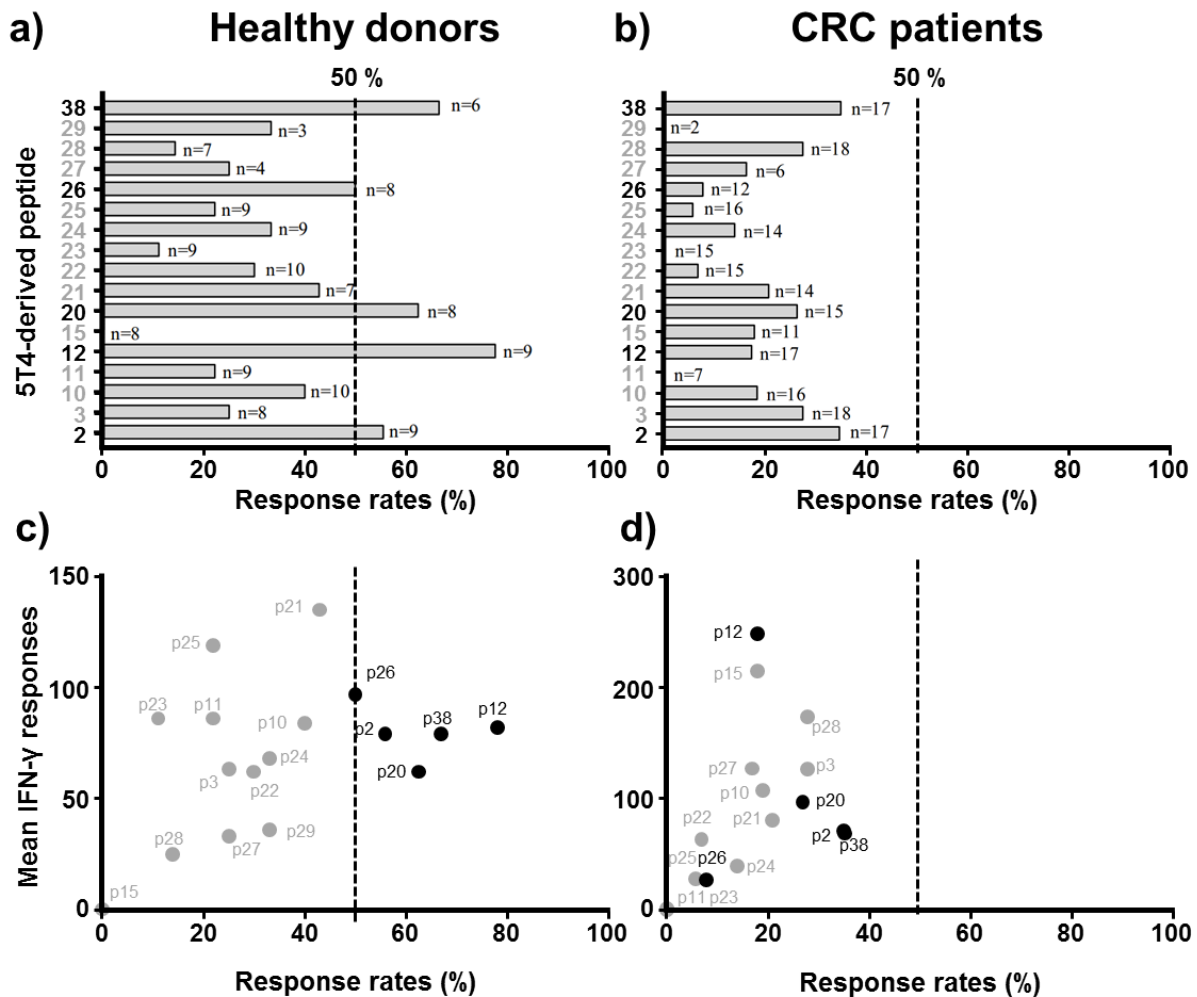
Figure 3.1 – Available data describing immunogenic 5T4 peptide epitopes:

a) Analysis of the percentage response rate of candidate 5T4 peptides (y-axis) to elicit IFNγ indicated activation of CD4^{+} T cell lines cultured *in vitro* from healthy donors via stimulation with queried peptide. 5T4 responses in healthy donors were robust in which responses to five peptides (bold) were observed in more than half of donors. Responders were classified as donors exhibiting ≥25 sfcs/10^5 cells above background and a two-fold increase above background. Inset *n* values represent number of donors tested for each peptide.

b) Analysis of the percentage response rate of candidate 5T4 peptides, as described in *a)*, to elicit CD4^{+} T cell activation of lines cultured from colorectal cancer (CRC) patients. CRC patients showed an overall decrease in percentage responders.

c) 2D-plot of percentage response rate, as described in *a)*, as a function of the magnitude of observed response (mean IFNγ sfcs/10^5 cells) in healthy donors. Five peptides (black dots) exhibited both high response rates and a strong magnitude of response.

d) 2D-plot of percentage response rate and magnitude as described in *c)* in CRC patients. Response rates were lowered in CRC patients, however, those responders exhibited an increased magnitude of response compared to healthy donors.

NB. All responses analysed using data obtained from Besneux, M. Thesis, 2015.

3.3.2 Clone generation strategy

Having reviewed five potential 5T4 epitopes which generated prevalent CD4^{+} T cell responses in the periphery of a cohort of healthy donors, each of the five peptides (*Table 3.1*) were used to generate CD4^{+} T cell clones using a T-cell library parallel generation approach by Dr Garry Dolton (Cardiff University) (Theaker et al. 2016). T cell clones were generated from a pool of CD4^{+} enriched PBMCs from an HLA-DR1^{+} healthy donor (HD216) (*Appendix 2*).

Cultured T cells from a CD4^{+} enriched library were expanded *in vitro* and successfully screened for peptide reactivity against the combined pool of five 5T4 candidate peptides and later individual peptides. IFNγ release in response to peptide was chosen as the principal selection criteria due to the cytokine's role in defining $T_H 1$ cell activation and it's key role in mediating T cell immunity to tumours (Dighe et al. 1994). This selection was achieved by IFNγ release detected by ELISpot assay in response to 5T4-peptide-pulsed HLA-DR1^{+} lymphoblastoid cell line (LCL) presenting cells, termed T2-DR1 cells (Czerkinsky et al. 1983). Thus, presentation of peptide by HLA-DR1 only expressing transduced T2-DR1 cells favoured the selection of T cell clones restricted to HLA-DR1 (HLA-DRB1*0101).

	Origin	Length (aa)	Sequence	Domain origin
5T4 p2	$5T4_{11-30}$	20	AGDGRLRLARLALVLLGWVS	Signal peptide
5T4 p12	$5T4_{111-130}$	20	FARRPPLAELAALNLSGSRL	Extracellular LRR 1-2
5T4 p20	$5T4_{191-210}$	20	QNRSFEGMVVAALLAGRALQ	Extracellular LRR 4-5
5T4 P26	$5T4_{251-270}$	20	YVSFRNLTHLESLHLEDNAL	Extracellular LRR 6-7
5T4 p38	$5T4_{371-390}$	20	LLVLYLNRKGIKKWMHNIRD	Transmembrane/Intracellular

Table 3.1 – Immunogenic 5T4-derived peptides selected for the generation of CD4$^+$ T cell clones

aa = amino acids, LRR = Leucine Rich Repeat

3.4   5T4-reactive CD4$^+$ T cell clones derived from healthy peripheral blood

Three 5T4-reactive T cell clones were generated: (i**) GD.D821** which was cloned in response to **5T4p2**, (ii) **GD.D104** cloned in response to **5T4p12** and (iii) **GD.C112** which was cloned in response to **5T4p38**.

   To examine their molecular phenotype, each clone was first analysed for its TCR clonotype and cell surface expression of TCR, co-receptor and the co-inhibitory molecule LAG-3. In order to characterise the function of these clones *in vitro*, each clone was examined for activation in response to cognate peptide presented on an allele of restriction, assayed for the production of functional cytokines/chemokines in response to cognate peptide and analysed for the comparative sensitivity of each clone.

3.4.1   Clonotyping

To clarify the clonality of each generated T cell clone and provide sequence definition of the TCRs expressed by each clone, the transcribed TCR sequences from each clone was sequenced through TCR clonotyping performed by Dr Meriem Attaf (Cardiff University). These data confirmed each T cell clone to indeed be clonal and derived from a unique recombination event as shown by three independent clonotypes (*Table 3.2*). Overall, the acquisition of these sequences characterise three unique 5T4-reactive clones with differential antigen binding receptors of which the translated protein sequence is known.

		TCRα			TCRβ			
Clone	Antigen	TRAV	TRAJ	CDR3	TRBV	TRBJ	TRBD	CDR3
GD.D821	5T4 p2	19	23	CALSEGLIYNQGGKLIF	7-2	1-5	2	CASSLESGLANQPQHF
GD.D104	5T4 p12	12-1	45	CVVNRYSGGGADGLTF	2	2-7	2	CASRGGSSYEQYF
GD.C112	5T4 p38	23/DV6	57	CAAEDQGGSEKLVF	5-1	2-4	2	CASSLVDGDIQYF

Table 3.2 – Unique clonotype of three 5T4-reactive T cell clones

TRAV = T cell receptor alpha variable, TRAJ = T cell receptor alpha joining, CDR = Complementarity determining region, TRBV = T cell receptor beta variable, TRBJ = T cell receptor beta joining & TRBD = T cell receptor beta diversity.

3.4.2 Unstimulated 5T4-reactive T cell clones are competent to antigen stimulation

In order to assess whether each T cell clone was antigen receptor and co-receptor replete, and thus liable to antigen stimulation, each clone was co-stained with CD4 and pan-TCR antibodies and analysed by flow cytometry. Each clone exhibited detectable surface co-expression of TCR and CD4 co-receptor (*Figure 3.2a*). GD.D821 and GD.D104 clones exhibited almost no heterogeneity in antigen receptor and co-receptor expression status as signified by 99 and 98 % of live T cell clones $CD4^+TCR^+$ dual-positive, respectively. Whilst the cultured GD.C112 clonotypic cells were also broadly $CD4^+ TCR^+$, dual-positive cells were limited to 88 % of live T cell clones highlighting an overall heterogeneity in TCR expression amongst the clonotypic population. Such heterogeneity was caused by an observed downregulation in TCR expression compared to GD.D821 and GD.D104 clones as signified by a population (11 % of live T cells) of $CD4^+ TCR^-$ cells. Such downregulation of TCR is typical in $CD4^+$ T cells as a result of recent T cell activation (Gallegos et al. 2016).

Having established that each of the T cell clones express antigen receptor and co-receptor, each clone was next checked for constitutive expression of the co-inhibitory molecule LAG-3 which, as discussed further in Chapter 4, can cause inhibition of T cell activation (Liang et al. 2008). LAG-3 expression by $CD4^+$ cells, across all clones, was minimal with less than 1 % of live $CD4^+$ T cells expressing the co-inhibitory molecule (*Figure 3.2b*). As a result, in unstimulated culture conditions, the generated 5T4-reactive T cell clones appear competent to receive antigen stimulation as indicated by the cell surface expression of markers tested.
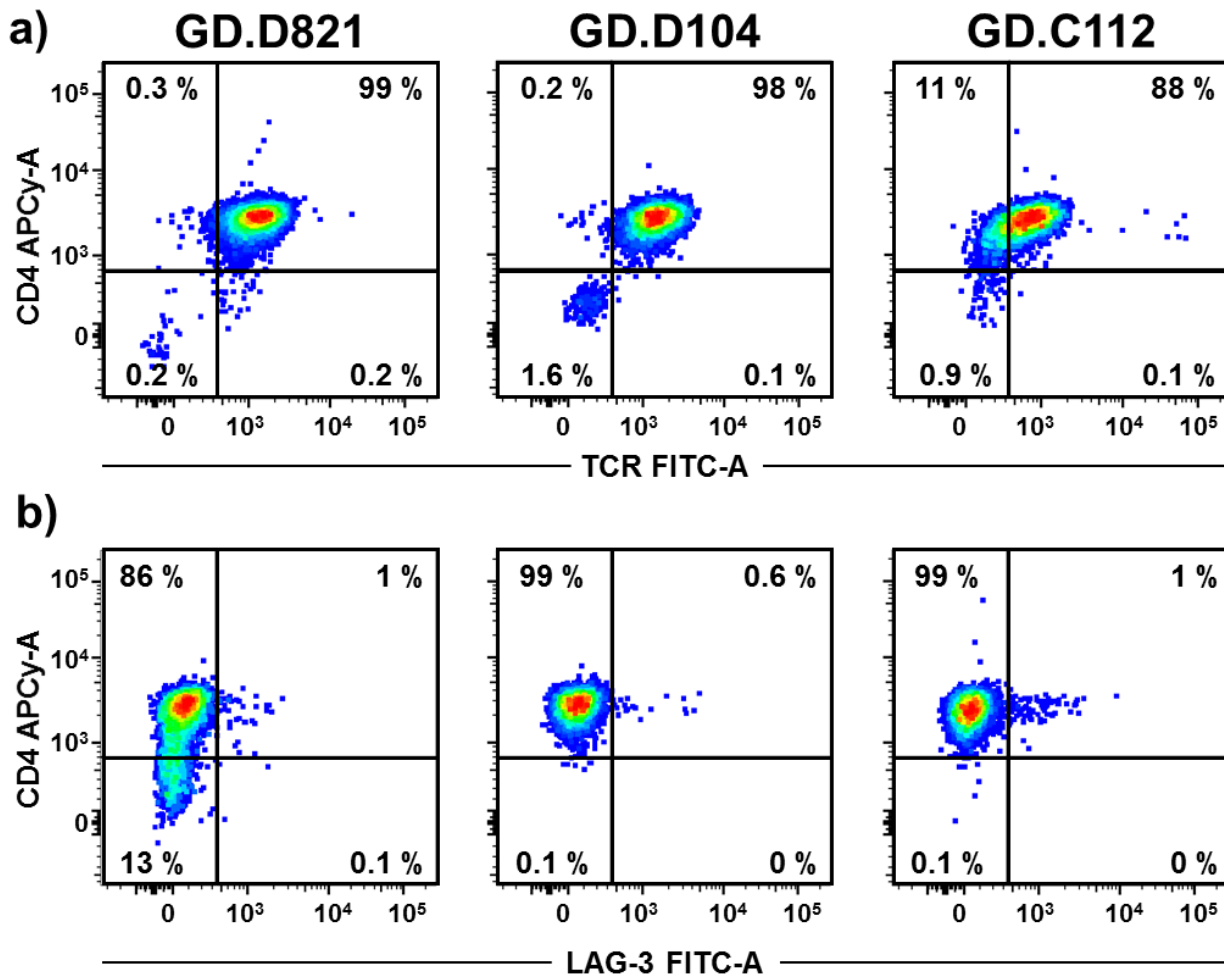
Figure 3.2 – Surface expression characterisation of 5T4-reactive T cell clones:

a) Flow cytometric analysis of CD4 and TCR expression of the three 5T4-reactive T cell clones. Each clone exhibited expression of both antigen receptor and co-receptor as indicated by > 88 % of cells CD4^{+} TCR^{+}. Quadrant gates set according to FMO/unstained negative control populations. 2D plots representative of two independent experiments.

b) Flow cytometric analysis of CD4 and LAG-3 expression of the three 5T4-reactive T cell clones. Each clone exhibited minimal staining of LAG-3 surface expression as indicated by < 1 % of CD4^{+} cells expressing detectable LAG-3. Quadrant gates set according to FMO/unstained negative control populations. 2D plots representative of two independent experiments.

3.4.3 Determination of restriction of 5T4-reactive T cell clones to HLA-DR

Whilst the selection criteria for the generation of these clones included an ability to respond and activate in the presence of HLA-DR1 replete presenting cells, such assays did not rule out the possibility of self-presentation between T cell to T cell on HLA molecules of other alleles expressed on the surface of the T cell clones themselves. As a result, each T cell clone was analysed for the ability to release IFNγ as a surrogate marker for T cell activation by ELISpot in response to peptide pulsed APCs performed at low T cell numbers (300 T cells per well) and an excess of presenting cells (50,000 per well).

Each of the three generated 5T4-reactive T cell clones showed peptide specific release of IFNγ in response to overnight incubation with autologous corresponding peptide-pulsed B lymphoblastoid cell line (B-LCL) presenting cells as shown by IFNγ ELISpot assay (*Figure 3.3a*). Each clone exhibited maximal IFNγ release compared to PHA control in response to autologous B-LCL presenters pulsed with 10^{-5} M of corresponding peptide as shown by equivalent number of IFNγ spot forming cells (sfcs) equating to approximately 100 % of maximal (PHA) response.

In order to indicate restriction to HLA-DR molecules, blockade of HLA-DR molecules with a pan anti-DR antibody, after peptide pulsing and before co-incubation with T cells, abrogated the IFNγ release by each corresponding cognate T cell clone. Blockade of -DR molecules was most effective on 5T4p2 presentation to GD.D821 in which activation was reduced to background levels of IFNγ release (~100 % blockade). Likewise, blockade of DR molecules on 5T4p38 presentation to GD.C112 abrogated IFNγ release by ~60 %. Blockade of 5T4p12 presentation to GD.D104 had a less marked effect (~30 % blockade) on peptide-specific activation and consequent IFNγ release thus suggesting that (i) the GD.D104 clone may not be restricted by HLA-DR, (ii) the GD.D104 may exhibit increased sensitivity to 5T4p12 compared to the GD.D821 and GD.C112 clones or (iii) the 5T4p12 peptide has an increased affinity for the restricted HLA molecule compared to 5T4p2 or 5T4p38.

In order to test whether each clone exhibited dose-dependent response to cognate peptide presented on pulsed APCs, T cell clones were stimulated with 10 times reduced concentration of peptide (10^{-6} M) and, once again, analysed for the effect of pan anti-DR blockade on T cell clone activation (*Figure 3.3b*). At 10^{-6} M GD.D821 and GD.C112 exhibited ablation or reduction of activation, respectively, whilst GD.D104 remained maximally stimulated despite reduction in peptide concentration.
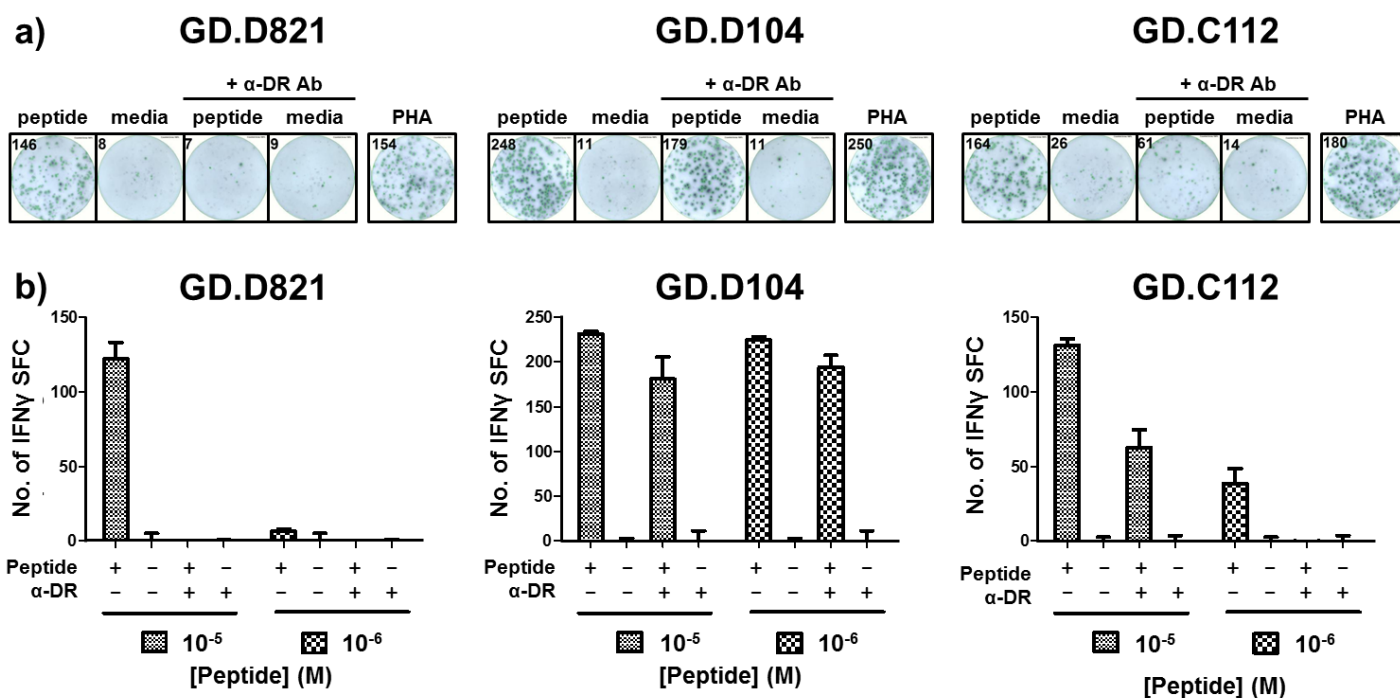
Figure 3.3 – Validation of HLA-DR restriction of 5T4-reactive CD4⁺ T cell clones:

a) IFNγ ELISpot assays on the three 5T4-reactive T cell clones showing peptide specific activation of T cell clones in response to overnight co-incubation with 10^{-5} M cognate peptide-pulsed autologous B-LCL presenter cells. Peptide-specific IFNγ release (peptide) is observed compared to no-peptide controls (media) and is abrogated by the blocking of DR molecules on peptide pulsed B-LCL presenter cells (+ α-DR Ab) prior to co-incubation with corresponding T cell clone. Phytohaemagglutinin (PHA) positive control wells indicate maximal IFNγ T cell clone response. Inset numbers represent raw spot forming cells (sfcs) counts. Presented ELISpot wells representative of experiments performed in duplicate on 300 T cells per well.

b) Mean background subtracted quantification of IFNγ sfcs for assays as shown in a) performed at 10^{-5} and 10^{-6} M concentration of peptide. Peptide-specific response (+) was observed compared to no-peptide control (-) as well as abrogation of IFNγ release by α-DR blocking (+) compared PBS control (-). Plotted mean values are background subtracted by equivalent no-peptide control and calculated from experiments in duplicate (error bars = SEM).

To further narrow the HLA restriction of the three generated 5T4-reactive T cell clones as being indeed restricted to 5T4-derived peptides presented on the HLA-DR1 molecule, each of the three clones were analysed for IFNγ release indicated activation by peptide-pulsed presenters which express HLA-DR1 as the only MHC-II molecule at the cell surface (T2-DR1 cells) in comparison to HLA-DR1 null cells (T2-WT).

As with autologous presenters, each T cell clone exhibited corresponding peptide specific activation of T cells as indicated by an increase in IFNγ sfcs compared to no-peptide media only control (*Figure 3.4a*). Such activation was observed in HLA-DR1 expressing cells (T2-DR1) only and not observed in HLA-DR1 deficient cells (T2-WT) providing direct evidence of HLA-DR1 restriction; including the GD.D104 clone, which, in B-LCL assays was minimally effected by anti-DR blockade. Moreover, inclusion of anti-DR blocking once more abrogated the degree of IFNγ indicated activation of each T cell clone in the presence of HLA-DR1 replete presenting cells. Sensitivity of each clone followed a similar trend compared to autologous B cell presented experiments described previously. All clones exhibited less activation using T2-DR1 presenters compared to B-LCLs except GD.D104. Similarly, only the GD.D104 clone was sensitive to 10^{-6} M peptide, suggesting this clone is the most sensitive to antigen (*Figure 3.4b*).

These data therefore show direct requirement for HLA-DR1 in the peptide specific activation of the generated CD4$^+$ 5T4-reactive T cell clones. In addition, these data once more highlight the difference in efficiency of the T cell activation-peptide presentation axis between each of the three 5T4-reactive T cell clones and their HLA-DR1 presented 5T4-derived peptides.
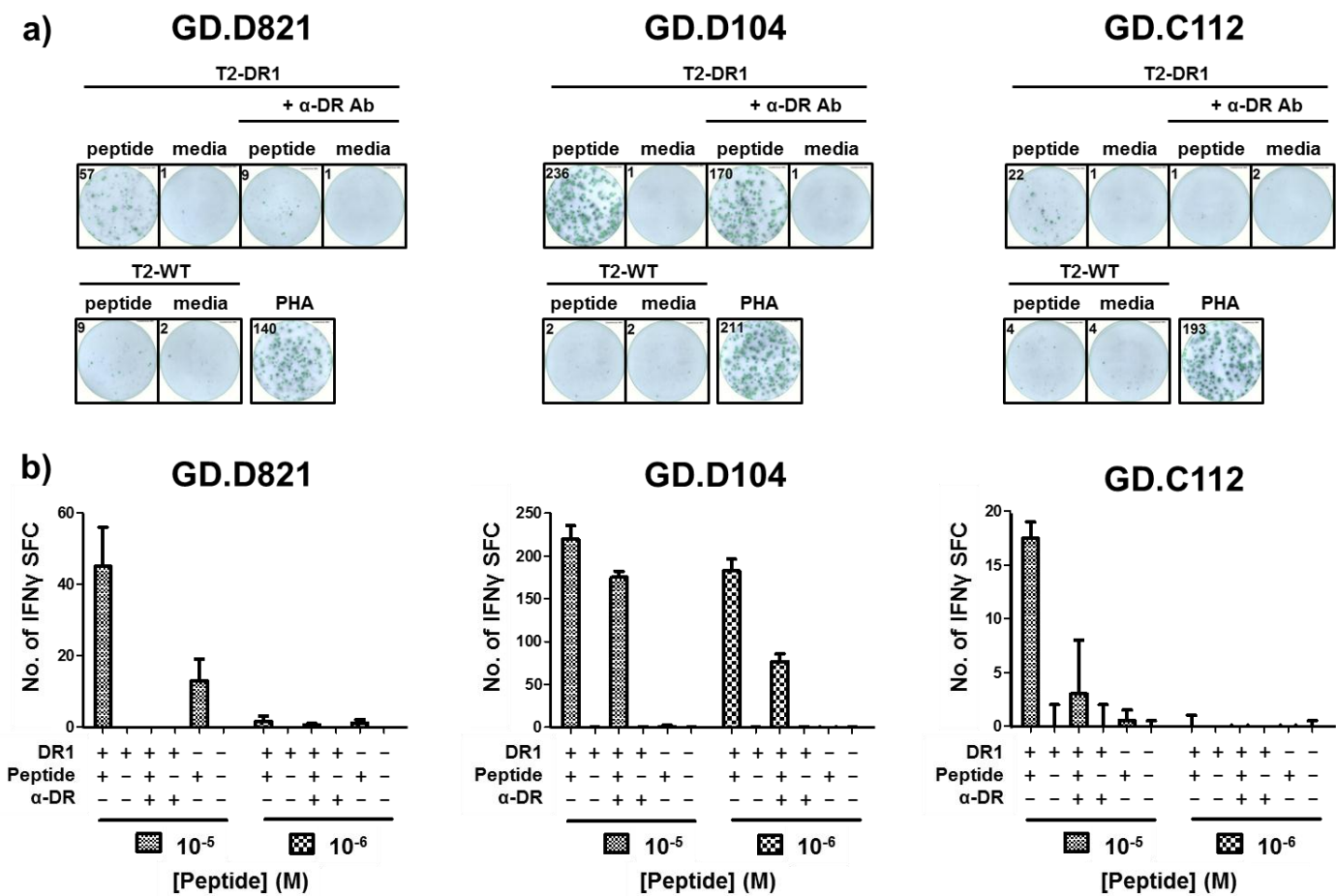
Figure 3.4 – Validation of HLA-DR1 restriction of 5T4-reactive CD4⁺ T cell clones:

a) IFNγ ELISpot assays on the three 5T4-reactive T cell clones showing peptide specific activation of T cell clones in response to overnight co-incubation with 10-5 M cognate peptide-pulsed DR1-transfected (T2-DR1) and DR1-null (T2-WT) presenters. Peptide-specific IFNγ release (peptide) was observed with T2-DR1 presenters compared to no-peptide controls (media) and was abrogated by the blocking of DR molecules on peptide pulsed T2-DR1 presenter cells (+ α-DR Ab) prior to co-incubation with corresponding T cell clone. Equivalent responses are not observed with DR1-null (T2-WT) presenters. PHA wells indicate maximal IFNγ T cell clone response. Inset numbers represent raw spot forming cells (sfcs). Presented ELISpot wells are representative of experiments performed in duplicate.

b) Mean background subtracted quantification of number of IFNγ sfc for assays as shown in a) performed at 10-5 and 10-6 M concentration of peptide. Peptide-specific responses (+) were observed compared to no-peptide control (-) with DR1-expressing (DR1 +) compared to DR1-null (DR1 -) presenters. Abrogation of IFNγ release by α-DR blocking (+) compared to PBS control (-) was also observed with DR1-transfected presenters. Plotted mean values are background subtracted by equivalent no-peptide control and calculated from experiments in duplicate (error bars = SEM).

3.4.4   Functional cytokine release in response to HLA-DR1 presented 5T4 epitopes

Having observed differences in sensitivity amongst the 5T4-reactive T cell clones, it was reasoned that each clone may produce different functional markers of activation. As a result, each clone was subjected to T cell activation assays in response to titrating concentration of cognate peptide presented by HLA-DR1 only expressing cells and functional cytokine/chemokine release measured by ELISA (*Figure 3.5*).

3.4.4.1   MIP-1β

Each clone, in response to titrating concentration of corresponding 5T4-derived peptides presented on T2-DR1 cells, produced titrating amounts of the early activation marker MIP-1β (*Figure 3.5a*). Each clone exhibited sensitivity to peptide within a similar sensitivity range and resulted in a similar maximal chemokine release. GD.D104 remained the most sensitive clone to cognate peptide as indicated by an EC_{50} of $10^{-7.0}$ M peptide. GD.D821 was the second most sensitive; EC_{50} of $10^{-6.3}$ M. Maximal MIP-1β response for GD.C112, and consequent calculation of an accurate EC_{50} sensitivity value, proved difficult to achieve due to lack of solubility at concentrations of peptide above 10^{-5} M. Despite this, using MIP-1β as a marker for T cell activation, all three T cell clones were indeed responsive to peptide presented in the context of HLA-DR1.

3.4.4.2   IFNγ

Analysis of the T_H1 type 1 inflammatory cytokine, IFNγ, expression by each clone highlighted that the GD.D821 and GD.C112 clones are poorer IFNγ producers in response to titrating peptide (*Figure 3.5b*). Whilst induction of IFNγ was possible in these two clones, considerable IFNγ release was not detected until high concentrations of peptide (GD.D821: 10^{-4} M and GD.D104: 10^{-5} M). The maximal release of IFNγ by these two clones was not determined due to the requirement of such high concentrations of peptide. It is worth noting, however, that maximal IFNγ release by GD.C112 may be hampered by the solubility of the 5T4p38 peptide at concentrations above 10^{-5} M.
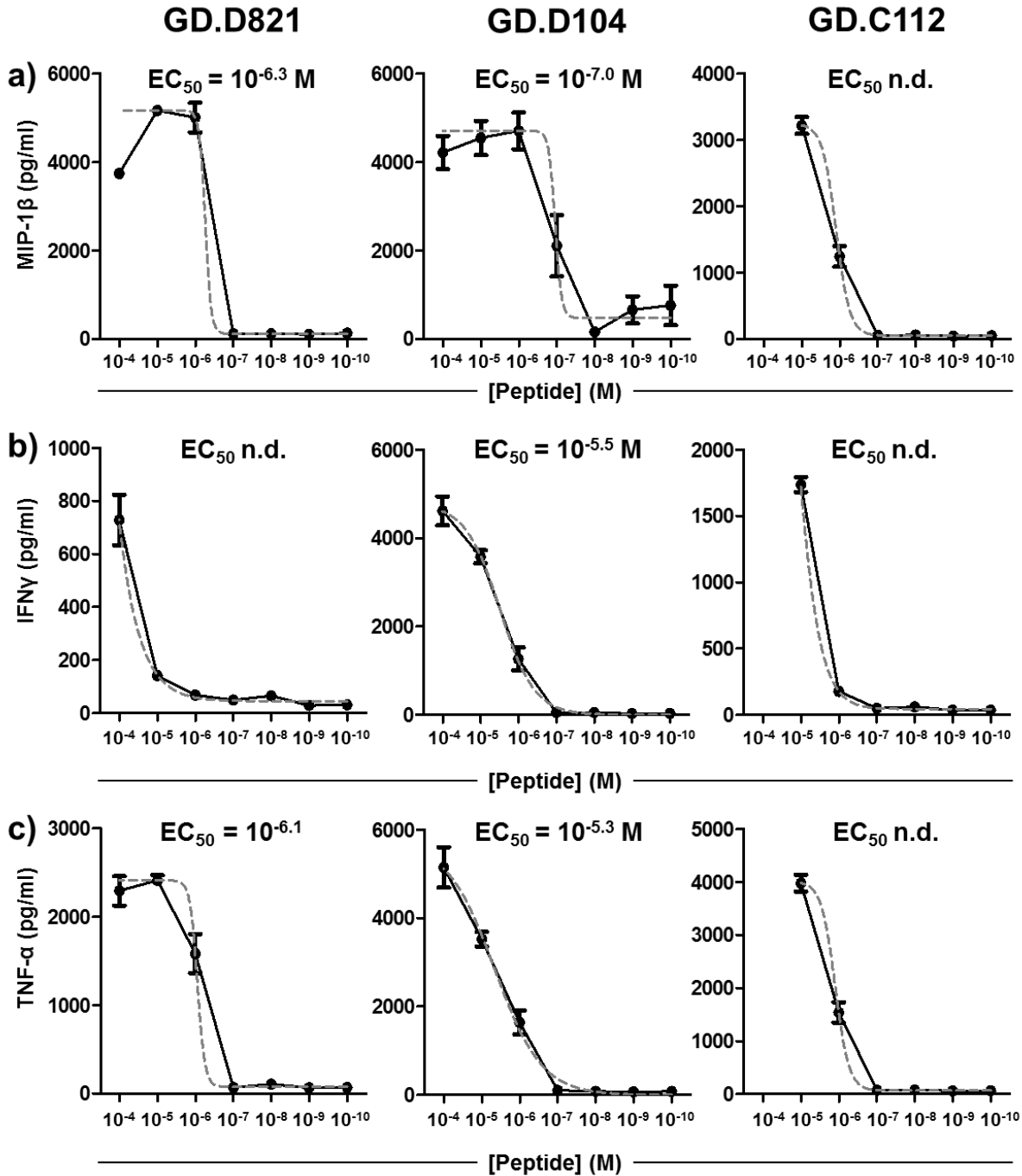
Figure 3.5 – 5T4-reactive T cell sensitivity and functional cytokine/chemokine release:

a) Background (no peptide) subtracted MIP-1β release in response to overnight co-culture of GD.D821, GD.D104 and GD.C112 clones with HLA-DR1 only (T2-DR1) presenting cells and titrated concentrations of cognate peptide. Dashed lines (grey) show non-linear log(agonist) vs response curve fitting from which EC_{50} value (inset, in Molar; n.d. = not determined) is calculated. Error bars = SEM, experiments performed in triplicate and representative of two independent experiments.

b) Background subtracted IFNγ release in response to HLA-DR1 presented cognate peptide as described in ***a).***

c) Background subtracted IFNγ release in response to HLA-DR1 presented cognate peptide as described in ***a).***

On the other hand, release of IFNγ by GD.D104 was robust and detectable down to lower concentrations of peptide (10^{-6} M). In addition, maximal release observed at 10^{-4} M or 10^{-5} M peptide was greatest amongst the three clones. As a result, the GD.D104 is a sensitive IFNγ producing 5T4-reactive T cell clone to cognate peptide characterised by a low EC_{50} of $10^{-5.5}$ M peptide. These data highlight that IFNγ remains a good marker for T cell activation of the GD.D104 clone, however, stimulation of GD.D821 and GD.C112 requires much higher concentration of peptide to induce IFNγ release.

3.4.4.3 TNF-α

Each clone was next tested for the release of TNF-α in response to peptide. Like MIP-1β, production of TNF-α release was much more consistent throughout the three clones (*Figure 3.5c*). Indeed GD.D821 and GD.C112 clones, which were poor IFNγ producers in response to peptide, exhibited robust release of TNF-α in response to lower titrated concentrations of peptide (10^{-4} M or 10^{-5} M). Similarly, GD.D104 also produced TNF-α in response to lower peptide concentrations suggesting that this clone is a strong dual producer of both these T_H1 cytokines. GD.D821 exhibited increased TNF-α sensitivity to peptide compared to GD.D104 with an EC_{50} of $10^{-5.3}$ M peptide. Despite an undeterminable EC_{50} value for the TNF-α sensitivity of GD.C112, production of TNF-α at the highest testable concentration of peptide (10^{-5} M) resulted in the highest TNF-α release quantified out of all three clones.

3.4.4.4 Summary of cytokine/chemokine profile

Each of the three 5T4-reactive T cell clones produce three markers of T cell activation and consequent function; MIP-1β, IFNγ and TNF-α, in response to cognate peptide and HLA-DR1 only expressing cells. The release of each cytokine/chemokine, however, occurred to varying degrees of sensitivity (summarised in *Table 3.3*). Expression of IFNγ and TNF-α strongly indicate that these 5T4-reactive T cell clones derived from the T_H1 subset of CD4^{+} T cells within the peripheral blood of a healthy donor.

Clone	Restriction	Antigen	MIP-1β	IFNγ	TNF-α
GD.D821	HLA-DR1	5T4 p2	+++ (-6.3)	+ (n.d.)	+++ (-6.1)
GD.D104	HLA-DR1	5T4 p12	+++ (-7.0)	+++ (-5.5)	++ (-5.3)
GD.C112	HLA-DR1	5T4 p38	+++ (n.d.)	++ (n.d.)	+++ (n.d.)

Table 3.3 – Summary of 5T4-reactive T cell clone cytokine/chemokine sensitivity to peptide
Scored sensitivity to release stated cytokine/chemokine in response to decreasing concentration of peptide. Sensitivity graded from least sensitive (+) to most sensitive (+++). Calculated $logEC_{50}$ values are recorded in parentheses. $logEC_{50}$ values for GD.C112 could not be determined (n.d.) due to lack of solubility at concentrations higher than 10^{-6} M. IFNγ release $logEC_{50}$ was also not determined due to failure to reach maximal IFNγ release by 10^{+4} M peptide.

3.5 Minimal detectable recognition by 5T4-reactive T cell clones

Differential sensitivities to antigen by the 5T4-reactive T cell clones may be contributed to (a) each 5T4-derived peptide exhibiting a different binding affinity for HLA-DR1, and hence peptide-HLA stability, and thus modulating the effective cognate pHLA-DR1 ligand concentration, (b) TCR engagement by each of the T cell clones occurring at differing affinities (c) a combination of both or (d) other factors out with TCR-pMHC engagement. As a result, cellular and biophysical analysis of cognate pHLA-DR1 engagement by each T cell clone were attempted using recombinantly produced 5T4-derived pHLA-DR1 molecules and 5T4-reactive T cell clone expressed TCRs to assay the effectiveness of presentation/recognition of antigen.

3.5.1 Prediction of 5T4-derived peptide binding affinity to HLA-DR1

To give an indication as to the potential affinity of each 5T4-derived peptide for HLA-DR1, each peptide was analysed for predicted binding affinity to HLA-DR1 using the peptide to HLA neural network prediction server *NetMHCII 2.2* (Nielsen & Lund 2009). As such, each peptide sequence was predicted to capably bind HLA-DR1 (*Table 3.4*). 5T4p2 and 5T4p12 were classified as predicted strong binders for HLA-DR1 (IC50 < 50 nM) whilst 5T4p38 was classified as a weak binder (IC50 = 50 - 500 nM). This analysis, therefore, gives an indication as to the quality of each 5T4-derived peptide to be presented to each corresponding cognate clone. Examination of the predicted core region of 5T4p38 binding to HLA-DR1 highlights a sub-optimal peptide sequence based on the known preference for amino acids at binding peptide binding pockets; most notably P4 and P9 where Arg and Lys, respectively, are not favoured residues (Cole & Godkin 2016).

Peptide epitope	Predicted binding core	Predicted affinity IC$_{50}$ (nM)
5T4p2	AGDGR<u>LRLARLALVL</u>LGWVS	14.1
5T4p12	FARRPP<u>LAELAALNL</u>SGSRL	8.0
5T4p38	LLVL<u>YLNRKGIKK</u>WMHNIRD	77.5

Table 3.4 – Prediction of 5T4-derived peptide binding core and affinity to HLA-DR1
Underlined peptide sequence = predicted binding core region

3.5.2   5T4-reactive T cell clones bind poorly to cognate pMHC-II multimers

Having shown T cell clone sensitivity to peptide and a requirement for HLA-DR1, each T cell clone was analysed for their ability to bind corresponding MHC-II multimers by flow cytometry.

3.5.2.1   Production of 5T4-derived MHC-II monomers for T cell clone multimer staining

To study the ability of TCR binding to cognate 5T4-derived pMHC-II epitopes, highly functional pHLA-DR1 monomers were successfully produced from *in vitro* refolding of human HLA-DR1 molecules produced in *E. coli* using methods described previously (Frayser et al. 1999). Each 5T4-derived pHLA-DR1 monomer was successfully biotinylated, in order to facilitate multimerisation, as shown by characteristic alteration in the electrophoretic mobility of the biotinylated HLA-DR1α chains in the presence of streptavidin (*Figure 3.6*). Moreover, each pHLA-DR1 monomer was shown to be functional by interaction with LAG-3^{+} cells as described in Chapter 4 (data not shown).

3.5.2.2   Multimer staining of 5T4-reactive T cell clones with cognate pMHC-II molecules

Given that each 5T4-reactive T cell clone successfully activated in response to cognate 5T4-derived peptide presented on HLA-DR1, each of the three T cell clones were stained with cognate 5T4-derived pMHC-II using dextramerised pHLA-DR1 molecules using an optimised protocol for the staining of low affinity self-antigen reactive T cells (Dolton et al. 2014; Dolton et al. 2015). Using this methodology, low affinity antigen specific T cells are detectable via multimer staining and have been used to stain viral-reactive MHC-II restricted T cell clones (Tungatt et al. 2015).

Despite this protocol, however, the 5T4-reactive T cell clones stained poorly with their cognate 5T4-derived pHLA-DR1 multimers (*Figure 3.7*). Only the GD.D821 clone marginally stained with cognate 5T4p2-HLA-DR1 multimers (*Figure 3.7a*) as shown by a small increase in tetramer positive cells (4.96 %) compared to irrelevant HLA-DR1 multimer control (0.03 %) and an approximate doubling (91 % increase) in geometric mean fluorescence intensity (gMFI) in HLA-DR1 5T4p2 multimer stained (gMFI = 222) compared to background fluorescence intensity observed with HLA-DR1 multimer stained control (gMFI = 116). In contrast, GD.D104 exhibited HLA-DR1 5T4p12 multimer staining (*Figure 3.7b*) only slightly above background (0.05 % tetramer positive) compared to irrelevant control staining (0.02 % tetramer positive), signified by a 34 % increase in gMFI (HLA-DR1 5T4p12 gMFI = 144, irrelevant pHLA-DR1 = 108). Similarly, GD.C112 exhibited HLA-DR1 5T4p38 multimer effectively equal to background (HLA-DR1 5T4p38: 0.04 % tetramer positive, irrelevant pHLA-DR1: 0.02 % tetramer
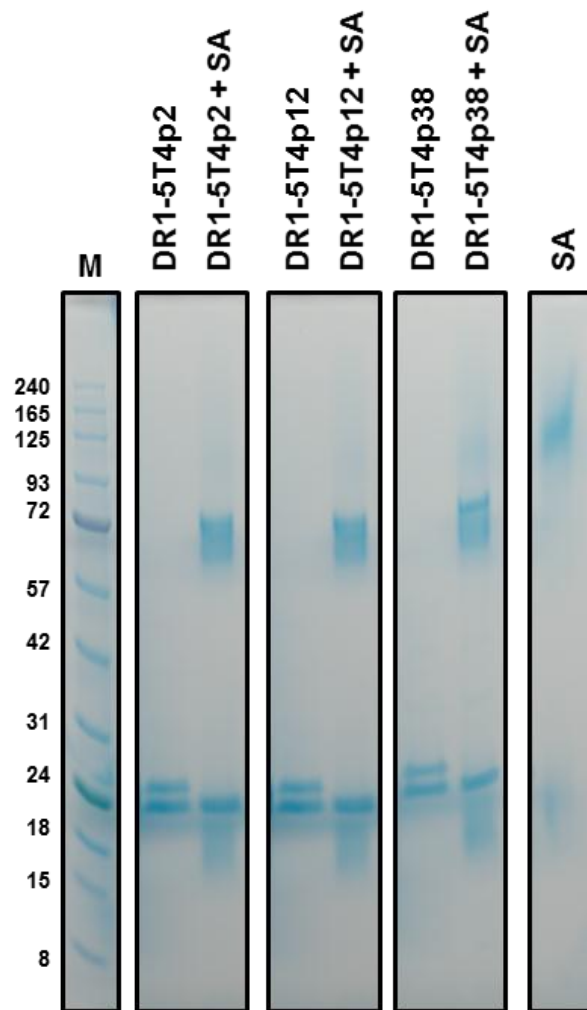
Figure 3.6 – Generation of biotinylated 5T4-derived pHLA-DR1 monomers:

SDS-PAGE analysis of purified biotinylated pHLA-DR1 monomers refolded with 5T4-derived peptides from inclusion bodies produced in *E. coli* in non-reducing conditions. Each monomer, DR1-5T4p2, DR1-5T4p12 and DR1-5T4p38, showed characteristic shift in electrophoretic mobility of biotinylated pHLA-DR1α chain when incubated with streptavidin (+ SA).

positive characterised by a less than 5 % increase in gMFI (5T4p38-HLA-DR1 gMFI = 113, irrelevant pHLA-DR1 = 108; *Figure 3.7c*).

These data, with the exception of 5T4p2-HLA-DR1 recognition by GD.D821, suggest a practically undetectable interaction between the 5T4-reactive T cell clones and cognate pHLA using enhanced methodologies to detect low affinity TCR-pMHC interactions. Detectable staining of 5T4p2-HLA-DR1 multimer binding to GD.D821 suggests the GD.D821 TCR may interact with the 5T4p2-HLA-DR1 antigen with the strongest affinity out of the three 5T4-reactive T cell clones.
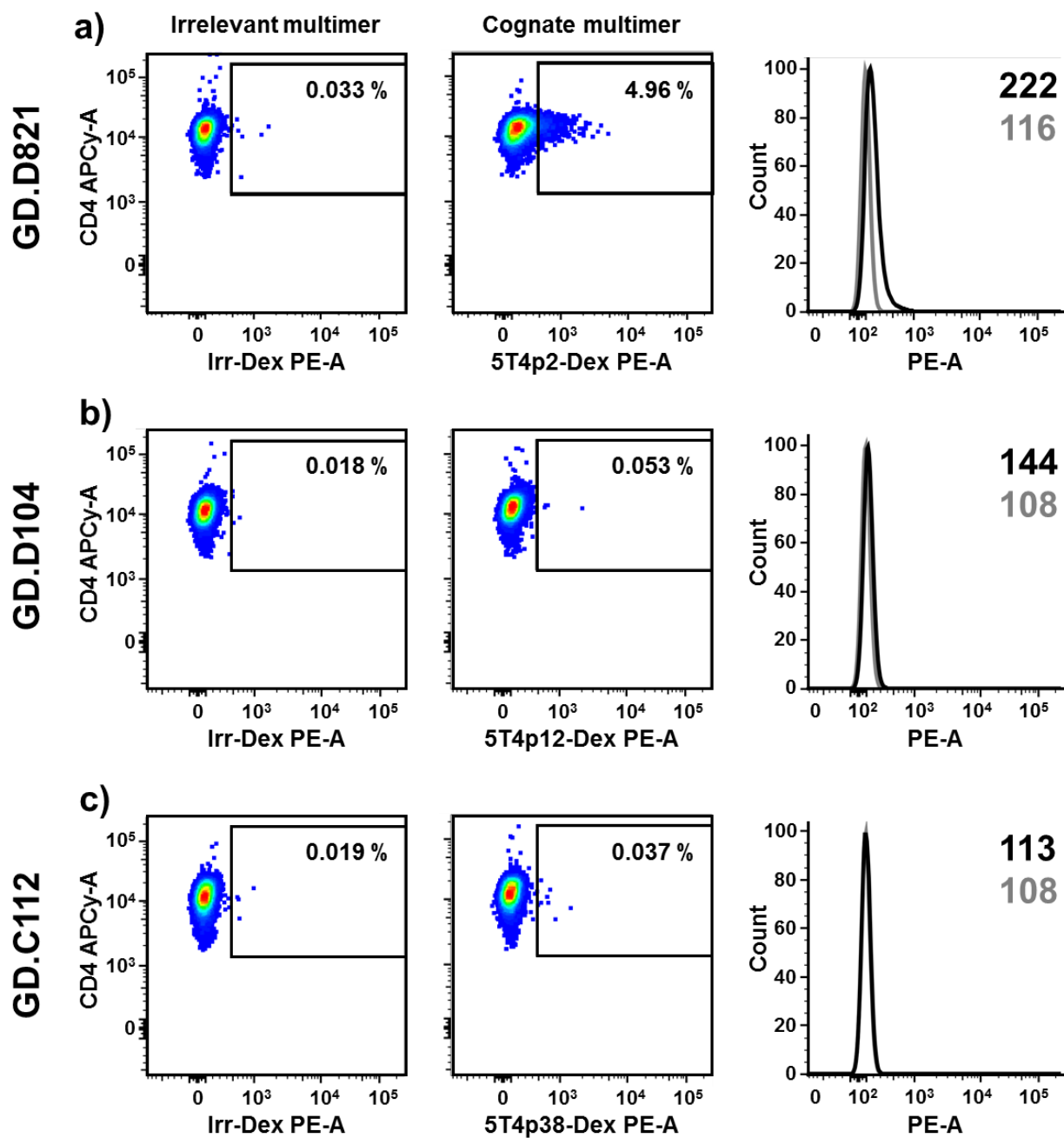
Figure 3.7 – Minimal staining of 5T4-reactive T cell clones by cognate pMHC-II multimers:
a) Flow cytometric analysis of pHLA-DR1 multimer staining of the 5T4p2-reactive clone GD.D821. 2D plots highlight difference in CD4$^+$ multimer$^+$ cells when stained with the cognate multimer (5T4p2-Dex) or irrelevant multimer (Irr-Dex) with onset numbers representing percentage of multimer$^+$ cells in parent gate. Histograms represent shift in fluorescence intensity observed when stained with the PE-conjugated cognate multimer (black) compared to irrelevant multimer (grey); inset numbers = gMFI. Plots and histograms representative of two independent experiments. Displayed plots gated on live, CD4$^+$ singlet lymphocytes.

b) Flow cytometric analysis of pHLA-DR1 multimer staining of the 5T4p12-reactive clone GD.D104 as described in ***a).***

c) Flow cytometric analysis of pHLA-DR1 multimer staining of the 5T4p38-reactive clone GD.C112 as described in ***a).***

3.5.3 Minimal binding of 5T4-reactive TCR to 5T4p38 presented on HLA-DR1

Having observed that three 5T4-reactive T cell clones all exhibited poor or no observable staining via MHC-II multimers, it was hypothesised that the expressed TCRs by each T cell clone bound cognate 5T4-derived pHLA-DR1 molecules with a weak affinity. In order to assay the binding affinity of TCRs expressed by the 5T4-reactive T cell clones directly, soluble TCRs and 5T4-bearing HLA-DR1 molecules were produced and measurement of binding attempted through surface plasmon resonance (SPR). In these preliminary studies, each TCR expressed as inclusion bodies using methodologies to produce soluble TCR molecules from *E. coli* (*Appendix 3a*) (Boulter et al. 2003). Despite expression of all chains in *E. coli*, refolding of each 5T4-reactive TCR encountered varying success (outlined in *Appendix 3b*). Out of the three available TCRs, only the HLA-DR1 5T4p38-reactive GD.C112 TCR was able to successfully refold *in vitro* as indicated by characteristic complexing of TCRα and TCRβ chains in non-reducing SDS-PAGE analysis (*Appendix 3c*). Analysis of GD.C112 TCR binding to HLA-DR1 5T4p38 via SPR resulted in a small but increasing signal in response to increasing TCR concentrations (*Appendix 4*). Such binding, therefore, suggested a weak but detectable interaction between the GD.C112 TCR expressed by this 5T4-reactive T cell clone and the 5T4p38 peptide restricted to HLA-DR1, however, further SPR experiments using higher TCR concentrations would be required to accurately measure the TCR binding affinity.

3.6 Structural characteristics of a 5T4 tumour epitope presented by HLA-DR1

The ability for CD4^{+} T cells to recognise tumour derived peptide antigens is determined by the ability to both present and recognise such peptide molecules presented on MHC-II molecules such as HLA-DR1. In order to therefore gain insights into (a) how the 5T4-derived peptides are able to be presented on their restricted MHC molecule, HLA-DR1 and (b) the molecular characteristics of the peptides presented to TCR molecules bound to MHC, the 5T4-derived peptides bound to HLA-DR1 were studied through recombinant production of protein samples for study via x-ray crystallography.

3.6.1 Production of HLA-DR1 presenting the 5T4p12 tumour antigen for structural analysis

Protein crystallisation generally requires a highly pure and highly homogenous soluble protein sample. Due to the low refold efficiency of HLA-DR1, typically between $1 - 10$ %, an affinity purification step, as published previous, was implemented into standard protocol for the production of HLA-DR1 molecules (*Figure 3.8a*) (Stern & Wiley 1992). These methodologies allowed separation of non-binding wash fractions from bound HLA-DR1 bearing elution fractions and allowed the highly efficient purification of desired protein in a single-step (*Figure 3.8b*). For this study HLA-DR1 molecules were refolded in the presence of the three 5T4-derived peptides, 5T4p2, 5T4p12 and 5T4p38 for crystallisation trials. Each 5T4-derived peptide successfully refolded with similar yield in order to obtain milligram quantities of highly pure protein sample required for screening of crystallisation conditions (*Figure 3.8c*).
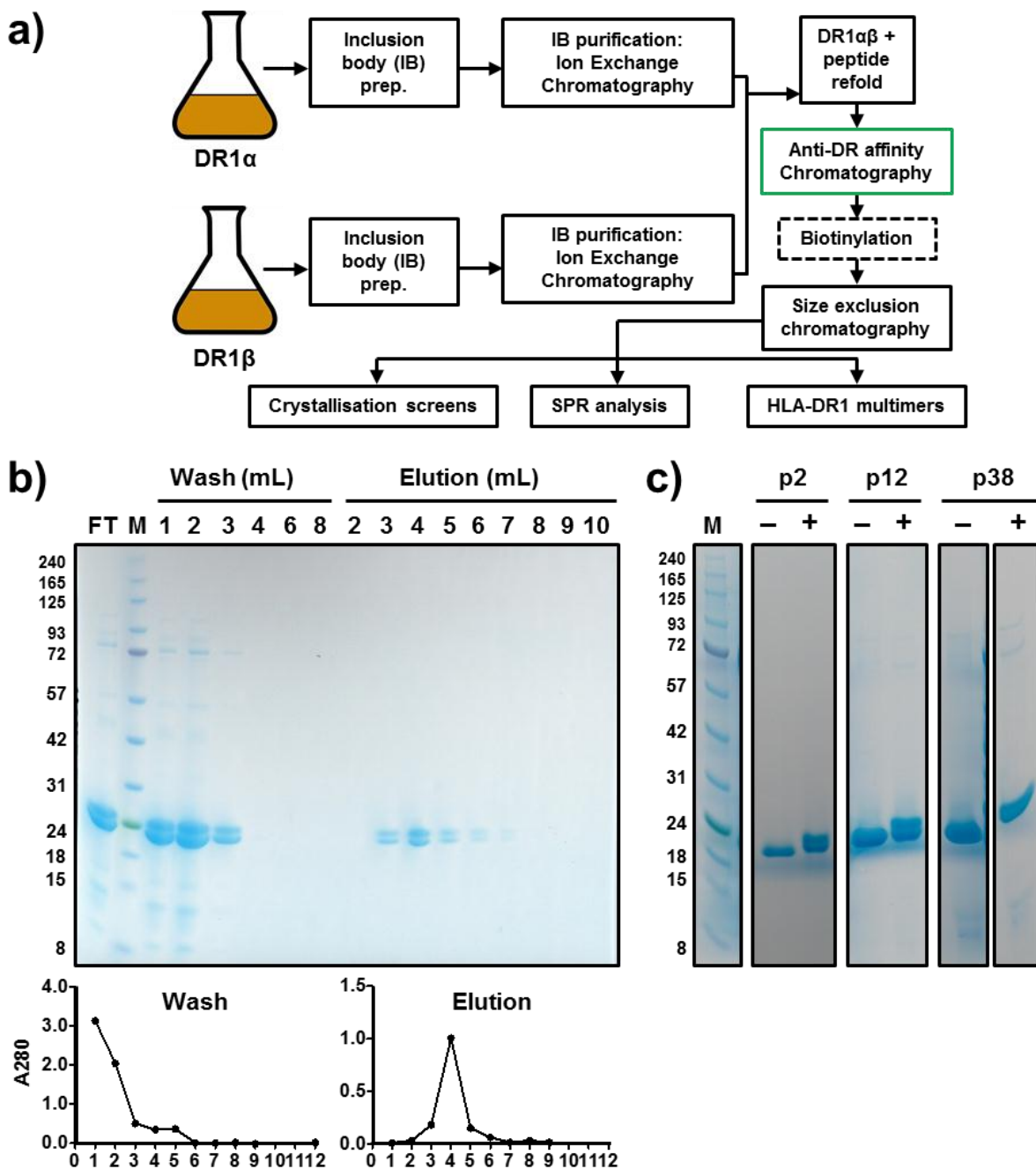
Figure 3.8 – Production of HLA-DR1 5T4p12 for x-ray crystallography:

a) Enhanced protocol for the production of HLA-DR1 molecules refolded in the presence of desired peptide *in vitro* from DR1α and DR1β inclusion bodies produced in *E. coli*. Addition of an anti-DR antibody affinity chromatography step after refold and before biotinylation and/or size exclusion chromatography is shown (green). Purified molecules were used for multiple analyses described. Biotinylation step required for SPR and multimer applications only.

b) SDS-PAGE and spectrophotometer (A280 nm) analysis highlighting separation of anti-DR non-binding wash fractions and anti-DR binding 1 mL elution fractions from an example HLA-DR1 *in vitro* refold. FT = flow through, M = MW marker.

c) SDS-PAGE analysis of refolded HLA-DR1 5T4p2 -p12 and -p38 protein samples produced for crystallisation trials. HLA-DR1 samples exhibited shift in electrophoretic mobility in the non-reducing (-) compared to reducing (1 M DTT, 5 min 95 °C) conditions (+).

3.6.2   Optimised crystallisation of HLA-DR1 5T4p12

HLA-DR1 molecules refolded in the presence of 5T4p2, 5T4p12 and 5T4p38 were subjected to crystallisation screening. Each protein sample was screened for formation of protein crystals using two commercially available screens (Molecular Dimensions PACT Premier & JBScreen) as well as the TCR-pMHC optimised protein crystallisation screen: TOPS (Bulek et al. 2012). Primary screens were performed at multiple concentrations (range 1 - 10 mg/mL) using sitting drop vapour diffusion. Later, secondary screens were performed by hanging drop in the presence prepared MHC-II microseeds.

From the panel of three 5T4-derived peptides, crystals suitable for x-ray diffraction were obtained for the HLA-DR1 5T4p12 complex (*Figure 3.9*). Primary crystallisation screening yielded few non-diffractable crystals in both TOPS and PACT screen conditions (*Figure 3.9a*). Such crystals, whilst exhibiting macroscopic crystalline appearance, were of 1D branched needle or small 3-Dimensional crystals which were not suitable for diffraction (*Figure 3.9b*). In order to optimise crystal formation, non-diffractable crystals were harvested and combined to form a self-microseed stock from which numerous large 3-Dimensional crystals were formed through crystal microseed screening (*Figure 3.9c*). Such crystals were obtained through the screening of various microseed stock, concentration and buffer conditions. The obtained crystal growth conditions are outlined in *Table 3.5*. Obtained crystals were harvested and diffracted at Diamond Light Source (Harwell, UK) to a resolution extending to 1.95 Å (*Table 3.6*).

3.6.3   High resolution structure of an MHC-II presented 5T4-derived peptide

Collected diffraction data of HLA-DR1 5T4p12 at a resolution of 1.95 Å was solved using phase information obtained via molecular replacement by a HLA-DR1 structure (PDB: 1DLH) published on the PDB (Stern et al. 1994) and refined until convergence of statistical parameters (*Table 3.6*). The HLA-DR1 5T4p12 structure was solved as two copies within the asymmetric unit formed by crystal contacts throughout the molecule. Such contacts are detailed in *Appendix 5*. Some crystal contacts were made between DR1β-Q110, within a flexible loop of the DR1 β2 domain, and the rigid central peptide core residues Glu3, Leu4 & Ala5. Likewise, Pro-2 and Arg-4 also made a few contacts with a flexible loop and N-terminal tail, respectively, of DR1β. Such contacts are detailed in *Appendix 5c*. These contacts are highly unlikely to significantly influence peptide side chain positioning due to the extensive contacts made between the peptide and HLA-DR1 (detailed to follow) and the lack of rigidity of contacting regions in symmetry mates.

Broad analysis of the obtained structure showed the produced protein, refolded from *E. coli*, to conform to HLA-DR1 structures of similar resolution published in the PDB
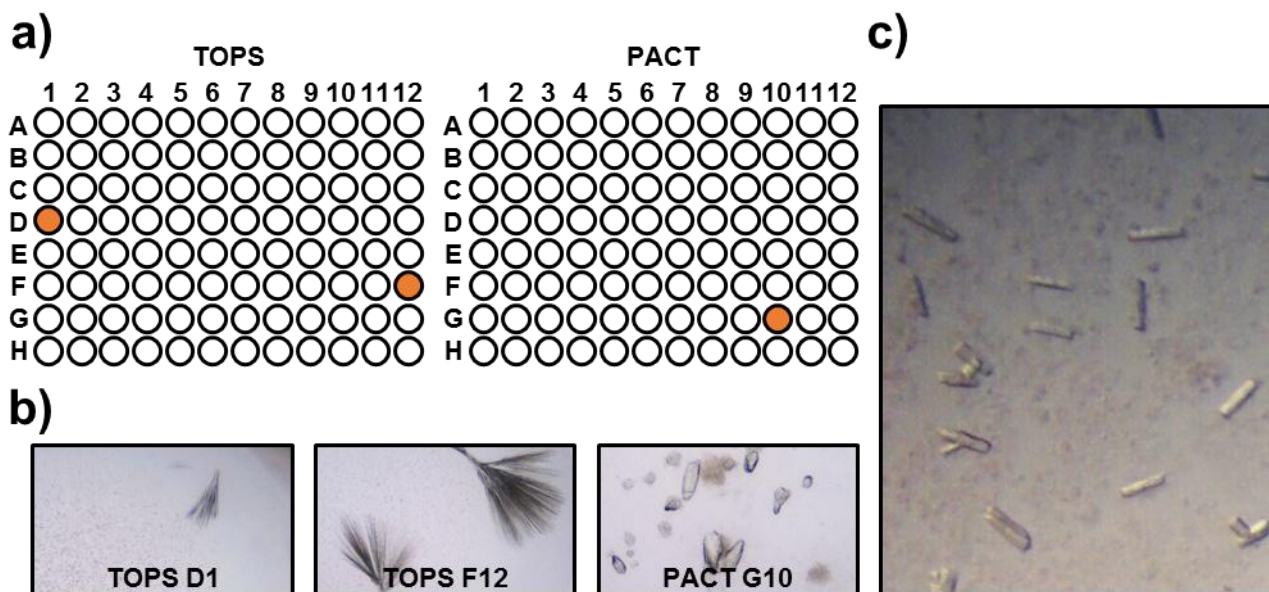
Figure 3.9 – Optimised growth of HLA-DR1 5T4p12 protein crystals through microseeding:
a) Schematic overview of crystal condition well locations (TOPS D1, TOPS F12 & PACT G10) in which primary screens yielded non-diffractable crystalline material (orange) later used as microseeds for crystal optimisation.

b) Stereomicroscope images highlighting non-diffractable crystal forms from primary crystal screening conditions as outlined in ***a)***.

c) Stereomicroscope images of high-resolution diffracting 3-Dimensional HLA-DR1 5T4p12 crystals grown at 4 mg/mL via hanging drop in PACT G10 buffer condition (0.02 M Sodium/potassium phosphate, 0.1 M Bis-Tris propane pH 7.5, 20 % PEG 3350) supplemented with microseed stocks produced from combined crystals shown in ***a)*** and ***b)***.

Crystallisation conditions	
Primary screening	
Screen conditions	
TOPS D1	0.1 M Hepes pH 7.0, 15 % Glycerol, 15 % PEG 4000
TOPS F12	0.1 M Tris pH 7.5, 0.2 M Amonium Sulphate, 25 % PEG 8000
PACT G10	0.02 M Sodium/potassium phosphate, 0.1 M Bis-Tris propane pH 7.5, 20 % PEG 3350
Protein concentration	4 mg/mL
Total drop volume	200 nL
Seeding	
Parent seed protein	Self (HLA-DR1 5T4p12)
Parent seed screen conditions	TOPS D1, TOPS F12, PACT G10
Seed dilution volume	1 in 100 (5 mL)
Seed dilution buffer	PACT G10
Reservoir buffer	PACT G10
Protein concentration	4 mg/mL
Total drop volume	3 µL

Table 3.5 – Crystallisation conditions from which HLA-DR1 5T4p12 crystals were obtained

TOPS = TCR-pMHC Optimised Protein Screen, PACT = PACT premier™ HT-96 MD1-36 (Molecular Dimensions), % = % w/v

(3PDO (Gunther et al. 2010) vs HLA-DR1 5T4p12: RMSD = 0.714 Å). All elements of the four globular domains (α1, α2, β1 and β2) were resolvable and described the tertiary fold of the two DR1α and DR1β chains non-covalently complexed to form the peptide-binding groove between α2 and β2 domains (*Figure 3.10*).

Within the binding groove, the presented 5T4p12 peptide, of 20 amino acids in length, was held non-covalently atop an anti-parallel β-sheet floor constructed from the α2 and β2 chains, in an extended conformation. The open ended conformation characteristic of MHC-II binding grooves allowed the extension of 20 amino acid long peptide antigen to far extend out of the nonamer binding core of HLA-DR1. Presence of the 5T4p12 peptide was confirmed via peptide omit map analysis, whereby the peptide model was omitted during refinement and difference map peaks were analysed for presence/absence of density[1]. Through omit map analysis, observation of positive difference map peak density which accurately described the modelled 5T4p12 peptide sequence, confirmed the presence of the desired peptide within x-ray diffraction data and thus not a consequence of refinement bias (*Figure 3.11a*)

Of the 20 amino acids, only the N-terminal Phe residue was unable to be modelled due to a lack of discernible continuous electron density (*Figure 3.11b*). Modelling of side chain and backbone positioning of the peptide within the peptide binding groove was achievable at contour levels of 1.0 σ whilst N- and C-terminal flanks required some approximated positioning at a contour level of 0.5 σ[2]. Deterioration of electron density at the extremities of the N- and C-termini caused an increase in assigned isotropic displacement B-factor parameters, an indicator of model flexibility and thus, quantified the positional uncertainty of modelled atoms within the three most N-terminal residues (**FAR**RPP**-)** and two most C-terminal residues (-SGS**RL**) (*Figure 3.11c*). Such increase in B-factor assignment indicates inherent flexibility at each flank extremity.

---

[1] Difference map peaks highlight areas of disagreement between the modelled structure and observed electron density data. Positive difference map peaks represent areas of observed electron density which have not been filled by the modelled structure. When the modelled peptide is removed from refinement during omit map analysis, positive difference map peaks should resemble the omitted peptide.

[2] Sigma (σ) is a statistical parameter which describes the intensity of electron density at a given point in terms of standard deviation from the mean electron density of the entire map. Thus areas of electron density with high σ represents areas of high electron density. A σ cut-off level therefore acts as a contour level that determines whether a given point is visualised as containing electron density. A σ level of 1.0 is generally used for presenting visualised electron density whilst a σ level of 0.5 can be used to model flexible protein residues.

Dataset statistics	
Space group	P 1 2$_1$ 1
Unit cell parameters	a=56.96, b=121.29, c=68.96 α=90.0°, β=107.3°, γ= 90.0°
Radiation source	DLS I02
Wavelength	0.9795 Å
Resolution range	60.65 – 1.95 (2.00 – 1.95) Å
CC-half	0.995 (0.589)
Total reflections	239,331 (17,960)
Unique reflections	64,792 (4,807)
Completeness	99.6 (99.8) %
Multiplicity	3.7
I/σ	8.3 (1.3)
R$_{merge}$	10.0 (91.3) %
Refinement statistics	
Phase determination	Molecular replacement (PHASER)
No. of reflections used	64,762
No. of reflections in R$_{free}$ set	3,165
R$_{cryst}$ (%)	19.31
R$_{free}$ (%)	24.11
Asymmetric unit (ASU) parameters	
Number of copies in ASU	2
Number of non-H atoms	6,784
Deviation from ideal geometry (RMSD)	
Bond lengths	0.0191
Bond angles	1.8659
Chiral volume	0.1086
Overall Wilson B factor (A^2)	39.2
Ramachandran statistics (MolProbity)	
Most favoured	756 (98.1 %)
Allowed	15 (1.9 %)
Outliers	0 (0.0 %)
MolProbity clash score	2.42
MolProbity score	1.48

Table 3.6 – Data reduction and refinement statistics of the HLA-DR1 5T4p12 structure

DLS = Diamond Light Source, Dataset statistics in parentheses represent statistical value for data in the outermost resolution shell. RMSD = Root-mean-square deviation.
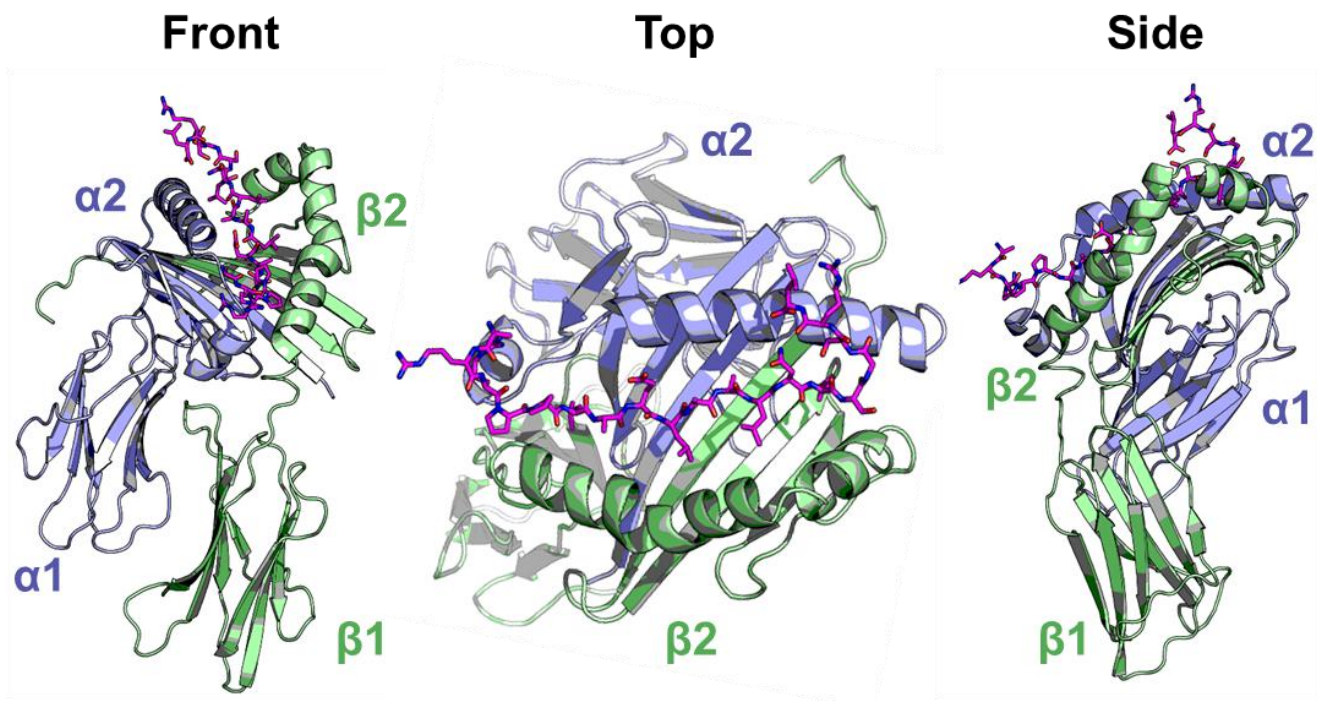
Figure 3.10 – Refined crystal structure of HLA-DR1 presenting 5T4p12 at 1.95 Å:
Cartoon representation of solved HLA-DR1 structure presenting the 5T4p12 peptide as stick representation (magenta). DR1α1 and α2 (blue) domains complex with DR1β1 and β2 domains (green) as depicted by front, top and side views. The 5T4p12 peptide is held within the open ended peptide binding groove as shown by top view. N-terminal and C-terminal peptide flanking residues protrude away from the peptide binding groove as shown in front and side views.
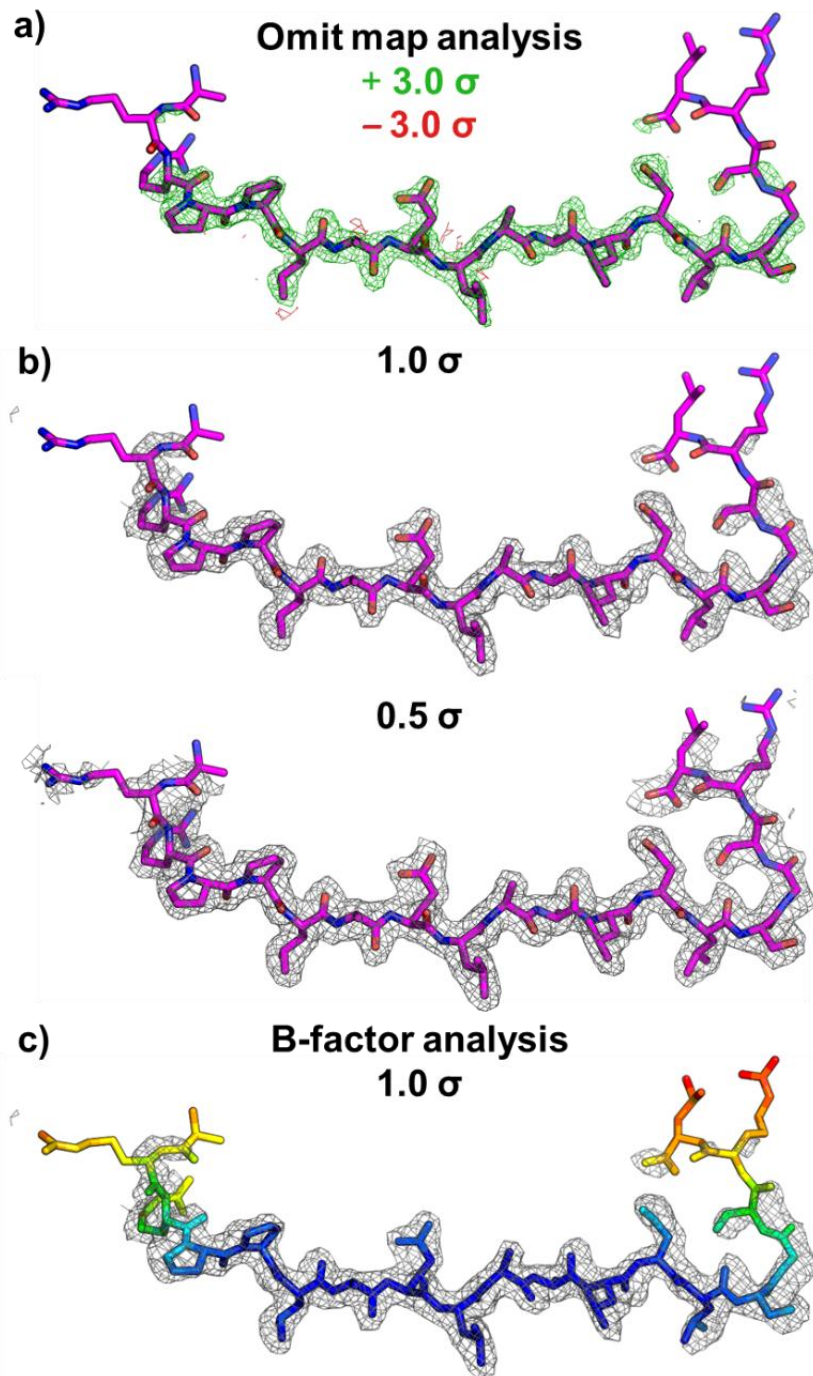
Figure 3.11 – Density plot analysis of peptide conformation within HLA-DR1 5T4p12:

a) Omit map analysis of observed difference map peaks in absence of peptide during refinement. Presence of positive difference map peaks (green mesh; + 3.0 σ) and not negative peaks (red mesh; - 3.0 σ) with highly related density to modelled peptide (magenta sticks; atoms coloured: C = magenta, O = red, N - blue) validated the presence of 5T4p12 within electron density.

b) Stick representation of modelled 5T4p12 peptide (magenta) within refined electron density map contoured at 1.0 σ and 0.5 σ (grey mesh). Peptide electron density allowed modelling of 19 of the 20 amino acids of 5T4p12 with no observed electron density of N-terminal Phe.

c) Stick representation of 5T4p12 peptide coloured by B-factor (blue to red; B-factor range = 21 to 130). B-factor analysis indicated a highly stable core binding region (B-factor < 40) flanked by stability extending to both N-terminal and C-terminal flanking regions. Extremities of termini exhibited high flexibility as indicated increase in B-factors to > 80.

3.6.4   Definition of the 5T4p12 core epitope presented by HLA-DR1

Previous ELISpot and ELISA experiments described the cognate 5T4-reactive GD.D104 T cell clone activation in response the 20 amino acid 5T4p12 (FARRPPLAELAALNLSGSRL) presented by HLA-DR1 only expressing cells. Likewise, preceding studies highlighting the 5T4p12 as immunogenic in healthy individuals and colorectal cancer patients defined the epitope only to the full length 20 amino acid sequence. Definition of the nonamer peptide binding core exhibited by HLA-DR1 for 5T4p12 had not previously been experimentally defined.

The peptide binding pockets of MHC-II molecules classically define the selection of peptides presented by each allele. Using the solved structure of HLA-DR1 5T4p12, definition of the nonamer peptide binding core of 5T4p12 was achieved by assignment of the register within the HLA-DR1 binding groove (*Figure 3.12a*). In agreement with the prediction by NetMHC2.2, described previously, this binding core was defined to the centre of the 20 amino acid peptide (FARRPP**LAELAALNL**SGSRL; binding core bold and underlined) and as a result, the core immunogenic epitope was derived from 5T4$_{117-125}$. Assignment of the peptide binding core, therefore, defined the 5T4p12 peptide to contain a six amino acid N-terminal flank (FARRPP) and five amino acid C-terminal flank (SGSRL).

3.6.5   HLA-DR1 presented 5T4$_{117-125}$ exhibits minimal potential TCR contact residues

Binding of cognate TCR to peptides presented on MHC molecules and consequent triggering of T cell signalling is mediated by the ability of paratopic CDR loops on the TCR to interact with residues on the combined peptide-MHC surface volume. As a result, determinant of binding is governed by peptide atoms, particularly those derived from peptide side chain residues, which orientate in a membrane distal direction – away from the MHC binding groove. Such atoms allow the formation of enthalpically favourable intermolecular contacts between the peptide MHC and cognate TCR (Bridgeman et al. 2012). Consequently, the dimensions and chemistry of such orientated side chain residues are a key factor in selecting TCRs with affinity for peptide antigen which can form a network of electrostatic interactions between peptide and TCR.

Analysis of the structure of 5T4p12 bound to HLA-DR1 revealed the likely residues involved in TCR contact within the peptide core binding region (5T4$_{117-125}$; **LAELAALNL)** as shown by residues protruding away from the MHC binding groove (*Figure 3.12b*). Overall, the 5T4$_{117-125}$ core peptide region of 5T4p12 exhibited a mostly flat surface volume. Only Glu3 and Asn8 form obvious TCR contact residues. The charged carboxyl side chain of Glu3 is positioned centrally within the peptide and projects perpendicularly away from the peptide binding groove and, thus,
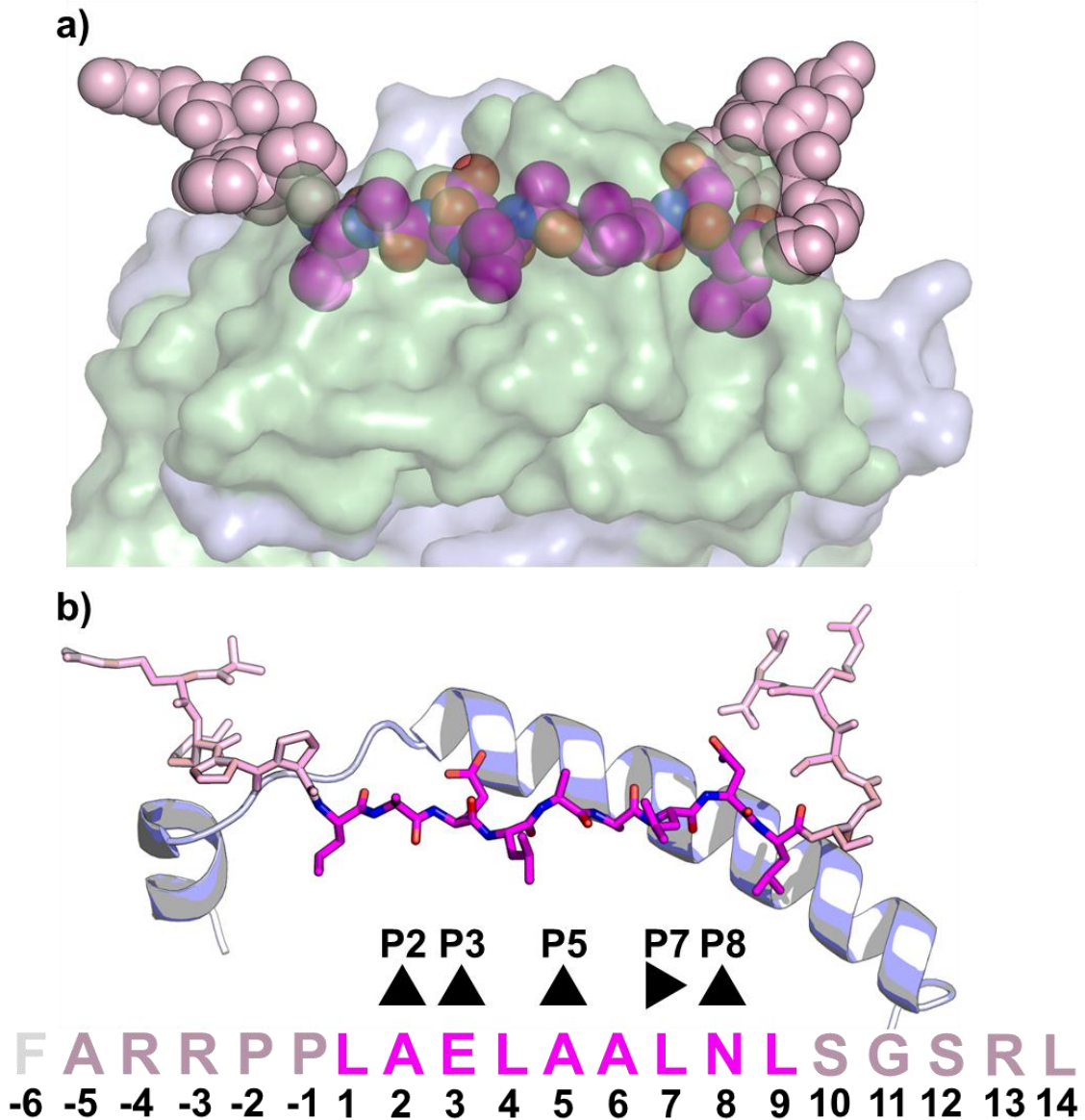
Figure 3.12 – Definition of the 5T4p12 core peptide region and potential TCR contact residues within:

a) Sphere and surface representation of the largely flat 5T4p12 core peptide binding region (magenta spheres) within the HLA-DR1 molecule (DR1α = blue, DR1β = green). Peptide flanking residues outside of the binding core are also shown protruding away from the HLA-DR1 molecule (light pink spheres).

b) Stick and cartoon representation of the defined 5T4p12 core peptide binding region (coloured as in *a)*) and the potential TCR contact residues within the binding core which protrude away from the peptide binding groove. Orientation of such residues are denoted by upwards facing arrowheads and corresponding HLA-DR1 binding position. Leu7 at position P7 is orientated parallel to the MHC molecule and is therefore partially available for TCR contact, thus, denoted as a sideways arrowhead.

available to form hydrogen bonds or salt bridges with the TCR. Likewise, the more C-terminally positioned Asn8 is available for hydrogen bonding via its amide bearing side chain. Due to the positioning of two short aliphatic alanine residues at P2 (Ala2) and P5 (Ala5) as well the partial burial of Leu at P7, which provide little contact atoms for TCR interaction, no other obvious high enthalpy TCR contact residues are present in the 5T4$_{117\text{-}125}$ peptide binding core of 5T4p12. NB.

3.6.6 Intramolecular interactions mediate a hairpin turn in the C-terminal flank of 5T4p12

Analysis of the solved HLA-DR1 5T4p12 structure demonstrated a lack of potential TCR contacts in the core peptide binding region of 5T4p12, however, observation of the flanking regions highlighted extended structures which protrude away from the MHC. Such residues, whilst exhibiting a degree of inherent isotropic displacement, as discussed previous, formed ordered conformational features.

At the N-terminal flank, the peptide remained in a relatively flat conformation by interacting with the MHC molecule through a network of interactions involving residues Arg-3, Pro-2 and Pro-1 of which these interactions, and their contribution to peptide binding to MHC are discussed in detail later. In general, these interactions extended the N-terminal flank over the top of the MHC-II binding groove and held the peptide backbone close to the DR1α chain (as visualised in *Figure 3.10; top view*). This exit from the binding groove was facilitated by the flexible loop region connecting the 3$_{10}$ helix and binding groove wall α-helix. Drop-off in electron density for the peptide backbone past Arg-4, and the Arg-4 side chain itself (as shown in *Figure 3.11a*) was observed as a result of the molecular dynamics of isolated polypeptide chains. Consequently, the exact locale of such atoms are not fixed, however, their orientation trended away from the MHC where they exhibit mobility in solution. As such, these residues at the N-terminal flank may be free to contact the TCR through interaction with the guanidinium side chain of Arg-4 or the aromatic phenyl group of Phe-6.

In comparison, at the C-terminal flank, the 5T4p12 exhibited an ordered structure that protruded away from the MHC binding groove in the form of a hairpin loop (*Figure 3.13*). This hairpin loop was mediated through few intermolecular contacts with the MHC, constrained to Ser12 interacting with Ile72α which, via four vdW interactions, was the only residue to scaffold the turned peptide above itself by the MHC.

The reverse turning of the peptide strand was instead mediated mainly through intramolecular contacts within the peptide (*Figure 3.13a*). The result of these interactions was the pulling

of the final three residues at the C-terminus into close proximity of the peptide binding core boundary. Such contacts within the peptide were the result of three residues, Ser10, Gly11 and Ser12, forming a tight reverse turn in the C-terminal flank of 5T4p12 that resembled the characteristics of a type II β-turn. This turn was mediated by residues Leu9, Ser10, Gly11 and Ser12; assigned *i, i+1, i+2 & i+3*, respectively, according to convention. Specifically, as per the criteria of β-turns, residue Ser12 (*i+3*) was brought within 7 Å of Leu9 (*i*); as measured between Cα atoms (*Figure 3.13b*). The resulting dihedral angles about Ser10 (*i+1*) and Gly11 (*i+2*) conformed to typical average values observed in type II β-turns (*Figure 3.13c*).

The presence of this turn was formed and constructed by interactions between the Ser12 side chain to Leu9 and Ser10 residues located before the turn – enabled through the locale of the Ser12 side chain hydroxyl group. This side chain allowed the formation of a hydrogen bond between the Ser12 hydroxyl and Leu9 carbonyl (*Figure 3.13d*). In order to accommodate this interaction, measured at 2.8 Å, the type II β-turn hairpin turn was opened and thus the observed turn was consequently more obtuse. As a result, the Ser10-Gly11-Ser12 turn did not form a fully recognised H-bond between the backbone carbonyl of residue *i* (Leu9) and backbone amide of *i+3* (Ser12) – a criterion for classification of β-turns. In the observed hairpin, this distance (3.6 Å) was marginally outside the general cut-off distance for H-bonds (<3.4 Å). At this distance, however, these atoms would still experience weak electrostatic attraction. No crystal contacts were made between the C-terminal hairpin loop and neighbouring symmetry mates (*Appendix 5c*).
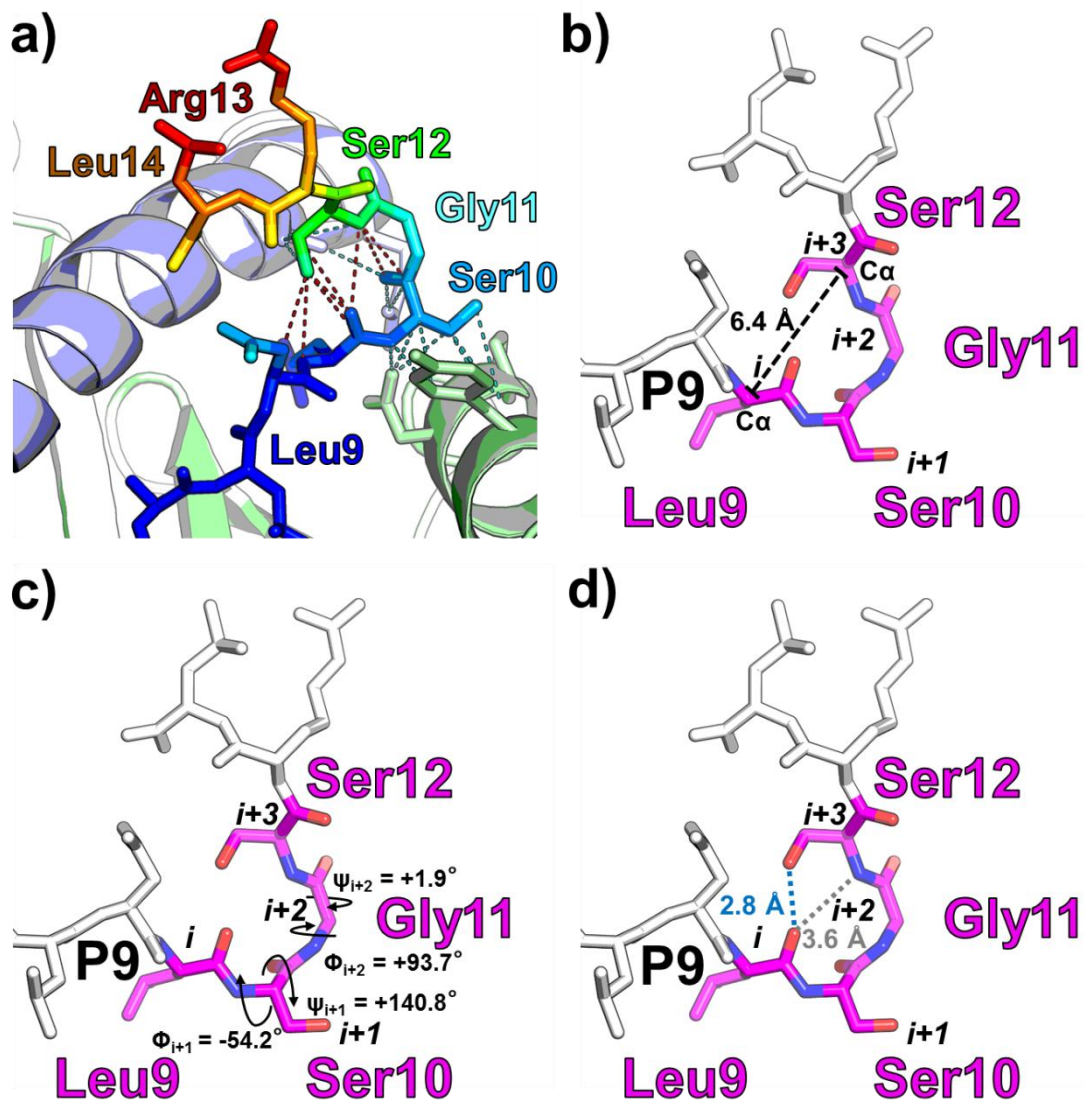
Figure 3.13 – Hairpin turn formation at the C-terminal flank of 5T4p12:

a) Stick representation of C-terminal flanking region of 5T4p12 (coloured by B-factor; blue to red; range = 21 to 130) bound to HLA-DR1 highlighting a hairpin loop mediated by intramolecular contacts within the peptide (red dashes) before increase in B-factors. Few intermolecular contacts (cyan dashes) with residues Ser10-Leu14 were observed.

b) C-terminal flanking region of 5T4p12 highlighting the hairpin loop formed by residues Leu9-Ser12 (magenta). Cα atoms of Leu9 and Ser12 (denoted i and i+3, respectively) are separated by a distance typical of β-turns (<7.0 Å).

c) C-terminal flanking region of 5T4p12 as in *b)* annotated with dihedral angles Φ/ ψ about Ser10 and Gly11. Observed dihedral angles conform to typical average values of type II β-turns: Φ_{i+1} = -60°, ψ_{i+1} = +120°, Φ_{i+2} = +80°, ψ_{i+2} = 0°.

d) C-terminal flanking region of 5T4p12 as in *b)* highlighting the lack of established H-bond between Leu9 carbonyl and Ser12 amide due to distance (grey dashes) above H-bond cut-off value (3.4 Å). Hairpin turn is, instead, held by the formation of a H-bond between Leu9 carbonyl and Ser12 side chain hydroxyl (blue dashes)

3.6.7 Enhanced intermolecular binding of 5T4p12 to HLA-DR1 via contacts throughout the extended tumour-antigen derived peptide

The 5T4p12-reactive T cell clone GD.D104 exhibited sensitivity to antigen presented by HLA-DR1 only expressing cells but did not stain effectively by HLA-DR1 5T4p12 multimers. Despite this, 5T4p12 was immunogenic to *in vitro* cultured CD4$^+$ T cells. In order to study the contribution to immunogenicity by 5T4p12 binding to MHC, the solved HLA-DR1 5T4p12 structure was interrogated for the intermolecular contacts that anchor and complex the peptide to MHC.

3.6.7.1 Anchoring of the 5T4p12 peptide to HLA-DR1 incorporating leucine into the P1 binding pocket

Differences in HLA-DR alleles are characterised by polymorphisms in the peptide binding groove which alter the array of presentable peptide ligands between MHC-II molecules and therefore between individuals. As a result of such polymorphisms, different HLA-DR alleles have preference for binding different peptide motifs into the polymorphic peptide binding pockets (Rammensee et al. 1995). Anchoring of 5T4p12 to the MHC was characterised by a classic HLA-DR1 binding motif (*Figure 3.14*). Binding residues at P4 (Leu4), P6 (Ala6) and P9 (Leu9) are within preferential and conventional residues for respective HLA-DR1 binding pockets (*Figure 3.14a&b*) (Cole & Godkin 2016). Such classical interactions confirm the 5T4p12 as a good ligand for HLA-DR1, in accordance with the predicted affinity of 5T4p12 for HLA-DR1, described previously.

In contrast to counterpart binding pockets, incorporation of Leu at P1 represents a sub-optimal residue for the P1 pocket of HLA-DR1 which has potential for binding larger hydrophobic and aromatic residues (Tyr, Phe, Trp & Ile) (*Figure 3.14c*). As such, there are currently no published structures in the PDB describing leucine binding at position P1 of HLA-DR1 (all structures assigned as using DRB1*01 beta chain; UniProtKB: P04229). Despite the smaller size of the leucine side chain, Ser53α, Phe54α, Phe32α, Val85β and Asn82β of the HLA-DR1 P1 pocket were able to contact Leu1.

The interactions between Leu1 and MHC were in the form of a network of sixteen contacts: fifteen van der Waals interactions and a single hydrogen bond to the peptide backbone (*Figure 3.14d*), listed in *Table 3.7*. Such interactions are comprised of contacts with the Leu1 peptide backbone (7/16 contacts) but, more significantly, with aliphatic side chain atoms (9/16 contacts). The most contacts with Leu1 were contributed to Asn82β (6/16 contacts) which made extensive interactions through the Leu1 side chain and backbone. In contrast, Phe54α interacted with the peptide backbone only through two van der Waals interactions. The single hydrogen bond contribution to binding was mediated through Ser53α interacting with the peptide bond amide group

Peptide		MHC			Contact	
Residue	**Atom**	**Chain**	**Residue**	**Atom**	**Distance (Å)**	**Type**
Peptide backbone contacts						
Leu1	N	A	Ser53	C	4	VW
	N	A	Ser53	O	2.8	HB
	Cα	B	Asn82	Oδ1	3.47	VW
	Cα	A	Ser53	O	3.82	VW
	C	B	Asn82	Oδ1	3.69	VW
	O	A	Phe54	Cε1	3.77	VW
	O	A	Phe54	Cδ1	3.32	VW
Peptide side chain contacts						
Leu1	Cβ	B	Asn82	Oδ1	3.95	VW
	Cβ	A	Ser53	O	3.78	VW
	Cγ	B	Val85	Cγ1	3.95	VW
	Cδ1	A	Phe32	Cε1	3.79	VW
	Cδ2	B	Asn82	O	3.94	VW
	Cδ2	B	Asn82	Cγ	3.9	VW
	Cδ2	B	Asn82	Oδ1	3.51	VW
	Cδ2	B	Val85	Cβ	3.89	VW
	Cδ2	B	Val85	Cγ1	3.69	VW
No. of total contacts						**16**
vdW						15
H-bonds						1
No. of contacts with peptide backbone						**7**
vdW						6
H-bonds						1
No. of contacts with side chain						**9**
vdW						9
H-bonds						0

Table 3.7 – Contacts enabling Leu1 mediated anchoring of 5T4p12 at position P1:
vdW = van der Waals (=< 4.0 Å cut-off), H-bonds = hydrogen bonds (=< 3.4 Å cut-off).
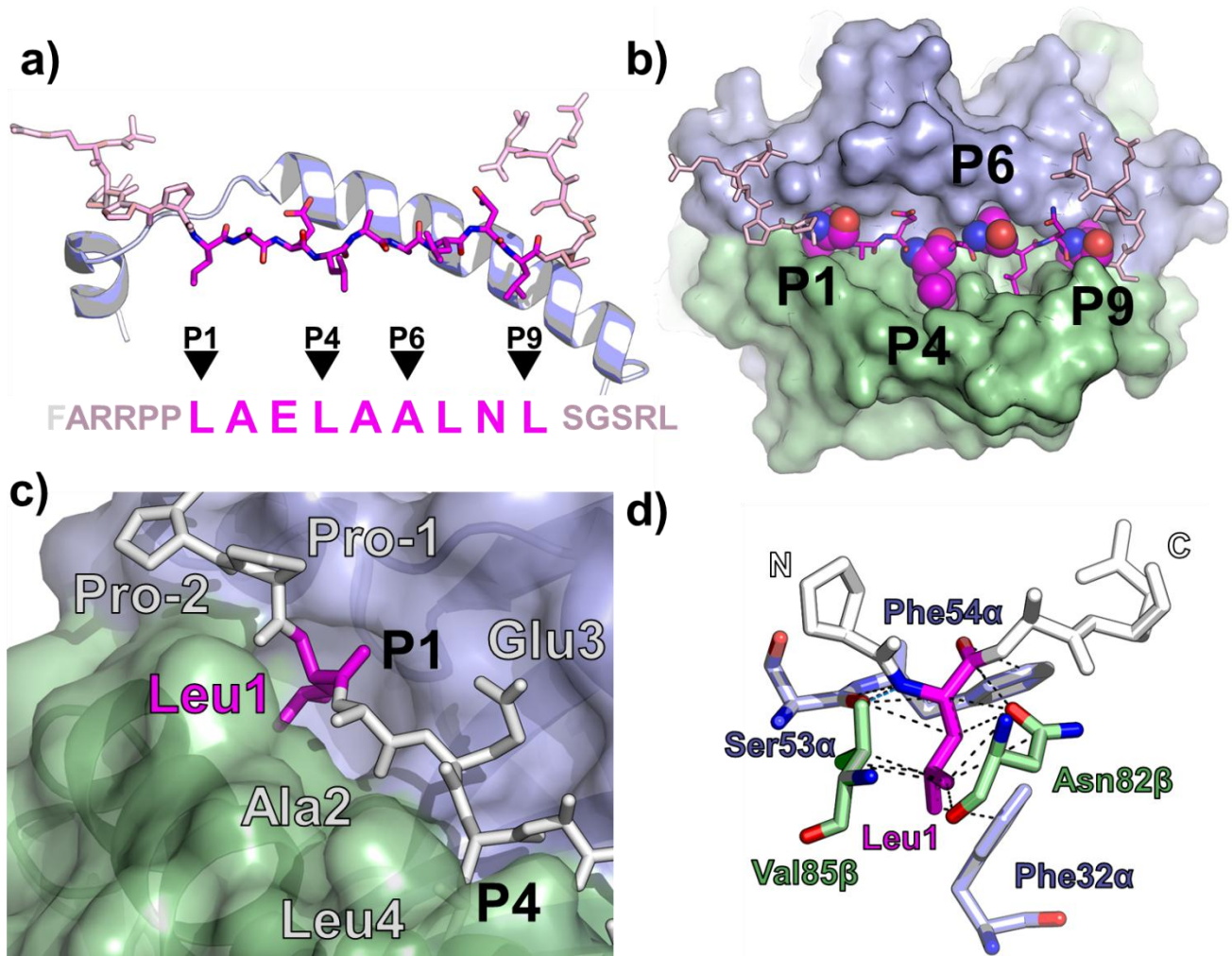
Figure 3.14 – Anchoring of 5T4p12 via partial occupancy of the P1 pocket by leucine:

a) Stick and cartoon representation of the 5T4p12 peptide (core region = pink, flanking regions = pale pink sticks) and assignment of peptide residues binding to P1, P4 P6 and P9 position HLA-DR1 binding pockets (downward arrowheads). α2 α-helix = blue cartoon.

b) Surface, sticks and sphere representation of top down view of 5T4p12 binding to HLA-DR1 coloured as in ***a)***. Spheres highlight peptide residues buried into HLA-DR1 binding pockets.

c) Surface and stick representation of the concaved P1 binding pocket constructed from HLA-DR1α (surface, blue) and -DR1β (surface, green) chains of which the aliphatic Leu1 side chain (pink) of the 5T4p12 peptide (white) partially fills.

d) Stick representation of contacts made between the Leu1 peptide residue (pink) with residues at the P1 binding pocket facilitating peptide binding to MHC. Leu1 made sixteen van der Waals contacts (black dashed lines) with the HLA-DR1α chain residues Ser53α and Phe54α (both green) as well as the -DR1β chain residues Phe32α, Val85β and Asn82β (all blue).

of Leu1 and is therefore unlikely to be impacted by side chain selection at P1. Due to the aliphatic nature of the Leu1 residue, no hydrogen bonding or salt bridging was observed with the Leu1 side chain. As a result, anchorage of Leu1 to the P1 pocket was not able to be enhanced by side chain linked hydrogen bonds, despite proximity of hydrogen bond capable polar residues such as Asn82β and Ser53α. As reference, anchoring of the influenza-derived 'universal epitope' $HA_{306-318}$ peptide to the P1 pocket of HLA-DR1 is mediated by a total of 23 contacts between MHC and the Tyr1 residue of $HA_{306-318}$ when analysed using the same contact criteria (Stern et al. 1994).

3.6.7.2 Peptide flanking residues contribute to HLA-DR1 binding

Whilst the core binding region of MHC-II restricted peptides is typically considered to define the ability of peptides to be selected for presentation on MHC alleles, contribution to binding by residues flanking the core region must also be considered. Indeed, increases in peptide flanking length have suggested an influence of peptide to MHC-II affinity *in vitro* and computationally (Sant'Angelo et al. 2002; O'Brien et al. 2008).

The 5T4p12 peptide tethered to HLA-DR1 via a network of non-covalent interactions including 168 vdW interactions and 19 H-bonds; 187 total contacts (*Figure 3.15a*). Flanking the defined nonamer core binding region of 5T4p12 was a six amino acid N-terminal flank (FARRPP) and five amino acid C-terminal flank (SGSRL). In order to analyse the contribution of these flanking residues to 5T4p12 peptide binding to HLA-DR1, the number of contacts by each residue in the full length peptide was quantified (*Table 3.8*) and stratified for the percentage contribution of contacts per peptide residue to observed interactions (*Figure 3.15b*).

Analysis of the distribution of contacts throughout the peptide sequence highlighted the residues bound into the HLA-DR1 binding pockets as shown by increases in contacts at P1 (Leu1), P4 (Leu4), P6 (Ala6) and P9 (Leu9) as expected. In addition, contribution of peptide to MHC binding by residues within the peptide flanking residues was observed. Of the 11 flanking residues, five residues contributed to peptide binding to HLA-DR1 through the formation of contacts between the complexed peptide and MHC molecule; N-terminal flanking Arg-3, Pro-2 & Pro-1 as well as the C-terminal flanking Ser10 & Ser12 (FAR**RPP**<u>LAELAALNL</u>**S**G**S**RL; highlighted in bold, core peptide underlined).
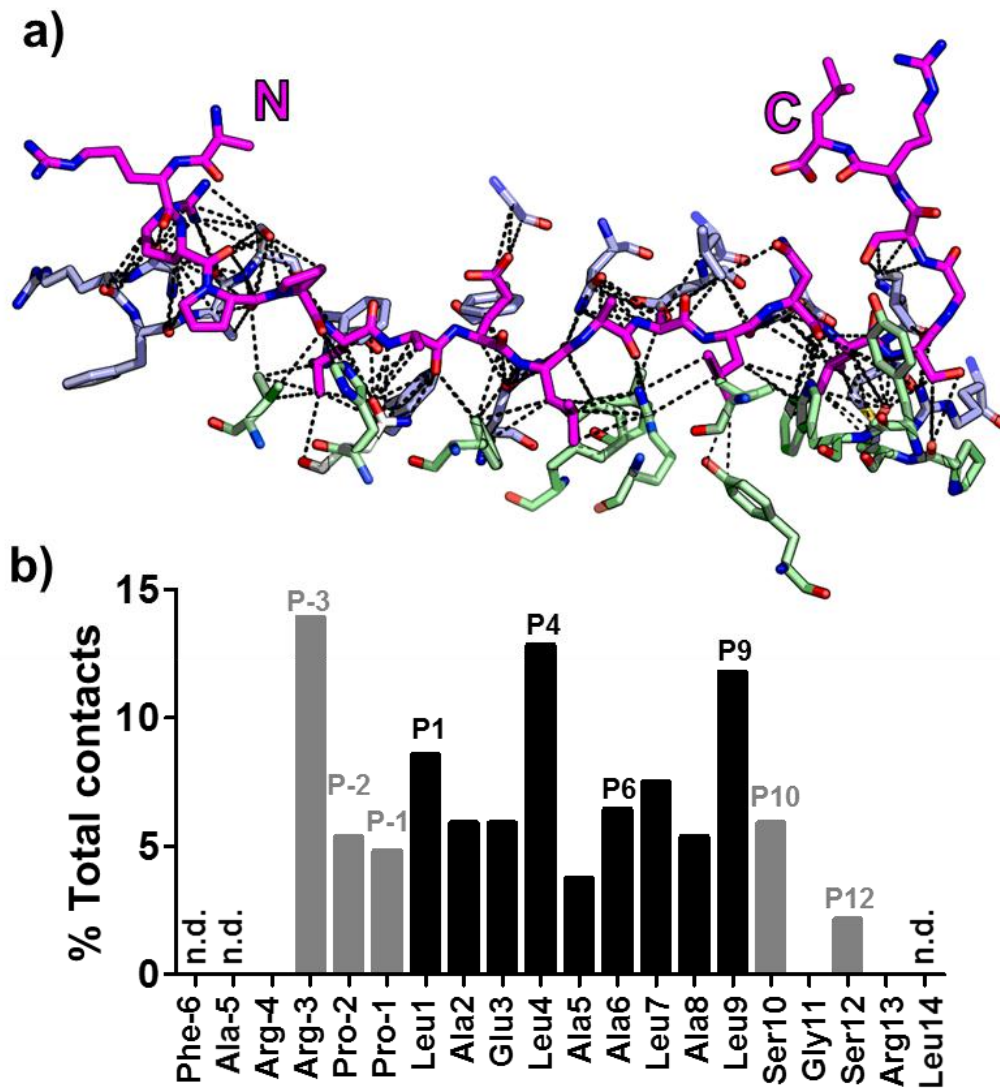
Figure 3.15 – The complex interaction network between 5T4p12 and HLA-DR1:

a) Stick representation of all contacts (=< 4.0 Å cut-off), between the 5T4p12 peptide (magenta) and residues of the DR1α (blue) and DR1β (green) chains.

b) Reduction of the 5T4p12 to HLA-DR1 contact network to the number of contacts mediated by each single amino acid within the peptide sequence. Quantified contacts across the peptide sequence are presented as a histogram stratified to percentage of total contacts observed across the 5T4p12 peptide chain. Simplification of the contact network demonstrates contribution to MHC binding by residues within the peptide binding core (black) and within the peptide flanking residues (grey). n.d. = not determined due to lack of positional certainty.

		Peptide to MHC contacts		
Residue	**Position**	**vdW**	**H-bonds**	**Total**
N-terminal peptide flanking residues				
Arg-3	P-3	23	3	**26**
Pro-2	P-2	9	1	**10**
Pro-1	P-1	8	1	**9**
Peptide binding core region				
Leu1	P1	15	1	**16**
Ala2	P2	9	2	**11**
Glu3	P3	11	0	**11**
Leu4	P4	21	3	**24**
Ala5	P5	5	2	**7**
Ala6	P6	11	1	**12**
Leu7	P7	13	1	**14**
Asn8	P8	9	1	**10**
Leu9	P9	21	1	**22**
C-terminal peptide flanking residues				
Ser10	P10	9	2	**11**
Ser12	P12	4	0	**4**
No. of total contacts				**187**
vdW				168
H-bonds				19
No. of contacts with peptide flanking residues				**60**
vdW				53
H-bonds				7
No. of contacts with peptide binding core				**127**
vdW				115
H-bonds				12

Table 3.8 – Contribution of peptide residues to 5T4p12 to MHC binding
vdW = van der Waals (=< 4.0 Å cut-off), H-bonds = hydrogen bonds (=< 3.4 Å cut-off).

3.6.7.3   Peptide to MHC contacts at the C-terminal flanking region

Binding of peptide to MHC at the C-terminal flank was mediated via the Ser10 and Ser12 residues (P10 & P12 respectively). At Ser10, extensive contacts with five residues across both DR1α (Ile72α and Arg76α) and DR1β (Pro56β, Asp57β and Tyr60β) chains were made through a total of eleven interactions including two hydrogen bonds (*Figure 3.16a*). Despite the polar hydroxyl group side chain of Ser10, these two hydrogen bonds were made to the peptide backbone only and therefore the Ser10 side chain did not facilitate additional peptide anchoring through a high energy H-bond. Such inability to form side chain H-bonds with MHC residues was in spite of the relative proximity of the polar atoms of Arg76α which remained too distal to Ser10. Despite this, the Ser10 hydroxyl and Cβ did interact with Pro56β and Asp57β by forming weaker vdW interactions.

Despite the hairpin loop observed at the C-terminal flank of 5T4p12 causing protrusion away from the binding groove, discussed previous, Ser12 at position P12 made some contacts with the MHC through interactions between the Ser12 side chain and Ile72α (*Figure 3.16b*). Similar to Ser10, contacts between MHC and Ser12 were mediated through vdW interactions and did not utilise the hydroxyl group of Ser12 to form contacts but instead formed four vdW interactions with Ile72α; two of which were contributed by side chain atoms. Presence of fewer observed contacts between peptide and MHC by Ser12 at P12 is expected due to the protrusion of the C-terminal hairpin loop away from the MHC molecule. Nevertheless, lack of Ser12 to MHC contacts was a correlate of the increase flexibility of the extremities of the C-terminal flank of 5T4p12 as shown by B-factor analysis previous.

Overall, analysis of the C-terminal flanking region reveals presence of interactions between peptide residues and the MHC, however, such interactions are far fewer than those observed in other regions of the peptide – specifically the peptide binding core and the HLA-DR1 binding pockets within. In addition, inclusion of serine residues at positions P10 and P12 have no obvious structural advantage to cause enrichment of such residues at these positions due to redundancy of the hydroxyl side chain in both positions in terms of contribution to peptide-MHC binding. Nevertheless, such interactions positively benefited peptide complexing to HLA-DR1.

Figure 3.16 – Intermolecular contacts between the C-terminal flank of 5T4p12 and HLA-DR1:

a) Stick representation of 5T4p12 peptide (white) highlighting residue Ser10 (magenta) interacting with DR1α residues Ile72α and Arg76α (blue) and DR1β residues Pro56β, Asp57β and Tyr60β (green). Van der Waals contacts (=< 4.0 Å) are shown as black dashed lines and H-bonds (=< 3.4 Å) shown as blue dashed lines between contributing atoms. Ser10 contacted MHC via both side chain and peptide backbone but showed no ability to form side chain hydrogen bonds with neighbouring polar residues such as Arg76α.

b) Stick representation of 5T4p12 peptide, as in ***a)*** highlighting Ser12 (magenta) interaction with DR1α residue Ile72α. Minimal contacts were observed including no side chain hydrogen bonding between the Ser12 hydroxyl group and the MHC molecule.

3.6.7.4   **Peptide to MHC contacts at the N-terminal flanking region**

Compared to the C-terminal counterpart, the N-terminal peptide flanking region made three times as many total contacts with HLA-DR1 (15 compared to 45, respectively). Such contacts involved the three most proximal residues to the binding core: Arg-3, Pro-2 and Pro-1.

Two consecutive proline residues proximal to the peptide binding core made a moderate contribution to binding, creating contacts with the MHC comparable to those exhibited by core peptide binding region residues outside the binding pocket positions. Contacts by Pro-1 were quantified as eight vdW interactions across three residues including Ser53α, which made contacts at position P1, and a single H-bond to the peptide backbone (*Figure 3.17a*). Similar contacts were observed for Pro-2 where a single H-bond between the Pro-2 backbone contacted Ser53α, further highlighting this MHC residue proximal to the P1 pocket as key to stabilisation of the 5T4p12 peptide (*Figure 3.17b*). Due to the cyclic nature of the proline side chain, however, no obvious advantage in enrichment of prolines at P-1 and P-2, in terms of direct interactions to the MHC by side chain atoms, was immediately clear.

Whilst both Pro-2 and Pro-1 made contributions to MHC binding themselves, incorporation of two consecutive proline residues allowed the 5T4p12 N-terminal flank to exhibit a di-proline kink in the peptide chain and subsequently positioned Arg-3 towards the DR1α chain proximal α2 domain of the peptide binding groove. This kinked conformation located Arg-3 above the linking region between the 3_{10} helical and α-subunit helix of the α2 domain. Consequently, Arg-3 was able to form a network of contacts with five residues, all localised to the DR1α chain (*Table 3.9*).

Quantification of 26 unique contacts (23 vdW & 3 H-bonds) between Arg-3 and the MHC molecule showed that Arg-3 made the most inter-molecular contacts out of any single residue throughout the length of the peptide. Arg-3 contacted a string of five consecutive residues Gly49α – Ser53α by making extensive vdW interactions with both the side chain and peptide backbone of Arg-3 (*Figure 3.17c*). Most contacts however, were mediated by the large positively charged side chain of arginine (backbone contacts = 4, side chain contacts = 22).

In addition to vdW interactions, contacts included three higher-energy H-bonds (2.75 - 3.0 Å bond length) between Arg-3 and the MHC. Firstly, the backbone carbonyl of Arg-3 contacted the hydroxyl of Ser53α describing how the peptide backbone of longer MHC-II restricted peptides can make interactions with the MHC at position P-3 (*Figure 3.17d*). Furthermore, the side chain NH_2 of Arg-3 made two H-bond interactions with Gly49α and Ala52α backbone carbonyls. Such interactions were enabled by the length of the Arg-3 side chain and it's positively charged

guanidinium end group and thus binding of peptides to HLA-DR1 may be preferentially enhanced by arginine inclusion at position P-3. Such interactions here described enabled a more fixed N-terminal flank that, for 5T4p12, theoretically enhanced the complexing of peptide to HLA-DR1 and thus may impact its immunogenicity *in vitro* and potentially *in vivo*.

Peptide		MHC			Contact	
Residue	Atom	Chain	Residue	Atom	Distance (Å)	Type
Peptide backbone contacts						
Arg-3	C	A	Ser53	Oγ	3.84	VW
	O	A	Ser53	N	3.78	VW
	O	A	Ser53	Cβ	3.67	VW
	O	A	Ser53	Oγ	2.82	HB
Peptide side chain contacts						
Arg-3	Cβ	A	Ala52	Cα	3.84	VW
	Cβ	A	Phe51	C	3.83	VW
	Cβ	A	Phe51	O	3.67	VW
	Cβ	A	Ala52	N	3.8	VW
	Cβ	A	Ala52	C	3.73	VW
	Cβ	A	Ser53	N	3.93	VW
	Cγ	A	Arg50	C	3.96	VW
	Cγ	A	Arg50	O	3.43	VW
	Cδ	A	Arg50	C	3.97	VW
	Cδ	A	Arg50	O	3.71	VW
	Cδ	A	Gly49	O	3.3	VW
	Nε	A	Gly49	O	3.85	VW
	C	A	Gly49	O	3.67	VW
	Cζ	A	Ala52	O	3.93	VW
	Cζ	A	Ser53	Cβ	3.89	VW
	NH1	A	Ser53	Cβ	3.58	VW
	NH2	A	Ala52	C	3.8	VW
	NH2	A	Ser53	Cα	3.96	VW
	NH2	A	Gly49	C	3.81	VW
	NH2	A	Gly49	O	2.75	HB
	NH2	A	Ala52	O	2.99	HB
	NH2	A	Ser53	Cβ	3.91	VW
No. of total contacts						**26**
vdW						23
H-bonds						3
No. of contacts with peptide backbone						**4**
vdW						3
H-bonds						1
No. of contacts with side chain						**22**
vdW						20
H-bonds						2

Table 3.9 – Intermolecular contacts mediating peptide binding to MHC by Arg-3
vdW = van der Waals (=< 4.0 Å cut-off), H-bonds = hydrogen bonds (=< 3.4 Å cut-off).

a) Pro-1 at P-1

His81β Pro-1 C N Val85β Ser53α

b) Pro-2 at P-2

Pro-2 C N Val85β Ser53α Ala52α Phe51α

c) Arg-3 at P-3 vdW

Ser53α Arg-3 N C Gly49α Arg50α Ala52α Phe51α

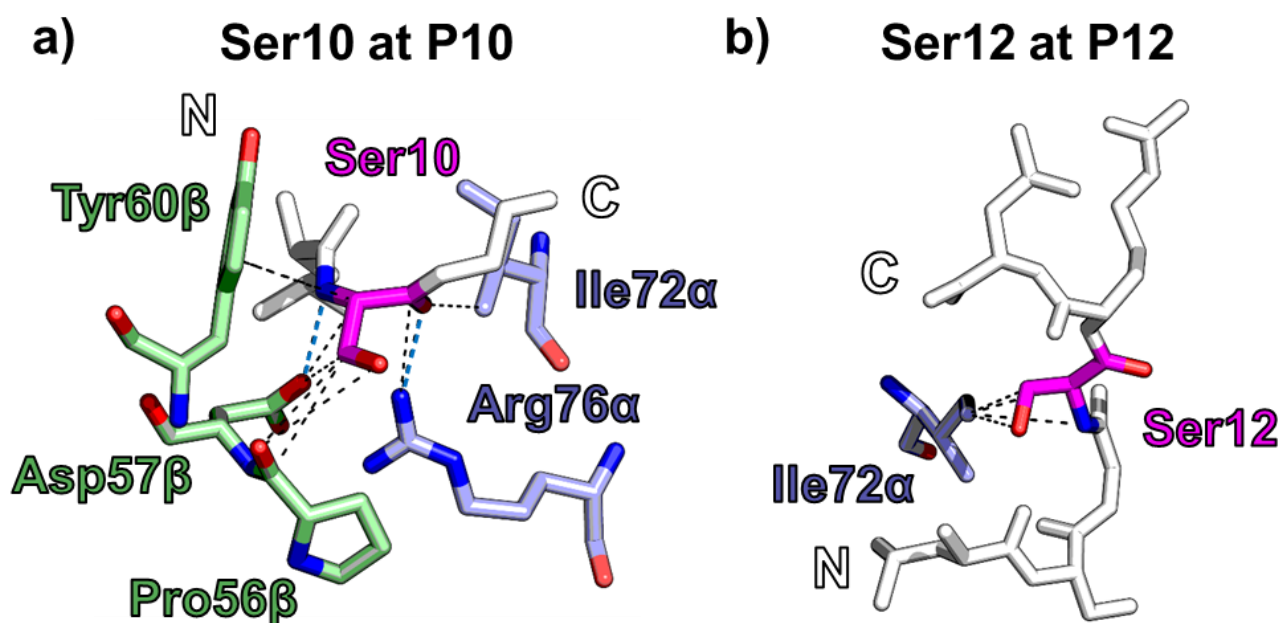**d) Arg-3 at P-3 H-bonds**

Ser53α Arg-3 N C Gly49α Ala52α
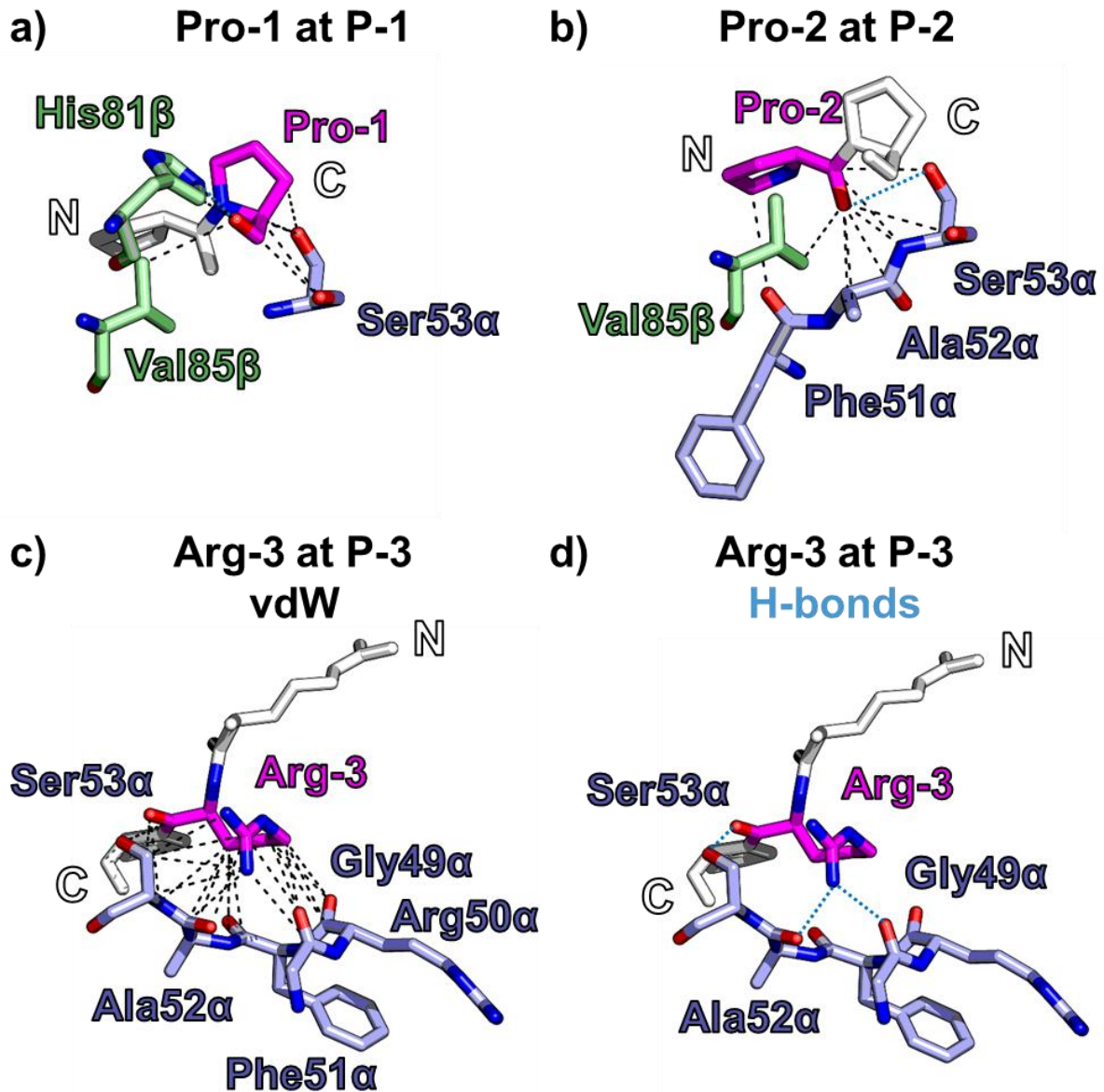
Figure 3.17 - Inter-molecular contacts between the N-terminal flank of 5T4p12 and HLA-DR1:

a) Stick representation of 5T4p12 peptide (white) binding to MHC highlighting residue Pro-1 (magenta) interacting with Ser53α (blue), His81β and Val85β (both green). Van der Waals contacts (=< 4.0 Å) are shown as black dashed lines and H-bonds (=< 3.4 Å) shown as blue dashed lines between contributing atoms.

b) Stick representation of 5T4p12 binding as in a) highlighting Pro-2 (magenta) interacting with Phe51α, Ala52α & Ser53α (blue) as well asVal85β (green).

c) Stick representation of van der Waals contacts (=< 4.0 Å) by Arg-3 at position P-3 allowing interaction with Gly49α to Ser53α (all blue). Contribution to MHC binding by Arg-3 was mediated mostly through interactions between Arg-3 side chain atoms.

d) Stick representation of H-bond contacts between Arg-3 and HLA-DR1α chain residues describing backbone Arg-3 carbonyl interacting with Ser53α and side chain NH2 contacting backbone carbonyls of Gly49α and Ala52α. The bond distance of all three H-bonds were in the intermediate range 2.75 - 3.0 Å.

- 130 -

3.7 Discussion

CD4^{+} T cells have been shown to recognise 5T4-derived antigens in human colorectal patients and loss of this recognition has been linked with tumour progression (Scurr et al. 2013). Protection against tumour formation in models of 5T4[+] tumours in mice treated with an attenuated 5T4 bearing vaccine MVA-5T4, as well as the boosting of anti-5T4 B cell immunity, highlighted a role for CD4^{+} T cell populations in the therapeutic response to vaccination against 5T4 presented in an inflammatory context (Castro et al. 2012). As a result, analysis at the clonal level of T cells circulating within individuals, the desired targets for boosting by vaccination, enables a molecular explanation of the initial quality of the T cell response against 5T4-derived antigens. Moreover, analysis of the ability to present 5T4-derived peptide antigens on MHC molecules describes how epitopes are selected for presentation to the T cell repertoire and thus enable immunogenicity.

In these studies, three generated CD4^{+} T cell clones were shown to be responsive to 5T4-derived peptides presented in the context of HLA-DR1. These clones were generated from the peripheral blood of an HLA-DR1^{+} donor. The T cell clones, in response to antigen *in vitro*, exhibited a T_H1 phenotype with all clones capable of producing the type 1 inflammatory cytokines IFNγ and TNF-α. These clones therefore did not display a regulatory T cell phenotype despite the self-derived nature of the 5T4 peptide antigens. Each clone, however, exhibited individual sensitivities to antigen with different levels of maximal cytokine release in response to antigen.

Despite ability to activate in response to peptide presented in the context of HLA-DR1 expressing cells only, multimer staining with HLA-DR1 complexed with cognate 5T4-derived peptides indicated poor antigen binding by the TCR. Such poor staining was observed despite using enhanced protocols for the detection of low affinity T cell clones (Tungatt et al. 2015). To try quantify this weak binding of 5T4-derived peptide antigens, soluble TCRs and MHC-II molecules were produced for biophysical analysis of the cognate interaction between 5T4-reactive TCR and 5T4-derived peptides presented on HLA-DR1. These studies, however, were hampered by an inability to produce two out of the three TCRs *in vitro* due to poor-to-no refolding efficiency. Despite this, using the single TCR which was obtainable – the TCR expressed by the 5T4p38 reactive GD.C112 – the weak engagement of cognate antigen observed in multimer staining analysis was replicated at the protein level by SPR. Here, GD.C112 was shown to exhibit some binding to 5T4p38 presented on HLA-DR1, however, this interaction occurred at a low affinity that was consequently unquantifiable and thus further experiments are required. Together, this molecular analysis of 5T4 TCR binding shows that engagement of cognate

pMHC-II by the TCRs expressed by each 5T4-reactive T cell clone appears weak, yet each T cell clone is responsive to peptide *in vitro* as shown by T cell activation assays.

pMHC structural data was sought to provide further insight into this weak TCR-pMHC interaction. Acquisition of structural data regarding MHC-II presented peptide epitopes within the literature has been hampered by the comparative difficulties in producing high quantities of pure conformationally correct MHC-II protein samples. As a result, the number of MHC-II derived x-ray crystallographic structurers deposited to the PDB are vastly outnumbered by MHC-I counterparts. Enabled by affinity purification of HLA-DR1 molecules, crystallisation of HLA-DR1 complexed with 5T4p12 was achieved and the structure solved at 1.95 Å. This structure defined the peptide binding core of the epitope, the residues which anchor the peptide to the MHC and the residues available for TCR contact.

The 5T4p12 peptide presented by HLA-DR1 exhibited few charged/polar residues within the core peptide and thus may explain the observed weak engagement by multimer stain. Glu3 and Asn8 exhibit the only obvious high-enthalpy contact points for TCR engagement. As a result, if the GD.C112 focuses binding to the peptide core, TCR engagement may be mediated by CDR loop binding close to the peptide backbone as well as the minimal side chains of Ala2, Ala5 and the partially buried Leu7 at positions P2, P5 and P7, respectively.

Analysis of the peptide flanking residues of 5T4p12, however, highlighted a hairpin loop in the C-terminal flanking region that protrudes away from the peptide MHC surface volume and thus available for TCR binding. This hairpin loop exhibited characteristics of a type II β-turn of which such structural features have been described previously in a HLA-DR1 restricted HIV-GAG peptide (Zavala-Ruiz et al. 2004). Indeed, *Zavala-Ruiz et al.* describe a hairpin loop structure that, when mutated, impacted activation of a cognate T cell clone. As a result of the hairpin loop observed in 5T4p12, the charged C-terminal carboxyl and Arg13 are brought back to the vacinity of the peptide binding core. Such residues may form high-enthalpy interactions with TCR and facilitate binding.

Aside from the potential involvement in TCR binding, the observed hairpin loop describes an interesting MHC-II phenomena in peptide binding. In support of the observed hairpin described by *Zavala-Ruiz et al.*, the structure of HLA-DR1 5T4p12 provides a further model example of secondary structure motifs in the C-terminal flanking region and thus provides evidence of structral order in the peptide flanks. Moreover, MHC-II presented peptides are generally thought to be flat and exhibit little elevation away from the MHC binding groove – in comparison to MHC-I presented peptides which can form large central bulges (Holland et al. 2013). As shown by HLA-DR1 5T4p12, extension of peptides at the flanks does not necessarily

result in an extension of peptide width, as generally perceived. Instead, through the formation of the described hairpin loop in 5T4p12, peptides can elevate away from the peptide binding groove, increasing the peptide height and the overall peptide-MHC surface volume height.

The observed hairpin was enabled by a Ser-Gly-Ser (SGS) sequence which is inherently very geometrically flexible, due to the central glycine residue, and is thus predisposed to forming secondary structure motifs. Analysis of the SGS structural arrangement observed at the C-terminal peptide flank of HLA-DR1 5T4p12 compared to the same residues within the published structure of the native 5T4 protein (Zhao et al. 2014) reveals structural parallels between the peptide antigen *in situ* and in presented form (*Figure 3.18*). Whilst not exhibiting exact geometric conformity to the SGS sequence observed bound to the MHC, there are similarities in the overall structure of the sequence in the native 5T4 antigen and bound to HLA-DR1; signified by a root mean squared deviation (RMSD) value of 0.794 upon alignment of the SGS sequence in both HLA-DR1 5T4p12 and the native 5T4 protein (RMSD of $5T4_{126-128}$ (SGS) in PDB: 4CNM vs HLA-DR1 5T4p12 = 0.794). Observation of the SGS sequence in the structure of the native folded 5T4 shows that the SGS sequence again forms a turn in the protein about the central glycine. Observation of such structural parallels may be conserved to MHC-II presented peptides only due to the open ended nature of the groove and its consequent loss of influence on extended peptide flanks; thus allowing flanking residues to form conformationally favourable motifs irrespective of the MHC molecule.

Despite the observed poor binding shown by multimer staining of cells, the 5T4p12 peptide has been shown to be immunogenic. Consequently, it was reasoned that 5T4p12 bound strongly to HLA-DR1 and thus contributed to this immunogenicity. As such, the solved structure of HLA-DR1 5T4p12 was interrogated for the interactions mediating peptide binding to MHC. Burial of P1 (Leu1), P4 (Leu4), P6 (Ala6) and P9 (Leu9) residues of 5T4p12 enclosed into binding pockets and provided a large network of intermolecular contacts between peptide and the MHC. Assignment of this peptide binding core defined the 5T4p12 peptide as able to be presented by APCs using a near ideal HLA-DR1 binding motif and thus adds rationale as to why the 5T4p12 is immunogenic. Only Leu1 incorporation into the P1 pocket could be described as sub-optimal. Despite numerous contacts with Leu1, the P1 pocket remains only partially filled allowing for incorporation of larger side chains capable of making more extensive contact networks with the MHC molecule. Such contacts, were fewer compared to those observed by P1 incorporation of tyrosine in another peptide-HLA-DR1 system (Stern et al. 1994). Nevertheless, the HLA-DR1 5T4p12 structure described how the P1 position of HLA-DR1 is able to accommodate and bind leucine residues through interaction with the leucine side chain atoms and is
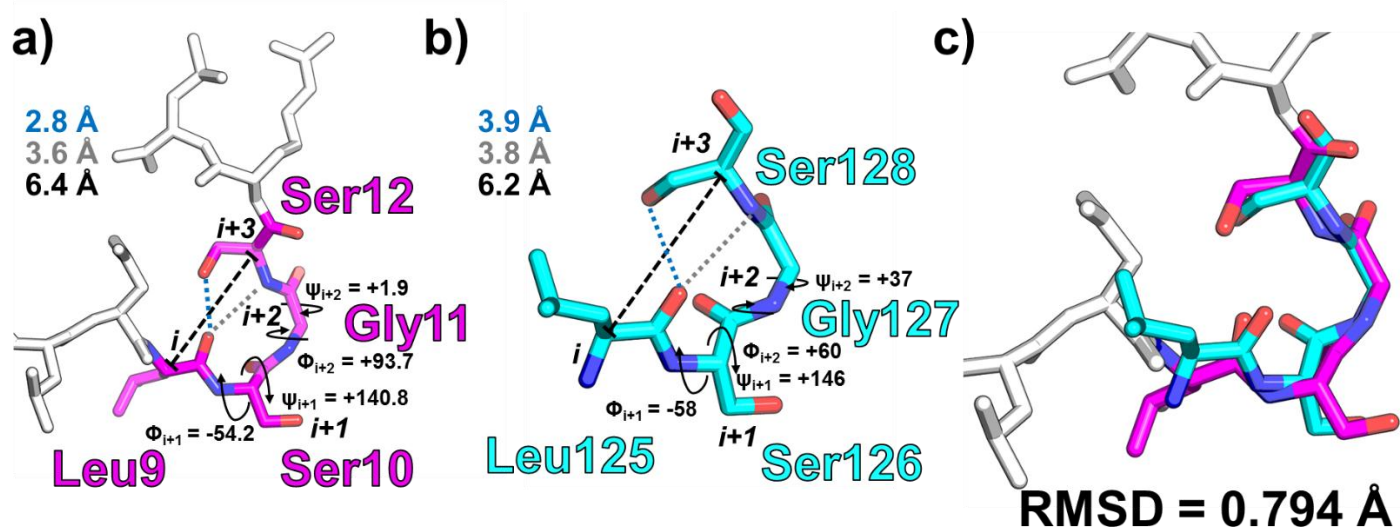
Figure 3.18 – Structural parallels between 5T4₁₂₅₋₁₂₈ bound to HLA-DR1 and native 5T4 protein:

a) Stick representation of C-terminal hairpin loop exhibited by Leu9-Ser12 of 5T4p12 (magenta) bound to HLA-DR1 and the parameters of geometry that characterised the loop. Inset distances are colour coded to corresponding and Φ/ψ about Ser10 to Gly11 are shown.

b) Equivalent stick representation of the sequence of amino acids described in ***a)*** within the structure of native 5T4 (PDB: 4CNM) (Zhao et al. 2014) corresponding to residues Leu125 to Ser128 (cyan) of full length 5T4. Distances and angles are annotated as described in ***a)***.

c) Aligned stick representation of 5T4₁₂₅₋₁₂₈ bound to HLA-DR1 and as part of the native 5T4 protein. In both structures, parallels are observed about the SGS turn sequence quantified by a root mean squared deviation of 0.794 Å across the three residues.

the first structure showing incorporation of leucine residues into the P1 binding pocket of HLA-DR1.

Contributions to peptide binding to the MHC-II molecules by the peptide backbone have been previously identified to also include residues outside the core nonamer e.g. P-2 and P10 (Painter & Stern 2012). Such interactions were in the form of hydrogen bonds to peptide back-bone with Ser53α and His81β at the P-2 position and Arg76α and Asp57β at the P10 position. Despite this, contribution of peptide flanking residues further extending out of the core peptide binding region is currently less understood and preference for amino acid side chains in flanks to enhance peptide to MHC binding has not been characterised in depth. Due to the length of peptide held within the MHC in the solved HLA-DR1 5T4p12 structure, these structural data provide an excellent model for the interrogation of peptide flanking region contribution to MHC binding.

In HLA-DR1 5T4p12, the single amino acid throughout the entire peptide which contributed the most contacts with MHC was attributed to Arg-3 in the N-terminal flank. Such contacts therefore suggest that this Arg-3 residue contributed to MHC binding on a similar capacity to that of a peptide residue within a classical binding pocket. Moreover, the majority of these con-tacts were mediated by the arginine side chain. Thus, incorporation of arginine residues at P-3 may be preferential for the enhanced binding of peptides to HLA-DR1. The locale of Arg-3 may have been dependent, however, on the diproline kinking sequence that superseded it and allowed the peptide to curve towards the DR1α chain whilst sitting atop the DR1α surface.

Together, analysis of structural data at the N- and C-terminal flanks highlight that whilst displaying a degree of mobility, as indicated by isotropic displacement parameters, peptide flanking residues can exhibit conformational structures that impact peptide binding to MHC and potentially the repertoire of MHC-II restricted TCRs by contributing to the conformation of the peptide MHC surface volume.

3.7.1 Future directions

The work presented in this chapter describes the efficiency of T cell recognition of 5T4-derived peptide antigens through the study of three epitopes and three corresponding clones. The efficiency of a T cell clone to respond to antigen is influenced by both the ability for TCRs to bind to cognate pMHC but also the ability for MHC molecules to present such peptides. As a result, experimental quantification of the ability for HLA-DR1 to bind and present each 5T4-derived peptide would provide a better understanding of the comparative contribution of peptide affinity to HLA-DR1 in the observed efficiency and sensitivity of each described clone. This

could be achieved through peptide binding assays to HLA-DR1 as opposed to relying on the predictions described in this study.

One limitation of this study is that whilst the three epitopes of 5T4 have been shown to be immunogenic *in vitro* through culturing and measuring responses by human T cells in the presence of synthetically produced peptide sequences, it is not guaranteed that these peptide epitopes are naturally processed through the MHC-II processing pathway and thus presented on professional antigen presenting cells. Nevertheless, in studies performed within our group, whole 5T4 protein has been shown to be immunogenic in *ex vivo* IFNγ release ELISpot assays stimulating with whole protein (Clarke et al. 2006). Moreover, primary responses to these epitopes have been repeatedly observed in both healthy donors and CRC patients. In order to assay whether each epitope is naturally processed by APCs, full length 5T4 protein could be used in the T cell clone activation assays similar to those described with peptide.

APCs process MHC-II peptide antigens usually by the uptake of exogenous protein via the endosomal or lysosomal pathway for protein digestion. To assay the abundance of the described 5T4 epitopes as part of the presented 5T4 peptide ligandome, whole 5T4 protein could be 'fed' to APCs and the resulting ligandome studied. Using mass spectrometry of HLA-DR elution products, the relative abundancy of 5T4p12 presentation compared to other 5T4-derived peptides, and the other peptides in the ligandome could be studied. Moreover, the nested set of peptides for the $5T4_{117-125}$ epitope within the 5T4p12 peptide could also be identified.

Determination of the importance of the C-termainal hairpin loop region to TCR binding could be assayed through T cell clone activation assays of modified peptides using the GD.D104 clone. Such modifications could include truncations to completely remove the N- and C-terminal flanking regions and alanine scan mutations across the whole peptide to assay the contribution of each residue to TCR binding of the GD.D104 TCR including at the C-terminal flank. Such experiments would show whether the C-terminal carboxyl and Arg13, which are brought back to the facinity of the peptide binding core by the hairpin loop, contribute to binding through high-enthalpy interactions with a TCR. In addition, disruption of the C-terminal hairpin loop by mutation of the central Gly11 residue within the SGS sequence which enables flexibility in dihedral angles could be assayed by mutation to residues which block dihedral angle flexibility such as proline.

Ultimately, the contribution of each residue to binding the GD.D104 TCR would be comprehensively revealed by the solving of the complexed structure between HLA-DR1 5T4-p12 and the GD.D104 clone TCR. Such studies would require optimisation of the production of the GD.D104 TCR which did refold but at poor efficiency. In addition, due to the likely low

affinity between GD.D104 TCR and HLA-DR1-5T4p12, as indicated by multimer staining, acquisition of complex crystals may prove challenging. Nevertheless, complexed structures between TCRs and pMHC-II molecules have been solved despite an inability to detect binding by either SPR or multimer staining (Deng et al. 2007; Beringer et al. 2015). Such structural data would reveal the role in which the C-terminal flanking region plays in TCR binding.

3.7.2   Implications of this study

In the studies outlined in this chapter, analysis of the CD4^{+} T cell immune response to 5T4 antigens has revealed the presence of 5T4-reactive T cell clones that are sensitive to antigen yet exhibit sub-optimal engagement of pMHC-II. In response to antigen, these T cell clones cultured from the peripheral blood of a healthy donor exhibit a strong T_H1 functional phenotype and adds evidence to the surveillance of tumour antigens within the periphery through expression of TCRs which are able to bind self-derived antigens presented on MHC-II molecules. In efforts to describe this presentation of self-antigens to T cells through the solving of the HLA-DR1 5T4p12 structure, a number of interesting observations were made regarding how HLA-DR1 is able to present a new peptide epitope. Firstly, this structure demonstrates that leucine can be an effective anchor for the P1 binding pocket of HLA-DR1. Secondly, this structure revealed that peptide flanking residues might contribute substantially to the binding of peptides to HLA-DR1 and consequently suggests a preference for large charged amino acid residues at position P-3 in the N-terminal flanking region. Thirdly, elucidation of the HLA-DR1 5T4 structure provides a second model example of an MHC-II specific phenomena in peptide binding in that C-terminal flanking regions can form ordered hairpin loop structures that drastically alter the pMHC surface volume presented to the TCR repertoire. Finally, it was observed that the structure of the C-terminal flanking hairpin loop resembled the folding of the 5T4p12 epitope in the native 5T4 protein. This consequently challenges the dogma that peptides presented on MHC molecules are held in an extended conformation dictated by the MHC that are absent in secondary structural similarity to the native antigen.

4 Chapter 4: Molecular characterisation of the LAG-3-MHC-II interaction

4.1 Abstract

Lymphocyte activation gene-3 (LAG-3) is expressed on a number of immune cells including activated CD4$^+$ T cells and suppressive T cell subsets. On activated effector T cells, LAG-3 functions as a co-inhibitory receptor and consequently limits T cell activation in response to antigen stimulus. Overexpression of LAG-3 on CD4$^+$ T cells extracted from tumour sites has implicated LAG-3 in suppressing T cell immunity to tumours and consequently highlighted the molecule as a potential target for enhancement of anti-tumour immunity through the blockade or removal of LAG-3. The function of LAG-3, however, is poorly described. Here, the molecular role of LAG-3 is interrogated through the study of LAG-3 binding to its putative ligand, MHC-II. Through cellular staining and flow cytometry, LAG-3 was shown to bind multimerised MHC-II molecules. This interaction was characterised at the protein-protein level by surface plasmon resonance where the moderate affinity ($K_D = 13$ μM) of MHC-II engagement by LAG-3 was defined. Moreover, preliminary efforts to describe LAG-3 structure via negative stain electron microscopy are documented with a future view to the study of LAG-3 and MHC-II using high-resolution structural techniques. Together, these molecular studies show LAG-3 is able to bind MHC-II with moderate affinity providing insights into the mechanism by which LAG-3 initiates T cell inhibition.

4.2 Introduction

Lymphocyte activation gene-3 (LAG-3) is a single pass transmembrane protein expressed on a number of immune cells including activated CD4$^+$ and CD8$^+$ αβ T cells, γδ T cells, B cells, NK cells and plasmacytoid dendritic cells. LAG-3 function is best described in activated CD4$^+$ T cells where it has been show to inhibit T cell activation (Triebel 2003). LAG-3 expression by CD4$^+$ T cells is upregulated after TCR mediated stimulation, is maximal at four days, and detectable at seven days, post-activation in T cells extracted from murine spleen or lymph nodes challenged *in vivo* (Sega et al. 2014).

Upon cell surface expression, LAG-3 is thought to localise to the immune synapse through an interaction with MHC-II molecules (Huard et al. 1996). Subsequently, suppression of T cell signalling mediated by LAG-3 has been shown to be dependent on the protein's short cytoplasmic tail (Workman et al. 2002). Further suppressive function may also be enhanced through competition for MHC-II binding with the CD4 co-receptor (Huard et al. 1995).The signalling mechanisms that enable LAG-3 mediated suppression of T cell signalling have not been defined, however, involvement of a co-precipitated accessory protein termed LAG-3-associated protein may be implicated (Iouzalen et al. 2001).

As well as a role in maintaining T cell homeostasis in the effector response against antigens, LAG-3 expression has also been implicated in maintaining the function of regulatory T cell subsets such as classical FoxP3$^+$ regulatory T cells (T$_{regs}$) (Huang et al. 2004). In addition, tumour infiltrating lymphocytes (TILs) extracted from human colorectal cancer patients exhibited an upregulation of LAG-3 expression compared to T cells extracted from matched PBMC and healthy colon and were not dependent on FoxP3 expression (Scurr et al. 2013). Moreover, LAG-3 expression, in conjunction with CD49b, identifies a population of highly suppressive FoxP3$^-$ regulatory cells termed type 1 regulatory (Tr1) cells (Gagliani et al. 2013). Similarly, this Tr1 subset of cells has also been implicated in tumour infiltration (Pedroza-Gonzalez et al. 2015).

Together, these studies highlight LAG-3 as a marker of a sub-optimal immune response to tumours, either through involvement of suppression on activated effector responses or on regulatory populations. The basis of LAG-3 function on such cells is thought to be mediated by an interaction with MHC-II which consequently implicates LAG-3 with the immune synapse.

4.2.1 Current understanding of LAG-3 binding to MHC-II

LAG-3 was first hypothesised to bind to MHC-II molecules upon characterisation of human *LAG3* as a gene upregulated upon activation of lymphocytes (Triebel et al. 1990). Such reasoning, in these early studies, was based on the similarity of LAG-3 with the already defined MHC-

II ligand, CD4, at the gene level. *Lag3* shared a neighbouring chromosomal locale with *CD4* (LAG-3: chromosome 12, p13.3; CD4 chromosome 12, pter-p12) as well as similar exon-intron organisation. *Lag3* and *CD4* genes exhibited regions of sequence homology which, importantly, translated to structural similarity at the gene level where both gene sequences encoded motifs characteristic of four Ig-like domain containing proteins.

The first experimental evidence of a LAG-3 interaction with MHC-II was achieved through the characterisation of the *Lag3* gene product at the protein level enabled through the generation of monoclonal antibodies against LAG-3 protein (Baixeras et al. 1992). Primate kidney derived fibroblast-like COS-7 cells expressing LAG-3 through transfection adhered to MHC-II sufficient B lymphocytes. Such adhesion was observed as LAG-3⁺COS-7 "rosetting" with a range of MHC-II⁺ cell lines. This adhesion was abrogated through the incubation of either αHLA-DR (mAb clone D1.12), pan-HLA-class II (mAb clone 9.49) or an αLAG-3 (mAb clone 17B4) antibody and thus indirectly indicated an interaction between LAG-3 and MHC-II proteins expressed on the surface of cells. Blockade of this surface interaction on cells was subsequently shown to have functional consequences on the activation of T cell clones (Huard et al. 1994).

Specific cellular detection of LAG-3 binding to MHC-II was achieved through the expression of a soluble LAG-3 protein sample constructed through the fusion of a human IgG1 fragment crystallisable (Fc) domain to the extracellular portion of LAG-3 (henceforth termed LAG-3:Fc). This protein molecule specifically stained HLA-DR4 transfected fibroblast cell lines as well as numerous HLA class II⁺ cell lines through secondary staining detected by flow cytometry (Huard et al. 1996). No such staining was observed in either non-transfected controls or HLA-class II⁻ cell lines and were again abrogated by the addition of the 17B4 clone αLAG-3 mAb whose epitope had been confirmed to the LAG-3 portion of the LAG-3:Fc protein.

Extension of these fluorescent staining experiments, whereby titrating concentrations of LAG-3:Fc were used to stain HLA-class II⁺ cells, showed LAG-3:Fc bound to MHC-II expressing cells with far superior capacity to CD4:Fc equivalent molecules due to detection of binding down to 100-fold lower concentrations of LAG-3:Fc protein compared to CD4:Fc (Huard et al. 1995). Using Scatchard plot analysis, the avidity of LAG-3:Fc – a *dimeric* form of LAG-3 – was deduced to a K_D of 60 nM at 37 °C. Moreover, the binding of LAG-3:Fc to MHC-II blocked consequent interaction of CD4 with MHC-II, thus suggesting that LAG-3 and CD4 compete for the same binding site. Similar analyses using murine derived fusion proteins replicated the enhanced binding of LAG-3:Fc to MHC-II expressing cells compared to CD4:Fc (C. J. Workman et al. 2002).

Biochemical analysis of LAG-3:Fc binding enabled regional localisation of the MHC-II binding domain on LAG-3. Truncation of LAG-3 to the two extracellular domains (D1 & D2) of LAG-3 and consequent fusion to IgG1 Fc to form LAG-3D1D2:Fc localised the binding site of LAG-3 to the N-terminal IgSF domain (Huard et al. 1997). This binding site was resolved down to a 30 amino acid additional loop sequence within the membrane distal D1 domain using mutational analysis and consequent impact on LAG-3 mediated adhesion to MHC-II expressing cells. This extra loop was unique to LAG-3 compared to CD4 and as a result, it was reasoned that LAG-3 binding to MHC-II occurred at a higher affinity to that of CD4 binding to MHC-II through residues contained within the unique loop sequence.

4.2.2   Evidence of LAG-3 multimerisation and implication on functional binding

Evidence of oligomerisation of CD4 molecules at the cell surface drove reasoning that, due to similarities to the co-receptor, LAG-3 may form multimers at the cell surface which mediate an increased functional avidity for MHC-II as well as stabilise solvent exposed LAG-3 (Huard et al. 1997). Data to support such hypotheses was shown by the mutation of residues within the membrane distal D1 domain of LAG-3, outside the defined extra-loop binding site for MHC-II, which were able to remove LAG-3 functional binding to MHC-II. Here, three mutations R88A, D109E, and R115A in LAG-3 transfected into COS-7 cells rendered LAG-3 unable to bind MHC-II via adhesion assay and, when co-transfected with wild type LAG-3, was able to inhibit wild type binding to MHC-II. Thus, these mutations inhibited MHC-II binding with a dominant negative-like effect and thus suggested that dimerisation was required to facilitate MHC-II binding. From this data, a proposed model whereby the D1 domain of LAG-3 contains a homotypic dimerization binding site (LAG-3 to LAG-3) as well as the ligand binding site (LAG-3 to MHC-II) was suggested (summarised in *Figure 4.1*).

Support for this described model was elucidated by the observation of LAG-3 post-translational cleavage products in murine systems. Here, a cleavage product of LAG-3 corresponding to the extracellular portion was shown to localise at the cell surface despite absence of the membrane anchoring transmembrane and cytoplasmic domains (Li et al. 2004). This extracellular domain cleavage product was co-precipitated with full length LAG-3 via a homotypic interaction with full length LAG-3 at the cell surface. Further evidence of oligomerisation mediated via the membrane distal D1 domain was achieved by the generation of D1 domain deficient LAG-3 constructs or LAG-3:CD4 chimeric constructs, whereby the D1 domain of LAG-3 was replaced with that of CD4. Such constructs once more revealed a dependency of wild type D1 domain on observed oligomerisation.
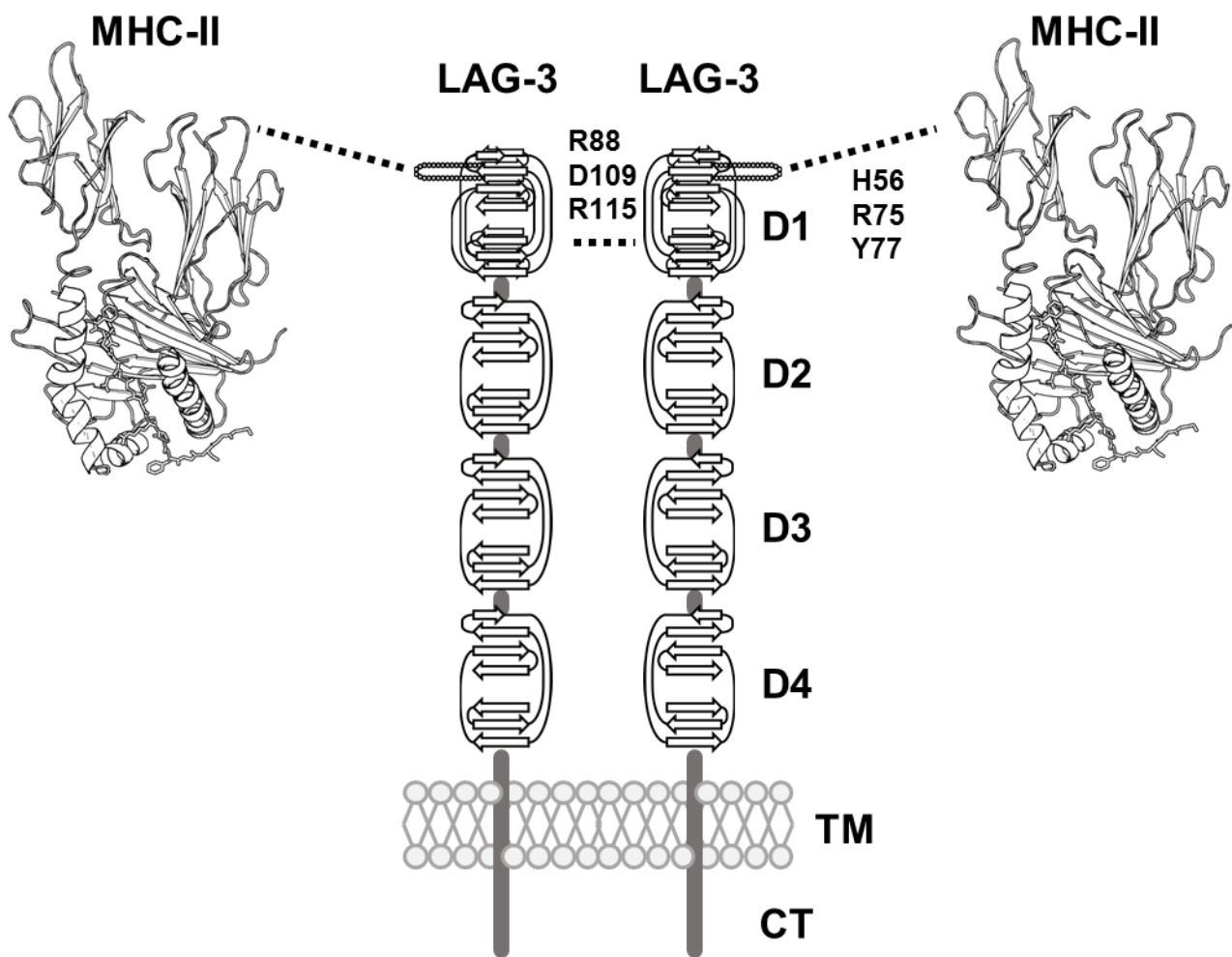
Figure 4.1 – Model of LAG-3 binding to MHC-II and potential oligimerisation:
Schematic overview of the hypothetic model of LAG-3 oligomerisation and MHC-II binding as proposed by Huard et al. 1997. LAG-3 was proposed to contain two binding sites: a homotypic (LAG-3-LAG-3) site and a heterotypic (LAG-3-MHC-II) binding site. Homotypic binding was proposed to be mediated by residues including R88, D109 & R115 whilst heterotypic binding was proposed to be mediated by residues including H56, R75 & R77 as shown by site-direct mutagenesis studies. Dimerisation through the D1 domain of LAG-3 was further evidenced by non-detection of a co-immunoprecipitating LAG-3 fusion product when the LAG-3 D1 domain was exchanged for the equivalent domain of CD4 (Li et al. 2004). TM = transmembrane domain , CT = cytoplasmic tail domain

Together, these indirect functional and biochemical assays provide evidence of dimeric forms of LAG-3 at the cell surface and therefore implicates the effect of multivalency in the functionality of LAG-3 binding to MHC-II molecules.

4.2.3 Electron microscopy and surface plasmon resonance as tools to study LAG-3 structure-function

The described avidity value of LAG-3:Fc for MHC-II ($K_D = 60$ nM) is used in the literature to describe the potency of LAG-3 function on inhibition of T cell activation through a perceived high affinity interaction with MHC-II (Workman & Vignali 2003; Li et al. 2007; Gagliani et al. 2013). Whilst the described analyses showed an ability of LAG-3:Fc molecules to exhibit enhanced binding compared to CD4:Fc molecules, these analyses do not take into account the potential contribution of avidity effects as a result of the dimerization of LAG-3 through the Fc portion of LAG-3:Fc. Moreover, differences in observed avidity between LAG-3:Fc and CD4:Fc molecules cannot be categorically attributed to differences in monovalent affinity between LAG-3 and CD4 for MHC-II. The ability of the dimeric fusion proteins to differentially bind multiple ligands may, for example, also be dependent on differences in steric hindrance or molecular flexibility between LAG-3:Fc and CD4:Fc molecules. Thus, in order to accurately describe the monovalent binding affinity of LAG-3 for MHC-II, molecular techniques which can account for the effects of bivalency are required.

Despite growing interest in the function of LAG-3 on T cell homeostasis, its role within diseases including cancer and the therapeutic targeting of LAG-3 expressing cells, the current understanding of human LAG-3 structure-function and the nature of the interaction with MHC-II has advanced little since the studies described. This stagnation is despite the evolution of structural and biophysical techniques for the study of protein structure and protein-protein interactions. As a result, indirect fluorescence measurements of binding through analyses such as the Scatchard plot are considered outdated and superseded by methodologies that directly measure protein-protein interactions such as surface plasmon resonance (SPR).

Whilst previous groups have endeavoured to prepare LAG-3 protein samples suitable for the study of LAG-3 structure at high resolution via x-ray crystallography, such efforts have not produced soluble protein able to be crystallised (F. Triebel, personal communications). As such, the only LAG-3 protein sample successfully produced *in vitro* documented in the literature is the dimeric LAG-3:Fc fusion protein, described previously, or variations thereof. The mammalian expression system used to produce this fusion protein, which incorporates extensive post-

translational glycosylation, has rendered the protein formulation averse to the formation of protein crystals. Nevertheless, study of the structure of LAG-3:Fc can be obtained using solution techniques such as single particle transmission electron microscopy (EM).

The molecular size of LAG-3:Fc makes the protein sample amenable, but difficult, to study by negative stain EM. Using this technique, protein in solution is applied to a grid after which a high molecular weight stain, such as uranyl acetate, is applied to grids in order to create contrast around the low-molecular weight protein envelope (Rames et al. 2014). Prepared grids are consequently analysed under a transmission electron microscope whereby single protein particles can by imaged. Collection of multiple EM frames is performed to achieve a dataset of particle "views". These particle views are described by their orientation in Euclidian space[3] and the parameters of which are termed the Euler angles[4]. Analysis of these particle views can be used to generate three-dimensional reconstructions of proteins through a series of image processing events (Tang et al. 2007). First, particle images are summated via 2D analyses to form a collection of image classes – termed class sums – whereby particle images are grouped according to similarity in "views" of the protein and thus increase the signal-to-noise ratio in particle images. Consequent 3D analysis determines the relationship between class sums and, as a result, assigns spatial 3D coordinates for classes. Subsequent rounds of model refinement through iterative 2D and 3D analyses yield reconstructions of proteins to resolutions typically capped at around 20 Å. This resolution range is limited due to the lack of mass-contrast[5] within the protein sample and, thus, structural information achieved through negative stain EM is mostly limited to that of the protein surface envelope (Boekema et al. 2009). Increasing the number of particle images, however, improves the accuracy and resolution of the obtained model and can reveal some secondary structure features (Zhang et al. 2008).

As a result, negative stain electron microscopy provides a feasible technique to study the overall protein structure of LAG-3:Fc as a model of LAG-3 expressed at the cell surface. Whilst negative stain EM does not yield atomic resolution protein structure information, analysis of the

---

[3] Euclidian space is the space that encompasses both the 2-dimensional plane and 3-dimensional space

[4] Euler angles are the angles that describe the orientation of an object in the 3-dimensional component of Euclidian space. This orientation is described by three angles: α, β, γ which represent the angle from the 3-dimensional planes x,y and z, respectively.

[5] Electrons passing through a sample will interact strongly with heavy atoms and weakly with light atoms. Proteins are generally made up of atoms of low mass, therefore interact weakly with electrons and are said to have low mass contrast. Proteins tend to exhibit a relatively even distribution of mass, thus, internal structural features – effectively differences in mass – are difficult to resolve.

overall shape and quaternary structure of LAG-3:Fc may aid understanding in the function of LAG-3 and it's interaction with MHC-II.

4.2.4   Aims

At present there is currently no high- or low-resolution data that describes LAG-3 protein structure and despite evidence of LAG-3 binding to MHC-II, the structural and biophysical characteristics which determine such binding are poorly described. As a result, insights into the three-dimensional fold of LAG-3 are based on sequence based predictions from which LAG-3 is thought to resemble the CD4 co-receptor. Whilst LAG-3 has been shown to bind specifically to MHC-II expressing cells in a series of studies, no direct detection of LAG-3 binding to MHC-II has been shown at the protein-protein level. As a consequence, no direct measurement of the affinity of LAG-3 for MHC-II has been accurately defined using modern instrumentation and kinetic analysis.

As a result, the overall aim of this chapter was to describe the nature of the LAG-3 interaction with MHC-II using biophysical techniques as well as structural investigations of LAG-3 with and without its putative ligand, MHC-II. This overall aim is divided into the following sub-aims:

(i)   To develop a stable LAG-3 expressing cell line as a model for LAG-3$^+$ T cells

(ii)   To measure multimeric MHC-II binding to LAG-3$^+$ cells using flow cytometry

(iii)   To measure LAG-3 binding to MHC-II at the protein-protein level using surface plasmon resonance (SPR)

(iv)   To try and establish an affinity value of *monovalent* LAG-3 binding to MHC-II

(v)   To gain insights into LAG-3 structure through the study of LAG-3:Fc via negative stain electron microscopy

4.3 Production of a stable LAG-3$^+$ cell line

In order to study the molecular interaction of LAG-3 and MHC-II on the surface of LAG-3 expressing cells and facilitate the studies described in Chapter 5, a stably expressing LAG-3$^+$ cell line was produced. The full length LAG-3 protein (Uniprot: P18627) was successfully cloned into the 3rd generation lentiviral transfer vector pELNsxv via restriction cloning (Dull et al. 1998). This construct, which contained LAG-3 and a P2A linked self-cleaving rat CD2 (rCD2) marker cassette under the constitutive EF-1α promoter, allowed the tracking of transduction through the rCD2 marker which is known to be detected and expressed well via lentiviral delivery in T cell lines.

Wild type JRT T3.5 Jurkat cells (henceforth JRT) were successfully transduced with LAG-3.P2A.rCD2 lentivirus, resulting in the detectable expression of both rCD2 and LAG-3 (*Figure 4.2*). After transduction, 98 % of cells were rCD2 positive highlighting a high transduction efficiency (data not shown). After 30 days of culture of the LAG-3.P2A.rCD2 transduced line, 79 % and 78 % of cells were positive for rCD2 and LAG-3 expression, respectively, highlighting a gradual loss of construct expression (*Figure 4.2a*). In order to maintain a stable homogenous population of LAG-3 expressing cells and prevent untransduced cell outgrowth, the transduced line was subjected to limit dilution cloning to obtain JRT derived LAG-3$^+$ clones (*Figure 4.2b*). This resulted in three clones: JRT LAG-3$^+$ C8, D4 & E11. Each clone exhibited 100 % LAG-3 expression as shown by no negative staining population whilst exhibiting similar LAG-3 expression (gMFI JRT LAG-3$^+$ C8 = 435, D4 = 340, E11 = 372). Due to the enhanced expression of LAG-3, the JRT LAG-3$^+$ C8 clone was selected for future studies. As a result, the LAG-3$^-$ JRT WT and JRT LAG-3$^+$ C8 cells as well as the MOLT-3 cell line, which would later be used as a LAG-3$^-$ CD4$^+$ control, were analysed for expression of TCR, LAG-3 and CD4 expression (*Figure 4.3*).
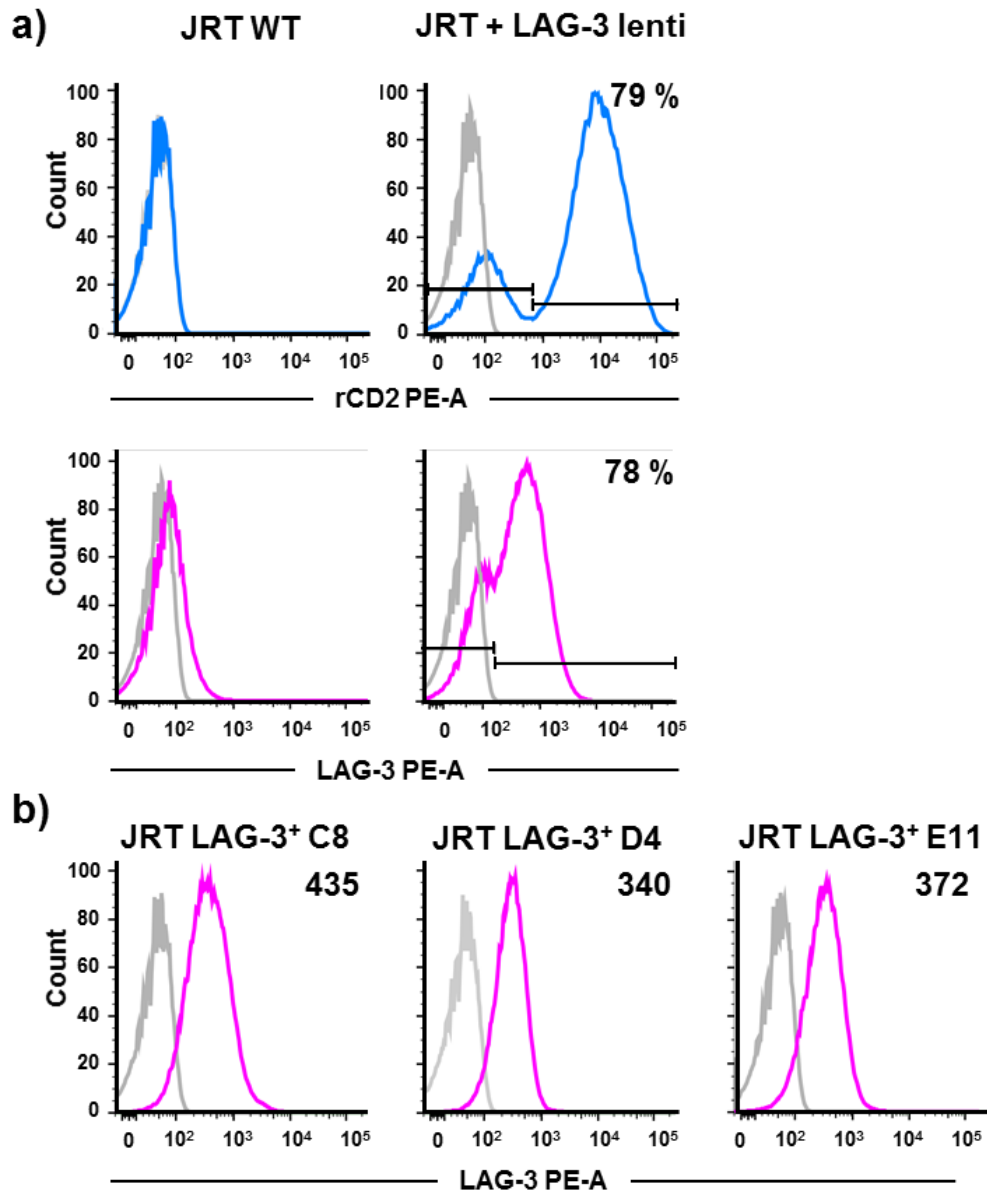
Figure 4.2 – Formation of the JRT LAG-3⁺ C8 cell line via lentiviral delivery:

a) Flow cytometry histogram plots of rCD2 and LAG-3 expression in wild type (WT) JRT cells and transduced JRT line following lentiviral delivery (JRT + LAG-3 lenti). Lentiviral transduction resulted in fluorescence intensity shift in rCD2 expression (blue) compared to unstained control (grey) as well as shift in LAG-3 staining (pink) compared to unstained control (grey). Post-transduction, 79 % of the resultant line were positive for the rCD2 transduction marker and 78 % of cells LAG-3⁺.

b) Flow cytometry histogram plots of LAG-3 expression in three consequent JRT LAG-3⁺ clones C8, D4 & E11 generated from the line described in ***a)***. Each clone expressed LAG-3 as shown by a shift in fluorescence intensity in LAG-3 stained (pink) compared to unstained control (grey). Inset numbers represent gMFI of LAG-3 staining. All three clones were 100 % LAG-3⁺ as shown by no negative population exhibited in the parent line.
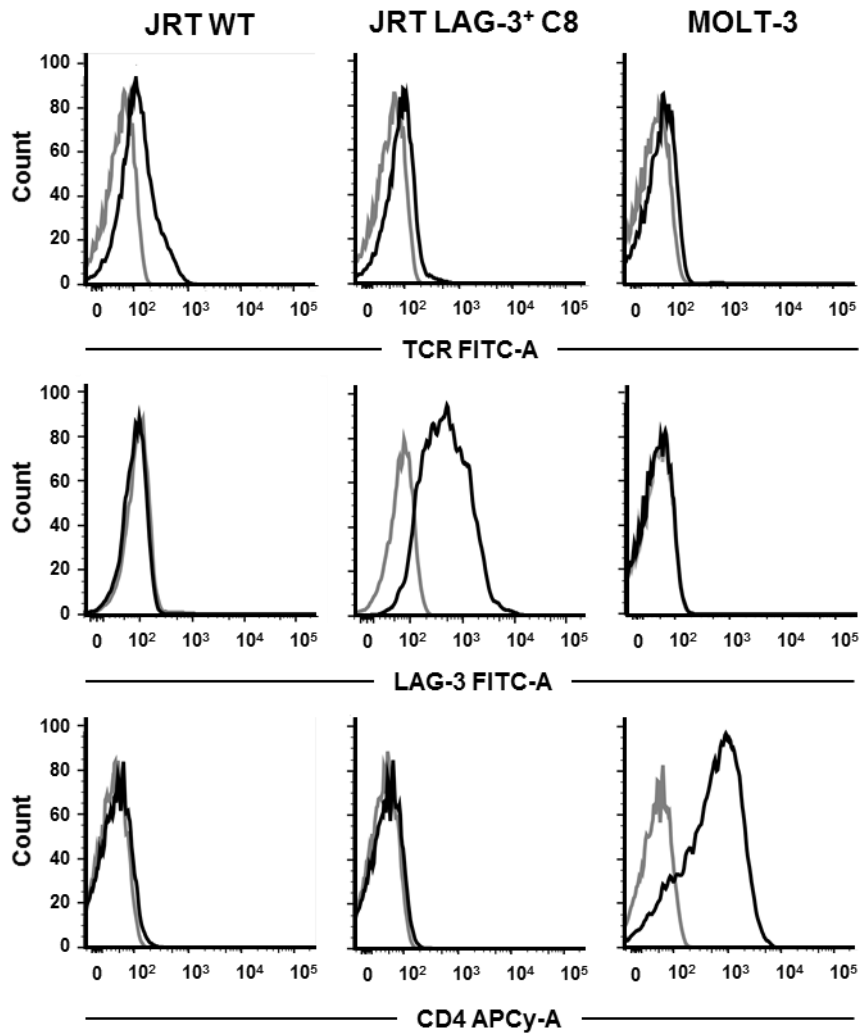
Figure 4.3 – Surface characterisation of T cell derived cell lines:
Flow cytometry histograms of TCR, LAG-3 and CD4 surface expression on LAG-3⁻ JRT WT, JRT LAG-3⁺ C8 and MOLT-3 cells. LAG-3⁻ JRT WT cells expressed no LAG-3 or CD4, JRT LAG-3⁺ C8 cells expressed LAG-3 but no CD4 and MOLT-3 cells expressed CD4 but no LAG-3. Each cell line showed low expression of TCR, as expected. Stained marker = black, FMO/unstained control = grey.

4.4 MHC-II multimers bind to LAG-3^{+} cells

Having generated a stably expressing LAG-3^{+} cell line as a model for T cells expressing LAG-3, it was hypothesised that MHC-II multimers would bind LAG-3^{+} cells through a TCR independent interaction with MHC-II. As such, LAG-3^{-} JRT WT and JRT LAG-3^{+} C8 cells were stained using PE labelled HLA-DR1 dextramers using a protocol optimised for low affinity interactions (Tungatt et al. 2015). Staining of JRT LAG-3^{+} C8 cells with HLA-DR1 Influenza HA$_{306-318}$ multimers resulted in modest detection of LAG-3 replete cells compared to both FMO and HLA-A2 multimer controls, whilst LAG-3^{-} JRT WT cells exhibited no staining (*Figure 4.4*). Staining of LAG-3 replete cells with HLA-DR1 multimers resulted in 19 % of cells exhibiting enhanced staining compared to background levels exhibited by -A2 multimers or either -DR or -A2 multimer staining of LAG-3 deplete cells (*Figure 4.4a*). Such detection resulted in a shift in fluorescence intensity in HLA-DR1 stained JRT LAG-3^{+} C8 cells only (*Figure 4.4b*). To ensure observed multimer staining did not arise due to multimer deposition on dead cells, experiments described were gated on live singlet cells by live/dead staining (*Figure 4.4c*). Despite the observed staining of JRT LAG-3^{+} C8 cells by HLA-DR1 multimers only, such staining was poor compared to staining of the HLA-DR1 Influenza HA$_{306-318}$-specific cognate T cell clone (DCD10) where 98 % of cells are detected as multimer[+] (*Figure 4.4d*). This was in spite of JRT LAG-3^{+} C8 exhibiting no LAG-3 negative population, described previously.

In order to confirm that the observed staining of LAG-3^{+} cells by HLA-DR1 multimers was indeed mediated by LAG-3, the effect of the LAG-3 blocking antibody clone 17B4 on HLA-DR1 multimer staining was assayed. Indeed, pre-incubation of JRT LAG-3^{+} C8 cells before multimer staining abrogated the shift in fluorescence intensity observed when staining with HLA-DR1 multimers (*Figure 4.4e*). To confirm antibody blockade had no effect on either HLA-A2 multimers staining of LAG-3 replete cells or -DR or -A2 multimer staining of LAG-3 deplete cells, corresponding blockade experiments were also performed on such controls and resulted in no significant impact on background staining (*Figure 4.4f*). Moreover, an irrelevant antibody (αCD4) was not able to abrogate the binding of HLA-DR1 multimers to JRT LAG-3^{+} C8 cells (*Figure 4.4g*).

Since CD4 also binds to MHC-II molecules, albeit via a notoriously weak interaction (Jönsson et al. 2016), it was reasoned that a similar staining of CD4^{+} cells by MHC-II multimers may be observed. The CD4^{+} LAG-3^{-} MOLT-3 cell line, however, showed no significant detection of multimer^{+} cells using HLA-DR1 multimers compared to -A2 multimers (*Figure 4.5a*). As a result, no shift in fluorescence intensity was observed between either FMO control of HLA-A2 multimer staining (*Figure 4.5b&c*).

Together, these data show that LAG-3 expressing cells are able to be modestly stained by MHC-II multimers characterised by a small shift in fluorescence intensity through an interaction mediated through LAG-3. Such staining was not comparable to that of a viral-derived MHC-II restricted cognate TCR interaction and was not observed in a LAG-3 deplete but CD4 replete cell line.
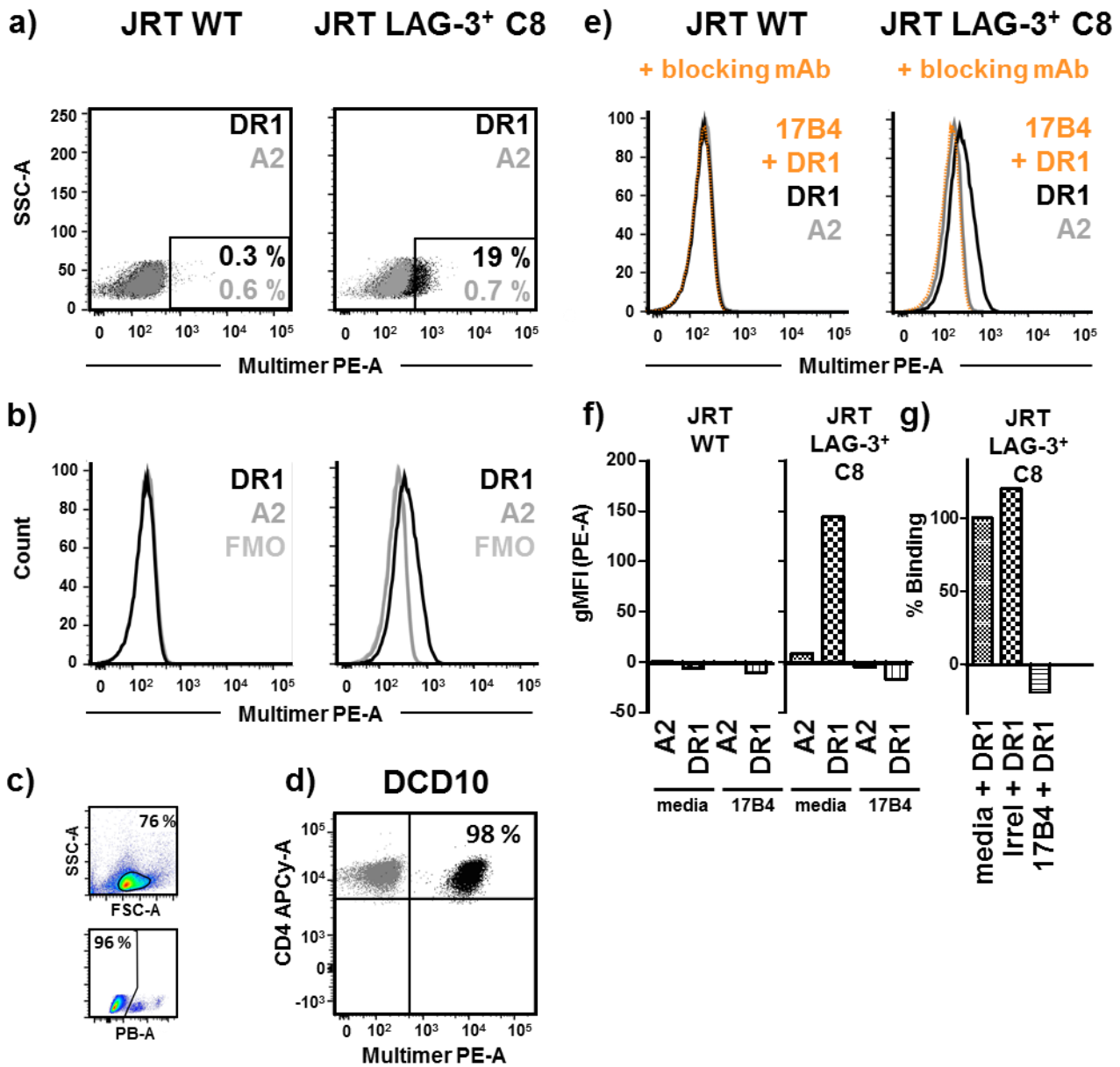
(Figure legend overleaf)

Figure 4.4 – Specific binding of HLA-DR1 multimers to LAG-3$^+$ cells:

a) 2D flow cytometry plots of MHC-multimer staining of LAG-3$^-$ JRT WT cells (left) and JRT LAG-3$^+$ C8 cells (right) with HLA-A2 multimers (grey) or HLA-DR1 multimers (black). Cells were multimer$^+$ above background in JRT LAG-3$^+$ C8 cells stained with HLA-DR1 multimers only. Inset numbers = percentage multimer$^+$, colour coded as described.

b) Flow cytometry histograms of MHC-multimer staining as in *a)* highlighting no increase in fluorescence intensity staining above FMO in LAG-3$^-$ JRT WT cells stained with HLA-A2 or -DR1 multimers. Increase in fluorescence intensity above FMO was observed in JRT LAG-3$^+$ C8 cells stained with HLA-DR1 but not -A2 multimers. Colours as described previously.

c) Example gating strategy of lymphocyte gate and live PB-A$^-$ cells used in *a)* and *b)*. Example shown is JRT LAG-3$^+$ C8 cells stained with HLA-DR1 multimers.

d) 2D flow cytometry plot of cognate CD4$^+$ T cell clone (DCD10) staining with HLA-DR1 multimers used in experiments described. Peptide specific staining of T cell clone exhibited significantly enhanced staining compared to peptide non-specific staining of LAG-3$^+$ cells.

e) Flow cytometry histograms of MHC-multimer staining of LAG-3$^-$ JRT WT cells (left) and JRT LAG-3$^+$ C8 cells (right) stained with HLA-DR1 multimers pre-blocked with unconjugated anti-LAG-3 mAb clone 17B4 (orange; dashed) or media control (black). HLA-DR1 specific shift in fluorescence intensity is removed to background -A2 levels (grey) by 17B4 blockade.

f) FMO subtracted quantification of gMFI in experiments described in *e)*. 17B4 blockade influenced HLA-DR1 multimer staining of JRT LAG-3$^+$ C8 cells only as shown by decrease in gMFI compared to media only control. Blockade with 17B4 had no influence on the negative staining of LAG-3$^-$ JRT WT cells or JRT LAG-3$^+$ C8 cells with -A2 multimers.

g) Quantification of HLA-DR1 binding to JRT LAG-3$^+$ C8 cells pre-incubated with control (media), irrelevant mAb (irrel) or anti-LAG-3 mAb (17B4). Percentage binding normalised to background subtracted gMFI observed for control blockade of -DR1 binding.
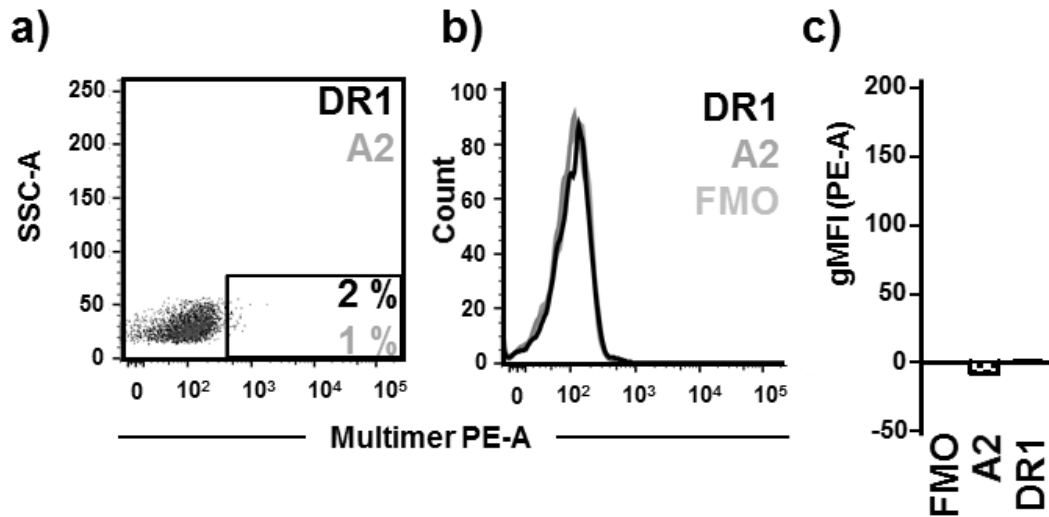
Figure 4.5 – No observed binding of HLA-DR1 multimers to LAG-3⁻ CD4⁺ cells:

a) 2D flow cytometry plots of MHC-multimer staining of LAG-3⁻ CD4⁺ MOLT-3 cells with HLA-A2 multimers (grey) or HLA-DR1 multimers (black). Multimer⁺ cells were equivalent with both HLA-DR1 and -A2 multimers. Inset numbers = percentage multimer⁺, colour coded as described.

b) Flow cytometry histograms of MHC-multimer staining as in *a)* highlighting no increase in fluorescence intensity staining above FMO in cells stained with HLA-A2 or -DR1 multimers. Colours as described previously.

c) FMO subtracted quantification of gMFI in experiments described in *b)*. Staining of LAG-3⁻ CD4⁺ MOLT-3 cells with either HLA-A2 or -DR1 multimers exhibited no increase in gMFI compared to FMO.

4.5 LAG-3 binds HLA-DR1 via a moderate affinity interaction

4.5.1 LAG-3:Fc as a model protein of LAG-3 function

Study of the molecular function of LAG-3 has been hampered by the difficulties in producing LAG-3 protein samples to facilitate the study of LAG-3 at the biophysical level. Initially, efforts were concentrated on producing recombinant LAG-3 protein via production of the extracellular domain of LAG-3 in monomeric form by both *E. coli* and *sf9* insect cells. Production of such protein was detectable in *sf9* cells, however, production yield was not efficient enough to generate sufficient protein mass for biophysical and structural studies in the given time frame (data not shown).

Through a collaboration with Professor Frédéric Triebel (Prima BioMed, Sydney, Australia), LAG-3 protein was instead obtained in the form of a LAG-3:Fc fusion protein (Huard et al. 1995). This construct of LAG-3 utilised the fusion of the extracellular domain of LAG-3 to a human IgG1 Fc domain in order to form a functionally viable and stable protein dimer. This dimer of LAG-3 has been used extensively to describe LAG-3 function, as previously described, and as a therapeutic agent (Brignone et al. 2007). The LAG-3 protein was obtained was GMP-grade protein expressed in glycosylation-sufficient *Chinese hamster ovary* (CHO) cells.

4.5.2 LAG-3 binds HLA-DR1 independent of peptide and expression system

In order to directly determine at the protein level whether LAG-3 binds to MHC-II molecules, LAG-3 binding to HLA-DR1 was assayed by surface plasmon resonance (SPR). Such experiments were designed to analyse LAG-3:Fc as analyte and MHC molecules as ligands immobilised to SPR sensor chips (*Figure 4.6a*).

To first confirm that LAG-3:Fc did not bind to an MHC-I molecule, LAG-3:Fc was assayed as analyte for binding to HLA-A2 complexed with the hTERT$_{540-548}$ peptide. Indeed, LAG-3:Fc exhibited no interaction with HLA-A2 as shown by no observed binding in blank flow cell reference subtracted sensograms (*Figure 4.6b*). No binding was observed to HLA-A2 using concentrations of LAG-3 analyte up to 57 µM. As a result, all future experiments were performed using reference subtraction from HLA-A2 immobilised flow cells.

In contrast, LAG-3:Fc bound specifically to HLA-DR1 complexed with the HA$_{309-318}$ peptide as shown by HLA-A2 reference subtracted sensograms (*Figure 4.6c*). Such binding was concentration dependent where binding was detectable down to the lowest tested concentration of analyte (0.11 µM). Binding to HLA-DR1 molecules was not altered by the peptide presented

- 154 -
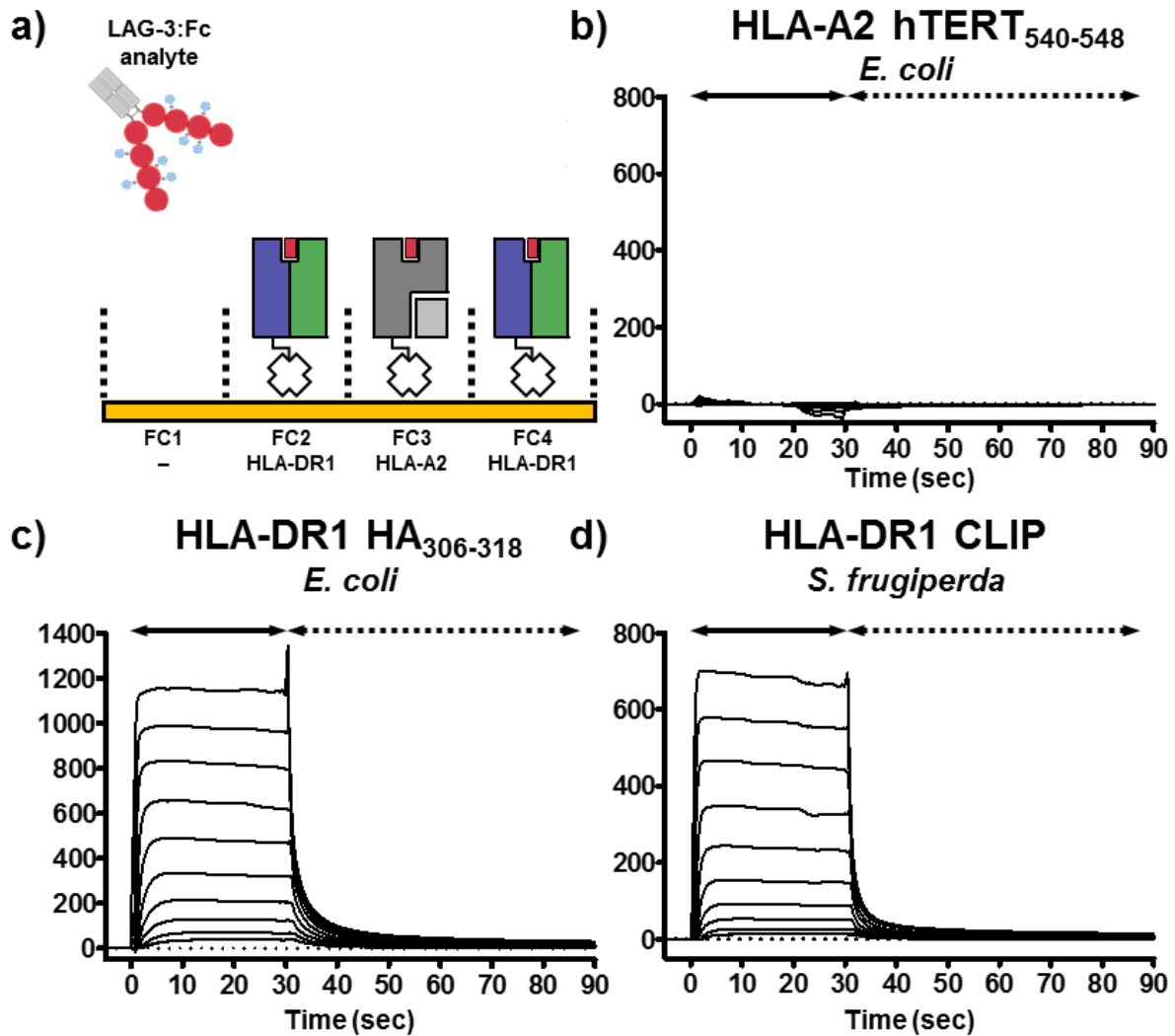
Figure 4.6 –Binding of LAG-3:Fc to HLA-DR1 observed via SPR:

a) Cartoon schematic describing formulation of SPR experiments performed using LAG-3:Fc as analyte injected over MHC immobilised sensor chips. Biotinylated MHC molecules were immobilised via coupling of streptavidin to sensor chips. FC = Flow cell.

b) SPR analysis of LAG-3:Fc injection over immobilised HLA-A2 complexed with the hTERT$_{540-548}$ peptide. Sensograms reference subtracted from a blank no-ligand control flow cell (FC3-FC1 as shown in *a)*) exhibited no binding across a titrating range of LAG-3:Fc concentrations (57 µM to 0.11 µM).

c) SPR analysis showing concentration-dependent binding of LAG-3:Fc to HLA-DR1 produced from *E. coli* by *in vitro* refolding in the presence of the HA$_{306-318}$ peptide. Binding was observed in HLA-A2 reference subtracted sensograms (FC2-FC3 as shown in *a)*) and was detectable at all concentrations throughout a dilution series of 57 µM to 0.11 µM.

d) SPR analysis as described in *c)* showing concentration-dependent binding of LAG-3:Fc to HLA-DR1 produced in *S.frugiperda* (*sf9*) insect cells expressed with covalently linked CLIP. Binding was observed at all concentrations in HLA-A2 reference subtracted sensograms.

within the HLA-DR1 binding pocket as well as independent of HLA-DR1 expression system, as shown by equal binding to HLA-DR1 produced via a covalently-linked CLIP construct in *sf9* insect cells (*Figure 4.6d*). Broad observation of the kinetics of LAG-3:Fc binding to HLA-DR1 were fast in nature – characterised by fast on-rate and fast off-rate.

4.5.3 LAG-3:Fc binds immobilised HLA-DR1 with weak bivalency

To determine the monovalent affinity between LAG-3 and MHC-II, the mode of valency exhibited by the dimeric LAG-3:Fc fusion protein was first required to be determined. To this end, various simultaneous k_{on}/k_{off} modelling curves were applied to observed binding sensograms at concentrations of 0.1 – 7 μM of LAG-3:Fc and compared for visual goodness-of-fit as well as analysis of χ^2 and residual plot parameters (*Figure 4.7*). An overview of the candidate binding models tested is described in *Table 4.1*.

No model demonstrated perfect matching to observed data across multiple concentrations, however, kinetic data was best described by the bivalent analyte model of binding by satisfying multiple analysed analyte concentration sensograms (*Figure 4.7a*). Bivalent analytes, however, can exhibit altered kinetics at different analyte concentrations making fitting global parameters that satisfy multiple LAG-3:Fc injection concentrations difficult. Analysis of kinetic fitting to a single intermediate concentration of analyte (local fitting) resulted in a similar good fit and comparable kinetic parameters to those observed in global fitting (*Figure 4.7b*). Thus, LAG-3:Fc binding was best described by bivalent binding to immobilised HLA-DR1.

This model can be rationally applied to the bivalent system being studied whereby two molecules (A & B) bind to form a complex (AB) which undergoes a second binding event with a second molecule of B forming a heterotrimeric complex (ABB):

$$A \quad + \quad 2\,B \underset{koff1}{\overset{kon1}{\rightleftharpoons}} \quad AB + B \underset{koff2}{\overset{kon2}{\rightleftharpoons}} \quad ABB$$

(Eq. 4.1)
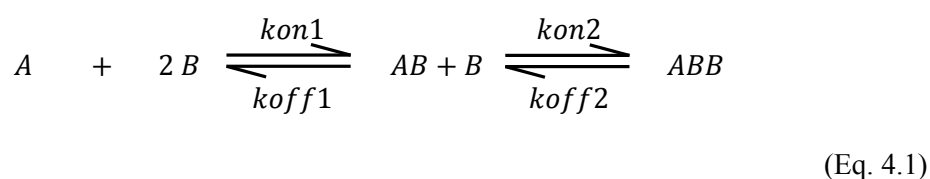
	Binding Model	Kinetic Parameters	Rate equations
1:1 Langmuir	A + B ⇌ AB	k_{on} k_{off}	$$\frac{dAB}{dt} = kon[A][B] - koff[AB]$$
Bivalent analyte	A + B ⇌ AB + B ⇌ ABB	k_{on1} k_{off1} k_{on2} k_{off2}	$$\frac{dAB}{dt} = ((2 \cdot kon1)[A][B] - koff1[AB]) - (kon2[AB][B] - (2 \cdot off2)[ABB])$$ $$\frac{dABB}{dt} = (kon2[AB][B] - (2 \cdot koff2)[ABB])$$
Two-state reaction	A + B ⇌ AB ⇌ ABx	k_{on1} k_{off1} k_{on2} k_{off2}	$$\frac{dAB}{dt} = (kon1[A][B] - koff1[AB]) - (kon2[AB] - koff2[ABx])$$ $$\frac{dABx}{dt} = kon2[AB] - koff2[ABx]$$

Table 4.1 – Candidate binding models to describe LAG-3:Fc binding to HLA-DR1
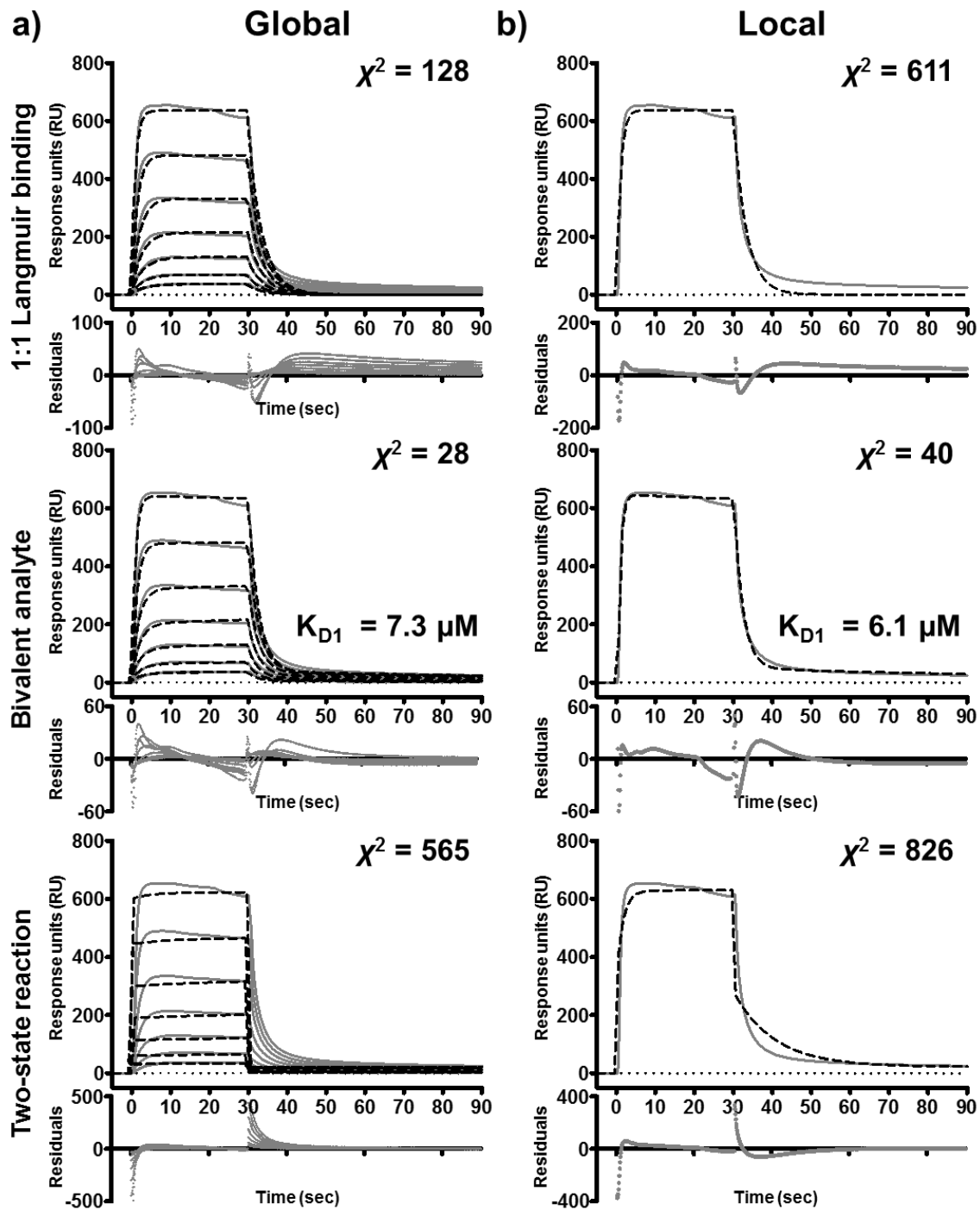
Figure 4.7 – LAG-3:Fc binding to HLA-DR1 exhibits bivalent analyte kinetics:

a) Global fit analysis of reference subtracted sensograms of LAG-3:Fc ($0.1 – 7$ μM) binding to immobilised (525 RU) HLA-DR1 fitted with three candidate models: 1:1 Langmuir binding, bivalent analyte and two-state reaction. Global fitting analysis highlight a good overall fit with the bivalent analyte model. Observed sensograms are shown as grey solid lines, fitted curves as black dashed lines with inset χ^2 value and kinetic derived dissociation affinity constant K_{D1} calculated as in Eq 4.6 according to bivalent analyte binding. Corresponding curve fit residual plots are shown below each fit.

b) Local fit analysis of the reference subtracted sensogram describing LAG-3:Fc binding at 7 μM to immobilised HLA-DR1 as described in *a)*. Local fitting analysis highlighted a good overall fit with the bivalent analyte model and similar K_{D1} value to global analysis.

$\chi^2 = \sum \frac{(observed - expected)^2}{expected}$; lower χ^2 values indicate better model fitting.

- 158 -

In the bivalent analyte model, there are four kinetic parameters (k_{on1}, k_{off1}, k_{on2} and k_{off2}) which describe the rates at which the two complex states (AB and ABB) of the reaction model form. These rate constants are described by the following rate equations:

$$\frac{dAB}{dt} = ((2 \cdot kon1)[A][B] - koff1[AB]) - (kon2[AB][B] - (2 \cdot koff2)[ABB])$$

(Eq. 4.2)

$$\frac{dABB}{dt} = (kon2[AB][B] - (2 \cdot koff2)[ABB])$$

(Eq. 4.3)

Application of this bivalent analyte model to the system being studied is visualised by the following schematic whereby Eq 4.1 has been modified to include terms of the LAG:Fc to HLA-DR1 system being studied:

$$LAG3Fc + 2\ DR1 \underset{koff1}{\overset{kon1}{\rightleftharpoons}} LAG3Fc{:}DR1 + DR1 \underset{koff2}{\overset{kon2}{\rightleftharpoons}} LAG3Fc{:}DR1{:}DR1$$

(Eq. 4.4)
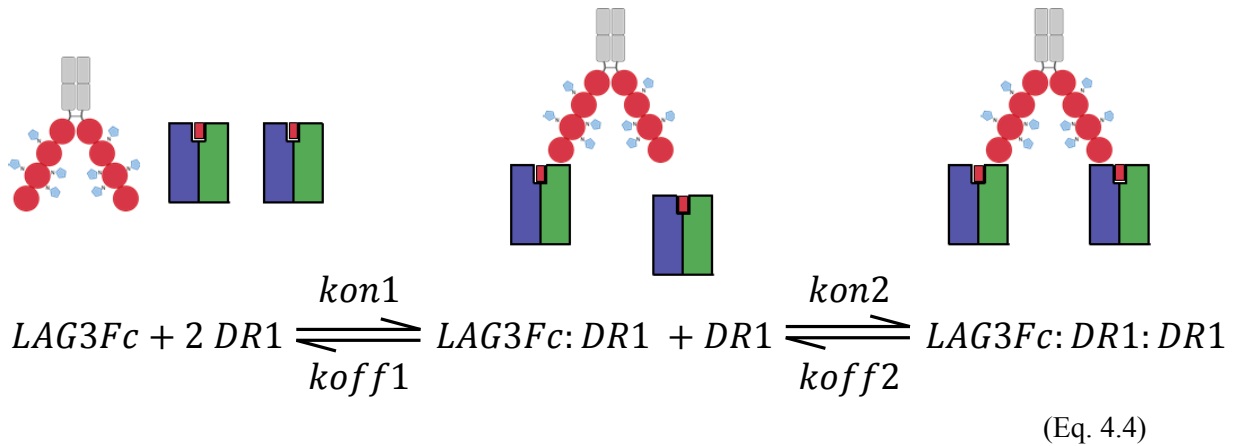
NB. Schematic drawings of binding are for illustrative purposes only and no inference of binding sites on LAG-3:Fc or HLA-DR1 should be made.

Whilst LAG-3:Fc binding was best described by the bivalent analyte model, it was observed that dissociation of LAG-3:Fc unexpectedly occurred with fast kinetics; within the timescale of seconds. Such fast kinetics are atypical of dimeric molecules binding with bivalency – as demonstrated by contrasting binding of antibody-antigen interactions in Chapter 5. To therefore determine the contribution of the rates of $LAG3Fc{:}DR1$ (AB) formation and $LAG3Fc{:}DR1{:}DR1$ (ABB) formation to overall observed kinetics, the kinetic parameters of bivalent binding (k_{on1}, k_{off1}, k_{on2} and k_{off2}) were calculated from kinetic fits as shown in *Figure 4.6* and are reported in *Table 4.2*.

Fit	[Analyte] (µM)	R_{max} (RU)	RI (RU)	χ^2	k_{on1} (1/Ms)	k_{off1} (1/RU)	k_{on2} (1/s)	k_{off2} (1/s)	K_{D1} (M)	K_{D2} (M)	K_{D1} (µM)
Local	7.1	1190	6.6	39.6	7.24×10^4	0.439	9.70×10^{-6}	4.30×10^{-3}	6.06×10^{-6}	4.43×10^2	6.06
Global	0.1 – 7.1	962	4.6 – 16.9	27.6	5.22×10^4	0.380	6.00×10^{-6}	4.10×10^{-3}	7.28×10^{-6}	6.83×10^2	7.28

Table 4.2 – Bivalent analyte model parameters of LAG-3:Fc binding to HLA-DR1
[Analyte] = Concentration of injected LAG-3:Fc analyte, RU = Response units,
R_{max} = Maximum analyte binding capacity in RU, RI = Bulk refractive index effect in RU,
$\chi 2 = \sum \frac{(observed - expected)^2}{expected}$; lower $\chi 2$ values indicate better model fitting.
K_{D1}= the affinity equilibrium association constant calculated as described by Eq. 4.6
K_{D2} = the affinity equilibrium dissociation constant calculated as described by Eq. 4.8

These kinetic parameters can consequently be used to deconvolute kinetic derived dissociation affinity constant measurements which determine both stages of LAG-3:Fc binding. Specifically, the affinity constant K_{D1}, which defines the monovalent component of the interaction, and the affinity constant K_{D2}, which defines the bivalent component, can be calculated.

Firstly, the monovalent affinity constant K_{D1} describes the formation of $LAG3Fc: DR1$ as follows:

$$LAG3Fc + 2\ DR1 \underset{}{\overset{K_{D1}}{\rightleftharpoons}} LAG3Fc: DR1\ + DR1 \underset{}{\overset{K_{D2}}{\rightleftharpoons}} LAG3Fc: DR1: DR1$$

(Eq. 4.5)
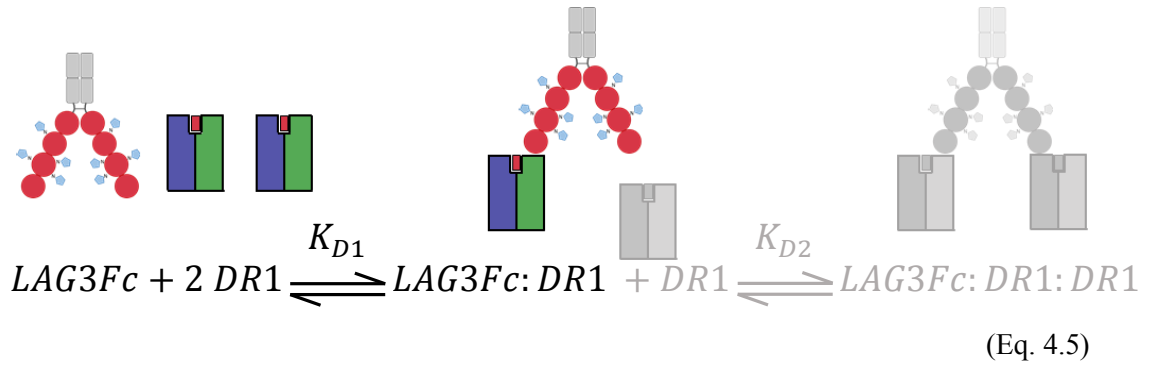
As a result, the affinity constant (K_{D1}) can be calculated from defined kinetic rate constants described in *Table 4.2* as follows:

$$K_{D1} = \frac{koff1}{kon1}$$

(Eq. 4.6)

Similarly, the equilibrium dissociation constant K_{D2}, which defines the bivalent component of observed kinetics due to the formation of the heterotrimeric $LAG3Fc: DR1: DR1$ is as follows:

$$LAG3Fc + 2\ DR1 \underset{}{\overset{K_{D1}}{\rightleftharpoons}} LAG3Fc: DR1\ + DR1 \underset{}{\overset{K_{D2}}{\rightleftharpoons}} LAG3Fc: DR1: DR1$$

(Eq. 4.7)
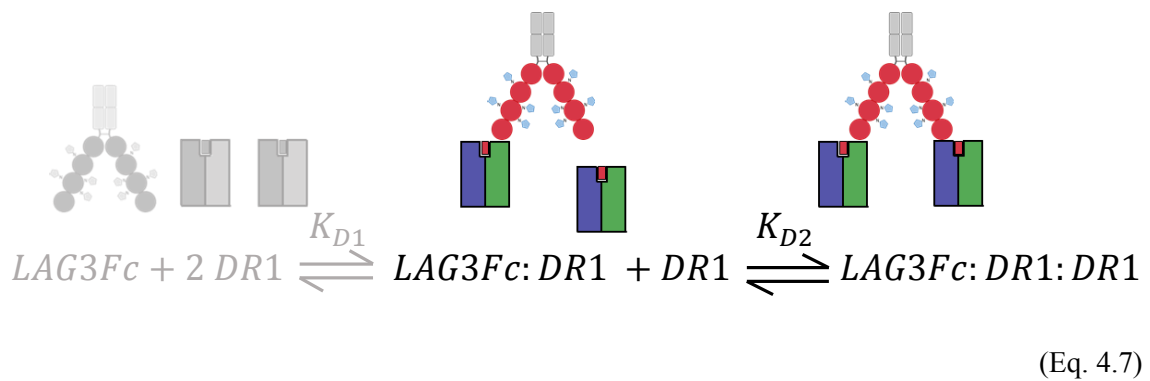
As a result, the affinity constant (K_{D2}) can be calculated from defined kinetic rate constants described in *Table 4.2* as follows:

$$K_{D2} = \frac{koff2}{kon2}$$

(Eq. 4.8)

Analysis of the kinetic derived equilibrium dissociation constants suggested that the contribution of bivalent effects to observed LAG-3:Fc binding in these experiments was minimal as signified by a calculated K_{D2} in excess of molar concentration (*Table 4.2*). Thus, in order to achieve occupancy of the heterotrimeric complex $LAG3Fc{:}DR1{:}DR1$ high concentrations of the preceding $LAG3Fc{:}DR1$ complex was required. As a result, the observed kinetics are dominated by 1:1 binding with minimal contribution of bivalency. These data suggest that, in these SPR experiments, LAG-3:Fc bound poorly to multiple MHC-II molecules.

Similarly, deconvolution of the kinetic derived equilibrium dissociation constant K_{D1} which describes the monovalent interaction between $LAG3Fc$ and $DR1$ and therefore represents an *estimated* affinity of LAG-3 for HLA-DR1 at 6.1 or 7.3 µM using local and global fitting, respectively (*Table 4.2 & Figure 4.7*). Kinetic fitting of binding systems exhibiting fast kinetics, however, can lead to inaccuracies in calculated affinity and therefore further analysis is required. Moreover, affinity values calculated from kinetic analysis can be skewed by mass transfer effects – particularly at high ligand concentrations[6].

4.5.4   LAG-3 binds HLA-DR1 with micromolar K_D affinity

Having shown that LAG-3:Fc bound MHC-II via a bivalent interaction estimated in the micromolar range, further SPR experiments were performed to elucidate an accurate affinity for monovalent LAG-3 binding to HLA-DR1. This was achieved using steady state analysis where kinetic affinity is calculated from the response observed during the steady state phase of association which is manifested in sensograms as a plateau during injections. This type of analysis is preferable over kinetic analysis when fast kinetics allow binding to establish steady state within short injection times. This was the case for LAG-3:Fc binding to HLA-DR1 system studied here, whereby steady state at multiple injection concentrations was reached by 20 seconds of analyte injection as can be seen in *Figure 4.7*. Calculation of a more accurate affinity by steady state analysis comes at a trade-off as through this analysis, no kinetic parameters (on- and off-rates) are obtained.

In order to deduce a monovalent affinity for LAG-3 binding to HLA-DR1, steady state experiments must be formulated such that the observed binding is either monovalent or dominated by monovalent binding. This is achievable for dimeric molecules such as LAG-3:Fc which, as

---

[6] Mass transfer effects can manifest as artefacts in SPR experiments whereby at high ligand densities observed affinity increases as dissociating analytes do not diffuse away from the ligand surface back to the bulk flow path of the flow cell. This causes faster rebinding of analyte. Such experiments are said to be mass transport limited as opposed to kinetic limited.

evidenced by kinetic analysis described previously, is able to bind with a weak capacity for bivalency. In order to observe binding dominated by a monovalent interaction, removal of bivalent binding can be achieved by lowering the density of ligand on the chip surface. This lower ligand density increases the spatial distance between ligand molecules on the chip surface and, as a result, reduces the availability of a second ligand species to engage with bivalently. The presence of bivalency can therefore also be confirmed by the increase in ligand density, thus, increasing bivalent binding character and consequent increase in observed affinity/avidity. A schematic overview of the effect of ligand density on observed affinity/avidity is presented in *Figure 4.8*.

To this end, different concentrations of HLA-DR1 was immobilised to flow cells of the same sensor chip such that the effect of LAG-3:Fc analyte binding to low, intermediate and high ligand densities could be studied (*Figure 4.9*). Here, increase in ligand density prolonged binding kinetics by lengthening the observed off-rate of LAG-3:Fc (*Figure 4.9a*). In agreement with described kinetic modelling of LAG-3:Fc binding, this lengthening of off-rate was likely contributable to bivalent binding of LAG-3:Fc at higher ligand densities. Similarly to previous kinetic analysis, at the highest ligand density tested, LAG-3:Fc did not exhibit antibody-like off-rate once more suggesting that LAG-3:Fc does not efficiently engage with multiple HLA-DR1 molecules.

In contrast to higher ligand densities, sensograms at low ligand concentration displayed fast kinetics and no extension of dissociation. As a result, LAG-3:Fc binding at low ligand density exhibited sensograms characteristic of kinetics predominated by one-to-one monovalent binding behaviour. Indeed, low ligand density sensograms did not adhere to bivalent kinetic model fitting (data not shown). As SPR data at low ligand density exhibited monovalent characteristic binding, in order to determine an accurate monovalent LAG-3 to HLA-DR1 monovalent affinity, sensograms were analysed under the assumption of the Langmuir 1:1 binding model for bimolecular interactions:

$$A \quad + \quad B \underset{koff}{\overset{kon}{\rightleftharpoons}} AB$$
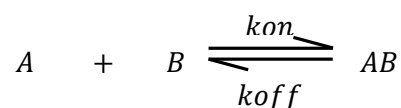
(Eq. 4.9)
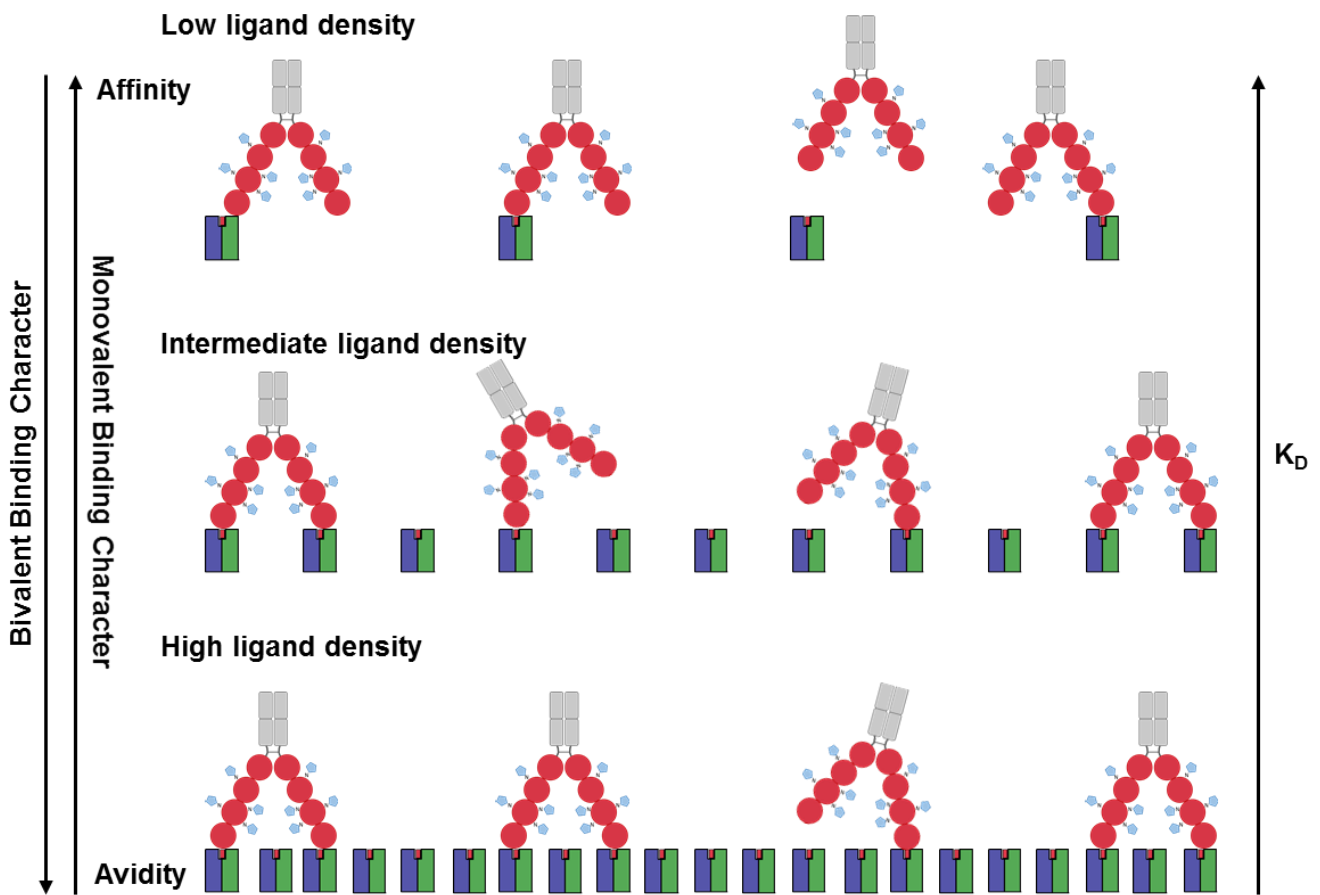
Figure 4.8 – Effects of ligand density on observed LAG-3:Fc bivalency:
Schematic overview of the effects of increasing concentration of ligand on the observed binding of LAG-3:Fc in SPR experiments. At low ligand density (top) spatial distance between HLA-DR1 ligand molecules (green/blue) is increased and thus LAG-3:Fc (red:grey) is unable to sterically bind multiple HLA-DR1 ligand molecules. The observed binding is therefore dominated by monovalent kinetics and thus affinity measurements are made. At high ligand density (bottom) spatial distance between HLA-DR1 ligand molecules is decreased and thus LAG-3:Fc is able to bind multiple HLA-DR1 ligand molecules. The observed binding is therefore dominated by bivalent kinetics and thus avidity measurements are made. Increase in bivalent binding character causes a decrease in observed K_D i.e. increase in affinity/avidity. Arrow direction represent increase from low→high.

In the Langmuir 1:1 binding model, there is a single complex species (AB) whose formation is described by the following single rate equation:

$$\frac{dAB}{dt} = kon[A][B] - koff[AB]$$

(Eq. 4.10)

Application of this monovalent analyte model to the system being studied, whereby at low ligand density engagement of a second ligand molecule by LAG-3:Fc is not achievable due to spatial separation of ligand, is visualised by the following schematic. Here, Eq 4.9 has been modified to include terms of the LAG:Fc to HLA-DR1 system being studied:

$$LAG3Fc + DR1 \underset{koff}{\overset{kon}{\rightleftharpoons}} LAG3Fc{:}DR1$$
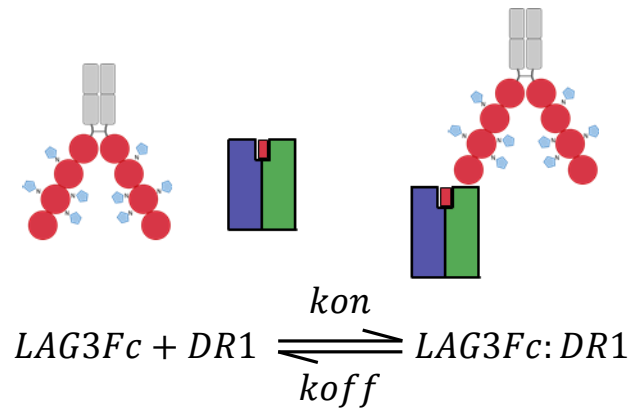
(Eq. 4.11)

As a result, a steady state derived affinity can be calculated from sensograms collected at low ligand density. At steady state, the equilibrium binding constant (K_D) can be calculated from the molecular ratio of unbound to bound components of the system. This is possible because at steady state the rate of formation of the complex ($LAG3Fc{:}DR1$) is equal to zero:

$$\frac{dLAG3Fc{:}DR1}{dt} = kon[LAG3Fc][DR1] - koff[LAG3Fc{:}DR1] = 0$$

(Eq. 4.12)

$$kon[LAG3Fc][DR1] = koff[LAG3Fc{:}DR1]$$

(Eq. 4.13)

$$\frac{koff}{kon} = \frac{[LAG3Fc][DR1]}{[LAG3Fc{:}DR1]}$$

(Eq. 4.14)

As the affinity constant (K_D) is equivalent to $\frac{koff}{kon}$:

- 165 -

$$K_D = \frac{[LAG3Fc][DR1]}{[LAG3Fc:DR1]}$$

<div align="right">(Eq. 4.15)</div>

As such, K_D can be calculated from plotted steady state response unit values (RU) at a series of concentrations. The relationship between which is fitted with a non-linear regression least squares ordinary fit in accordance with the Michaelis-Menten model formulated for protein-protein interactions:

$$LAG3Fc:DR1 = \frac{[LAG3Fc] \cdot LAG3Fc:DR1_{max}}{K_D + [LAG3Fc]}$$

<div align="right">(Eq. 4.16)</div>

In SPR experiments, observed response unit values, RU, are an observed measure of $LAG3Fc:DR1$ complex formation, thus:

$$RU = \frac{[LAG3Fc] \cdot LAG3Fc:DR1_{max}}{K_D + [LAG3Fc]}$$

<div align="right">(Eq. 4.17)</div>

As $LAG3Fc:DR1max$ is the maximal complex formation when the system is saturated and RU is an observed measure of $LAG3Fc:DR1$ complex formation, $LAG3Fc:DR1max$ is calculated as the maximal observed RU during saturated binding, termed R_{max}. This is achievable experimentally providing high concentrations of analyte are used in order to either saturate available ligand molecules or such that the saturation point can be accurately calculated during model fitting. As a result:

$$RU = \frac{[LAG3Fc] \cdot R_{max}}{K_D + [LAG3Fc]}$$

<div align="right">(Eq. 4.18)</div>

In order to determine K_D in terms of $[LAG3Fc]$ the equation is reduced to the following, when $K_D = [LAG3Fc]$:

$$RU = \frac{[LAG3Fc] \cdot R_{max}}{[LAG3Fc] + [LAG3Fc]}$$

<div align="right">(Eq. 4.19)</div>

$$RU = \frac{[LAG3Fc] \cdot R_{max}}{2[LAG3Fc]}$$

<div align="right">(Eq. 4.20)</div>

$$RU = \frac{R_{max}}{2}$$

<div align="right">(Eq. 4.21)</div>

Therefore, the K_D of the interaction between LAG-3:Fc and HLA-DR1 was calculated as the concentration of LAG-3:Fc at which RU is equal to half of R_{max} i.e. $(\frac{R_{max}}{2})$.

Using this described steady-state analysis, the monovalent affinity of LAG-3 binding to HLA-DR1 is calculated at 13.1 μM (*Figure 4.9b*). Moreover, application of one-to-one equilibrium analysis to intermediate and high ligand densities resulted in a modest decrease in $\frac{R_{max}}{2}$, thus, further evidencing LAG-3:Fc binding via weak bivalency in experiments designed to allow bivalent binding.

Since the lowest ligand density tested may still contain mixed kinetics with contribution of bivalent binding, the calculated monovalent K_D value under the assumption of one-to-one binding may over-calculate the monovalent affinity. In order to therefore further validate the assumption of one-to-one binding, SPR data at intermediate density was analysed by kinetic analysis. Global and local fitting of the bivalent analyte model analysed as described in Eq. 4.1 – 4.7 revealed an equilibrium dissociation constant (K_{D1}) for the monovalent affinity for LAG-3 to HLA-DR1 within a similar range as shown by equilibrium binding analysis (*Figure 4.9c*). This similar kinetic rate derived affinity constant validates the assumption that low ligand density steady-state analysis was predominated by monovalent binding character and thus, 1:1 Langmuir binding kinetics can be applied. Together, these data therefore define the affinity of LAG-3 for HLA-DR1 to be 13 μM at 25 °C and consequently in the range of high affinity MHC-II restricted TCR binding to MHC-II.

a)

b)

Low ligand density (244 RU)

$$K_D= 13.1\ (\pm 2.4)\ \mu M$$

Intermediate ligand density (792 RU)

$$[LAG3Fc]\frac{R_{max}}{2} = 3\ \mu M$$

High ligand density (3659 RU)

$$[LAG3Fc]\frac{R_{max}}{2} = 1\ \mu M$$

c)

Bivalent kinetics at intermediate ligand density

Global

$$\chi^2 = 28$$

$$K_{D1} = 7.3\ \mu M$$

Local

$$\chi^2 = 22$$

$$K_{D1} = 6.9\ \mu M$$
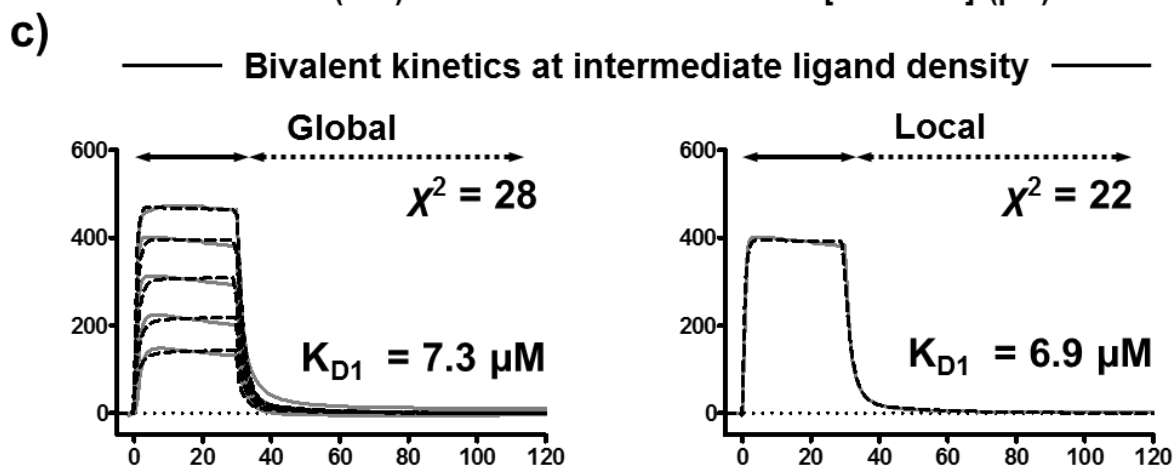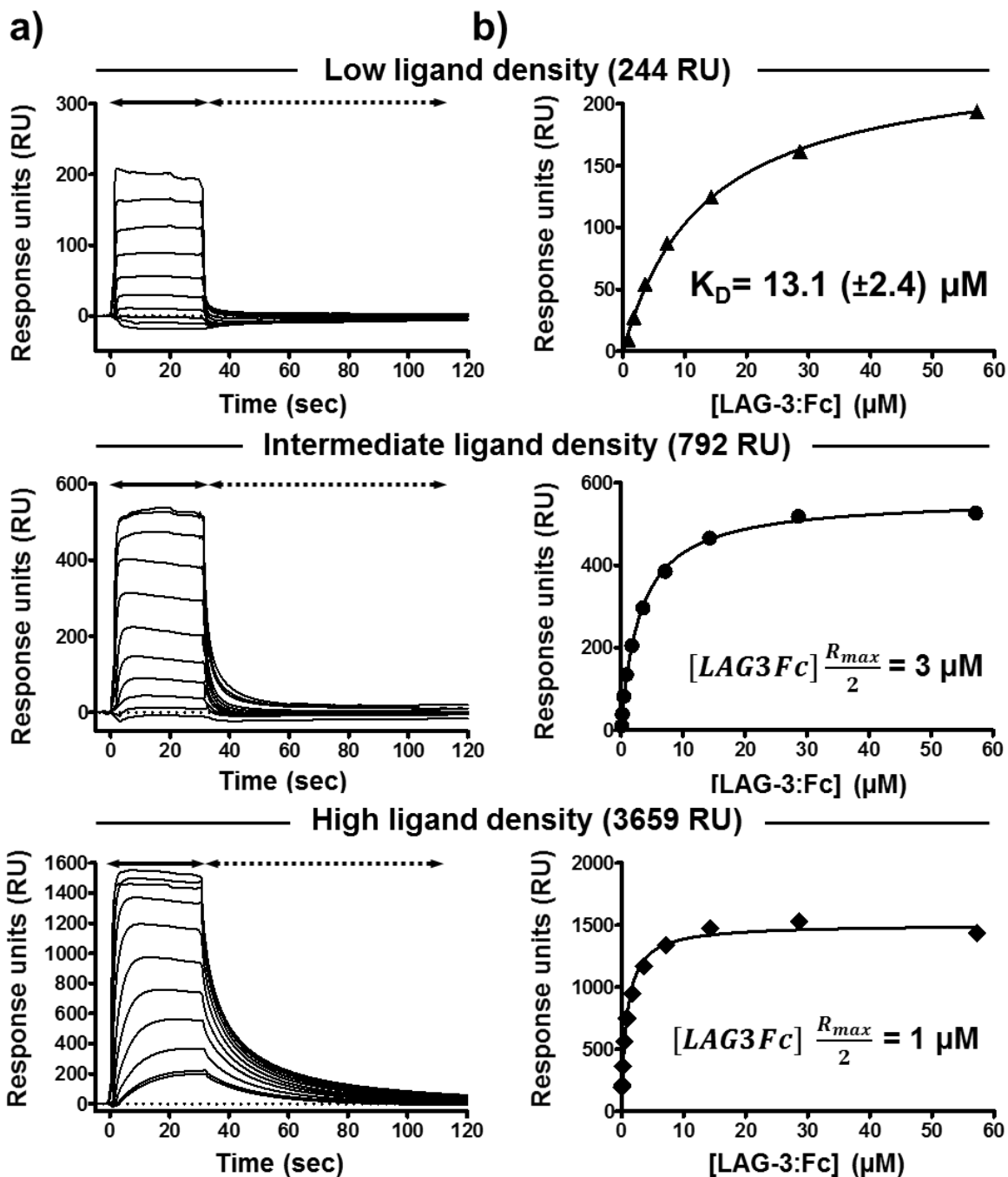
(Figure legend overleaf)

Figure 4.9 – LAG-3 binds HLA-DR1 with micromolar affinity:

a) SPR analysis of LAG-3:Fc binding to HLA-DR1 immobilised at low (244 RU), intermediate (792 RU) and high (3659 RU) ligand concentrations. Titrating concentrations of LAG-3:Fc (57 – 0.1 µM) bound HLA-DR1 with prolonged kinetics to higher ligand concentrations as shown by reference subtracted sensograms. Binding of LAG-3:Fc to low ligand density HLA-DR1 exhibited kinetics characteristic of one-to-one binding kinetics.

b) Steady-state analysis of LAG-3:Fc binding to HLA-DR1 at varying ligand concentrations analysed from sensograms as described in *a)* by plotting RU increase from baseline during steady-state (25 seconds into injections) against concentration of LAG-3:Fc. Under the assumption of one-to-one binding, LAG-3 monovalent affinity (K_D) was defined (inset on low ligand density only) for low ligand density only (top) at 13 µM. Saturation of HLA-DR1 binding was observed at lower concentrations of LAG-3:Fc when ligand density was increased. This difference in saturation concentration is attributable to the increase in bivalent binding character as spatial distance between ligands is decreased. The effect of this bivalency can be quantified by observation of $[LAG3Fc] \frac{R_{max}}{2}$ (inset at intermediate and high ligand density).

c) Kinetic analysis of LAG-3:Fc binding to HLA-DR1 at intermediate ligand density (792 RU) exhibited some bivalent binding as shown by kinetic modelling. Global fitting (left) of LAG-3:Fc binding at 0.9 – 14.3 µM as well as local fitting (right) at the concentration closest to perceived K_{D1} (7.2 µM) described a similar monovalent affinity as calculated by steady-state analysis described in *b)*. K_{D1} was calculated through the first step complex formation affinity constant K_{D1} in accordance with the bivalent binding model as shown by Eq. 4.6 and is thus equivalent to a monovalent affinity.

4.6 Preliminary studies of LAG-3 structure by negative stain electron microscopy

There is currently no structural data describing LAG-3, and as a result, knowledge of the protein domain organisation of LAG-3 is based on interference at the gene level, and comparison to homologous proteins whose structure may have been elucidated. As a result, little is known about how LAG-3 functionally impinges on the immune synapse resulting in T cell inhibition (C. C. J. Workman et al. 2002).

This lack of structural data has stemmed from the lack of soluble LAG-3 protein samples suitable for high-resolution studies by x-ray crystallography. The soluble LAG-3:Fc fusion protein used to describe HLA-DR1 binding is produced in Chinese hamster ovary (CHO) cells and is post-translationally modified to include approximately 18 kDa of N-linked glycosylation (F. Triebel, personal communications). In this formulation, protein crystal formulation is highly unlikely due to carbohydrate flexibility and heterogeneity. However, recent advances in electron microscopy techniques for protein samples have enabled the study of protein structure to resolutions nearing that of x-ray crystallography (Egelman 2016). Such techniques are not dependent on crystal formation and, thus, can be performed on glycosylated protein samples. Furthermore, enhanced techniques are enabling the study of smaller proteins, near to the 161 kDa LAG-3:Fc, which have previously been too small to study via EM (Ciuffa et al. 2015).

Despite advances in cryo-EM based methodologies, access to microscope time on such instruments is limited at present and requires a pre-requisite knowledge of sample at low resolution before preceding to high resolution studies. To this end, these studies outline the preliminary results in efforts to define LAG-3 structure through the study of LAG-3:Fc at near atomic-resolution using negative stain electron microscopy with a view to future study at atomic-resolution using cryo-electron microscopy.

4.6.1   Collection of LAG-3:Fc and LAG-3:Fc + HLA-DR1 negative stain EM datasets

In order to gain knowledge of the overall size and shape of the LAG-3:Fc protein envelope, as well as validate the quality of the protein preparation, LAG-3:Fc was studied by negative stain EM (*Figure 4.10*). Obtainment of EM datasets first required the generation of LAG-3:Fc and LAG-3:Fc in complex with HLA-DR1 protein grids optimally stained with the contrasting agent uranyl acetate, outlined in *Figure 4.10a*, modified from methodologies previously described (Rames et al. 2014). Using grids prepared under the described conditions, LAG-3:Fc and LAG-3:Fc combined with HLA-DR1 were imaged at 50,000 times magnification using a 200 kV transmission electron microscope (TEM). Micrographs of LAG-3:Fc showed that the protein
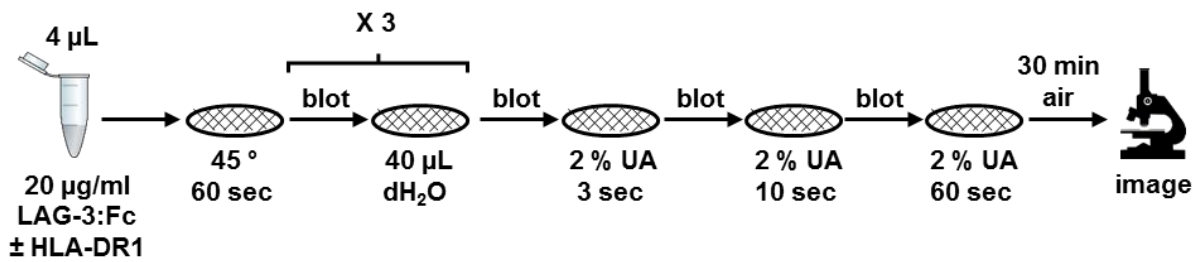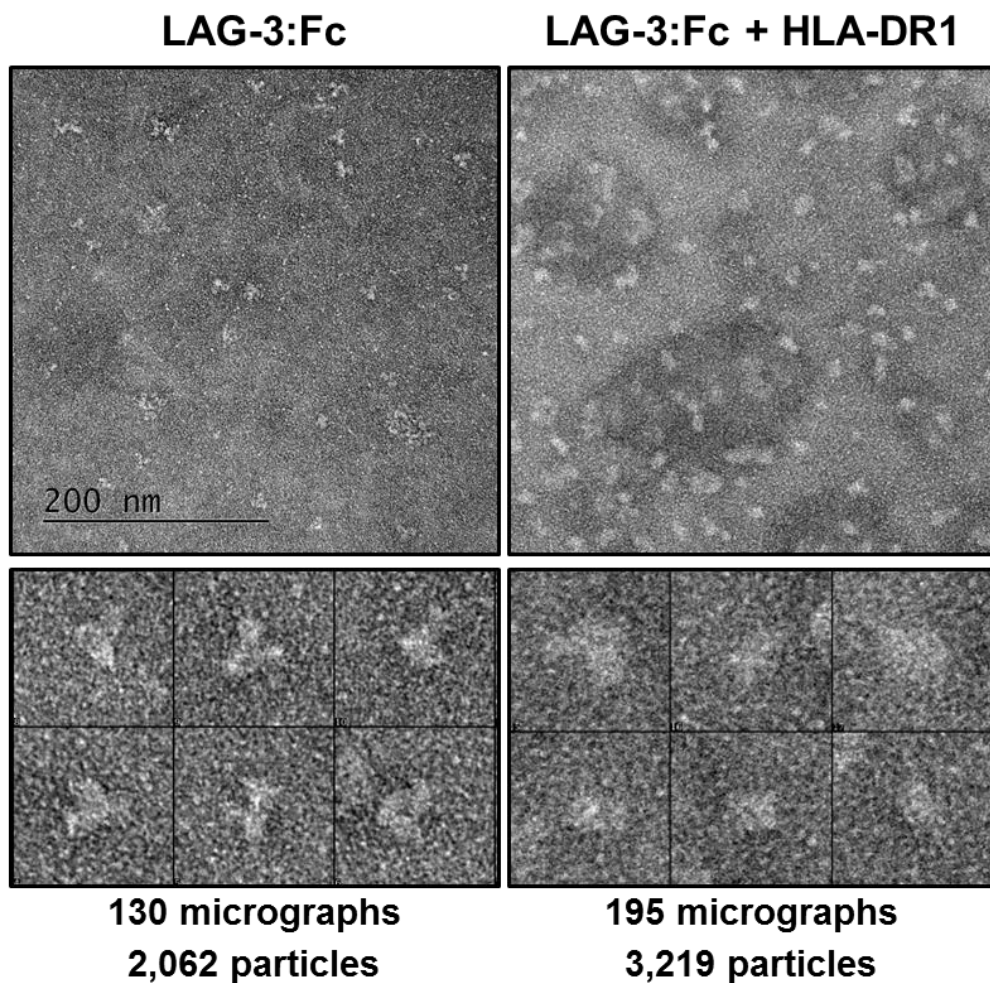
Figure 4.10 – Preparation of samples and collection of negative stain EM datasets:

a) Schematic overview of the optimised conditions for preparation of negative stained LAG-3:Fc and LAG-3:Fc + HLA-DR1 complexed sample grids for imaging via transmission electron microscopy (TEM). Protein samples were applied to grids at an angle of 45 ° over ice, washed three times with deionised water before undergoing three consecutive incubations in 2 % uranyl acetate (UA) for time periods indicated. Grids were air dried before imaging.

b) Overview of current datasets for LAG-3:Fc and LAG-3:Fc + HLA-DR1 samples. Example micrographs at 50k X magnification at 200 kV acceleration voltage and detected using a charged coupled device (CCD) camera (top). Example particles from each dataset using manual particle picking in the EMAN 2.1 software package (bottom). LAG-3:Fc particles exhibited good stain contrast and homogenous particles across micrographs. LAG-3:Fc + HLA-DR1 datasets exhibited less contrast and heterogeneity in particle size across micrographs. Current dataset sizes indicated below.

sample was homogenous and devoid of large aggregation and exhibited no visible oligomerisation or polymerisation (*Figure 4.10b*). Distinct LAG-3:Fc single particles were visible and suitable for single particle reconstruction. As a result, 130 micrographs of LAG-3:Fc were collected from which a limited dataset of 2,062 particles were picked for single particle reconstruction analysis.

Imaged LAG-3:Fc grids complexed with HLA-DR1, however, exhibited sample heterogeneity and some aggregation (*Figure 4.10c*). Nevertheless, micrographs were dominated with particles of a similar to slightly enlarged size suggesting inclusion of complexed particles. A total of 195 micrographs were consequently collected from which a dataset of 3,219 picked particles has been obtained. Due to the heterogeneity of the particle dataset, however, and its limited size, the current dataset, at present, was not suitable for single particle reconstruction analysis.

4.6.2   A single particle reconstruction of the LAG-3:Fc surface envelope

The 2,062 particle dataset of LAG-3:Fc was subjected to single particle reconstruction analysis using the EMAN2.1 project workflow[7] (Tang et al. 2007). Multiple symmetry restrained initial models were built from 2D class averages[8] generated from particles exhibiting the best signal-to-noise ratio. From these initial models, refined reconstructions of LAG-3:Fc were achieved by iterative refinement through gradual inclusion of particle images and increasing resolution targets. Refinements of LAG-3:Fc models restraining for different symmetry groups revealed that the protein exhibited *c1* point group symmetry i.e. no symmetry. At low-resolution, therefore, LAG-3:Fc exhibits asymmetry and does not possess a symmetry axis about the plane of the dimerisation interface.

The refined reconstruction shows LAG-3:Fc as a non-spherical protein with three distinct globular domains (*Figure 4.11*). Each globular domain combines to form a Y-shaped molecule with approximate maximal dimensions of 150 x 140 x 130 Å (width, height, depth; as viewed from front). One globular domain exhibits smaller dimensions (65 x 65 Å) and is therefore likely the Fc portion of the molecule. The second two domains were matched in overall size (65 x 75 Å) and appearance and thus likely represent the two LAG-3 components of the fusion protein.

---

[7] EMAN2.1 is a software suite comprised of software packages that allow analysis of raw micrograph data to particle reconstructions (protein models).

[8] 2D class averages are the resulting particle image generated from the summation of particles assigned to similar views (class sums).
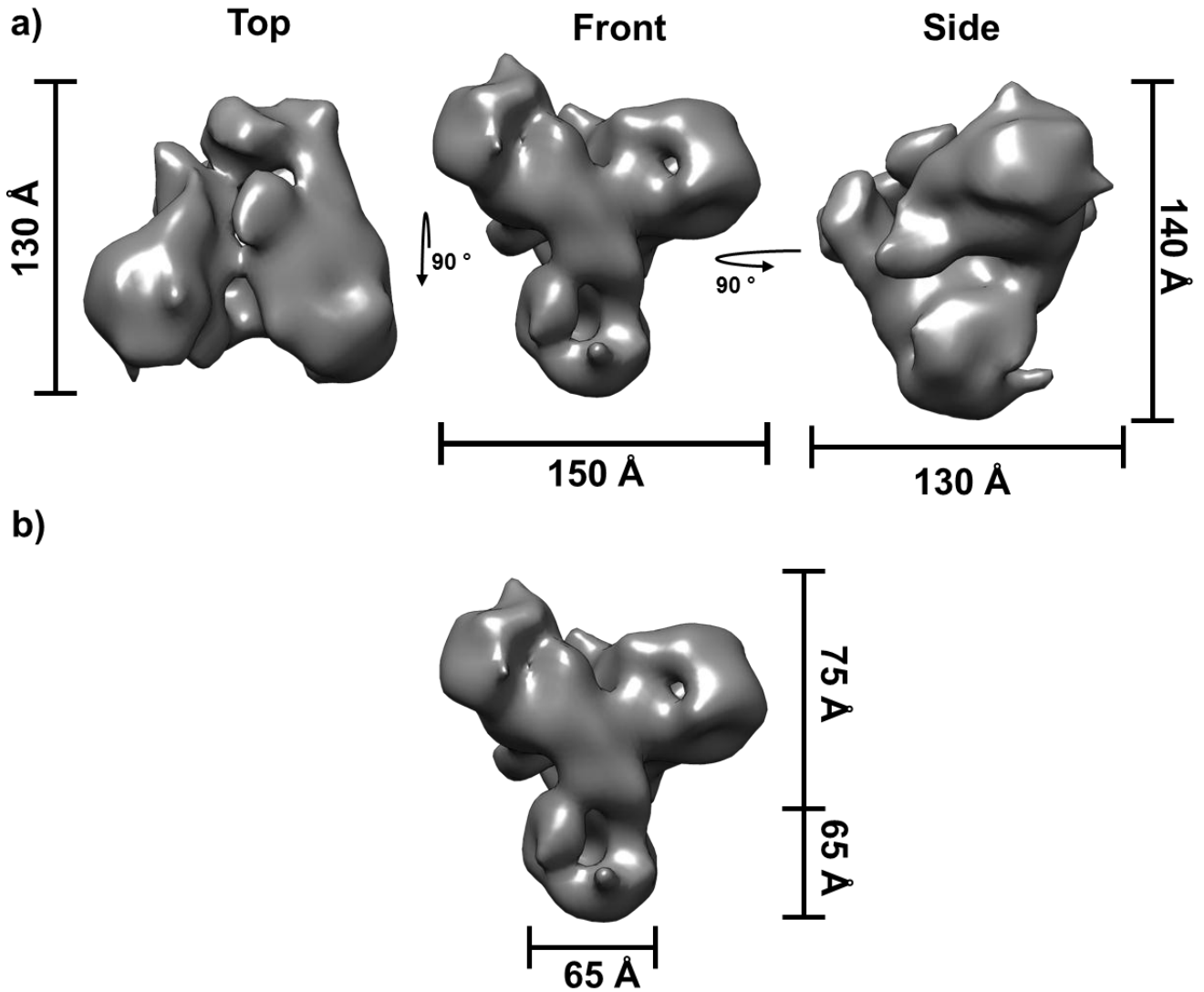
Figure 4.11 – Single particle reconstruction of LAG-3:Fc by negative stain EM:

a) 3D single particle reconstruction of LAG-3:Fc shown by surface volume contoured at 0.41 σ contour level. LAG-3:Fc exhibits an antibody-like Y-shape surface envelope as shown by front view. Top and side views show the globular nature of two LAG-3 domains and third Fc domain. The approximate overall dimensions of the LAG-3:Fc are defined as 150 x 140 x 130 Å (width, height, depth; as viewed from front).

b) Measurements of the globular domains of LAG-3:Fc single particle reconstruction front view. The reconstruction suggested two globular domains of similar size (top of model) and a third smaller domain (bottom of model) which likely represents the LAG-3 and Fc domains, respectively.

Due to the quality of the model, however, domain matching with known structures of the Fc domain were unable to confirm such assignments (data not shown).

The refined LAG-3:Fc model was reconstructed from inclusion of the full particle dataset (2,062 particles). Class averages and corresponding model projections showed good overall agreement[9]. However, better matching was observed in class averages of front views of LAG-3:Fc suggesting better model accuracy of front view projections (*Figure 4.12a*). Analysis of the Euler map of class averages – a plotted representation of the assigned Euler angles to each class average – showed that angular assignment of class averages exhibited good coverage across particle views[10] (*Figure 4.12b*). Class averages which were comprised of larger image stacks (typically 8 to 16 particles per class average) were clustered to front views, once more highlighting increased image data skewed towards front views. Top and side view class averages were formed typically from only 3 to 8 particle images per class. As a result, to improve model accuracy and resolution, further particle images from a larger dataset of LAG-3:Fc micrographs are required; particular containing LAG-3:Fc top and side views. For assessment of resolution, LAG-3:Fc model of Fourier shell correlation (FSC) curves[11] were subjected to the gold-standard resolution criteria (*Figure 4.12c*) (Scheres & Chen 2012). The resolution of the model using these criteria is estimated to between 23.2 – 24.0 Å depending on applied masking criteria. A conservative resolution of the LAG-3:Fc model is therefore estimated at 24.0 Å.

The solution of this reconstruction of LAG-3:Fc, therefore, described LAG-3:Fc as a non-polymerising asymmetric protein consisting of three distinguishable globular domains that combined to overall dimensions similar to that of an antibody. Moreover, imaging of the LAG-3:Fc

---

[9] Model projections are computed views through the reconstructed model. In effect, model projections represent a computed representation of a particle view from a given angle. Thus, model projections can be used to validate that observed particle views are equivalent to modelled particle views.

[10] To generate an accurate 3D reconstruction of a protein molecule, the particle dataset must contain particle views that encompass all possible views. A perfect Euler map would describe an even distribution of 2D class averages (views) with a similar number of images per class average (image stacks).

[11] FSC curves allow the assessment of resolution of structural information. Fourier shell correlation (FSC) is the cross-correlation coefficient between two 3-dimensional volumes. This correlation is calculated by reconstructing two models from half the available dataset each. In an FSC curve, FSC is plotted as a function of spatial frequency. At low resolutions (low spatial frequencies) each of the two compared models have high FSC i.e. a high degree of correlation and are in agreement between models. At higher resolutions (high spatial frequencies) the two models exhibit low FSC i.e. no correlation, as they trend towards random noise. If high resolution structural information is contained within the model, high FCS extends out into higher spatial frequencies and the FSC curve reaches baseline at higher spatial frequencies.

protein by negative stain EM showed that the current protein formulation was largely homoge-
nous, devoid of aggregation and thus a viable sample for the study of LAG-3 using higher-
resolution EM techniques.
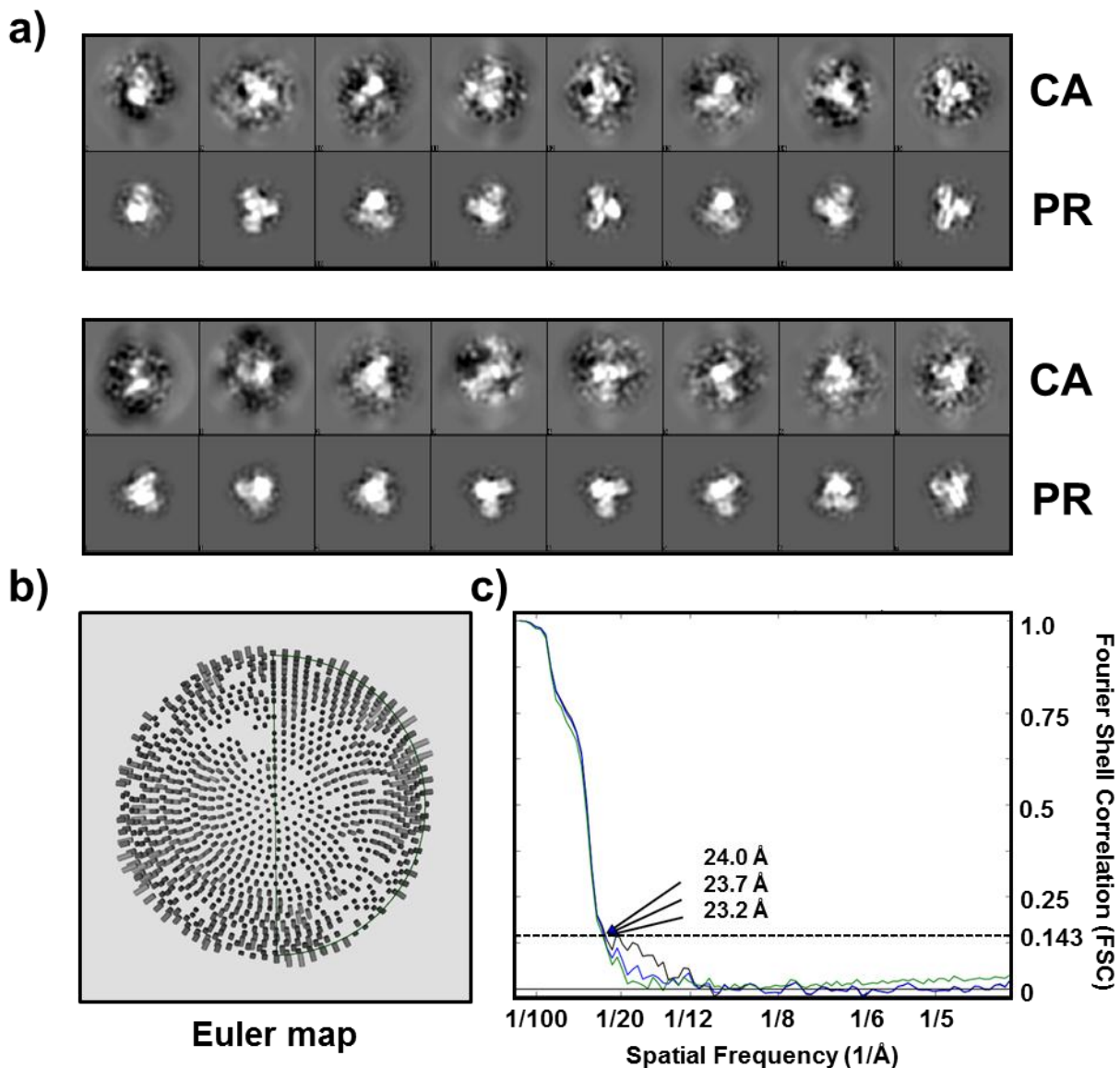
Figure 4.12 – Validation of the current LAG-3:Fc single particle reconstruction:

a) Sixteen example class averages (CA) and corresponding projections (PR) from the refined model of LAG-3:Fc based on current particle dataset. CA and PR matched at certain Euler angles, particularly front views. CA and PR at other angles, particular side views, exhibited poorer matching due to the limited dataset.

b) Distribution of Euler angles assigned to class averages of LAG-3:Fc represented by cylinders scaled to particle stack size. Cylinders represent a single class average which is derived from a number of particles images of similar 'views'. Class averages were relatively evenly spread across all possible 'views' meaning few 'views' of LAG-3:Fc were missing from the dataset. Each class average had a relatively even number of constituent particle images, however, some skewing towards LAG-3:Fc front views was observed as shown by increased stack height of cylinders about the map circumference.

c) Fourier shell correlation (FSC) curves and gold-standard resolution criteria of the refined LAG-3:Fc reconstruction which can be used to give an indication of model resolution. FSC curves are shown of unmasked (green) loose (blue) and tight (black) masks applied to the refined model which show extension of FSC out to moderate spatial frequencies only and no data out to high spatial frequencies. Resolution is estimated at 23.7 Å using the most conservative tight masking in accordance with the gold-standard resolution criteria (Scheres & Chen 2012).

4.7   Discussion

LAG-3 has been shown to bind MHC-II expressed at the cell surface (Huard et al. 1995). This interaction has not been characterised at the protein level, nor has an affinity value been attributed to LAG-3 binding MHC-II through direct protein measurements.

Studies into the functional binding of LAG-3 were enabled by the development of a LAG-3 expressing cell line. The resulting transduced Jurkat cells clone expressed high levels of LAG-3 and remained as a homogenous LAG-3$^+$ population throughout prolonged culture periods of ~90 days. This JRT LAG-3$^+$ C8 cell line developed was also essential for the studies described to follow in Chapter 5.

LAG-3 was first shown to interact with the MHC-II molecule HLA-DR1 by the staining of LAG-3$^+$ cells with HLA-DR1 multimers. Such multimers were shown to stain LAG-3 replete and not LAG-3 deplete cells. Moreover, the binding of multimers to LAG-3 replete cells was observed only with HLA-DR1 multimers and not MHC-I multimers of HLA-A2. Such staining could not be attributed to TCR binding due to the lack of TCRβ chain expression in the JRT3 T3.5 Jurkat cell line as confirmed by minimal staining of JRT LAG-3$^+$ C8 cells with a pan-αβ TCR antibody. The observed staining was instead shown to be LAG-3 dependent by the blockade of multimer staining by the 17B4 clone αLAG-3 antibody.

Despite 100 % LAG-3 expression by JRT LAG-3$^+$ C8 cells, only a fraction of cells were detected as HLA-DR1 multimer$^+$. Staining of cells was characterised by only a moderate shift in fluorescence intensity. Indeed, the HLA-DR1 multimers used (batch matched) had the capacity to achieve near complete recovery of cells when staining a cognate T cell clone. These data initially suggested that the LAG-3 interaction with HLA-DR1, at least as a multimeric molecule, stained LAG-3 cells with a weaker avidity compared to the cognate interaction between HLA-DR1 and TCR. Poorer staining could, however, be attributed to a number of factors that are difficult to deduce from cell surface expressed LAG-3 staining.

To this end, LAG-3 binding to the MHC-II molecule HLA-DR1 was interrogated at the protein level using surface plasmon resonance (SPR) experiments. Such experiments required the acquisition of LAG-3 and HLA-DR1 protein samples. Production of a monomeric LAG-3 protein has proved difficult in-house and thus hampered the ability to measure the affinity of the LAG-3-MHC-II interaction through monovalent SPR experiments. As a result LAG-3 binding to HLA-DR1 was measured using the bivalent LAG-3:Fc fusion protein.

SPR experiments directly confirmed, as previously observed at the cell surface, that LAG-3 binds to the MHC-II molecule HLA-DR1 at the protein level and shows no specific interaction

with the MHC-I molecule HLA-A2. This interaction with HLA-DR1 was shown to be independent of complexed peptide and thus supports a model of LAG-3 binding uninfluenced by presented peptide. Moreover, LAG-3 similarly bound to HLA-DR1 molecules produced in either *E. coli* or *sf9* insect cells and is therefore appears uninfluenced by MHC glycosylation differences.

This interaction between LAG-3 and HLA-DR1 was described in terms of its affinity through a combination of kinetic and steady-state SPR analyses. These analyses quantified the affinity of binding between LAG-3 and HLA-DR1 as 13 μM (K_D) using steady-state analysis. This affinity is comparable to that of TCR engagement of pathogen-derived pMHC-II and is slightly higher than average TCR-pMHC-II binding (D. Cole et al. 2007). This micromolar affinity is considerably weaker than the calculated avidity of dimeric LAG-3 binding in indirect cell surface experiments (K_D = 60 nM at 37 °C) (Huard et al. 1995).

Despite a weaker affinity than previously described, these studies show LAG-3 binds HLA-DR1 at a significantly higher affinity that CD4; for which a soluble affinity of binding has not been determined by SPR due to its weak nature. Indeed, CD4 binding to MHC-II was unable to be detected at concentrations as high as 2.5 mM (Jönsson et al. 2016). As LAG-3 binding to MHC-II molecules has been shown to block consequent CD4 binding, at the cell surface (Huard et al. 1995), competition between LAG-3 and CD4 for MHC-II binding would favour engagement by LAG-3. Thus, this enhanced engagement by LAG-3 may contribute to the potency of LAG-3 mediated T cell inhibition.

Although LAG-3 binds MHC-II via a higher affinity interaction compared to CD4, LAG-3 dissociation was shown to have very fast kinetics. These data suggest that LAG-3 engagement of MHC-II at the cell surface is likely a transient process maintained by fast rebinding to MHC-II as opposed to prolonged attachment at the cell surface. Such kinetics are observed for co-receptor binding to MHC, whereby co-receptor binding affinity is tuned with TCR affinity such that T cell signalling remains highly sensitive yet maintains specificity to cognate TCR-pMHC stimulation (Hoerter et al. 2013). As a result, T cell signalling by agonist interaction between TCR and cognate pMHC can be initiated by very few binding events (Irvine et al. 2002). For CD4, despite a weak affinity, MHC-II binding maintains TCR phosphorylation at an active basal level by recruitment of Lck and thus poises T cells for cognate TCR-pMHC engagement (Jönsson et al. 2016). Since LAG-3 also exhibits fast kinetic binding to MHC-II, parallels between LAG-3 and co-receptor maintenance of antigen specificity may exist. Indeed, surface bound LAG-3 mediated inhibition of dendritic cell maturation has been shown to be antigen specific and require TCR-pMHC-II engagement by LAG-3 expressing regulatory T cells (Liang et al. 2008). Thus, the affinity of LAG-3 engagement of MHC-II expressing APCs must be tuned

such that ligand discrimination is maintained. The effect of LAG-3 expression on antigen specific stimulation on human T cells, however, is poorly understood. Consequently, further knowledge of LAG-3 signalling is required to understand how this observed affinity for MHC-II affects LAG-3 mediated T cell homeostasis.

Definition of LAG-3 affinity for MHC-II at 13 μM describes a similar affinity to that of the MHC-I co-inhibitory molecule Immunoglobulin-like transcript 2 (ILT2) which impairs T cell signalling in MHC-I restricted T cells (Liang et al. 2006). Exhibiting parallels to LAG-3, ILT2 inhibits T cell activation through an interaction through CD8 co-receptor competitive binding with MHC-I; measured at 7 μM using similar SPR analyses (Moysey et al. 2010). Unlike CD4 binding, CD8 co-receptor binds to HLA-A2 with a measurable affinity defined at 137 μM (Cole et al. 2007). As a result, ILT2 binding to MHC-I is approximately 20-fold higher affinity than that of CD8 binding. In contrast, the relative affinity of LAG-3 for MHC-II is >200-fold compared to CD4 binding (assuming a CD4-MHC-II K_D of >2.5mM). Thus, despite a slightly weaker affinity compared to ILT-MHC-I binding, the enhanced ability of LAG-3 to out-compete CD4 binding may make LAG-3 a more potent inhibition of MHC-II restricted T cell activation compared to ILT2 mediated inhibition in MHC-I restricted T cells.

Whilst the dimeric LAG-3:Fc molecule exhibited some bivalent effects, the contribution of bivalency to LAG-3:Fc binding was minimal. At high ligand concentrations, where spatial density of MHC-II molecules should enable multivalent interactions, LAG-3:Fc off-rate was only minimally extended through bivalency. As a result, functional binding of the LAG-3:Fc fusion protein exhibited poor ability to engage multiple MHC-II molecules. Since there is evidence that LAG-3 forms dimeric molecules at the cell surface, dimerisation of LAG-3 molecules may contribute to an increase in functional potency (Li et al. 2004). These data, however, suggest that dimerisation of LAG-3 does not drastically influence the strength of MHC-II engagement. Such observations should be made with caution, however, as it is not known how representative the LAG-3:Fc protein is of dimeric LAG-3 forms found at the cell surface.

Having shown that LAG-3 bound MHC-II with a micromolar (K_D) affinity, structural data to describe this interaction was sought. Initially, efforts were made to produce samples for study by x-ray crystallography. Despite detectable expression of LAG-3 products, which comprised of the four extracellular domains of LAG-3 expressed in insect cells, sufficient yield required for structural studies was not achieved. As a result, the dimeric LAG-3:Fc fusion protein remained the best available reagent for the study of LAG-3 structure function.

Insights into LAG-3 structure by study of LAG-3:Fc by electron microscopy were instead initiated. Using negative stain electron microscopy, a low-resolution model of LAG-3:Fc, estimated at 24 Å resolution, was produced which described the fusion protein's overall surface envelope. This reconstruction showed that the LAG-3:Fc molecule did not form any unexpected oligomerisation events. In addition, the LAG-3:Fc protein formed a Y-shaped globular structure reminiscent of immunoglobulins. At this resolution, however, little inference about LAG-3 structure-function can be made. Instead, these data represent preliminary experiments required in order to progress towards the study of LAG-3:Fc at higher resolution by cryo-electron microscopy. Importantly, these data show that the quality of the LAG-3:Fc preparation is sufficient to proceed to more complex structural analyses.

4.7.1 Future directions

In these studies, LAG-3:Fc binding was described to a single MHC-II molecule: HLA-DR1. To this end, it is unknown whether LAG-3 binds to other MHC-II alleles with similar affinity. Having established methodologies to quantify LAG-3 affinity to HLA-DR1, similar experiments could be performed using different HLA-DR, HLA-DQ and HLA-DP molecules. Indeed, CD8 co-receptor affinity for different MHC-I molecules ranges from (K_D) affinity of 100 μM for HLA-A11 to >1000 μM for HLA-A68 binding (Gao et al. 2000). Analysis of binding of these alleles could also be studied by HLA allele multimer staining of LAG-3^{+} cells.

In addition, some evidence has emerged of a second potential ligand for LAG-3 in the cell-adhesion molecule LSECtin/CLEC4G (Xu et al. 2014). Such binding has been proposed as a potential mechanism of LAG-3 mediated inhibition of CD8^{+} T cell activation. Dependent on availability of LSECtin samples, SPR experiments using LAG-3:Fc could be performed to robustly determine the presence of such an interaction and again describe its affinity.

At present, there is still a vast gap in understanding in how LAG-3 mediates inhibition of T cell activation, particularly at the structural level. As described, the next steps in efforts to gain high-resolution insights into LAG-3 structure would be the study of LAG-3:Fc via cryo-electron microscopy which, through the development of advanced microscopes, automated imaging, advanced reconstruction software and expanding computation power has begun to yield protein structures at near-atomic resolution (Egelman 2016). Moreover, recent implementation of Volta phase plate (VPP) technology into TEM set-ups, which increase contrast at the focal plane, will allow the study of smaller proteins, such as LAG-3:Fc, via high-resolution cryo-EM imaging (Danev & Baumeister 2016). In order to access such microscopes, LAG-3:Fc cryo-protected grids must first be produced and shown to be of sufficient quality for high-resolution TEM. Such

methodologies could also be applied to the study LAG-3:Fc complexed with HLA-DR1 which, at higher-resolution, would be easier to filter out sample heterogeneity.

Despite unsuccessful attempts to produce suitable protein sample, study of LAG-3 structure may still be achievable by x-ray crystallography. In order to try generate soluble LAG-3 samples, a high-throughput construct screening process may prove to be a viable approach. Here, multiple LAG-3 derived constructs could be designed *in silico* to include (a) sequential truncation of Ig-like domains (b) mutation of glycosylation signal sequences and/or (c) fusion protein screening. Indeed, production of a monomeric form of LAG-3:Fc, by mutation of the disulphide mediating residues, resulted in inefficient expression indicating that monomeric forms of LAG-3 *in vitro* may not be achievable (Huard et al. 1996). These high-throughput screens could therefore focus on constructs which enable LAG-3 stability through dimerisation. These constructs could consequently be screened for production in different expression systems which are either glycosylation deficient or impaired (Chang et al. 2007).

4.7.2 Implications of this study

Firstly, initial experiments describing binding of MHC-II multimers to LAG-3^{+} pose an indirect implication in CD4^{+} T cell biology experimental design. MHC-II multimers are used to specifically stain and sort antigen-specific T cells based on a desired interaction with the pMHC-II epitope. These experiments highlight a requirement for the use of irrelevant multimer controls in such experiments in order to prevent misdetection of LAG-3^{+} cells as perceived antigen-specific multimer^{+} cells. Such controls become increasingly important in self-derived MHC-II multimer experiments where low affinity clones do not exhibit a considerable increase in fluorescence intensity as a result of multimer binding. To this end, these data show that flow cytometric gating of multimer^{+} cells should be performed using matched HLA multimers and that use of MHC-I irrelevant controls in staining MHC-II restricted T cells may result in the aberrant antigen non-specific detection of LAG-3^{+} cells and are thus not suitable.

In terms of LAG-3 function, these studies provide the most comprehensive evidence of LAG-3 binding to MHC-II at the protein level. Moreover, definition of the affinity of the interaction alters the perception that LAG-3 binds MHC-II via a high affinity interaction as the data presented in this Chapter describes a more moderate interaction strength. Nevertheless, this binding affinity is significantly higher than the immeasurably low CD4-MHC-II soluble affinity. As a result, these data add evidence to a model where LAG-3 is able to out compete CD4 for MHC-II binding as one potential mechanism of LAG-3 mediated T cell suppression.

5 Chapter 5: Molecular tools for the characterisation and molecular targeting of LAG-3$^+$ T cells

5.1 Abstract

Immune responses to tumours are sub-optimal leading to immune evasion and consequent progression of malignancies. Efforts to improve T cell responses to tumours by tuning the activation of T cells in human cancers has shown promising clinical benefit and have been licensed for use in some cancers. As a result, therapeutic agents which target T cells expressing surface markers involved in immune suppression are of clinical interest. Lymphocyte activation gene-3 (LAG-3), a protein expressed on activated T cells and regulatory T cells, is associated with a highly suppressive T cell phenotype. LAG-3$^+$ cells are enriched in lymphocytes extracted from colorectal cancer tumours and as a result, LAG-3 has been highlighted as a potential therapeutic target for enhancement of anti-tumour T cell responses. To this end, a panel of mouse monoclonal anti-LAG-3 antibodies were generated using the whole protein immunisation of mice. Consequent antibody responses were quantified by direct ELISA and flow cytometry allowing for the cloning of six monoclonal antibodies reactive to LAG-3 expressing cells. Antibodies were subsequently characterised by sequence, function and antibody-antigen binding strength. Generated antibodies were able to bind LAG-3 specifically by flow cytometry and Western blot via a sub-nanomolar (K_D) avidity with antigen, as shown by surface plasmon resonance measurements. The development of such antibodies will aid in the detection of LAG-3 expressing cells, the generation of LAG-3 protein samples and represent the starting pipeline in the generation of antibody therapeutics to target LAG-3 expressing cells in human cancers.

5.2 Introduction

Tumour-specific T cells are detected within tumours as tumour infiltrating lymphocytes (TILs) and play an important role in the regulation of malignancies. Despite a correlation between the presence of TILs and 5 year survival in colorectal cancer patients, T cells cannot prevent tumour occurrence (Galon et al. 2006). Current immunotherapy research is focusing on the modulation of checkpoint inhibitor proteins, such as CTLA-4 and PD-1, which can downregulate anti-tumour T cell responses (Sharma & Allison 2015). For example, in a phase III study, treatment of unresectable stage III or stage IV metastatic melanoma patients with ipilimumab and nivolumab, which target CTLA-4 and PD-1 respectively, showed a significant increase in progression free survival (11.5 months) compared to monotherapy (ipilimumab alone: 2.9 months, nivolumab alone: 6.9 months) (Larkin et al. 2015). Despite success of such agents in the clinic, increased progression free survival is not observed in all patients, highlighting a need to identify further immune checkpoint targets for tailored treatment or combination treatment across different individuals. One such potential target is LAG-3, which, as discussed previously, plays a complex role in suppressing adaptive immunity.

Interest in depleting LAG-3 expressing T cells in tumours, or blocking the action of LAG-3 by such T cells, stems from the glycoprotein's expression on inhibitory T cell populations. LAG-3 in $CD4^+$ $CD25^+$ Tregs is upregulated and its function is required for maximal suppressive activity (Huang et al. 2004). As a result of LAG-3 expression, such cells are inherently anergic to proliferation upon exposure to antigen. In addition, $CD4^+$ TILs extracted from human colorectal cancer tumours have shown a significant upregulation of LAG-3 expression compared to $CD4^+$ T cells from matched healthy colon and PBMCs (Scurr et al. 2013). These T cells, taken from tumour, were 50-fold more suppressive than classical $CD25^{hi}$ $FoxP3^+$ $CD4^+$ Tregs as shown by *in vitro* suppression assays. LAG-3 expression is also a characteristic marker on Tr1 cells, a highly suppressive T cell subset found in the periphery as well as infiltrating in human hepatocellular carcinomas (Pedroza-Gonzalez et al. 2015).

Whilst LAG-3 is expressed on T cells with regulatory function, expression of LAG-3 on effector activated T cells must also be considered (Wojciech et al. 2014). Depletion of LAG-3 expressing T cells, either possessing anti-tumour effector function, or the capacity to regain functionality as memory T cells, might impact on T cell immunity as a whole. Depletion of LAG-3 expressing activated effector T cells, in a primate model of type IV hypersensitivity, reduced T cell mediated symptoms and reversed T cell driven pathology (Poirier et al. 2011). These data would suggest that removal of such cells in a cancer setting might in theory be a detrimental intervention. Studies involving ipilimumab, which specifically targets CTLA-4 to

block and induce depletion, have shown that antigen-target depletion of T cells is compartment specific and it is hypothesised that whilst therapeutic depletion of CTLA-4 expressing activated effector T cells may occur, providing the depletion of CTLA-4 expressing cells shifts the effector to regulatory T cell ratio in favour of increased anti-tumour effector cells, an enhanced immune response is observed (Simpson et al. 2013).

Whilst LAG-3 is expressed on activated effector T cells, the role of LAG-3 on such cells is to inhibit their further T cell activation signalling (Workman et al. 2002). It can therefore be hypothesised that depletion of such cells would have less impact on potential anti-tumour immunity due to their impaired function. LAG-3 has also been shown as a marker of T cell exhaustion and, thus, mediate the proliferative and functional impairment of tumour-reactive T cells within tumours (Woo et al. 2012). Moreover, blockade of LAG-3, in combination with PD-1 blockade, is able to reverse T cell exhaustion and promote enhanced clearance of parasite load in chronic infections, a model of chronic antigen exposure (Butler et al. 2012).

Together, these data highlight LAG-3 as a potential target for combination or monotherapeutic modulation of T cell immunity in colorectal and other cancers. To study the effect of blockade and depletion of LAG-3 expressing cells *in vitro* and later in human studies, accessible monoclonal antibodies designed with the correct formulation to promote such blockade or depletion are required.

5.2.1   Antibodies as biotherapeutic agents

Antibodies provide an essential molecular tool in immunology, diagnostic medicine and biology as a whole. In the last ~20 years, these protein molecules have come to importance in clinical medicine as biotherapeutic agents. These proteins, like T cell receptors, exhibit exquisite specificity to target molecules through the somatic recombination of immunoglobulin genes. The resulting antibody proteins therefore provide an effective solution to target specific molecules *in vivo* to disrupt or block native biological systems, or reverse pathophysiological transformations of biological systems. In addition, due to being derived from the immune system themselves, these biotherapeutic antibodies are able to modulate the host recipient's immune system into targeting an immune response against the antigenic target. This function, therefore, allows the therapeutic targeting of cells expressing cellular markers, such as LAG-3, through the recruitment of the host's immune networks.

Antibodies are multivalent protein molecules. IgG class antibodies, the focus of this chapter and most of the on-the-market antibody therapeutics, contain two antigen binding sites. As a result of bivalency, IgG molecules have exceptionally long off-rates in the order of hours and thus, immunoglobulins such as IgG class antibodies are effective at coating antigen expressing

cells (Weiner 2015). This high avidity property along with their long half-lives, 15 days for ipilimumab and 12 to 20 days for nivolumab (depending on dose), make IgG proteins an ideal molecular solution for targeting certain cell populations based on their antigenic expression (Fellner 2012; Glassman & Balthasar 2014). Moreover, the large protein volume of antibodies enables the inhibition of interactions to be mediated via the steric blockade of protein-protein interactions at the surface of cells (Shih et al. 2014).

5.2.2 Antibody isotypes and recruitment of immune effectors

As well as enabling blockade of molecular function, antibody molecules are also able initiate depletion of antigen-bearing cells through the recruitment of immune cells or proteins. Such processes are dependent on the antibody isotype of a developed antibody agent. A cellular based response against surface expressed antigen is dependent on the Fc receptor (FcR) family of proteins which bind antibodies at varying affinities dependent on subclass of both receptor and antibody (Guilliams et al. 2014).

Natural killer (NK) cell mediated depletion, through the process of antibody dependent cellular cytotoxicity (ADCC) occurs through the activating FcγRIIIa (CD16a) receptor expressed by NK cells and, as a result, IgG1 and IgG3 subclass antibodies are the choice isotype for ADCC induction (Seidel et al. 2013). Similarly, antibody dependent cellular phagocytosis (ADCP) by macrophages, which express a wide range of FcγR proteins, can be mediated through IgG molecules (Nimmerjahn & Ravetch 2008). Preference for the IgG1 subclass to initiate functional depletion by macrophages is based on its preferential binding to activating FcγRs such as FcγRIIa and FcγRIIIa compared to the inhibitory FcγRIIa – the latter of which can limit the efficacy of cellular depletion by macrophages (Beers et al. 2016).

In concurrence with a cellular based response, complement activation has also been shown as a mechanism of depletion of antigen-bearing target cells *in vivo* (Weiner 2010). Complement dependent cytotoxicity (CDC), against antibody opsonised targets, is facilitated by IgM, IgG1 and IgG3 molecules and enabled through an ability to interact with the C1q component of the classical complement activation pathway (Poons et al. 1985; Bindon et al. 1988).

Due to the ability to activate ADCC, ADCP and CDC immune networks, the IgG1 isotype is regarded as the most effective antibody isotype for the therapeutic targeting of antigen-bearing cells (Beers et al. 2016).

5.2.3 Anti-LAG-3 antibodies currently described in the literature and beyond

The generation of antibodies targeting human LAG-3 has been achieved previously by a number of academic laboratories, pharmaceutical companies and commercial biotechnology companies.

There are currently twelve available monoclonal antibodies targeting human LAG-3 protein (*Table 5.1*). As well as those available to purchase commercially, a number of additional antibody formulations are documented in the literature and are either in the possession of laboratories that are not distributed commercially or their use has been halted (Huard et al. 1994; Baixeras et al. 1992). In addition, a number of antibodies against LAG-3 are being developed as part of therapeutics by pharmaceutical companies of which, at the time of writing, little is known about their formulation, function and therapeutic potential.

Clone or Identifier	Species	Isotype	Availability	Immunogen	Function	Origin
Commercially available antibodies						
17B4	Mouse	IgG1	Enzo Lifescience	The unique 30 aa loop of the first N-terminal D1 domain of human LAG-3	Blocking	(Triebel group)[1]
28C5	Mouse	IgG1	Creative Diagnostics	Synthetic peptide covering the 30 aa extra loop of human LAG-3 (aa70-99)		
22F4	Mouse	IgG1	Creative Diagnostics	N-terminal D1 domain of human LAG-3		
FQS5403(3)	Rabbit	IgG	Creative Diagnostics	Synthetic peptide within C-terminus of human LAG-3 sequence		
DOB.53	Mouse	IgM	Creative Diagnostics	n.s.		
3DS223H	Mouse	IgG1	eBioscience	Human LAG-3 (no further specification)		
3C39	Mouse	IgG2	GeneTex	Human recombinant LAG-3 (no further specification)		
11E3	Mouse	IgG1	LifeSpan Biosciences	Baculoviralsf9 expressed human LAG-3. Recognizes the D1 domain		(Triebel group)[2]
8G6	Mouse	IgG2b	OriGene	Human recombinant aa66-332 of human LAG3 produced in E.coli		
10E7	Mouse	IgG2a	OriGene	Human recombinant aa66-332 of human LAG3 produced in E.coli		
5C3	Mouse	IgG2b	OriGene	Human recombinant aa66-332 of human LAG3 produced in E.coli		
874501	Mouse	IgG1	R&D Systems	Whole nS0-derived, recombinant human LAG3		
Unavailable antibodies						
15A9	Mouse	IgG1	None	Baculoviral sf9 expressed human LAG-3.		(Triebel group)[2]
4F4	Mouse	IgM	None	30 aa extra-loop of the first N-terminal D1 domain of human LAG-3		(Triebel group)[1]
13E2	Mouse	IgG1	None	n.s.	Non-blocking	(Triebel group)
Documented pharmaceutical agents						
BMS-986016	Human	n.s.	None (BMS)	n.s.	n.s.	
LAG525	Humanised	n.s	None (Novartis)	n.s.	Blocking	IMP701 (Triebel group)
GSK2831781	Humanised	n.s.	None (GSK)	n.s.	Depleting	IMP731 (Triebel group)

Table 5.1 – Summary of available anti-LAG-3 antibodies

Anti-LAG3 antibodies that are commercial available, currently unavailable or are known to be developed as pharmaceutical agents are listed. BMS = Bristol-Myers Squibb, GSK = GlaxoSmithKline. Antibodies of 'Triebel group' origin represent antibodies commercialised or derived from the laboratory of F. Triebel. [1]Generation referenced in (Baixeras et al. 1992), [2]Generation referenced in (Huard et al. 1994).

5.2.4   Aims

Despite a number of anti-LAG-3 antibodies having already been generated, such antibodies are currently unavailable for academic laboratories to analyse the efficacy of LAG-3$^+$ cell depletion either as a monotherapy or in combination therapy with agents aimed at enhancing immune responses to tumour antigens in cancer patients. Furthermore, none of these antibodies have yet shown clinical efficacy for the treatment of cancer, demonstrating the need for more investigation. In addition, dissection of the mechanisms involved in LAG-3 mediated T cell suppression have been hampered by a lack of suitable soluble LAG-3 protein. The development of an in-house supply of LAG-3 binding antibody would assist in the generation of recombinant LAG-3 protein for future cellular, biochemical, biophysical and structural studies.

As a result, the overall aim of this chapter was to develop an in-house monoclonal antibody which could be used as (i) an experimental tool for identifying LAG-3 expressing cells (ii) a molecular tool for the study of LAG-3 structure-function and (iii) a potential therapeutic agent for clinical cancer therapy. The overall aim of this chapter is divided into the following sub-aims:

(i)   To develop a panel of monoclonal antibodies with specificity for human LAG-3

(ii) To produce the large (milligram) quantities of antibody required for *in vitro* assays and LAG-3 protein chemistry.

(iii) To characterise each mAb in terms of their clonotype and isotype.

(iv) To assess the functional binding characteristics of generated monoclonal antibodies for LAG-3.

(v)   To assess the binding strength of the interaction between generated antibodies for LAG-3 protein *in vitro*.

(vi) To assess the ability to block the LAG-3-MHC-II interaction

5.2.5   Strategy of monoclonal antibody generation

The generation of antigen specific antibodies against human molecules is typically performed through the immunisation of small mammals (mice, rats or rabbits etc.) and consequent generation of clonal immortalised B hybridoma cell lines such that the cost and ethical expense of animals is minimised. More recent methodologies in generating human antibodies, driven by the generation of antibodies for therapeutics, utilise either immunoglobulin gene humanised mice or the complete bypassing of experimental mammals by generating human monoclonal antibodies through phage or yeast display libraries techniques (Lonberg 2005; Jespers et al. 1994).

Due to the expertise within the Division of Infection and Immunity, Cardiff University, the immunisation of mice with human derived LAG-3 immunogen approach was taken. This process was performed in collaboration with Professor Paul Morgan.

5.2.5.1   Choice of immunogen

When developing monoclonal antibodies against a specific target, the immunogen used must be selected based on the desired application of the developed antibodies. Generally, mouse antibody responses are raised against recombinately expressed whole protein or short peptides derived from the whole protein.

Generating monoclonal antibodies against short peptide epitopes (typically 6 – 25 amino acids in length) is the most commonly used tactic for generating highly specific antibodies to a desired target. As small, low molecular weight compounds are not immunogenic when injected into the host species, short peptide epitopes are typically conjugated to a carrier protein such as keyhole limpet hemocyanin (KLH) which increases the mass of the immunogen and consequently the immunogenicity. This method is preferable as a certain locale of the antigen can be targeted as the raised epitope. For example, if the rationale for antibody development is to block a protein function, such as interaction with a ligand or multimerisation, peptide-KLH immunogens can be used to narrow the generated B cell repertoire to have this desired functionality.

Narrowing the immunogen, however, limits the diversity of the B cell response which, in turn, can have a negative impact on the ability to generate high affinity antibodies against the protein target. This can occur if the narrow peptide epitope does not contain favourable chemical properties for the formation of a high affinity antibody-antigen interaction. This can be overcome by *in vitro* affinity maturation techniques such as phage or yeast display, however, this process can be lengthy and resource heavy. In addition, use of peptide-KLH immunogens requires some knowledge of the antigen's protein structure to ensure that the target epitope

sequence is surface exposed and sterically accessible in the antigen's native conformation. For this reason, the peptide-KLH approach is less suited in the generation of antibodies against proteins such as LAG-3 where the high resolution protein structure is not known. Antibody epitope prediction programs can, however, be used to assess whether the peptide-KLH antigen contains a favourable amino acid sequence for epitope generation, however, these programs result in a prediction only.

An alternative approach involves the immunisation of the host animal with whole antigenic protein. This method generates a diverse B cell response against the immunogen, within which the polyclonal response will be spread across epitopes of the whole heterologous protein. This is advantageous as the B cell repertoire is not limited to a narrow portion of the protein. Instead, antibodies are generated against the whole available protein surface, allowing the host B cell repertoire to sample molecular surfaces for all available potential epitopes. In the same respect, the disadvantage of this approach is that the epitope repertoire generated is far less focused, thus, if an antibody with a specific function is required, as discussed previously, this function must be screened for from the generated polyclonal B cell response via a functional assay – as opposed to selected for at the point of generation as in the case for peptide-KLH antibody generation.

For whole protein antigens larger than approximately 20 kDa in size, whole protein immunogens do not require carrier protein conjugation. As a result, carrier protein specific antibodies do not need to be affinity purified out (at the protein level) or cloned out (at the cellular level). Most importantly, the probability of generated antibodies having the capacity to bind natively folded antigen is significantly higher than if peptide-KLH conjugates are used as the immunogen is presented to the B cell repertoire in a similar (or the same) conformational state to that of the endogenously expressed target protein.

In this study, the whole protein approach was taken to generate anti-LAG-3 antibodies using the LAG-3:Fc fusion protein. The decision to opt for the whole protein approach was due to (i) the lack of LAG-3 structural data (ii) the increased probability of obtaining antibodies with binding capacity for *in vivo* cellularly expressed LAG-3 and (iii) the increased probability of achieving high affinity antibodies without requiring *in vitro* affinity maturation. Furthermore, the LAG-3:Fc fusion protein was chosen as the whole protein immunogen due to (i) the availability of the reagent through commercial sources (ii) the functionality of the molecule as demonstrated in the literature and (iii) the comparative stability of LAG-3:Fc compared to other LAG-3 reagents.

5.2.5.2 Anti-LAG-3 specific antibody screening strategy

In order to select for host sera or B cell hybridoma clone supernatants which contained antibodies specific for LAG-3, a two-fold screening approach was used which incorporated both direct ELISA and fluorescent antibody staining of LAG-3 expressing cells. This two-fold strategy was essential due to the nature of the LAG-3:Fc immunogen used.

Firstly, antibody containing samples were screened for specificity to the LAG-3:Fc immunogen by direct ELISA. In this assay, antibodies which are able to bind the LAG-3:Fc immunogen were first captured by their interaction with LAG-3:Fc and secondly detected by a HRP-conjugated anti-mouse Ig specific antibody. Thus, assay wells which produced a colorimetric output could be attributed to the presence of a substance with affinity to LAG-3:Fc, as test sample is subjected to extensive washing after incubation with the immunogen. Secondly, use of a mouse Ig specific secondary antibody confirms that such substance is indeed mouse immunoglobulin. This secondary antibody used was a Fab specific anti-mouse Ig to avoid potential cross-reactivity to the human Fc portion of the LAG-3:Fc fusion protein. This screening step has the advantage of being high-throughput.

Due to the LAG-3:Fc fusion protein containing a human Fc domain, one must consider the impact this portion will have on the generated mouse B cell response, as human and mouse Fc portions of immunoglobulins are also heterologous. As a result, a second screening procedure, which selected for antibodies generated against the LAG-3 portion of LAG-3:Fc was required. As production of unfused LAG-3 protein has proven to be challenging, an alternative non-protein based method of selection was required. Here, anti-sera or culture supernatant were screened for their ability to stain LAG-3 expressing cells via flow cytometry using the lentivirally transduced LAG-3$^+$ C8 Jurkat cell line developed as described in Chapter 4. This assay is much lower-throughput; hence this step was not used as the primary screening step.

As a result, this two stage screening process validated mouse antibody responses which could bind LAG-3 as both soluble protein and as a cell surface bound antigen. Additionally, antibodies raised against LAG-3:Fc may be dependent on post-translational carbohydrates added by the non-human cell line in which the LAG-3:Fc was produced – Chinese hamster ovary (CHO) cells. As a result, screening of binding to LAG-3 surface expressed on the human derived Jurkat cell line provides a better selection model of specificity for *in vivo* human LAG-3 glycoprotein.

5.3   Generation of monoclonal anti-human LAG-3 antibodies

Through the subcutaneous injection of mice, in the presence of adjuvant, immunised mice generated a robust peripheral antibody response to heterologous LAG-3. Such responses were experimentally quantified in the sera of immunised mice through reactivity to LAG-3:Fc, as shown by direct ELISA and, secondly, through specific binding by flow cytometry to LAG-3$^+$ cells. Immunised mouse B cells were extracted by splenectomy and fused with a myeloma derived cell line to form a library of polyclonal immortalised B cells. Anti-LAG-3 specific hybridomas were present within the repertoire of B cell fusion products and were subsequently cloned to form a panel of monoclonal anti-LAG-3 expressing hybridomas. Subsequent hybridoma clones were high-density cultured and produced antibodies harvested and purified for consequent characterisation. The immunisation of mice and production of initial hybridomas was performed by and in collaboration with Professor Paul Morgan (Cardiff University).

5.3.1   Anti-LAG-3 antibody responses in immunised mouse serum

During the immunisation schedule, at day 14 post initial treatment, all mice were screened for the presence of secreted anti-LAG-3 specific immunoglobulins in the serum of circulating peripheral blood via direct ELISA. The mouse sera with highest ELISA reactivity was screened for the ability to stain cellular expressed human LAG-3 protein through flow cytometric staining of JRT LAG-3$^+$ C8 cells, developed as described in Chapter 4, when secondary-stained with a FITC conjugated anti-mouse Ig antibody (*Figure 5.1*). Background staining by both control sera and immunised sera was observed when staining LAG-3$^-$ JRT WT cells compared to secondary only control and clarifying a background sera fluorescence intensity shift (*Figure 5.1a*). Furthermore, immunised sera showed no significant fluorescence intensity increase compared to control sera.

In JRT LAG-3$^+$ C8 cells, immunised mouse serum was able to stain the LAG-3 expressing cells as indicated by a fluorescence intensity shift compared to control sera (*Figure 5.1b*). This staining capacity was compared to the FITC-conjugated anti-LAG-3 clone 17B4 which binds JRT LAG-3$^+$ C8 but not JRT WT cells.
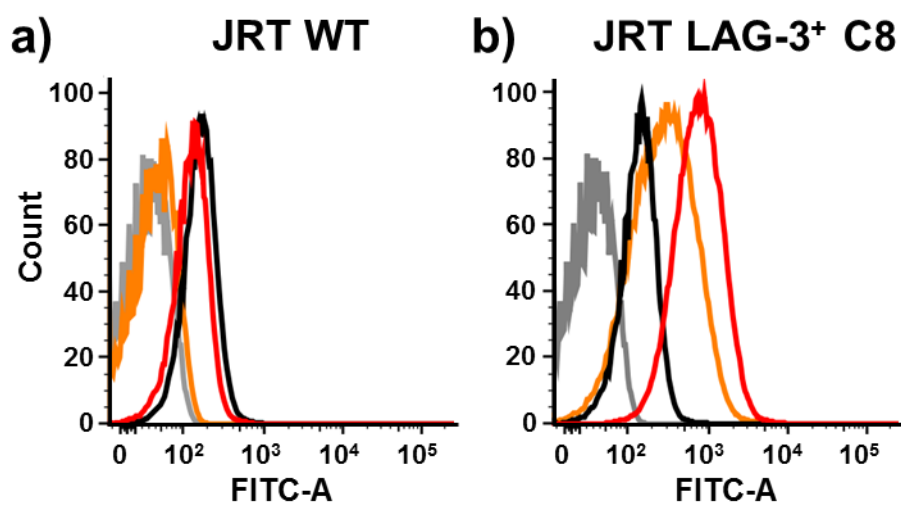
Figure 5.1 – LAG-3 dependent staining capacity of immunised mouse anti-sera:

a) Fluorescence histograms from flow cytometry analysis of anti-sera from LAG-3:Fc immunised mice (red) and control mouse (black) exhibiting no significant binding to LAG-3⁻ JRT WT cells detected using FITC-conjugated anti-mouse secondary staining. Both control and immunised anti-sera show significant background staining compared to FMO plus secondary only control (dark grey) and commercial anti-LAG-3 clone 17B4 (orange).

b) Flow cytometric analysis of LAG-3:Fc immunised mouse anti-sera (red) binding to JRT LAG-3⁺ C8 cells detected using FITC-conjugated anti-mouse secondary staining as demonstrated by a shift in fluorescence intensity compared to control mouse anti-sera (black) and FMO plus secondary only control (dark grey). LAG-3:Fc immunised mouse anti-sera exhibited enhanced staining compared to the commercial anti-LAG-3 clone 17B4 (orange).

5.3.2 Cloning of α-LAG-3 specific B cell hybridomas clones

Having established anti-LAG-3 specific antibody responses within the serum of an immunised mouse, the mouse was sacrificed, spleen removed, splenocytes harvested and fused to an immortalised B cell line to form a polyclonal library of B cell hybridomas. This polyclonal library was cloned by serial dilution and individual culture wells were screened for LAG-3 reactivity by ELISA and flow cytometry as described previously. In the first round of cloning, 960 culture well supernatants were screened by direct ELISA using LAG-3:Fc as the adsorbed antigen. ELISA positive wells were observed and defined as a significant increase in colorimetric output compared to an irrelevant adsorbed antigen.

Of the ELISA positive wells, ten culture supernatants were selected for screening for reactivity to LAG-3 via flow cytometry. These wells were selected from an array of ELISA positive wells due to (i) the highest colorimetric output (ii) the degree of dilution factor, with preferences for wells subject to more dilution and (iii) wells which derived from distinct starting populations i.e. wells from different cloning plates. These criteria were used in order to increase the probability of selecting high affinity antibodies, of monoclonality or low polyclonality and of distinct clonotypes. Of the ten ELISA positive cultures screened, seven cultures were LAG-3 positive, as defined by a significant increase in gMFI in JRT LAG-3$^+$ C8 but not JRT WT cells. The seven candidate clones were subjected to three further rounds of limiting dilution cloning to ensure single cell clonality. During this process, one clone, 6D3, lost expression of anti-LAG-3 specific antibodies. This left a final candidate antibody panel consisting of six monoclonal hybridomas termed 1B5, 6F7, 6D6, 4C10, 10C8 and 4B1 which all expressed LAG-3 specific antibodies within their culture supernatants (*Figure 5.2*).

5.3.3 Production of anti-human LAG-3 specific antibodies

Having successfully cloned six anti-LAG-3 antibody expressing hybridomas and confirmed their clonality (described in section 5.5), all six hybridoma clones were taken forward for large scale antibody production and purification for downstream experiments. These experiments, such as biophysical, cellular and *in vitro* characterisation assays require purified antibody of known concentration, as opposed to the crude culture supernatants used in screening selection. Through high-density culture in bovine Ig depleted serum, milligram quantities of antibody were purified using affinity chromatography of varying yields ranging from 5.5 – 75.4 mg (*Appendix 6*). The resulting purified mAb preparation was of high purity, demonstrated by SDS-PAGE analysis, and showed molecular mass separation indicative of immunoglobulin (Ig): a single ~150 kDa band in non-reduced conditions and two bands, ~50 kDa and ~25 kDa, in reduced conditions representing Ig heavy and light chains, respectively (*Figure 5.3*).
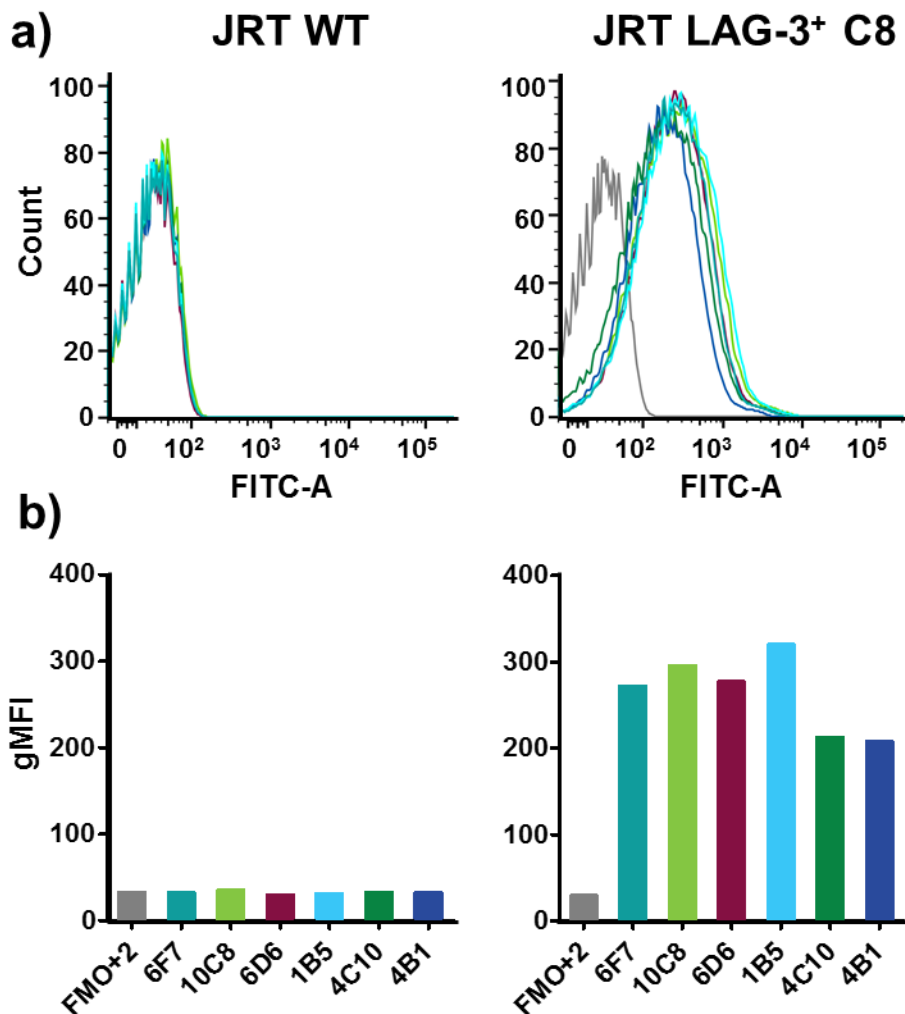
Figure 5.2 –LAG-3 specific antibody responses in screened hybridoma supernatants:

a) Fluorescence histograms from flow cytometry analysis showing LAG-3 specific binding of generated mouse hybridoma supernatants to JRT LAG-3$^+$ C8 cells (right) and not JRT LAG-3$^-$ WT cells (left), detected using FITC-conjugated anti-mouse secondary antibody staining. Each monoclonal hybridoma culture supernatant is coloured as in *b)*, background FMO plus secondary antibody (grey).

b) Raw geometric mean fluorescence intensity (gMFI) values generated from flow cytometry data shown in *a)* demonstrating specific binding of all hybridoma culture supernatants to JRT LAG-3$^+$ C8 cells (right) with significant staining above background FMO plus secondary control (FMO+2). Staining in JRT LAG-3$^-$ WT cells (left) is equivalent to background.
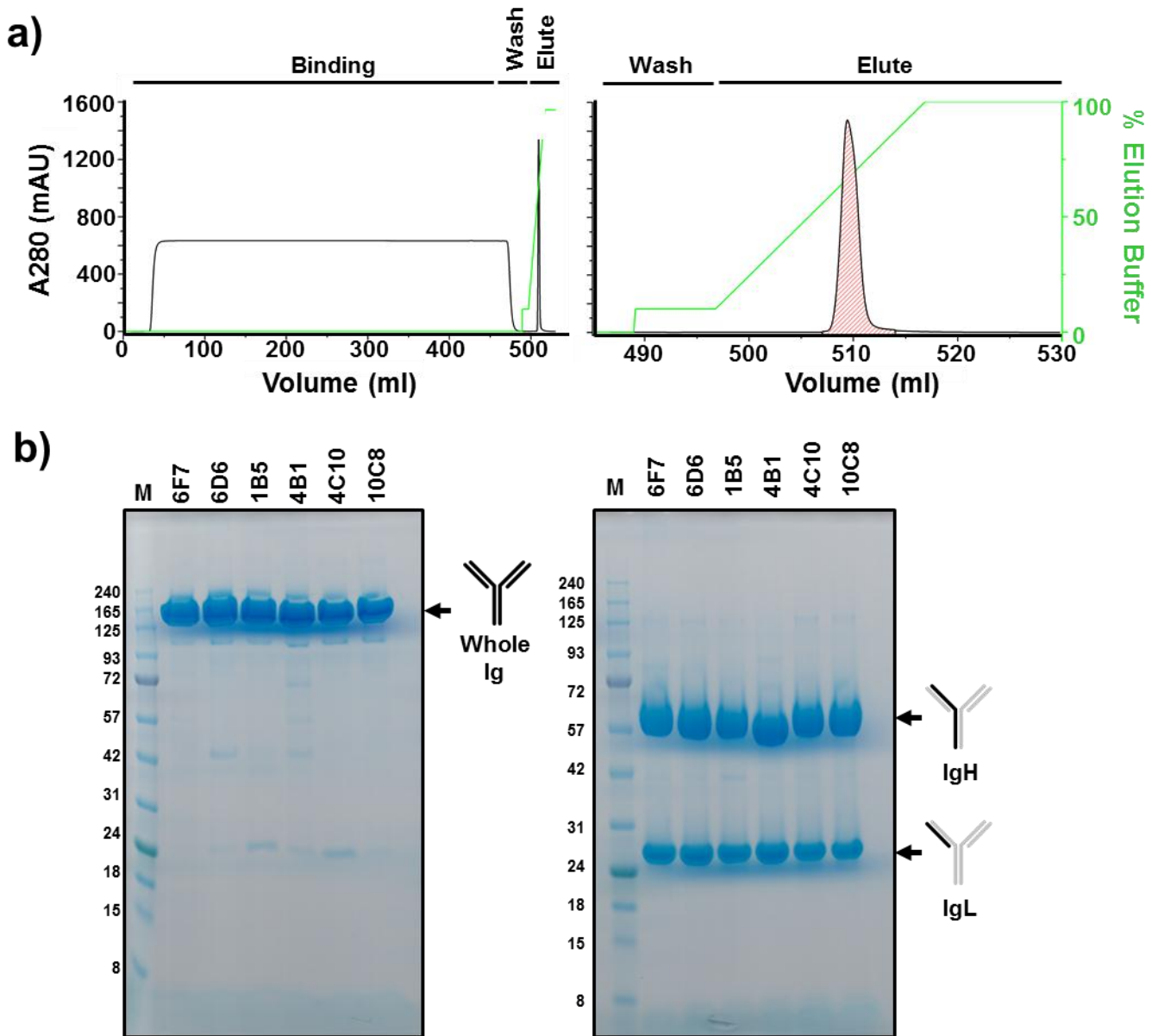
Figure 5.3 – Generation of high purity anti-LAG-3 monoclonal antibody samples:

a) Example affinity chromatography purification of mouse mAbs from monoclonal hybridoma culture supernatants. Absorbance at 280nm (A280) FPLC trace of binding, wash and elute phases of purification (left) shows separation of non-specific proteins during binding and wash phase and elution of mAb during elute phase. Enlargement of the elute phase trace (right) high-lights single-peak protein species within affinity column bound eluents.

b) SDS-PAGE analysis showing protein purity after affinity and size exclusion chromatography purification of the six candidate mAbs highlighting in-tact whole Ig in non-reducing conditions (left) and individual heavy (IgH) and light (IgL) chains in reducing conditions (right).

5.4 Sequence characterisation of generated anti-LAG-3 monoclonal antibodies

Having established and produced a panel of six candidate anti-LAG-3 antibodies, each mAb clone was characterised in terms of their genetic and protein sequence. This process was followed for a number of reasons. Firstly, knowledge of antibody protein sequences allows the production of the antibodies recombinately in alternative cell lines or expression systems should (i) a hybridoma stop expressing and secreting antibody or (ii) the antibodies are required to be reformatted i.e. chimerisation or humanisation. Secondly, knowledge of the protein sequence, particularly that of the complementarity determining regions (CDRs) is required for patent application to demonstrate the novelty of the intellectual property. Thirdly, analysis of each sequence with respect to each other gives an indication of the diversity of the candidate antibody panel with respect to the epitopes of LAG-3 each antibody binds to.

As cloning of each mAb was performed at the cellular stage, each mAb can be defined at the protein level by inference to the corresponding B cell hybridoma cells mRNA sequences of the translated clonal antibodies. As a result, each candidate antibody was sequenced from RNA in order to obtain the variable domain sequence of each antibody and isotyped to determine the constant domain sequence usage of each antibody. From this information, one can determine the full protein sequence of each generated anti-LAG-3 antibody.

5.4.1 Candidate LAG-3 antibodies have narrow isotypes

Antibodies *in vivo* are able to mediate a diverse range of functions through the usage of different antibody classes. As a result, the isotype of a raised anti-LAG-3 antibody would influence its functional ability in future studies, when used in their current form i.e. without isotype switching. Experimentally, antibody isotype influences the affinity of antibody for Fc binding agents such as Protein A and Protein G which are often used in purification or in the immobilisation of antibodies in a favourable orientation for antigen binding. Moreover, knowledge of the antibody isotype is a pre-requisite in the determination of variable chain usage and clonotype in the process of antibody sequence determination. To this end, the isotype of each antibody was determined.

Antibody isotype was firstly assayed at the protein level through the use of isotype immunoassay shift sticks by testing soluble antibody within culture supernatants (*Appendix 7*). This isotype was then used in the selection of sequencing primers for the determination of each heavy and light variable chain V_H and V_L, respectively. The success of this experimental procedure,

therefore, confirmed and consolidated the isotyping initially shown through immunoassay shift sticks (*Table 5.2*).

The six candidate antibodies consisted of two different isotypes as defined by their constant heavy (C_H) gene usage: five antibodies (1B5, 6D6, 6F7, 10C8 & 4C10) were all IgG2b isotype and one antibody (4B1) of IgG2a isotype. All candidate antibodies had kappa constant light chain usage (C_L). This moderate diversity in isotype suggested either a diversity in generated clonotypes against the LAG-3:Fc immunogen, or alternatively, a single isotype shifting event as a result of the maturing B cell response by the immunised mouse across the boosted immunisation schedule.

Both forms of IgG2 used by the generated antibodies have favourable affinities for the activating Fc receptor (FcR) found on mouse macrophages and natural killer cell (NK) cells, FcγRIII (CD16) (Bruhns et al. 2012). Binding of antibodies by NK cells via their Fc domain signals the lysis of antibody coated target cells through the antibody-dependent cellular cytotoxicity (ADCC) capabilities of NK cells. These antibodies, in the current protein formulation, therefore provide a useful reagent in studying the capacity of each antibody to perform mouse NK cell ADCC *in vitro*. Likewise, IgG2a and IgG2b isotypes have favourable affinities for the antibody binding protein C1q and could therefore be theoretically capable of triggering classical complement pathway activation. C1q complex formation can consequently promote complement dependent cytotoxicity (CDC), making these antibodies in their current formulation of favourable isotype for the capacity of CDC using mouse serum proteins *in vitro* (Neuberger & Rajewsky 1981).

5.4.2 LAG-3 antibodies are highly related clones

Having determined the isotype of each mAb, each hybridoma clone had their antibody variable chains (V_H and V_L) sequenced. Due to the highly variable nature of a V_H and V_L RNA sequence, performing PCR amplification of Ig sequences, sufficient for sequencing from a cDNA library, is not trivial and requires a library of degenerate primers. As a result, each hybridoma was sequenced commercially from frozen cell samples (Absolute Antibody, UK).

The resulting data yielded the full length V_H and V_L DNA sequences for each of the six candidate hybridoma clones as well as the heavy and light chain signal sequences for five (6F7, 4B1, 10C8, 6D6, 1B5) of the six hybridoma clones. The sixth clone, 4C10, proved to be difficult to sequence likely due to low levels of V_H and V_L mRNA transcript obtained during RNA extraction. This observation correlated with the low protein yield obtained during large scale expression and purification of each mAb described previously (section 5.3.3). A full length sequence for the V_H and V_L of 4C10, however, was still obtained. The ability to determine a reliable Sanger sequencing chromatogram for each of the six candidate mAbs confirmed their clonality and therefore confirmed purified antibody samples contain a single mouse anti-LAG-3 antibody sequence. In addition, each antibody was confirmed to contain functional Ig recombination events based on its sequence, which is expected since antibodies were screened and selected for based on functionality.

Sequence analysis of six candidate V_H and V_L sequences identify each mAb as being unique but highly related clones. This low sequence variability, particularly across the Ig framework region, is caused by the usage of the same IGH and IGL gene segments during antibody rearrangement. Each V_H sequence had the same V, D & J-segment usage, V1-19*01, D2-3*01 and J2*01 respectively, according to sequence alignment to the IMGT/V-QUEST reference directory sequences for mouse immunoglobulins (*Table 5.2*). Likewise V_L sequences were assigned to use identical V & J-genes, V19-93*01 and J2*01 (Lefranc 2008).

For both V_H and V_L sequences, the query antibody sequences did not contain complete identity to the reference directory sequences, ranging from 89.36 % to 100 % sequence identity. This indicates mutations incorporated into the V_H and V_L sequences outside of the hypermutated CDRs. This is commonly found in hybridoma cultures where mutations occur due to genomic instability within the first 1-2 weeks after fusion and stabilise over culture time and rounds of single cell cloning (Maynard & Georgiou 2000). These mutations, although outside of the antigen binding site, can also influence antigen binding affinity and can result during the process of affinity maturation (Wedemayer et al. 1997).

These mutational differences can be visualised through analysis of the Shannon positional entropy across the length of the six V_H and V_L sequences (*Figure 5.4a*). Despite these mutations occurring throughout the sequence, all six antibodies show no variability, $H(x) = 0$, across the conserved residues Cys23, Trp41, Met89, Cys104 & Trp118. Mutations in these residues, away from those that are allowed, would result in a non-functional Ig sequence and would, therefore, be selected against during screening.

5.4.3 LAG-3 antibodies contain highly related but unique paratopes

Like the framework regions, all six generated candidate clones exhibit different, but related, CDR loop sequences as assigned by the IMGT/V-QUEST reference sequence alignment tool (*Table 5.2*). As the CDR loops, in combination, make up the sequence specificity of the antigen binding site, the fact that all sequences have highly related CDR loops suggests that each antibody binds to a similar, or the same, epitope.

Despite similarities of CDR usage between each mAb, subtle differences between each antibody are present across the CDR loop regions (*Figure 5.4a*). This diversity is not consistent throughout the different CDR loops i.e. each loop does not contain an equal range of diversity. Similarly, certain CDR loop positions exhibit a greater degree of diversity, such as V_L CDR3 residue 5 which has three possible amino acids across the mAb panel and is the single contributor to diversity across this CDR loop compared to V_L CDR2 which exhibits no diversity across the dataset (*Figure 5.4b*).

By analysing each CDR loop as a fixed string of amino acids, one can assign usage similarity of each individual CDR string by each mAb clone (*Figure 5.4c*). For example, 1B5, 6F7, 6D6 & 4C10 all used a common V_L CDR3 sequence string, whereas 10C8 and 6F7 used a unique sequence string each resulting in three possible V_L CDR3 sequence strings. In contrast, as previously stated, all V_L CDR2 sequences were identical across all mAb clones, thus, resulting in one single possible sequence string. The greatest whole CDR sequence string diversity within the mAb candidate clones was exhibited by V_H CDR3 which incorporated four different possible sequence strings. This variation aligns with knowledge of V_H CDR3 diversity which, due to D-segment incorporation during immunoglobulin rearrangement, is the most variable CDR loop in immunoglobulins (Jung et al. 2006).

Despite similarities in CDR usage, no two candidate mAbs had identical amino acid sequences across the length of the variable domain (V_H & V_L) or, more relevantly, the full paratope (V_H CDR1, 2 & 3, V_L CDR1, 2 & 3) as shown by no common identical sequence string usage (*Figure 5.4d*). Moreover, analysis of the phylogeny of each protein sequence, either entire V_H V_L or the full paratope, ($V_H V_L$ CDRs) revealed the common ancestry of each antibody sequence

(*Figure 5.4e*). Here, each antibody can be compared, either at the full length or paratope level, to one another in terms of their overall sequence similarity.

Together, these data summarise the similarities between each of the generated anti-LAG-3 mAb clones in terms of their protein sequence and the antigen binding sites encoded within them. As each mAb clone had a unique but highly related antigen binding site sequence, one can hypothesise that each mAb will bind to the same or similar epitope. Due to subtle differences being present, however, one can also hypothesise that each mAb may bind to the epitope with varying binding affinity and thus potentially varying functionality. By correlating sequence usage with later functional characterisation, it may be possible to attribute sequence specific explanation for observed functional capacity.

mAb	Chain	Type	V-Gene	% Identity	J-Gene	% Identity	D-Gene	CDR1	CDR2	CDR3
1B5	H	IgG2b	V1-19*01	93.06	J2*01	89.36	D2-3*01	GYRITDFY	INPYNGDT	CARDDGNYVRFDYW
	L	κ	V19-93*01	95.34	J2*01	97.30		QDIKRF	YTST	CLQYDNLYTF
4B1	H	IgG2a	V1-19*01	95.49	J2*01	87.50	D2-3*01	GFRITDYY	INPYNGDT	CTRDDGNYVRFDYW
	L	κ	V19-93*01	97.49	J2*01	97.30		QDINKF	YTST	CLQYVNLYTF
6D6	H	IgG2b	V1-19*01	96.18	J2*01	89.36	D2-3*01	GYTITDYY	INPYNGVT	CARDDGNYVRFDYW
	L	κ	V19-93*01	98.93	J2*01	100		QDINKF	YTST	CLQYDNLYTF
6F7	H	IgG2b	V1-19*01	96.18	J2*01	89.36	D2-3*01	GYRITDFY	INPYNGDT	CARDDGNYIRFDYW
	L	κ	V19-93*01	98.92	J2*01	94.59		QDIKKF	YTST	CLQYDNLYTF
10C8	H	IgG2b	V1-19*01	97.92	J2*01	89.36	D2-3*01	GYTITDYY	INPYNGVT	CARDDGNYVRFDYW
	L	κ	V19-93*01	97.85	J2*01	100		QDINKF	YTST	CLQYFNLYTF
4C10	H	IgG2b	V1-19*01	97.57	J2*01	89.36	D2-3*01	GYTITDYY	INPYNGDT	CARDDGNYVRFDYW
	L	κ	V19-93*01	97.85	J2*01	100		QDINKF	YTST	CLQYDNLYTF

Table 5.2 – Sequence characterisation of α-LAG-3 antibodies aligned to IMGT reference database

a)

V_H

CDR1 CDR2 CDR3

V_L

CDR1 CDR2 CDR3

b)

c)

V_H CDR1 V_H CDR2 V_H CDR3 V_L CDR1 V_L CDR2 V_L CDR3

d)

V_H V_L V_H V_L CDRs

e)

V_H V_L V_H V_L CDRs
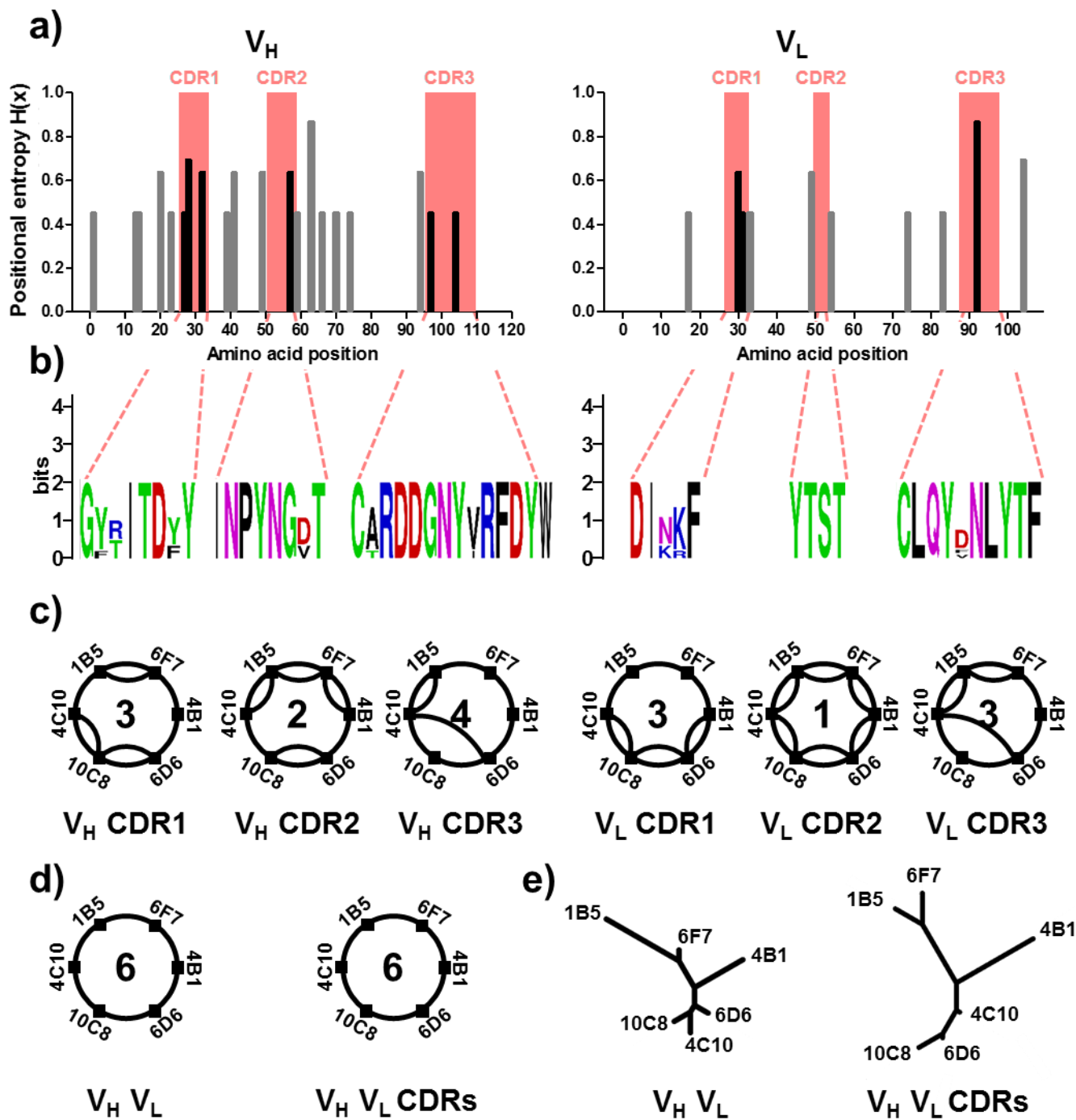
(Figure legend overleaf)

Figure 5.4 –Bioinformatic analysis of aligned anti-LAG-3 mAb amino acid sequences:

a) Shannon positional entropy plots highlighting entropy (variation) in V_H and V_L sequences by the six candidate mAb clones. Sequence differences, quantified by higher entropy, are found within (black bars) and outside (grey bars) the CDR loop regions (red).

b) Sequence logo plots of amino acid usage and variation within the CDR loops of the six candidate mAb clones coloured by amino acid properties: polar (green) basic (blue) acidic (red) hydrophobic (black).

c) Circular relationship graphs highlighting identical sequence string usage at each CDR loop by the six candidate mAb clones. Connected nodes represent clones with identical sequence usage for the given CDR loop. Inset numbers show the number of unique sequence strings within the dataset for the given CDR loop.

d) Circular relationship graphs, as in *c)*, highlighting the uniqueness (no connected nodes) of each candidate mAb clone at both the full length variable region ($V_H V_L$) and the full paratope ($V_H V_L$ CDRs).

e) Unrooted neighbour joining phylogenetic tree for both the full length variable region ($V_H V_L$) and the full paratope ($V_H V_L$ CDRs) highlighting sequence relationships between mAb clones.

5.5 Functional binding characterisation of anti-LAG-3 antibodies

Having determined that the panel of anti-LAG-3 monoclonal antibodies have unique antigen binding sites, each antibody was characterised for its ability to bind to LAG-3 in a cellular and *in vitro* protein context. As the primary aim of generating these anti-LAG-3 antibodies is to bind human LAG-3 expressed *in vivo* on LAG-3$^+$ T cells in order to induce the functional depletion of those cells, generated antibodies must be able to (i) bind to LAG-3 protein on the surface of cells (ii) discriminate LAG-3 from other human proteins i.e. maintain specificity. Thus, the candidate antibody panel was screened to establish which antibody, or antibodies, best satisfied these criteria. This characterisation would lead to rational preference for an antibody, or antibodies, to be used in downstream effector functional characterisation experiments.

As a result, purified antibody samples were firstly assayed for their capacity to stain LAG-3$^+$ cells and not cross-react with CD4$^+$ cells by flow cytometry. Secondly, antibodies were tested for the ability to detect LAG-3 protein by Western blot.

5.5.1 Mouse monoclonal antibodies specifically bind LAG-3$^+$ cells

In order to confirm that purified antibody samples bound LAG-3 expressing cells, and to assay the staining capacity of each generated anti-LAG-3 antibody within the candidate panel, each antibody was characterised by their ability to bind a LAG-3 expressing cell line by flow cytometry at varying concentrations. The JRT LAG-3$^+$ C8 lentivirally transduced cells, described previously, were once again used as a LAG-3 expressing cell model. Purified antibody samples were used as primary antibody stains at a concentration series from 2 µg/mL to 3.2 ng/mL by serial dilution. Staining capacity was detected through a fixed concentration of secondary antibody (2 µg/mL) and performed on fixed cell numbers (0.1 x10^6 cells).

As shown using hybridoma culture supernatants, all generated mAb bound LAG-3$^+$ cells where each mAb exhibited concentration-dependent binding to LAG-3$^+$ cells as indicated by increasing fluorescence intensity shifts at increasing mAb concentration (*Appendix 8a*). Each mAb showed similar binding capacity, with no obvious differences in fluorescent staining. Each antibody exhibited sigmoidal log(dose) response when background subtracted geometric mean intensity (gMFI) values were taken as response values (*Appendix 8b*). Identical experiments were also performed using the commercially available 17B4 anti-LAG-3 antibody (*Appendix 8c&d*).

Alignment of the log(dose) response of each antibody show that each of the generated clones exhibit similar dose responses (*Figure 5.5a*). Despite similarities, subtle differences in staining capacity were observed. Three antibodies, 6F7, 10C8 and 1B5 exhibited enhanced staining at 0.4 µg/mL which is in the range of a typical starting point concentration used for flow cytometric

analysis. All generated antibodies, however, performed very similarly at low concentrations (0.016 µg/mL) and, thus, no single antibody had significant performance advantage at low concentration.

By stratifying each mAb by the gMFI observed at the highest concentration, it was demonstrated that one clone, 6F7, exhibited enhanced staining compared to the mAb panel as well as the commercial clone 17B4 (*Figure 5.5b&c*). In addition, all antibodies exhibited an enhanced staining capacity compared to 17B4 at this concentration. These data suggest that the antibody panel presents comparable experimental functionality compared to the 17B4 commercial antibody, which is typically used throughout the literature to quantify the expression of human LAG-3 expressing cells by flow cytometry (Baixeras et al. 1992; Tian et al. 2015).
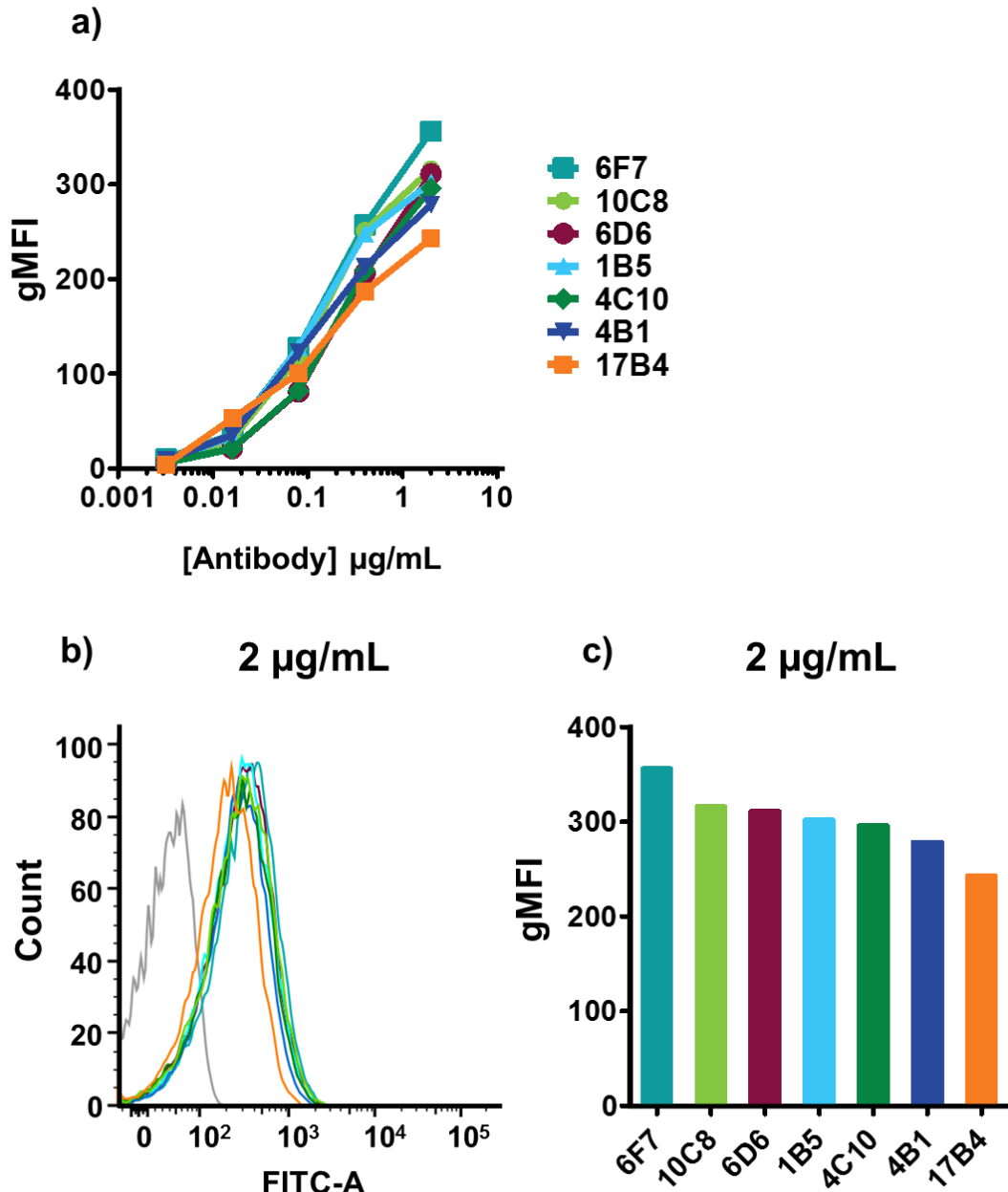
Figure 5.5 – Comparative analysis of anti-LAG-3 antibody binding to LAG-3^{+} cells:

a) Combined background subtracted geometric mean fluorescence intensity (gMFI) response values as a function of $\log_{10}$ antibody concentration for each of the six candidate and commercial (17B4) anti-LAG-3 mAbs. Log(dose) response curves show similar binding capacity of generated candidate mAbs and enhanced staining capacity compared to 17B4 at higher, experimentally relevant, concentrations.

b) Fluorescence histograms from flow cytometry analysis of each anti-LAG-3 mAb clone (coloured as in *a)* and *c)*)at 2 µg/mL binding JRT LAG-3+ C8 cells detected by secondary staining with FITC-conjugated anti-mouse secondary antibody staining.

c) Background subtracted geometric mean fluorescence intensity (gMFI) values at 2 µg/mL (calculated from data shown in *b)*) stratified by decreasing response. All generated mAb clones exhibit enhanced staining capacity compared to the 17B4 commercial anti-LAG-3 antibody with 6F7 generating the largest response.

5.5.2 Mouse monoclonal antibodies demonstrate no cross reactivity to CD4 expressing cells

As the immunogen used to generate the anti-LAG-3 specific responses in mice was a whole protein, the probability of generating antibodies with off target affects is greater than that of a short peptide-KLH conjugated immunogen approach (Hancock & OReilly 2005). Whilst generated antibodies demonstrated no significant background binding to LAG-3⁻ JRT WT cells, this cell line does not express CD4 protein at the cell surface (as described in Chapter 4). CD4 is predicted to have a highly related protein structure to LAG-3, despite its low sequence homology (Baixeras et al. 1992). As a result, the epitope(s) of the generated anti-LAG-3 mAbs may have commonality in CD4 and could, thus, exhibit cross-reactivity.

In order to assess any potential cross-reactive binding, the MOLT-3 T lymphoblast cell line was stained with the candidate mAb panel and analysed by flow cytometry. MOLT-3 cells have been shown to be LAG-3⁻ by flow cytometry using the 17B4 anti-LAG-3 mAb clone (Chapter 4), as this clone was raised against the unique D1 loop region not found in CD4 (Baixeras et al. 1992). Likewise, MOLT-3 cells have also been shown to express CD4 (Chapter 4). Consequently, the six candidate anti-LAG-3 antibodies were used to stain MOLT-3 cells to which no binding was observed (*Figure 5.6a*). LAG-3 staining by the candidate antibodies resulted in no significant shift in fluorescence intensity or gMFI compared to controls or MOLT-3 staining by the 17B4 clone. In addition, pre-incubation of MOLT-3 cells with the 1B5 mAb clone made no impact on consequent CD4 staining which is also replicated by 17B4 (*Figure 5.6b*). Together, these data show that the generated anti-LAG-3 antibodies show no ability to bind cell surface expressed CD4⁺ by flow cytometry and that the generated antibodies do not compete with a CD4 specific antibody staining of CD4⁺ cells.
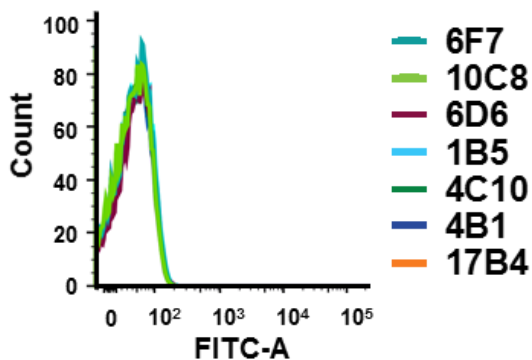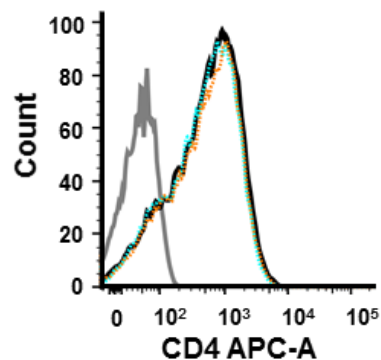
Figure 5.6 – Anti-LAG-3 mAbs show no cross-reactive binding to LAG-3$^-$ CD4$^+$ cells:

a) Fluorescence histograms from flow cytometry analysis of each anti-LAG-3 mAb clone (coloured as indicated) on LAG-3$^-$ CD4$^+$ MOLT-3 cells detected by secondary staining with FITC-conjugated anti-mouse antibody. All mAb clones show no significant binding to LAG-3$^-$ CD4$^+$ MOLT-3 compared to FMO + secondary control (grey).

b) Fluorescence histograms from flow cytometry analysis of CD4 staining on LAG-3$^-$ CD4$^+$ MOLT-3 cells pre-stained with buffer control (black; solid) or anti-LAG-3 antibody clone 1B5 (cyan; dashed) or 17B4 (orange; dashed). Pre-staining with LAG-3 antibodies showed no abrogation of CD4 staining observed compared to FMO control (grey).

5.5.3 Mouse monoclonal antibodies specifically bind LAG-3 by Western blot

Having established that the LAG-3 antibodies bind LAG-3 expressing cells, each antibody was tested for the ability to bind full length LAG-3 protein from cell lysates. Analysis of binding by Western blotting reveals the molecular weight of the antigen and can thus be used to confirm binding antigen is of a molecular mass known for that antigen. In addition, detection of antigen via Western blot is a strong indicator that the antigen epitope is a linear epitope as tertiary protein fold is not maintained during SDS-PAGE separation. Moreover, Western blotting provides a sensitive method for detecting low levels of protein analyte or, alternatively, lower affinity and less specific interactions. Whilst these low specificity interactions typically manifest themselves as unwanted background, Western blots can also give an indication of cross-reactivity and consequently an antibodies ability to discriminate towards the desired antigen.

Given this, each of the six mAbs were assayed for binding to JRT LAG-3$^+$ C8, LAG-3$^-$ JRT WT and LAG-3$^-$ CD4$^+$ MOLT3 cell lysates (*Figure 5.7*). Each antibody bound a single band, with varying intensity, at approximately 72 kDa in size in LAG-3 expressing JRT LAG-3$^+$ C8 cells only. Despite a theoretical molecular mass of 54 kDa as defined by the protein component of LAG-3, Western blot analysis using anti-human and anti-mouse LAG-3 antibodies have identified full length LAG-3 at ~72 kDa attributed to the extensive carbohydrate post-translational modifications (Baixeras et al. 1992; Li et al. 2004). This size band was also observed using the 17B4 and 13E2 mAb clones as a primary probe. By normalising protein mass loaded, secondary antibody conditions and blot exposure between mAb probe antibodies, each antibody can be compared for ability to bind LAG-3 in a Western blot assay. 4B1 and 1B5 clone antibodies produced the largest signal, however, some background detection due to potential LAG-3 degradation or cleavage products was observed. The 6D6 clone demonstrated the most desirable detection qualities by distinguishing an intense single protein band.

Since previous flow cytometry experiments did not give an indication of molecular weight of their binding antigen, these previous experiments did not rule out the, albeit highly unlikely, chance that antibodies bound to rat CD2 protein inserted as a marker alongside LAG-3 as a marker of lentiviral transduction. Rat CD2, which was also present in JRT LAG-3$^+$ C8 but not JRT WT cells, is detected at a molecular weight of approximately 45 kDa and is thus distinguishable from LAG-3 via Western blot. These results clarify that the anti-LAG-3 antibodies detect a protein present in the LAG-3 expressing cell lysates of a molecular mass similar to that of previously documented full length LAG-3 glycoprotein and identical to that of commercial and independently generated anti-LAG-3 antibodies.

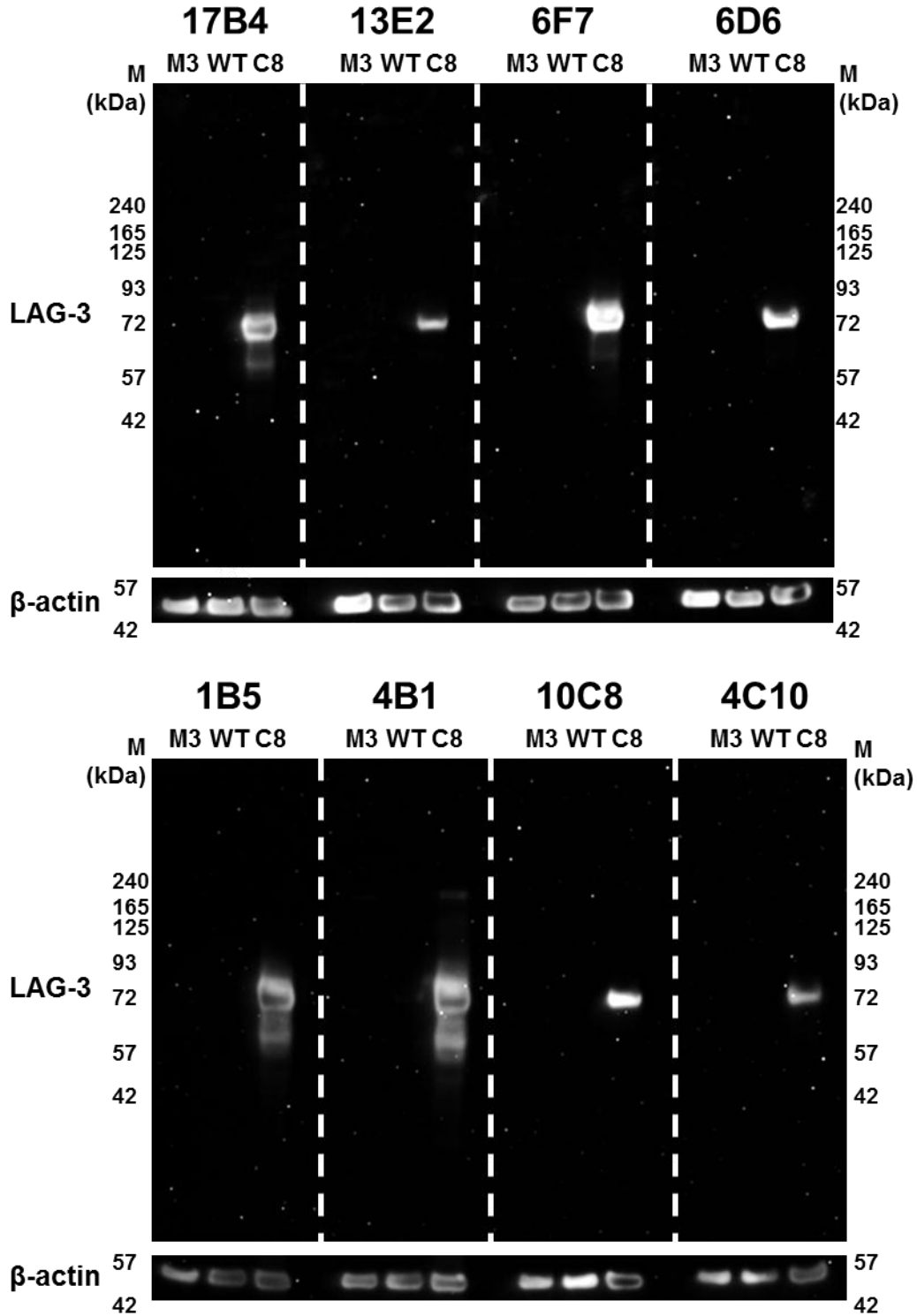***Figure 5.7 – Western blot characterisation of generated anti-LAG-3 antibodies:***

Detection of a single band protein at approximately 72 kDa in size present in JRT LAG-3$^+$ C8 cells (C8) and not LAG-3$^-$ JRT WT cells (WT) or LAG-3$^-$ CD4$^+$ MOLT3 cells (M3) by primary probing with the six indicated candidate mAb clones. Dashed white lines represent cuts made to incubate membrane with differing primary antibodies.

5.6 Generated antibodies bind LAG-3 antigen at high avidity

In order to further characterise each antibody and quantify an accurate measure of antibody to antigen binding, the six mAb candidate clones were assayed in terms of their binding avidity for their antigen. Whilst previous experiments have indicated varying capacities for binding LAG-3 in experimental systems, these assays do no accurately quantify binding strength for LAG-3 protein.

To fulfil the primary aim of generating anti-LAG-3 mAbs which bind human LAG-3 expressed *in vivo* on LAG-3$^+$ T cells in order to induce the functional depletion of those cells, the binding of generated antibodies must (i) occur with sufficient on rate such that dosage relevant concentrations effectively bind LAG-3 and (ii) bind LAG-3 long enough to facilitate functional depletion of those cells. Since one of the most important criteria for a good therapeutic agent is the strength or potency at which the agent can bind to its target, an accurate measurement of this potency could define the rationale for selection of that agent for further development.

5.6.1 LAG-3 mAbs bind LAG-3:Fc immunogen via a monogamous bivalent two-state binding reaction

Binding avidity/affinity measurements between the anti-LAG-3 mAb panel and LAG-3:Fc were determined via surface plasmon resonance (SPR) analysis of immobilised LAG-3:Fc. Binding of antibodies was measured by the individual single-injection of mAbs as analyte. Due to the bivalent nature of both LAG-3:Fc ligand and mAb analyte, SPR experiments were performed at low ligand densities in order to reduce mixed reaction kinetics.

All generated antibodies specifically bound LAG-3:Fc demonstrated by response unit binding curves observed in control surface subtracted sensograms (*Figure 5.8a*). The sensograms revealed binding kinetics typical of an antibody binding with bivalency, characterised by a slow association rate and orders of magnitude slower dissociation rate. The anti-LAG-3 mAbs demonstrated matching broad kinetics to that of the commercial 17B4 clone antibody (*Figure 5.8b*). This analysis suggests all antibodies tested exhibit binding strength within a similar range in agreement with observed cellular binding capacity shown by flow cytometry.

To quantify this binding strength and explain the valency of binding being observed, a number of single injection kinetic binding models were applied and fitted to the observed experimental data as shown in Chapter 4 (*Table 4.1*). Applied models were compared for quality of fit by visual observation of the curve fit quality, analysis of χ^2 values and residual plots. Simultaneous curve fit analysis determined that anti-LAG-3 antibody binding to LAG-3:Fc was best described by the two-state reaction model. As a result, the binding strength observed in these SPR experiments was the result of avidity effects.

Application of the two-state reaction model generated a good fit across all the generated mAbs (*Figure 5.8a*) as well as the commercial 17B4 clone (*Figure 5.8b*). This model, which can rationally be applied to the system being studied, is described by the following reaction equation, where two ligands (A & B) bind to form a complex (AB) which undergoes a second binding event to form a second state complex (ABx):

$$A \quad + \quad B \quad \underset{koff1}{\overset{kon1}{\rightleftharpoons}} \quad AB \quad \underset{koff2}{\overset{kon2}{\rightleftharpoons}} \quad ABx$$

(Eq. 5.1)
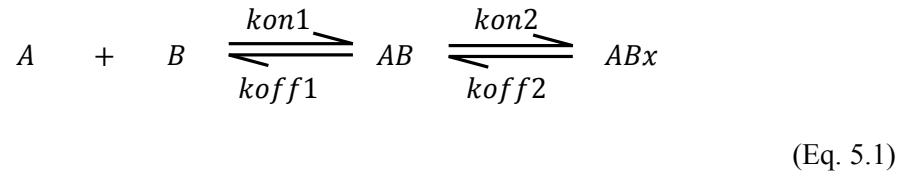
In the two-state reaction model, there are four kinetic constants (k_{on1}, k_{off1}, k_{on2} and k_{off2}), which describe the rates at which the two complex states (AB and ABx) of the reaction model form. These rate constants are described by the following rate equations:

$$\frac{dAB}{dt} = (kon1[A][B] - koff1[AB]) - (kon2[AB] - koff2[ABx])$$

(Eq. 5.2)

$$\frac{dABx}{dt} = kon2[AB] - koff2[ABx]$$

(Eq. 5.3)

Relation of this model to the system being studied, whereby bivalent mAbs are binding LAG-3:Fc, with independent but identical binding sites, allowed the formation of a monogamous bivalent mode of binding, visualised by the following schematic and equation. Here, Eq.5.1 has been modified to include terms of the antibody-antigen system being studied:

$$LAG3{:}Fc \quad + \quad mAb \quad \underset{koff1}{\overset{kon1}{\rightleftharpoons}} \quad LAG3Fc{:}mAb \quad \underset{koff2}{\overset{kon2}{\rightleftharpoons}} \quad LAG3Fc{:}mAbx$$

(Eq 5.4)
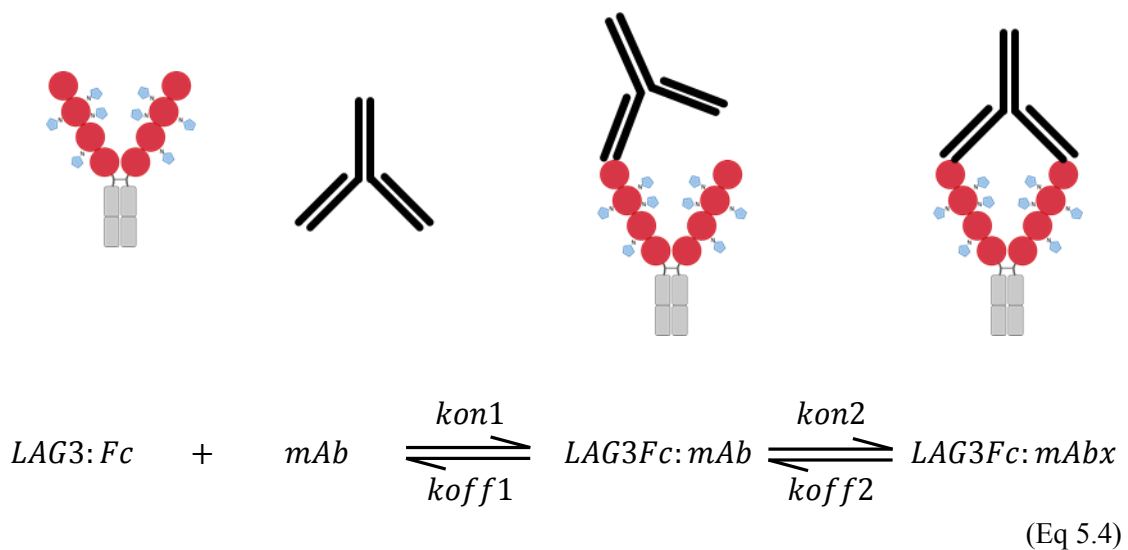
Having applied the two-state reaction model to the observed data, the four kinetic parameters which describe the rate of binding (k_{on1}, k_{off1}, k_{on2} and k_{off2}) were determined from the model

(*Table 5.3*). Whilst these kinetic parameters can, themselves, yield comparative information about the strength of each antibody-antigen interaction, the observed avidity or affinity is an accumulation of all of the four kinetic parameters. These kinetic parameters are, therefore, best used to form the basis for the mathematical determination of consequent anti-LAG-3 mAb equilibrium constant avidity measurements for LAG-3:Fc. The application of the two-state binding model with acceptable fit, however, strongly suggests a mode of binding measured as a result of monogamous bivalent binding as opposed to observed polygamous binding, which would favour a bivalent interaction kinetic model.

a)

1B5

$\chi^2 = 1.77$

4B1

$\chi^2 = 0.37$

10C8

$\chi^2 = 6.43$

4C10

$\chi^2 = 6.22$

6F7

$\chi^2 = 18.0$

6D6

$\chi^2 = 5.63$
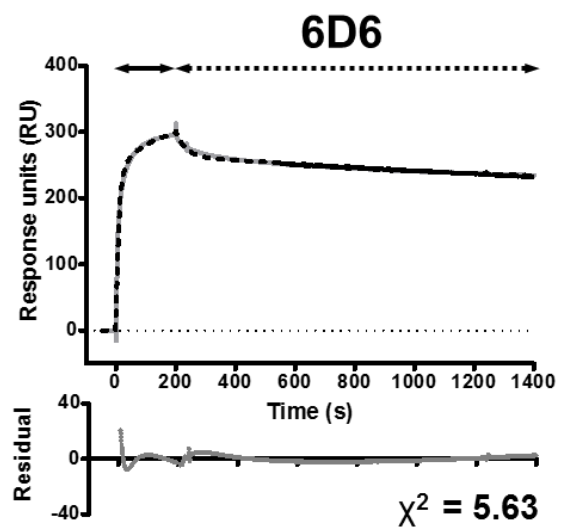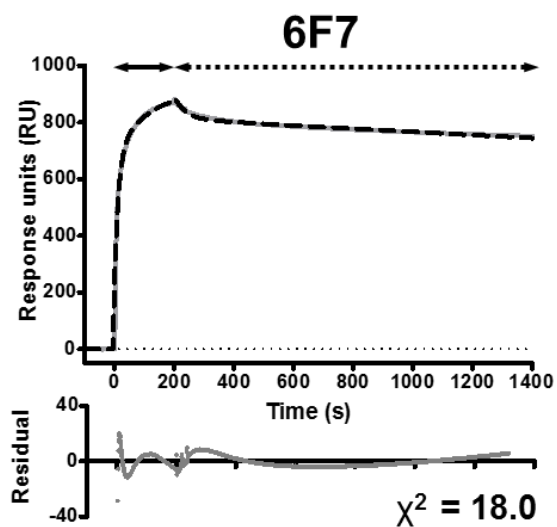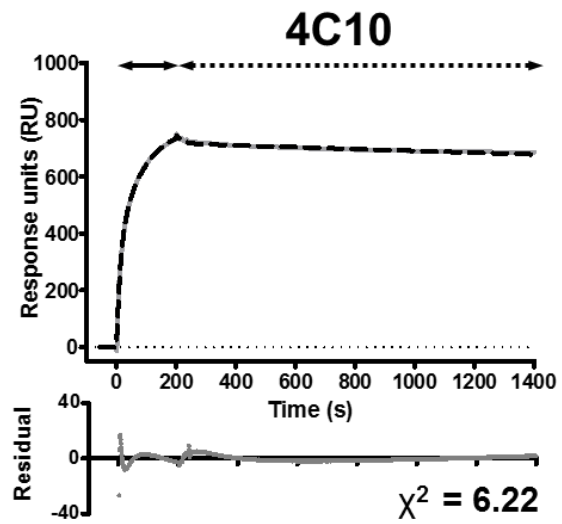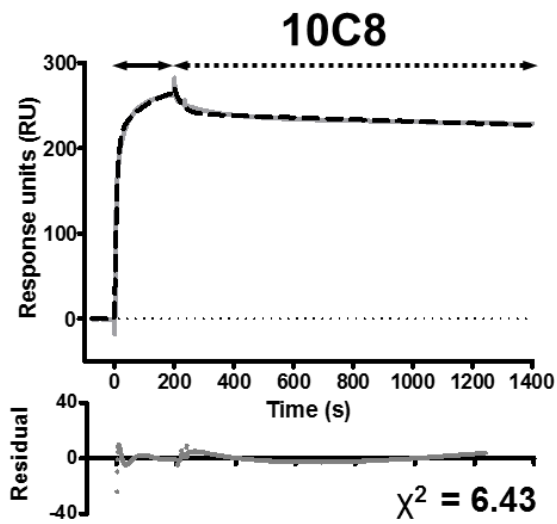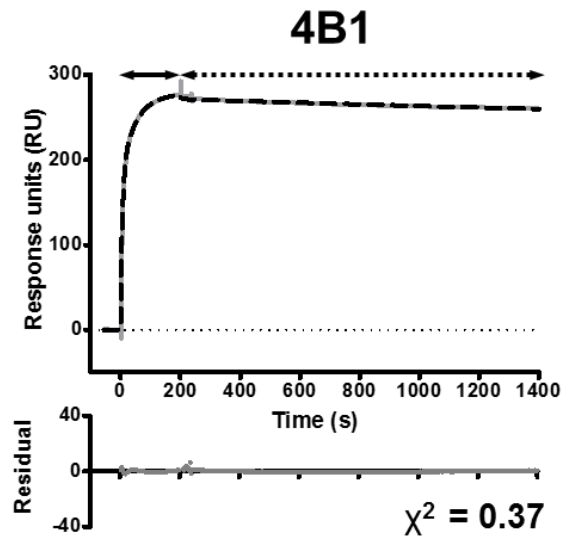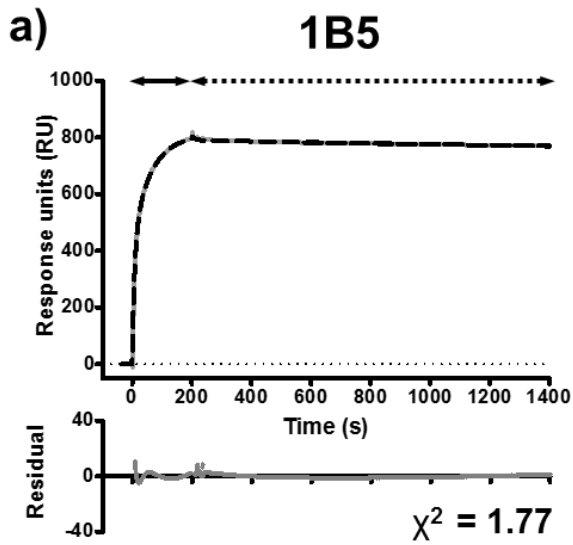
(Continued overleaf)
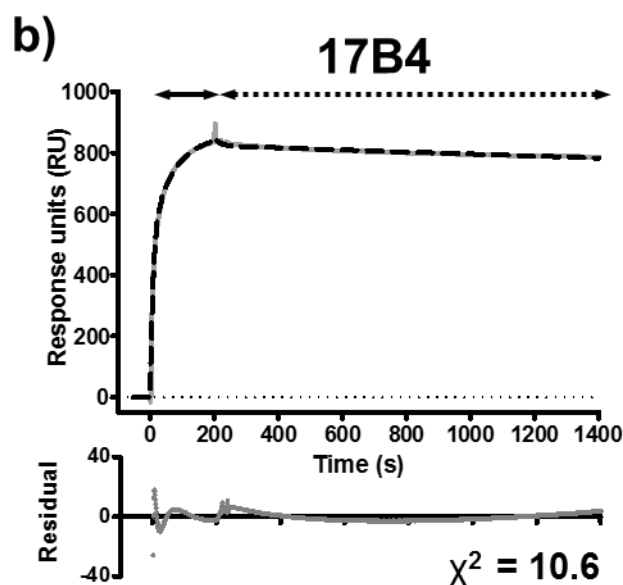
Figure 5.8 – Anti-LAG-3 mAbs bind LAG-3:Fc with monogamous bivalent two-state kinetics:
a) Surface plasmon resonance (SPR) analysis of each indicated candidate mAb binding to LAG-3:Fc. Analyte contact time is shown by arrowhead lines where injection length (solid) and dissociation time (dashed) are indicated. Experimental sensograms (grey) and two-state kinetic model fits (black; dashed) from which kinetic parameters of binding are calculated are shown. Residual plots and χ^2 values show the quality of fit of the two-state kinetic model to the observed data.

b) Surface plasmon resonance (SPR) analysis the commercial 17B4 mAb binding to LAG-3:Fc as described in *a)*.

mAb	k_{on1} (1/Ms)	k_{off1} (1/s)	k_{on2} (1/s)	k_{off2} (1/s)	[Analyte] (μM)	R_{max} (RU)	RI (RU)	χ^2
1B5	5.94×10^4	0.0409	0.0274	3.56×10^{-5}	1.29	817	-6.78	1.77
4B1	9.28×10^4	0.0453	0.0298	6.00×10^{-5}	1.29	275	2.83	0.371
10C8	8.28×10^4	0.0268	0.0109	6.76×10^{-5}	1.29	283	-5.95	6.43
4C10	3.30×10^4	0.0265	0.0208	8.28×10^{-5}	1.29	793	-12.6	6.22
6F7	4.64×10^4	0.0155	0.0155	1.28×10^{-4}	1.29	930	-12	18.0
6D6	6.30×10^4	0.0207	0.0100	1.56×10^{-4}	1.29	317	-2.31	5.63
17B4	5.72×10^4	0.0334	0.0212	6.87×10^{-5}	1.37	869	-8.96	10.6

Table 5.3 – Two state reaction model fit parameters of mAb to LAG-3:Fc binding

[Analyte] = Concentration of injected mAb analyte, RU = Response units, R_{max} = Maximum analyte binding capacity in RU, RI = Bulk refractive index effect in RU,

$\chi^2 = \sum \frac{(observed-expected)^2}{expected}$; lower χ2 values indicate better model fitting.

5.6.2   LAG-3 mAbs bind LAG-3:Fc with subnanomolar-to-nanomolar avidity

Once a suitable kinetic model which explained the observed kinetics of mAb binding to LAG-3:Fc had been applied, these kinetic fits were used to calculate the avidity observed for each mAb binding to the LAG-3:Fc protein. As a result, this obtained avidity could be used to compare (i) each antibody to each other within the mAb panel, (ii) the generated antibodies with the commercial 17B4 clone and (iii) the generated antibodies with other published therapeutically relevant antibody-antigen avidity data.

Due to the formulation of the SPR experiment, the applied model and its observed relevance to the experimental data, the detected binding strength is a result of monogamous bivalency and are therefore avidity measurements. From the kinetic parameters determined and shown previously (*Table 5.3*), association equilibrium constants (K_A) and dissociation equilibrium constants (K_D) can be calculated as was discussed for one-to-one as discussed in Chapter 4. Due to the valency of the binding model, however, these constants are defined by altered equilibrium equations. To distinguish these equilibrium constants as avidity values, the terms K_{Av} and K_{Dv} will be used to represent association and dissociation constants, respectively.

The formation of the final LAG-3:Fc-mAb complex (ABx) is dependent on the rate of formation of the intermediate AB complex. As a result, the cumulative association constant, K_{Av}, is a function of the formation of AB and ABx which themselves can be represented by their own equilibrium constants K_{A1} and K_{A2} respectively. The associated equilibrium affinity constant representing the formation of AB, described as K_{A1} is as follows:

$$K_{A1} = \frac{kon1}{koff1}$$

(Eq 5.5)

Likewise, the associated equilibrium affinity constant representing the formation of ABx, described as K_{A2} is as follows:

$$K_{A2} = \frac{kon2}{koff2}$$

(Eq 5.6)

As K_{Av} is an avidity constant as a consequence of the cumulative equilibrium from A and B as unbound ligands, through AB to ABx (as shown in Eq 5.1), K_{Av} is calculated by the following:

$$K_{Av} = K_{A1} + (K_{A1} \cdot K_{A2})$$

(Eq. 5.7)

Which, by substitution of K_{A1} with Eq. 5.5 and K_{A2} with Eq. 5.6, results in the following:

$$K_{Av} = \frac{kon1}{koff1} + \frac{kon1 \cdot kon2}{koff1 \cdot koff2}$$

<div align="right">(Eq 5.8)</div>

Finally, by the reduction of Eq. 5.8, K_{Av} can now be calculated from the kinetic parameters *kon1*, *koff1*, *kon2* and *koff2* shown previously (*Table 5.3*) by the following:

$$K_{Av} = \frac{kon1}{koff1} \cdot (1 + \frac{kon2}{koff2})$$

<div align="right">(Eq 5.9)</div>

However, as the units of K_{Av} are M^{-1}, dissociation equilibrium constant (K_{Dv}) values, whose units are in molar (M), represent a more digestible explanation of the avidity between mAb and LAG-3:Fc. As a result, K_{Dv} is calculated by taking the reciprocal of K_{Av}:

$$K_{Dv} = \frac{1}{\frac{kon1}{koff1} \cdot (1 + \frac{kon2}{koff2})}$$

<div align="right">(Eq. 5.10)</div>

Which reduces to the following, from which K_{Dv} values have been calculated:

$$K_{Dv} = \frac{1}{kon1} \cdot (\frac{koff1 \cdot koff2}{koff2 + kon2})$$

<div align="right">(Eq 5.11)</div>

As a result, K_{Dv} values for each of the six mAb candidate clones and the commercial 17B4 mAb, calculated from the experimental SPR measurements described, are presented in *Table 5.4*. The resulting avidities for each of the generated anti-LAG-3 antibodies show binding to LAG-3:Fc with nanomolar range dissociation constant avidity K_{Dv} (0.89 – 5.05 nM). In addition, two generated anti-LAG-3 antibodies bound with higher avidity than that of the commercial 17B4 clone antibody (K_{Dv} =1.89 nM). These two antibodies, 1B5 and 4B1 bound LAG-3:Fc with subnanomolar avidity (K_{Dv} = 0.89 and 0.98 nM, respectively). These results therefore allow the ranking of each antibody, based on their avidity for the LAG-3:Fc immunogen.

This range of avidity is typical of antibody binding to antigen with bivalent effects and is comparable to measurements of free antibody binding to high density ligands by other antibodies against different antigens either by SPR or ELISA based methods.

mAb	k_{on1} (1/Ms)	k_{off1} (1/s)	k_{on2} (1/s)	k_{off2} (1/s)	K_{Av} (1/M)	K_{Dv} (M)	K_{Dv} (nM)
1B5	5.94×10^{4}	0.0409	0.0274	3.56×10^{-5}	1.12×10^{9}	8.93×10^{-10}	0.89
4B1	9.28×10^{4}	0.0453	0.0298	6.00×10^{-5}	1.02×10^{9}	9.80×10^{-10}	0.98
10C8	8.28×10^{4}	0.0268	0.0109	6.76×10^{-5}	5.00×10^{8}	2.00×10^{-9}	2.00
4C10	3.30×10^{4}	0.0265	0.0208	8.28×10^{-5}	3.14×10^{8}	3.18×10^{-9}	3.18
6F7	4.64×10^{4}	0.0155	0.0155	1.28×10^{-4}	2.98×10^{8}	3.36×10^{-9}	3.36
6D6	6.30×10^{4}	0.0207	0.0100	1.56×10^{-4}	1.98×10^{8}	5.05×10^{-9}	5.05
17B4	5.72×10^{4}	0.0334	0.0212	6.87×10^{-5}	5.3×10^{8}	1.89×10^{-9}	1.89

Table 5.4 – Avidity equilibrium constant analysis of anti-LAG-3 antibodies for LAG-3:Fc
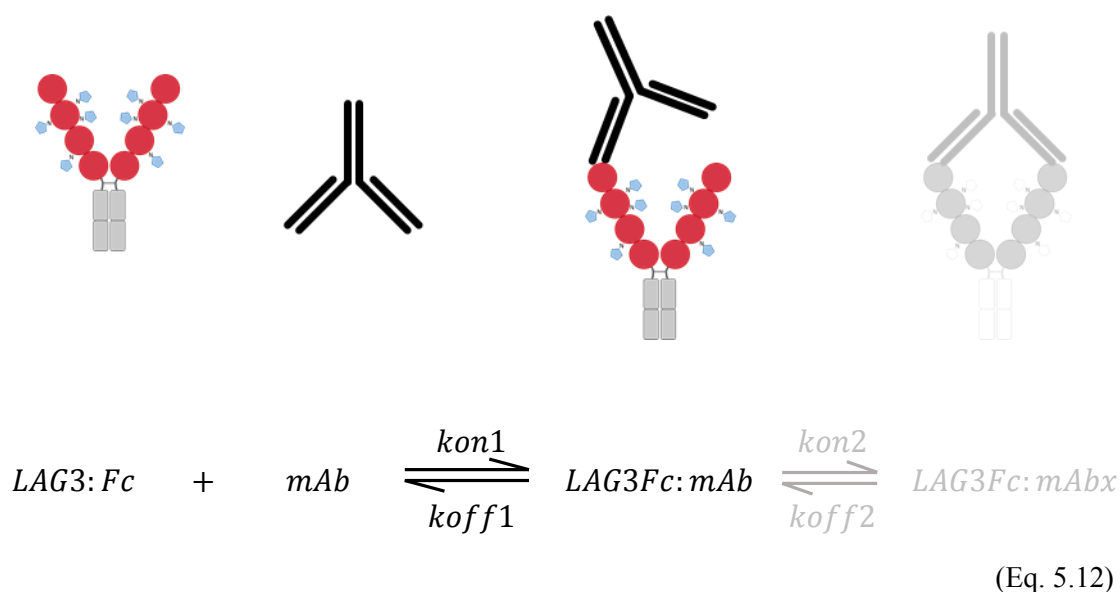K_{Av} = the avidity equilibrium association constant calculated as described by Eq. 5.9
K_{Dv} = the avidity equilibrium dissociation constant calculated as described by Eq. 5.11

5.6.3 Antibody-antigen single site binding affinity occurs at micromolar affinity

Analysis of SPR data obtained for mAb binding to the LAG-3:Fc protein can be used to infer an affinity measurement for one mAb antigen binding site binding to one LAG-3 epitope antigen. This is possible using the two-state reaction model and kinetic parameters applied previously and using an equilibrium constant term described previously, K_{A1} (Eq. 5.5).

Since K_{A1} is the equilibrium association constant associated with the formation of the intermediate AB complex, from unbound A and B, this constant describes the formation of a complex by which one single mAb arm binds to one LAG-3 arm:

$$LAG3{:}Fc \quad + \quad mAb \quad \underset{koff1}{\overset{kon1}{\rightleftharpoons}} \quad LAG3Fc{:}mAb \quad \underset{koff2}{\overset{kon2}{\rightleftharpoons}} \quad LAG3Fc{:}mAbx$$

(Eq. 5.12)

Considering the kinetic parameters k_{on1} and k_{off1} which, as illustrated in Eq. 5.5 describes the equilibrium association constant of LAG-3:Fc and mAb to form LAG-3Fc:mAb (K_{A1}), a single binding event affinity can be inferred. It is worth clarifying that whilst the formation of ABx and its contribution to the observed binding measurements are, in this analysis, ignored, these kinetics are still present in the model. Instead, the contribution of the first step binding event, described by K_{A1}, are deconvoluted from the overall observed two-state reaction model kinetics. The same analysis can be performed on the second step interaction i.e. K_{A2}, however, this interaction step has less biological relevance in describing the antibody-antigen interaction at the single site level. Like with avidity measurements, K_{A1} has units of M^{-1} and as a result, $K_{D1,}$ with units in M, is preferred and therefore used in the analysis:

$$K_{D1} = \frac{koff1}{kon1}$$

(Eq 5.13)

Observation of calculated K_{D1} affinity values suggests an alternative hierarchy of binding strength amongst the tested anti-LAG-3 antibodies (*Table 5.5*). All antibodies exhibit affinity

dissociation constants in the submicromolar range ($K_{D1} = 0.32 - 0.80$ µM). Four of the generated mAbs (10C8, 6D6, 6F7 and 4B1) demonstrated higher affinity K_{D1} values than the commercial 17B4 antibody ($K_{D1} = 0.80$ µM). Using this analysis, the highest affinity binding antibody was 10C8 which bound at $K_{D1} = 0.32$ µM.

To this end, the results presented in this section show that the generated anti-LAG-3 antibodies specifically bind LAG-3 glycoprotein at a subnanomolar to nanomolar avidity typical of a high affinity immunoglobulin (*Figure 5.9*). Fine differences in binding kinetics were apparent in each of the mAb-antigen interactions and these measurements can thus be used to distinguish a hierarchy of binding in which some of the generated antibodies bind with higher affinity and avidity than the 17B4 commercial antibody which is most commonly used in the literature. In addition, these data show that the generated antibodies and the commercial 17B4 clone are able to bind two independent binding sites of LAG-3:Fc through kinetic model fitting of measured analyte-ligand binding interactions at low ligand density.

mAb	kon1 (1/Ms)	koff1 (1/s)	K_{A1} (1/M)	K_{D1} (M)	K_{D1} (µM)
10C8	8.28×10^4	0.0268	3.09×10^6	3.24×10^{-7}	0.32
6D6	6.30×10^4	0.0207	3.04×10^6	3.29×10^{-7}	0.33
6F7	7.48×10^4	0.0335	2.99×10^6	3.34×10^{-7}	0.33
4B1	9.28×10^4	0.0453	2.05×10^6	4.88×10^{-7}	0.49
1B5	5.94×10^4	0.0409	1.45×10^6	6.89×10^{-7}	0.69
4C10	3.30×10^4	0.0265	1.25×10^6	8.03×10^{-7}	0.80
17B4	5.72×10^4	0.0334	1.71×10^6	5.84×10^{-7}	0.58

Table 5.5 – Affinity equilibrium constant analysis of anti-LAG-3 antibodies for LAG-3:Fc
K_{A1}= the affinity equilibrium association constant calculated as described by Eq. 5.5
K_{D1} = the affinity equilibrium dissociation constant calculated as described by Eq. 5.13
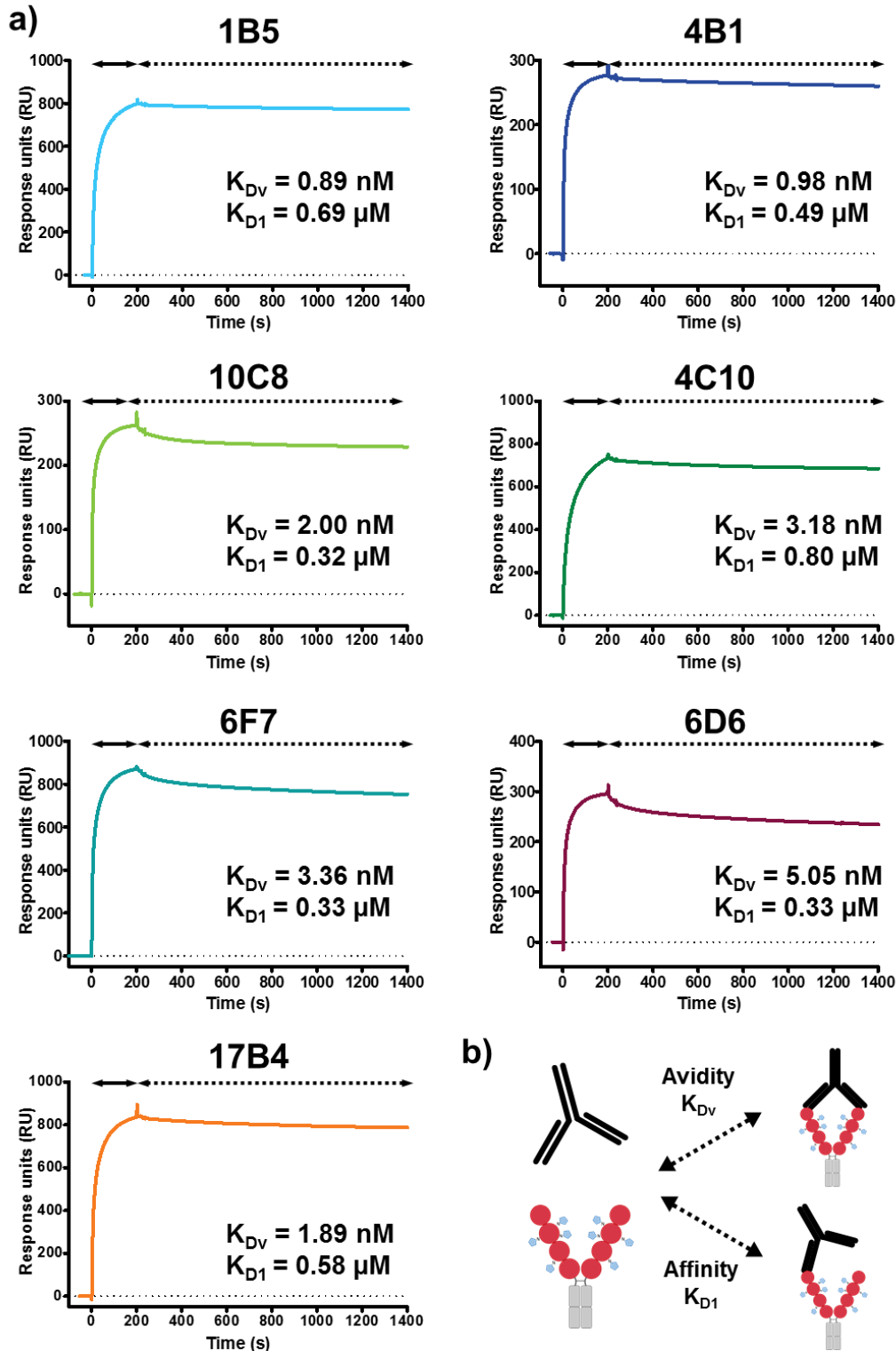
Figure 5.9 – Kinetic summary of anti-LAG-3 antibodies binding to LAG-3:Fc:

a) Observed binding curves of each of the indicated anti-LAG-3 antibodies binding to immobilised LAG-3:Fc. Inset numbers indicate the avidity (K_{Dv}) and affinity (K_{D1}) equilibrium dissociation constants determined by simultaneous kinetic model fitting.

b) Schematic of mAb (black) binding to LAG-3:Fc (red:grey) via a monogamous bivalent interaction and the definition of avidity and affinity values used in *a)*.

5.7 The LAG-3 mAb panel bind a similar or the same LAG-3 epitope

Given the similarity in sequence, functional and biophysical characteristics of each antibody, the capacity of each antibody to block one-another was investigated using a 'pulse-chase' competitive binding approach. Binding of mAb was once again measured against immobilised LAG-3:Fc using SPR. Determination of binding site competition (epitope competition) was achieved by first saturating the available binding sites on the immobilised LAG-3:Fc chip surface with a first 'pulse' antibody before injecting a second 'chase' antibody immediately after. Due to the slow mAb dissociation kinetics discussed previously, the second 'chase' antibody injection was made whilst the epitope of the first 'pulse' antibody remained near saturation. Should the 'chase' antibody be sterically hindered by the 'pulse' antibody, due to binding to the same or similar epitope on the surface volume of LAG-3:Fc, the resulting association measurement of the 'chase' antibody would be considerably diminished. Thus, by comparison of the binding profile of the 'chase' antibody with or without pre-bound 'pulse' antibody, such steric blocking can be deduced.

Using this described methodology, each of the six candidate mAb clones were shown to block the binding of one-another suggesting each antibody binds to the same or similar epitope (*Figure 5.10a*). In order to minimise the protein required to deduce cross-blocking between the mAb panel, 'pulse-chase' experiments were performed in a cyclic chain; applying the assumption that capacity to block was transferred throughout the chain. For example, if mAb A blocks mAb B, and mAb B blocks mAb C, it is assumed that mAb A would also block mAb C. Using this assumption, it was possible to deduce that each antibody within the panel blocked one another's binding. In addition, the 17B4 clone, of which the generated epitope is known, was able to be blocked by one of the generated mAb clones (10C8) as well as block one of the generated mAb clones (6F7). These data therefore suggest that 17B4 and the generated mAbs also bind to a similar or the same epitope.

In order to ensure that antibody blocking was in fact dependent on the antigenic epitope, a second anti-LAG-3 antibody from outside of the generated six mAbs (13E2) was tested for its capacity to block binding of candidate or 17B4 antibodies. This antibody is known to bind to a unique epitope from 17B4 (F. Triebel, personal communications). As such, saturation of LAG-3:Fc with 13E2 as the 'pulse' antibody was not able to impact on the association of the generated 6D6 mAb clone (*Figure 5.10b*). These data suggest that 13E2 binds to a distinct epitope from a shared or similar epitope of the candidate mAb panel and 17B4, based on the assumption described previously. These results were replicated in a pair-wise sandwich ELISA assay in which the generated mAbs and 17B4 used as binding pairs, were unable to detect LAG-3:Fc in the

ELISA assay (data not shown). On the other hand, 13E2 was able to pair with any of the generated mAbs or 17B4 and successfully detect LAG-3:Fc as antigen (data not shown).

In corroboration with the sequencing data described in this section, these competitive binding assays strongly suggest that each of the six generated mAbs bind to the same epitope which is in a similar proximity to the epitope for the 17B4 antibody but distinct from the 13E2 antibody.
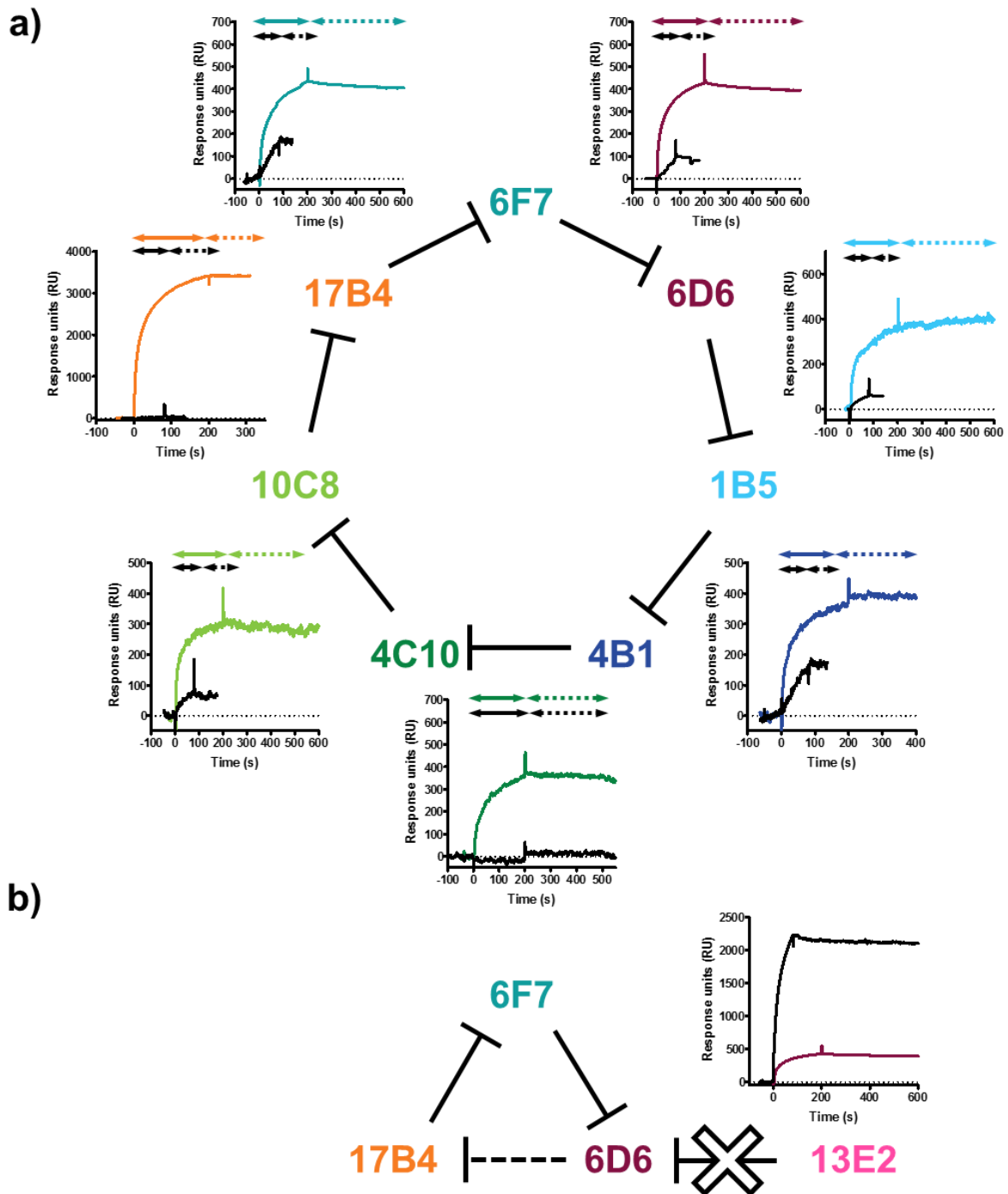
Figure 5.10 – Competitive blocking of anti-LAG-3 antibodies:

a) Overlay kinetic binding curves of anti-LAG-3 antibody binding to immobilised LAG-3:Fc with (black sensograms) and without (colour coded sensograms according to text) saturation of the LAG-3:Fc surface with a competitor anti-LAG-3 antibody. Competitor (pulse) antibody in each experiment is shown by flat-ended arrow indicating inhibition of query (chase) antibody. Classification of inhibition was made by the reduction of association kinetics compared to unblocked injections. Chain of inhibition proceeds in a clockwise orientation. Colour coded double headed arrows indicate analyte contact time as described in *Figure 5.8*.

b) Overlay kinetic binding curves as described in *a)* highlighting no capacity of mAb 13E2 clone antibody to block mAb 6D6 clone binding to LAG-3:Fc thus binding to a distinct epitope of LAG-3:Fc.

5.8   Molecular blockade of LAG-3-MHC-II binding

Given that the generated mAbs bind to a similar or the same epitope as the commercial 17B4 antibody clone, which is known to block the LAG-3-MHC-II interaction (Baixeras et al. 1992), it seemed likely that the generated new mAbs would also block the LAG-3-MHC-II interaction. As a result, this blocking ability was assayed using SPR binding analysis of the LAG-3:Fc-HLA-DR1 interaction as established in Chapter 4. In addition, the ability of antibodies to block the staining of cellularly expressed full length LAG-3 by HLA-DR1 multimers was assayed using the JRT LAG-3 C8 cell line as described in Chapter 4.

5.8.1   Direct blockade of LAG-3:Fc binding to HLA-DR1

To directly study the ability of generated antibodies to block the protein-protein interaction between LAG-3 and MHC-II, LAG-3:Fc protein was incubated with anti-LAG-3 antibodies (17B4, 13E2 and 6F7) and analysed for binding of analyte to a HLA-DR1 immobilised sensor chip via SPR. Incubation and co-injection of an excess of each anti-LAG-3 antibody (17B4, 13E2 and 6F7) with LAG-3:Fc did indeed result in the abrogation of LAG-3:Fc binding to HLA-DR1 compared to unblocked and an irrelevant antibody control (*Figure 5.11a&b*). This abrogation was observed as a complete reversal of binding in reference subtracted sensograms (*Figure 5.11a*). Quantification of the observed response units at 20 seconds into LAG-3:Fc injection highlighted the complete blockade of LAG-3:Fc binding to HLA-DR1 when co-injected with 17B4, 13E2 or one of the generated anti-LAG-3 antibodies, 6F7 (*Figure 5.11b*).

To confirm LAG-3:Fc-HLA-DR1 blockade by 6F7, LAG-3:Fc, at a fixed concentration (0.3 mg/mL, 2.0 µM), was incubated and co-injected with titrating concentrations (0.6 µM − 13.2 µM) of 6F7. Observed reference subtracted sensograms exhibited clear titratable reversal of LAG-3:Fc binding to HLA-DR1 at increasing concentrations of 6F7 antibody (*Figure 5.11c*). Moreover, quantified response units at 20 seconds into LAG-3:Fc injection highlighted titratable inhibition of binding (*Figure 5.11d*). This blockade was observed at limiting (0.1 mg/mL, 0.6 µM), comparable (0.5 mg/mL, 3.2 µM) and excess (2.0 mg/mL, 13.2 µM) concentrations of antibody compared to LAG-3:Fc (0.3 mg/mL, 2.0 µM). These data, therefore, show a direct ability of the generated 6F7 antibody to block the protein-protein interaction between LAG-3-MHC-II in the context of LAG-3:Fc-HLA-DR1 binding, similarly to two other anti-LAG-3 antibodies.
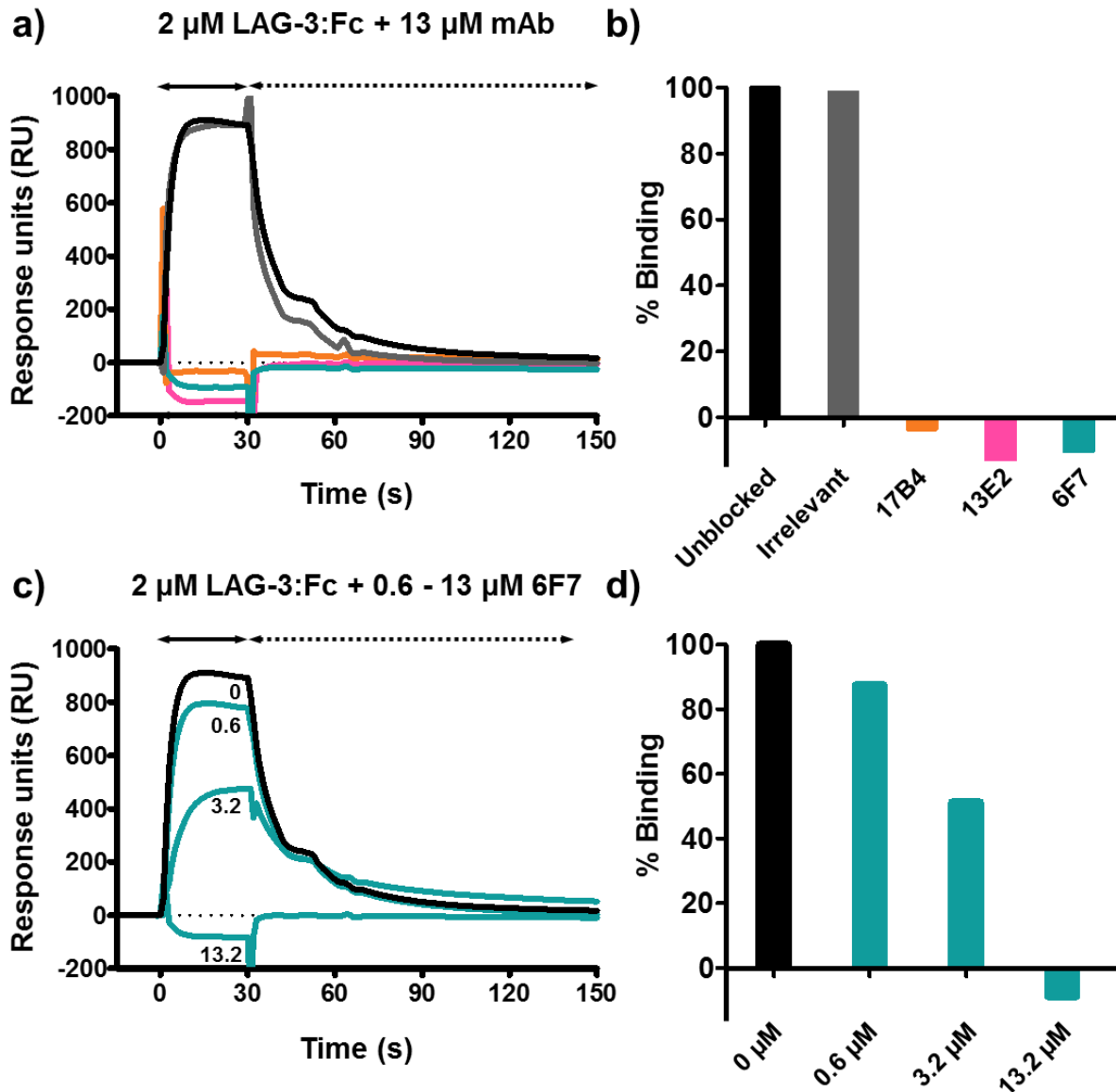
Figure 5.11 – Direct blockade of the LAG-3:Fc-HLA-DR1 protein-protein interaction:

a) Surface plasmon resonance (SPR) analysis of LAG-3:Fc binding to immobilised HLA-DR1 in the presence and absence of anti-LAG-3 antibodies. Co-injection of 2 μM LAG-3:Fc with 13.2 μM 17B4, 13E2 and 6F7 antibodies (colours as shown in *b)*) abrogated observed binding in reference subtracted sensograms compared to in the absence of antibody (unblocked, black) or a control antibody (irrelevant, grey).

b) Normalised quantification of binding at 20 sec into co-injection of 13.2 μM irrelevant, 17B4, 13E2 and 6F7 antibodies with 2 μM LAG-3:Fc or 2 μM LAG-3:Fc alone (unblocked). Percentage binding values are normalised to unblocked binding response from sensograms shown in *a)*.

c) SPR analysis of LAG-3:Fc binding to immobilised HLA-DR1, as described in *a)*, performed at titrated concentrations of 6F7 anti-LAG-3 antibody. Increasing concentrations of 6F7 during co-injection correlated with inhibition of observed binding in reference subtracted sensograms compared to in the absence of antibody (black). Inset numbers mark co-injection concentration in μM of 6F7 antibody.

d) Normalised quantification of binding at 20 sec into co-injection of 6F7 antibodies at given concentrations with LAG-3:Fc or LAG-3:Fc alone (0 μM). Percentage binding values are normalised to unblocked (0 μM) binding response from sensograms shown in *c)*.

5.8.2 Blockade of HLA-DR1 multimer binding to cellularly expressed LAG-3

Having established direct blockade of LAG-3:Fc binding to HLA-DR1 using SPR, the ability of a generated LAG-3 mAb to block MHC-II binding to cellularly expressed LAG-3 was confirmed using flow cytometric analysis of multimerised HLA-DR1 staining of JRT LAG-3$^+$ C8 cells. The capacity to inhibit multimerised HLA-DR1 staining of JRT LAG-3$^+$ C8 cells, as shown in Chapter 4, was assayed by pre-staining cells with three anti-LAG-3 antibodies (17B4, 13E2 and 1B5) prior to HLA-DR1 multimer staining.

In agreement with SPR data shown previously, 17B4 and 13E2 antibodies both blocked multimerised HLA-DR1 binding to cellularly expressed LAG-3 where 19 % of cells exhibited increased fluorescence staining above background in unblocked conditions compared to 0.1 and 0.3 % of cells in the presence of 17B4 and 13E2 anti-LAG-3 antibodies, respectively. The generated mAb tested, 1B5, blocked binding to MHC-II as shown by a reduction in multimer positive cells to 0.1 % (*Figure 5.12a*). Such reduction in staining was highlighted by a complete reversal of HLA-DR1 staining; to fluorescence intensities observed for control multimer (HLA-A2) binding to JRT LAG-3$^+$ C8 cells (*Figure 5.12b*). Reversal of HLA-DR1 multimer binding to JRT LAG-3$^+$ cells was not observed using an irrelevant antibody control as shown by equivalent binding to unblocked multimers (*Figure 5.12c*).

These data, therefore, show a direct ability of a generated anti-LAG-3 antibody, 1B5, to block binding between MHC-II and LAG-3 expressed in a cellular context. In combination with the ability to block LAG-3:Fc binding to HLA-DR1 at the protein level, these results show an ability of anti-LAG-3 antibodies of the generated panel, which bind the same or similar epitope, to modulate the interaction between LAG-3 and MHC-II.
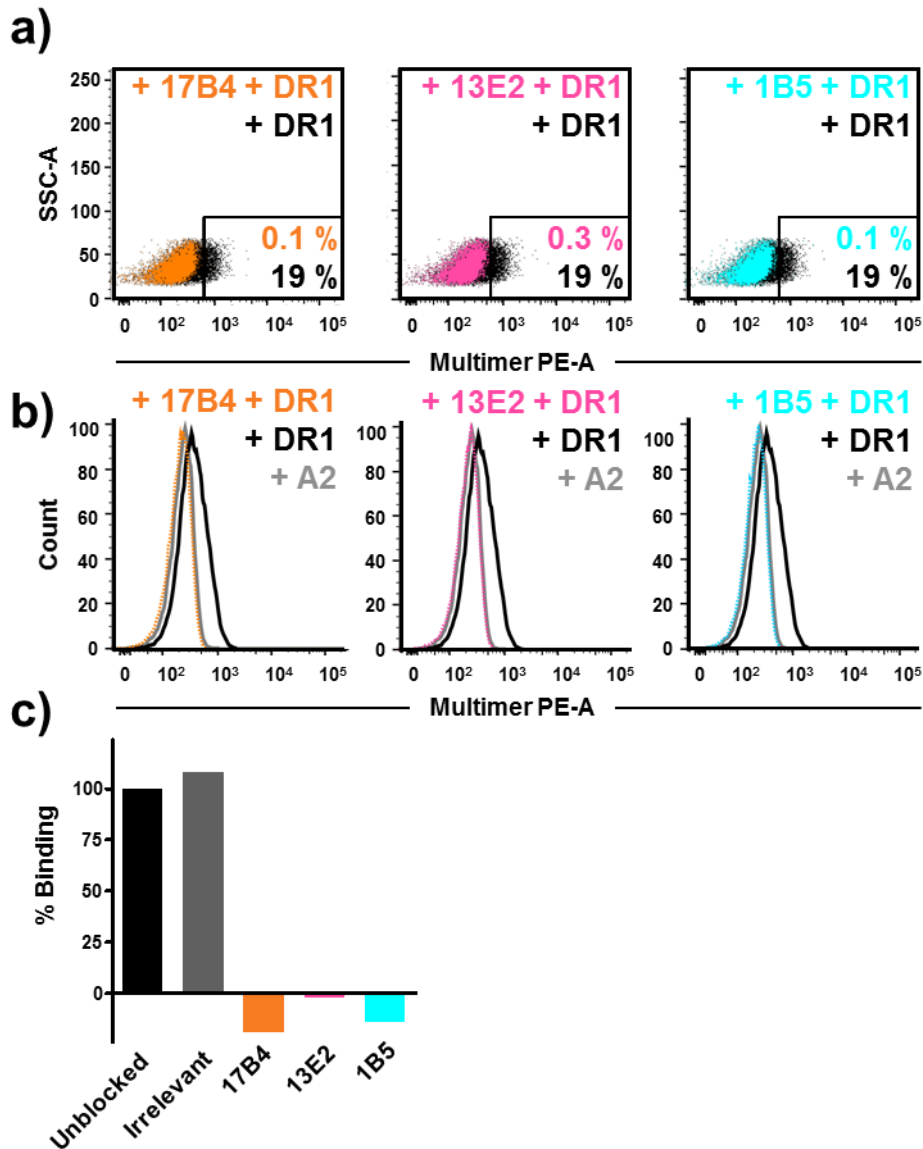
Figure 5.12 – Antibody mediated inhibition of HLA-DR1 multimer staining of LAG-3+ cells:

a) Flow cytometric analysis of HLA-DR1 multimer staining of JRT LAG-3+ C8 cells following pre-staining with unconjugated anti-LAG-3 antibodies. Pre-staining of cells with 17B4, 13E2 and 1B5 anti-LAG-3 antibodies (coloured, + mAb + DR1) reversed staining by PE conjugated multimers compared to PBS control (black, + DR1). Multimer positive gate set by HLA-A2 negative control multimer staining.

b) Fluorescence histograms of multimer staining of JRT LAG-3+ C8 cells as described in *a*). Observed binding of unblocked HLA-DR1 binding to cells (black, + DR1) was reversed to levels observed by control HLA-A2 multimers (grey, + A2) by pre-staining with 17B4, 13E2 and 1B5 anti-LAG-3 antibodies (coloured, + mAb + DR1).

c) Normalised quantification of HLA-DR1 multimer binding in the presence of an irrelevant, 17B4, 13E2 and 1B5 antibodies compared to unblocked (PBS) multimer staining. Percentage binding calculated by background subtraction of HLA-A2 multimer gMFI from observed HLA-DR1 multimer gMFI, from experiments as shown in *b*) normalised to unblocked control.

5.9 Discussion

The blocking of LAG-3 function or depletion of LAG-3 expressing cells has gathered great therapeutic interest due to the role of LAG-3 in suppressing T cell responses (Sega et al. 2014; Turnis et al. 2015). Moreover, the upregulation of LAG-3 on highly suppressive T cells extracted from within human colorectal tumours suggest a role for LAG-3 in the sub-optimal immune response to tumours (M Scurr et al. 2013). Indeed, pre-clinical studies have shown that blocking of LAG-3 function, in combination with PD-1 blockade unleashed an effective anti-tumour response in multiple mouse models of cancer (Woo et al. 2012). The blockade and/or depletion of such suppressive cells in tumours, through the expression of LAG-3, is therefore a desirable therapeutic goal in the field of cancer immunotherapy.

To this end, in these studies, a panel of anti-LAG-3 antibodies were successfully generated by the whole protein immunisation of mice. The resulting monoclonal antibody panel highlighted a robust and focused B cell response against the immunogen. Of the six mAb generated, each antibody exhibited high similarity, at the DNA, protein, functional and biophysical level. This occurred despite a wide immunisation and selection approach. The generated antibodies, therefore, likely arose from a single dominant parent clonotype generated from a single recombination event *in vivo* as a response to exposure to heterologous LAG-3 protein. Despite overall similarity, subtle differences at the protein sequence level were observed which likely arose from either affinity maturation of the parent clone or through random mutations inserted throughout the antibody sequence as a consequence of hybridoma culture. Nevertheless, subtle difference in protein sequence between antibodies translated into subtle differences in binding characteristics; both in terms of functional binding and binding kinetics.

The analysis of each antibody by SPR allowed the accurate characterisation of such binding strength. Dissection of these kinetic parameters will aid in the narrowing of the antibody panel for further functional characterisation. In depth analysis of the kinetic properties of antibody-antigen binding allowed the determination of avidity and affinity measurements for each antibody. As such, this comprehensive view of antibody-antigen binding will allow the selection of antibodies based on subtle differences in kinetics depending on application. Experiments or therapeutic scenarios where LAG-3 ligand density is lower would favour an antibody with higher affinity as opposed to avidity. Indeed, affinity measurements of each antibody show better correlation with maximum fluorescence cytometry staining compared to avidity measurements, albeit both not reaching significance (two-tailed Spearman's rank correlation; K_{D1} to max gMFI (p= 0.1389, r= -0.6487) K_{Dv} to max gMFI (p= 0.2357, r= 0.5357)). Thus, it is suggested that selection of an antibody with strongest affinity (lowest K_{D1}) may be preferential for ligand densities such as those found at the cell surface. In turn, strongest avidity (lowest K_{Dv}) may be more

favourable for high ligand density experiments such as ELISAs and Western blots. Consideration of binding strength on therapeutically relevant target cells would enable the design of an antibody with optimal therapeutic potency.

Initial experiments identifying the binding region of each of the generated mAbs revealed that each of the candidate antibodies competed for binding with one another. Alongside the described sequencing data, it is concluded that each antibody binds to the same epitope. Moreover, competitive binding was also exhibited with a commercial anti-LAG-3 mAb which was raised via peptide-KLH immunisation against a 30 amino acid extra loop unique to LAG-3 within the D1 domain (LAG-3$_{70-99}$) with the purpose of generating an antibody able to block the LAG-3-MHC-II interaction (Baixeras et al. 1992). Indeed, a representative antibody was able to block the binding of LAG-3 and MHC-II in competitive SPR binding analysis and MHC-II multimer staining. Future characterisation of the generated mAbs would benefit from defining the epitope recognition sequence at higher resolution and thus compound the capacity to block the LAG-3-MHC-II interaction, based on these initial competitive binding assays. The benefit of blocking LAG-3 and/or depleting such human cells could consequently be investigated *in vitro.* Indeed, both blocking and depletion of CTLA-4 cells has been shown to contribute to the clinical efficacy of ipilimumab (Peggs et al. 2009; Simpson et al. 2013).

5.9.1 Future directions

The work presented in this chapter represent the initial stages of a translational project to synthesise antibodies targeting the suppressive T cell molecule LAG-3 with them aim of future development of therapeutic agents targeting LAG-3 expressing cells. The use of such agents clinically requires the human-mouse chimerisation or full humanisation of generated mouse antibodies in order to minimise the effects of an anti-mouse Ig immune response against the protein agent, which results in low efficacy due to poor pharmacokinetic outcome (Weiner 2015). Moreover, in order to most effectively recruit human immune effector networks, mAb humanisation or chimerisation is required to optimally initiate LAG-3$^+$ cell depletion *in vivo* through favourable affinities with human antibody binding receptors or soluble proteins such as Fcγ receptors or C1q complement factors.

Humanisation of antibodies, through the grafting of CDR regions to human framework Ig sequences can be used to increase pharmacokinetic half-life by minimising, but not eliminating, anti-mouse recipient immunogenicity (Harding et al. 2010). The process of humanisation, however, can be time and resource heavy due to loss of antigen specificity requiring consequent back-mutation screening. Chimerisation of antibodies, whilst exhibiting increased immunogenic risk and comparatively shorter half-lives, can still be clinical beneficial. Rituximab, a chimeric

mouse/human anti-CD20 antibody, is an effective depleting antibody in a range of human diseases where pathophysiology is driven by aberrant B cells such as B cell lymphoma (McLaughlin et al. 1998).

As a result, to assay ability of the mAbs to initiate *in vitro* antibody dependent cellular phagocytosis (ADCP) by macrophages, complement dependent cytotoxicity (CDC) and antibody dependent cellular cytotoxicity (ADCC) by NK cells, the candidate antibody/antibodies would first be chimerised through the exchange of mouse constant region domains with human constant domain gene sequences. Ability of chimeric anti-LAG-3 mAbs to deplete LAG-3 human cells *in vitro* could initially be performed using JRT LAG-3$^+$ C8 cells, and later *ex vivo* human LAG-3 expressing T cells. Selection of human Fc domain sequences, determining the antibody isotype, would require careful consideration to ensure maximum recruitment of the three described effector networks (ADCP, ADCC & CDC) to allow consequent depletion of LAG-3 opsonised cells (Isaacs et al. 1998). For example, the therapeutic antibody rituximab, which uses human IgG1 isotype, has been shown to be the most effective Fc domain due to its preference for binding activating Fcγ receptors such as FcγRIIIA (Beers et al. 2016). Likewise, through an IgG1 Fc domain, B cell depletion by rituximab is enhanced by C1q binding and consequent complement activation (Idusogie et al. 2000). Ability to generate an effective depletion *in vivo*, however, would be dependent on effector cells expression of suitable activating FcγRs as well as complement availability within the desired target depletion site or organ. Thus, chimerisation of anti-LAG-3 mAbs could be performed using multiple Fc isotypes to find an optimal isotype for the given therapeutic setting. Indeed, engineering of generated mAbs to incorporate a depletion inert isotype would enable the dissection of phenotype as a result of LAG-3$^+$ cell depletion and LAG-3 blockade in *in vitro* assays.

5.9.2 Implications of this study

In the studies outlined in this chapter, a panel of high avidity and highly specific anti-LAG-3 antibodies have been generated that will be used for a number of different applications. Firstly, high quantities of mouse anti-LAG-3 antibodies will be used in the ongoing effort to produce soluble LAG-3 proteins for structural, biophysical and molecular characterisation of this high interest, yet difficult to characterise, immune regulator protein. Secondly, these antibodies will be used to help characterise LAG-3 expression on T cells found infiltrating in human colorectal cancer tumours whom have the potential to suppress an anti-tumour immune response. Finally, these antibodies will be developed and engineered with the ultimate goal of being tested for safety and efficacy in the clinic. Such efforts will require, and has already involved, collaboration of laboratory groups throughout Cardiff and beyond.

6 Chapter 6: Discussion

6.1 Implications of this thesis

The studies outlined in this thesis described the recognition and presentation of a colorectal tumour-derived antigen, 5T4, by CD4$^+$ T cells through the TCR-pMHC-II interaction. Moreover, LAG-3 was shown to bind MHC-II which, given its involvement in T cell regulation and high expression on CD4$^+$ T cells in colorectal cancer, may suppress T cell immunity to 5T4 antigen through this interaction. Thirdly, specific monoclonal antibodies were developed which efficiently bound, targeted and blocked this interaction and provide a platform for development of therapeutics aimed at depleting suppressive LAG-3$^+$ cells with the aim of enhancing immunity against 5T4 and other tumour antigens.

6.1.1 5T4-reactive CD4$^+$ T cell clones are present in the periphery

In Chapter 3, three CD4$^+$ T cell clones derived from the peripheral blood of a healthy donor were described in terms of their MHC restriction, ability to activate in response to tumour-derived peptides, functional cytokine release and ability to engage with cognate pMHC. These studies showed that within peripheral blood were CD4$^+$ T cell clones that were able to activate in response to presented 5T4-derived peptides on the MHC-II molecule HLA-DR1. These clones were sensitive to peptide in response to *in vitro* stimulation resulting in the release of T_H1 cytokines IFNγ and TNFα. Such activation occurred despite little to no detectable binding by cognate pMHC multimers. The ability of these clones to be sensitive in response to peptide yet exhibit weak engagement with cognate peptide MHC raises interesting questions about the origin of these clones from within the T cell repertoire such as (i) the nature of the optimal peptide agonist for these 5T4-reactive TCRs and (ii) whether the described clones were derived from naïve or memory T cell pools.

6.1.2 Structural definition of the 5T4$_{117-125}$ tumour-derived CD4$^+$ T cell epitope

In Chapter 3, the presentation of a 5T4-derived peptide by the MHC-II molecule HLA-DR1 was studied at high resolution by x-ray crystallography. These studies revealed structural insights into the presentation of a 5T4-derived peptide at 1.95 Å resolution. This structure of HLA-DR1 presenting the 5T4p12 peptide defined the core epitope to 5T4$_{117-125}$. It was revealed that the core epitope 5T4$_{117-125}$ bound with a near optimal HLA-DR1 binding motif with the exception of the partial filling of the P1 peptide binding pocket. The 5T4$_{117-125}$ core epitope was able to incorporate leucine into the P1 peptide binding pocket of HLA-DR1 and, despite its shorter side chain, made a number of contacts with the MHC molecule to anchor the peptide into the peptide

binding groove. This near optimal binding motif may have contributed to the *in vitro* immunogenicity of the 5T4$_{117-125}$ bearing 5T4p12. Nevertheless, the potential for further enhancement of the presentation of 5T4$_{117-125}$ by HLA-DR1 could be assayed by the generation of an altered peptide ligand of 5T4$_{117-125}$ by substitution of the Leu1 residue for a more favoured residue such as tyrosine, tryptophan or phenylalanine (Cole & Godkin 2016).

Altered peptide ligands which enhance peptide-MHC binding have been studied extensively in MHC-I systems. Modifications of melanoma antigen gp100 epitopes, for example, have been shown to enhance CD8$^+$ T cell responses in *in vitro* cultures of PBMCs from melanoma patients (Parkhurst et al. 1996). In MHC-II systems, however, similar tactics have resulted in the generation of heterogeneity in the consequent CD4$^+$ T cell response as incorporation of peptide-MHC-II enhancing peptide modifications had subtle structural implications on TCR contact residues (Chen et al. 2013). Consequently, an understanding of the impact on recognition by the T cell repertoire as a result of 5T4$_{117-125}$ Leu1 candidate modifications would also be required.

6.1.3 Peptide flanking residues can contribute to MHC-II anchoring

The HLA-DR1 5T4p12 structure described the presentation of a peptide longer than any current published pMHC-II structure. HLA-DR1 presented 5T4p12 with six and five amino acid PFRs at the N- and C-terminus, respectively. This structure therefore provided a model for the study of PFR interactions with the MHC-II.

In addition to the near ideal HLA-DR1 motif, contribution to binding between the MHC-II and the peptide flanking residues – particularly at the N-terminus – was observed. Indeed, through the large guanidinium side chain of Arg-4, binding by the P-4 residue to the HLA-DR1α chain contributed the most intermolecular contacts between peptide and MHC-II by any residue out of the entire peptide. This observation suggests that preference for lysine residues at P-4 may allow enhanced binding of peptide epitopes to HLA-DR1. Indeed, this enhanced binding contribution by the PFRs, in combination with the near ideal epitope of 5T4$_{117-125}$, may have contributed to the observed immunogenicity of the 5T4p12 peptide *in vitro*.

6.1.4 Formation of secondary structure elements reminiscent of native antigen in MHC-II peptide flanking residues

Further analysis of the peptide flanking residues of the HLA-DR1 5T4p12 structure revealed a novel structural feature of MHC-II presentation. Loss of influence imposed on the peptide by HLA-DR1 due to extension of the C-terminus of the peptide outside the peptide binding groove allowed the formation of a hairpin turn in the peptide with type II β-turn characteristics. This turn was mediated primarily by intramolecular (peptide to peptide) contacts and with smaller contributions by intermolecular (MHC to peptide) contacts.

Formation of this turn was enabled by a Ser10-Gly11-Ser12 series of amino acids which allowed flexibility in the peptide chain and formation of a high-energy hydrogen bond between the Ser12 side chain hydroxyl and the backbone carbonyl that preceded the Ser10-Gly11-Ser12 motif. A similar structural motif has been documented previously in a HLA-DR1 presented HIV-gag derived peptide, however, this hairpin loop was mediated primarily by a peptide backbone-to-backbone contact (Zavala-Ruiz et al. 2004). The studies described in this thesis, together with those reported by *Zavala-Ruiz et al.,* suggest that secondary structure elements such as hairpin turns may be a common feature of MHC-II peptide presentation.

Due to the open-ended nature of the peptide binding groove and the minimal contacts observed between the 5T4p12 hairpin turn and the MHC molecule, it is hypothesised that this structural motif likely arose due to the loss-of-influence on the peptide at the N-terminal flank. Indeed, comparison of the 5T4p12 sequence within the published structure of the 5T4 native antigen (Zhao et al. 2014) and the HLA-DR1 presented 5T4p12 revealed structural similarity; where in the native protein, the Ser-Gly-Ser sequence also forms a hairpin with type II β turn characteristics. This observation poses interesting questions about MHC-II peptide presentation such as (i) whether this structural motif would form in solution before MHC-II loading or after and (ii) how the low pH exhibited during peptide loading in the MHC-II compartment would affect secondary structure formation within the 5T4p12 C-terminal peptide flanking region.

6.1.5   LAG-3 function is mediated by a moderate affinity interaction with MHC-II

Using SPR analysis of a LAG-3:Fc fusion protein, supported by cellular flow cytometry staining of LAG-3^{+} cells, a direct interaction between LAG-3 and MHC-II was confirmed and described kinetically in Chapter 4. Through kinetic and equilibrium analysis, the affinity of the LAG-3-MHC-II interaction was defined as 13 μM. This moderate affinity is higher than the immeasurably low affinity between MHC-II and the competing CD4 co-receptor. This affinity is at least 200-fold higher than CD4 binding to MHC-II based on the current upper limit of solution affinity between CD4 and MHC-II (Jönsson et al. 2016).

LAG-3 binding was characterised by fast kinetics typical of MHC co-receptors and suggests that out-competition of CD4 for MHC-II may be mediated by rapid rebinding of MHC-II by LAG-3. Indeed, it is known that cytoplasmic signalling through LAG-3 is required for inhibitory function, therefore, CD4 out-competition is not the only potential mechanism of LAG-3 mediated suppression of T cells. This moderate affinity is weaker than the antibody-like avidity reported in the literature as a result of indirect fluorescence measurements of LAG-3:Fc at the surface of MHC-II expressing cells (Huard et al. 1995) and therefore alters the perception of how LAG-3 is able to inhibit T cell activation with such potency. As a result of the observed weaker affinity, it is likely that the potency of LAG-3 mediated T cell suppression is mediated

through the effectiveness of LAG-3 negative signalling; as opposed to simply the competitive blockade of CD4 binding to MHC-II and consequent removal of activating T cell signalling.

6.1.6 Implications in LAG-3:Fc adjuvant therapy

These data defining the affinity of LAG-3 for MHC-II, as well as the effects of bivalency by dimeric LAG-3:Fc, described in Chapter 4, pose interesting questions about the functionality of LAG-3:Fc as a cancer therapeutic. LAG-3:Fc (termed IMP321 in the clinical setting) has been shown to enhance immunity through agonizing MHC-II mediated dendritic cell activation (Brignone et al. 2007). Indeed, in a phase II trial incorporating LAG-3:Fc in combination with chemotherapy, treatment resulted in increased activation of monocytes and dendritic cells and subsequent increase in NK and cytotoxic effector-memory $CD8^+$ T cells (Brignone et al. 2010). Subcutaneous injection of LAG-3:Fc up to 2 mg/injection in combined therapy with chemotherapy resulted in no severe adverse events in a cohort of pancreatic adenocarcinoma patients (Wang-Gillam et al. 2013). Subcutaneous injection of up to 30 mg/injection as a monotherapy or at lower doses with chemotherapy has been well tolerated (Brignone et al. 2009; Wang-Gillam et al. 2013). Despite this, induction of an enhanced T cell immunity required doses higher than 6 mg of LAG-3:Fc and, as a consequence, tumour growth was reduced in patients with advanced renal cell carcinoma only at these higher doses (Brignone et al. 2009).

In light of the data described in this thesis, the effectiveness of LAG-3:Fc to induce dendritic cell maturation may be open to enhancement by improving the engagement of MHC-II molecules by LAG-3 – given the described micromolar K_D affinity. As LAG-3:Fc is derived from an antibody format, it may have been assumed that LAG-3:Fc binding to MHC-II with multivalent avidity may exhibit antibody-like kinetics i.e. greatly enhanced off-rates, as shown by antibody binding in Chapter 5. Kinetic analysis of LAG-3:Fc binding with bivalency in SPR experiments, however, did not support an antibody-like avidity.

Improvement of the LAG-3:Fc avidity may be possible via the enhancement of the monovalent LAG-3 to MHC-II affinity. Indeed, mutations which enhance LAG-3 binding to MHC-II as shown by indirect cell adhesion assays have been previously described (Huard et al. 1997). Analysis of the impact of such mutations on MHC-II engagement could be assayed as described in this thesis as a methodology for the screening of mutations which would enhance MHC-II binding and may facilitate enhanced LAG-3:Fc pharmacokinetics.

6.1.7 Working towards a high-resolution structure of LAG-3

Despite interest in modulating the function of LAG-3 for therapy, the high-resolution structure of LAG-3 remains undescribed. In Chapter 4, preliminary efforts were made to describe LAG-

3 function through the study of LAG-3:Fc at low resolution by negative stain electron microscopy. These studies showed that the available sample of LAG-3:Fc is homogenous, devoid of higher oligomeric species and suitable for study at higher resolution via cryo-electron microscopy. These preliminary studies provide required pre-requisite knowledge before proceeding to imaging cyro-preserved samples.

High-resolution understanding of LAG-3 binding to MHC-II would not only elicit detailed insights into LAG-3 function but would also be beneficial in the development of therapeutics to block LAG-3 function and thus modulate immunity – whether by monoclonal antibody blockade, as described in Chapter 5, or by protein-protein interface disruption using small molecule agents. Structural understanding of this molecular interface could be used to design a candidate small molecule library for the development of a protein-protein interaction inhibitor. Such inhibitors have been designed to disrupt the LFA-1-ICAM-1 interaction at the immune synapse and have consequently shown inhibition of T cell adhesion and activity (Semba & Gadek 2016). This therapeutic tactic may provide an alternate route of LAG-3 functional blockade by the implementation of small-molecule kinetics (and cost benefits) associated with small molecule drugs.

6.1.8   Monoclonal antibodies for the study and targeting of LAG-3

In Chapter 5, a panel of anti-LAG-3 monoclonal antibodies were produced and characterised. These antibodies were shown to be specific for LAG-3 and could discriminate LAG-3 from CD4. They were characterised as binding with comparable or higher affinity and avidity compared to a commercially available anti-LAG-3 antibody and bound to a similar or the same epitope as shown by cross-blockade and were able to block LAG-3 interacting with MHC-II at the cell surface, by flow cytometry, and at the protein level, by surface plasmon resonance.

These antibodies may provide valuable tools in the efforts to describe LAG-3 function by serving as a molecular probe for purifying LAG-3 protein formulations generated *in vitro* for structural studies. Such studies would not be feasible with commercially purchased antibodies due to the large quantities of reagents required. Moreover, the ability of these antibodies to modulate T cell function *in vitro* can be studied either by blockade of LAG-3 or by depletion of LAG-3 expressing cells. This study represented the first steps of a translation project towards an overall goal of developing antibody molecules for checkpoint inhibitor therapy.

6.2   Concluding remarks

The studies in this thesis focused on two aspects of cancer immunology which represent future avenues for immunotherapy: (i) the presentation and recognition of a tumour antigen, 5T4, by CD4+ T cells whose presence have the potential for boosting through cancer vaccines and (ii)

the suppression of immune responses by the inhibitory molecule LAG-3, which has the potential for enhancing immunity by removal of this inhibitory signal. Many developing immunotherapeutic interventions are combined therapies such as those combining multiple checkpoint inhibitors (Larkin et al. 2015). Indeed, an ongoing phase I/IIa clinical trial for solid tumours is aimed at assessing the safety of anti-LAG-3 and anti-PD-1 therapeutics as a combined treatment (ClinicalTrials.gov Identifier: NCT01968109). Combination therapies, however, need not be limited to multiple checkpoint inhibitors. In one study, treatment of cancer patients with the MVA-5T4 (Trovax®) vaccine enhanced IFNγ mediated immunity (Harrop et al. 2007) whilst in a second study depletion of $CD25^+$ T_{reg} cells revealed an enhanced $CD4^+$ T cell response (Elkord et al. 2008). Together, these studies provide rationale for the initial depletion of T cells with regulatory function, such as LAG-3 expressing cells, followed by the boosting of immunity through vaccination against cancer antigens, such as 5T4. Such tactics may enable the priming of T cell responses to 5T4 vaccine in a less suppressive environment and thus promote better anti-tumour immunity. The studies described in this thesis add basic understanding of these two aspects of anti-tumour immunology and have developed molecules for its potential modulation.

REFERNCES

Aleksic, M. et al., 2012. Different affinity windows for virus and cancer-specific T-cell receptors: Implications for therapeutic strategies. *European Journal of Immunology*, 42(12), pp.3174–3179.

Alexander, J. et al., 1993. Functional consequences of engagement of the T cell receptor by low affinity ligands. *The Journal of Immunology*, 150(1).

Ali, A. et al., 2001. The pattern of expression of the 5T4 oncofoetal antigen on normal, dysplastic and malignant oral mucosa. *Oral Oncology*, 37(1), pp.57–64.

Amin, K., 2012. The role of mast cells in allergic inflammation. *Respiratory Medicine*, 106(1), pp.9–14.

Andreae, S. et al., 2002. Maturation and Activation of Dendritic Cells Induced by Lymphocyte Activation Gene-3 (CD223). *The Journal of Immunology*, 168(8), pp.3874–3880.

Angiolillo, A.L. et al., 1995. Human interferon-inducible protein 10 is a potent inhibitor of angiogenesis in vivo. *The Journal of experimental medicine*, 182(1), pp.155–62.

Annunziato, F. et al., 1996. Expression and release of LAG-3-encoded protein by human CD4+ T cells are associated with IFN-gamma production. *The FASEB journal*, 10(7), pp.769–776.

Apostolou, I. & von Boehmer, H., 2004. In vivo instruction of suppressor commitment in naive T cells. *The Journal of experimental medicine*, 199(10), pp.1401–8.

Appleman, L.J. & Boussiotis, V. a, 2003. T cell anergy and costimulation. *Immunological Reviews*, 192, pp.161–180.

Baixeras, E. et al., 1992. Characterization of the lymphocyte activation gene 3-encoded protein. A new ligand for human leukocyte antigen class II antigens. *The Journal of Experimental Medicine*, 176(August), pp.327–337.

Beers, S.A., Glennie, M.J. & White, A.L., 2016. Influence of immunoglobulin isotype on therapeutic antibody function. *Blood*, 127(9), pp.1097–1101.

Beringer, D.X. et al., 2015. T cell receptor reversed polarity recognition of a self-antigen major histocompatibility complex. *Nature Immunology*, 16(11).

Besneux, M., 2015. *Elucidating the role of regulatory T cells in colorectal cancer progression*. Cardiff University.

Betts, G. et al., 2012. Suppression of tumour-specific CD4^{+} T cells by regulatory T cells is associated with progression of human colorectal cancer. *Gut*, 61(8), pp.1163–71.

Bindon, C.I. et al., 1988. Human monoclonal IgG isotypes differ in complement activating function at the level of C4 as well as C1q. *The Journal of experimental medicine*, 168(1), pp.127–42.

von Boehmer, H., 2005. Opinion: Unique features of the pre-T-cell receptor α-chain: not just a surrogate. *Nature Reviews Immunology*, 5(7), pp.571–577.

Boekema, E.J., Folea, M. & Kouřil, R., 2009. Single particle electron microscopy. *Photosynthesis research*, 102(2–3), pp.189–96.

Boesteanu, A.C. & Katsikis, P.D., 2009. Memory T cells need CD28 costimulation to remember. *Seminars in Immunology*, 21(2), pp.69–77.

Boniface, J.J. et al., 1999. Thermodynamics of T cell receptor binding to peptide-MHC: evidence for a general mechanism of molecular scanning. *Proceedings of the National Academy of Sciences of the United States of America*, 96(September), pp.11446–11451.

Boulter, J.M. et al., 2003. Stable, soluble T-cell receptor molecules for crystallization and therapeutics. *Protein Engineering Design and Selection*, 16(9), pp.707–711.

Brenner, H., Kloor, M. & Pox, C.P., 2014. Colorectal cancer. *The Lancet*, 383(9927), pp.1490–1502.

Bridgeman, J.S. et al., 2012. Structural and biophysical determinants of αβ T-cell antigen recognition. *Immunology*, 135(1), pp.9–18.

Brignone, C. et al., 2009. A phase I pharmacokinetic and biological correlative study of IMP321, a novel MHC class II agonist, in patients with advanced renal cell carcinoma. *Clinical cancer research : an official journal of the American Association for Cancer Research*, 15(19), pp.6225–31.

Brignone, C. et al., 2007. A Soluble Form of Lymphocyte Activation Gene-3 (IMP321) Induces Activation of a Large Range of Human Effector Cytotoxic Cells. *The Journal of Immunology* , 179(6), pp.4202–4211.

Brignone, C. et al., 2010. First-line chemoimmunotherapy in metastatic breast carcinoma: combination of paclitaxel and IMP321 (LAG-3Ig) enhances immune responses and antitumor activity. *Journal of translational medicine*, 8, p.71.

Brown, J., Jardetzky, T. & Gorga, J., 1993. Three-dimensional structure of the human class II histocompatibility antigen HLA-DR1. *Nature*.

Bruhns, P. et al., 2012. Properties of mouse and human IgG receptors and their contribution to disease models. *Blood*, 119(24), pp.5640–9.

Bulek, A.M. et al., 2012. TCR/pMHC Optimized Protein crystallization Screen. *Journal of immunological methods*, 382(1–2), pp.203–10.

Butler, N.S. et al., 2012. Therapeutic blockade of PD-L1 and LAG-3 rapidly clears established blood-stage Plasmodium infection. *Nature immunology*, 13(2), pp.188–95.

Camisaschi, C. et al., 2010. LAG-3 expression defines a subset of CD4(+)CD25(high)Foxp3(+) regulatory T cells that are expanded at tumor sites. *Journal of immunology (Baltimore, Md. : 1950)*, 184(11), pp.6545–51.

Cancer Research UK, 2016. Cancer Statistics for the UK. *Cancer Research UK*. Available at: http://www.cancerresearchuk.org/health-professional/cancer-statistics [Accessed September 9, 2016].

Carsberg, C.J., Myers, K.A. & Stern, P.L., 1996. Metastasis-associated 5T4 antigen disrupts cell-cell contacts and induces cellular motility in epithelial cells. *International Journal of Cancer*, 68(1), pp.84–92.

Castro, F. V et al., 2012. Regulation of autologous immunity to the mouse 5T4 oncofoetal antigen: Implications for immunotherapy. *Cancer Immunology, Immunotherapy*, 61(7), pp.1005–1018.

Center, M.M., Jemal, A. & Ward, E., 2009. International trends in colorectal cancer incidence rates. *Cancer epidemiology, biomarkers & prevention : a publication of the American Association for Cancer Research, cosponsored by the American Society of Preventive Oncology*, 18(6), pp.1688–94.

Chang, V.T. et al., 2007. Glycoprotein structural genomics: solving the glycosylation problem. *Structure (London, England : 1993)*, 15(3), pp.267–73.

Chen, J. & Chen, Z., 2014. The effect of immune microenvironment on the progression and prognosis of

colorectal cancer. *Medical Oncology*, 31(8), p.82.

Chen, S. et al., 2013. Structure-based design of altered MHC class II-restricted peptide ligands with heterogeneous immunogenicity. *Journal of immunology (Baltimore, Md. : 1950)*, 191(10), pp.5097–106.

Chothia, C., Boswell, D.R. & Lesk, A.M., 1988. The outline structure of the T-cell alpha beta receptor. *The EMBO journal*, 7(12), pp.3745–55.

Ciuffa, R. et al., 2015. The Selective Autophagy Receptor p62 Forms a Flexible Filamentous Helical Scaffold. *Cell Reports*, 11(5), pp.748–758.

Clarke, S.L. et al., 2006. CD4+CD25+FOXP3+ regulatory T cells suppress anti-tumor immune responses in patients with colorectal cancer. *PloS one*, 1(1), p.e129.

Claverie, J.M., Prochnicka-Chalufour, A. & Bougueleret, L., 1989. Implications of a Fab-like structure for the T-cell receptor. *Immunology Today*, 10(1), pp.10–14.

Clemente-Casares, X. et al., 2016. Expanding antigen-specific regulatory networks to treat autoimmunity. *Nature*, 530(7591), pp.434–440.

Cole, D. et al., 2007. Human TCR-Binding Affinity is Governed by MHC Class Restriction. *The Journal of Immunology*, 178(9), pp.5727–5734.

Cole, D. & Godkin, A., 2016. *The Peptide Ligands Presented by MHC Class II Molecules*,

Cole, D.K. et al., 2007. Computational design and crystal structure of an enhanced affinity mutant human CD8 αα coreceptor. *Proteins: Structure, Function, and Bioinformatics*, 67(1), pp.65–74.

Cole, D.K. et al., 2012. Modification of the carboxy-terminal flanking region of a universal influenza epitope alters CD4$^+$ T-cell repertoire selection. *Nature communications*, 3, p.665.

Corse, E., Gottschalk, R. a & Allison, J.P., 2011. Strength of TCR-peptide/MHC interactions and in vivo T cell responses. *Journal of immunology (Baltimore, Md. : 1950)*, 186(9), pp.5039–45.

Corthay, A. et al., 2005. Primary antitumor immune response mediated by CD4+ T cells. *Immunity*, 22(3), pp.371–83.

Curiel, T.J. et al., 2004. Specific recruitment of regulatory T cells in ovarian carcinoma fosters immune privilege and predicts reduced survival. *Nature medicine*, 10(9), pp.942–949.

Czerkinsky, C.C. et al., 1983. A solid-phase enzyme-linked immunospot (ELISPOT) assay for enumeration of specific antibody-secreting cells. *Journal of Immunological Methods*, 65(1–2), pp.109–121.

Dai, S. et al., 2008. Crossreactive T Cells Spotlight the Germline Rules for alphabeta T Cell-Receptor Interactions with MHC Molecules. *Immunity*, 28(3), pp.324–334.

Danev, R. & Baumeister, W., 2016. Cryo-EM single particle analysis with the Volta phase plate. *eLife*, 5(6220), p.e13046.

Davis, M.M. & Bjorkman, P.J., 1988. T-cell antigen receptor genes and T-cell recognition. *Nature*, 334(6181), pp.395–402.

Deng, L. et al., 2007. Structural basis for the recognition of mutant self by a tumor-specific, MHC class II-restricted T cell receptor. *Nature immunology*, 8(4), pp.398–408.

Denzin, L.K. & Cresswell, P., 1995. HLA-DM induces clip dissociation from MHC class II alphabeta dimers and facilitates peptide loading. *Cell*, 82(1), pp.155–165.

Deo, S.S. et al., 2010. Role played by Th2 type cytokines in IgE mediated allergy and asthma. *Lung India : official organ of Indian Chest Society*, 27(2), pp.66–71.

Dighe, A.S. et al., 1994. Enhanced in vivo growth and resistance to rejection of tumor cells expressing dominant negative IFNγ receptors. *Immunity*, 1(6), pp.447–456.

Dolton, G. et al., 2014. Comparison of peptide-major histocompatibility complex tetramers and dextramers for the identification of antigen-specific T cells. *Clinical and experimental immunology*, 177(1), pp.47–63.

Dolton, G. et al., 2015. More tricks with tetramers: a practical guide to staining T cells with peptide-MHC multimers. *Immunology*, 146(1), pp.11–22.

Dong, C. & Martinez, G.J., 2010. T cells : the usual subsets. *Nature Reviews Immunology*, 10(9).

Dull, T. et al., 1998. A third-generation lentivirus vector with a conditional packaging system. *Journal of virology*, 72(11), pp.8463–71.

Dunn, G.P. et al., 2002. Cancer immunoediting : from immuno- surveillance to tumor escape. *New York*, 3(11), pp.991–998.

Egelman, E.H., 2016. The Current Revolution in Cryo-EM. *Biophysical Journal*, 110(5), pp.1008–1012.

Elkord, E. et al., 2008. CD4+ T-cell recognition of human 5T4 oncofoetal antigen: Implications for initial depletion of CD25+ T cells. *Cancer immunology immunotherapy CII*, 57(6), pp.833–847.

Emsley, P. & Cowtan, K., 2004. Coot: Model-building tools for molecular graphics. *Acta Crystallographica Section D: Biological Crystallography*, 60(12 I), pp.2126–2132.

Eto, D. et al., 2011. IL-21 and IL-6 are critical for different aspects of B cell immunity and redundantly induce optimal follicular helper CD4 T cell (Tfh) differentiation. *PLoS ONE*, 6(3).

Falk, K. et al., 1991. Allele-specific motifs revealed by sequencing of self-peptides eluted from MHC molecules. *Nature*, 351(6324), pp.290–296.

Fearon, E.R., 2011. Molecular Genetics of Colorectal Cancer. *Annual Review of Pathology: Mechanisms of Disease*, 6(1), pp.479–507.

Fehling, H. et al., 1995. Crucial role of the pre-T-cell receptor alpha gene in development of alpha beta but not gamma delta T cells. *Nature*, 375(6534), pp.795–798.

Fellner, C., 2012. Ipilimumab (Yervoy) Prolongs Survival In Advanced Melanoma Serious Side Eff ects and a Hefty Price Tag May Limit Its Use. *P&T*, 37(9), pp.503–512.

Feng, D. et al., 2007. Structural evidence for a germline-encoded T cell receptor-major histocompatibility complex interaction "codon". *Nature Immunology*, 8(9), pp.975–83.

Frayser, M. et al., 1999. Empty and peptide-loaded class II major histocompatibility complex proteins produced by expression in Escherichia coli and folding in vitro. *Protein expression and purification*, 15(1), pp.105–14.

Fukaura, H. et al., 1996. Induction of circulating myelin basic protein and proteolipid protein-specific transforming growth factor-beta1-secreting Th3 T cells by oral administration of myelin in multiple sclerosis patients. *The Journal of clinical investigation*, 98(1), pp.70–7.

Gagliani, N. et al., 2013. Coexpression of CD49b and LAG-3 identifies human and mouse T regulatory type 1 cells. *Nat Med*, 19(6), pp.739–746.

Gallegos, A.M. et al., 2016. Control of T cell antigen reactivity via programmed TCR downregulation.

Nature Immunology, 17(4), pp.379–386.

Gallegos, A.M. & Bevan, M.J., 2004. Central tolerance to tissue-specific antigens mediated by direct and indirect antigen presentation. *The Journal of Experimental Medicine*, 200(8), pp.1039–49.

Galon, J. et al., 2006. Type, density, and location of immune cells within human colorectal tumors predict clinical outcome. *Science (New York, N.Y.)*, 313(5795), pp.1960–4.

Gandhi, M.K. et al., 2006. Expression of LAG-3 by tumor-infiltrating lymphocytes is coincident with the suppression of latent membrane antigen-specific CD8+ T-cell function in Hodgkin lymphoma patients. *Blood*, 108(7), pp.2280–9.

Gao, G.F. et al., 2000. Classical and Nonclassical Class I Major Histocompatibility Complex Molecules Exhibit Subtle Conformational Differences That Affect Binding to CD8alpha alpha. *Journal of Biological Chemistry*, 275(20), pp.15232–15238.

Garboczi, D.N.D.D.N. et al., 1996. Structure of the complex between human T-cell receptor, viral peptide and HLA-A2. *Nature*, 384(6605), pp.134–141.

Garcia, K.C. et al., 1996. An alphabeta T cell receptor structure at 2.5 A and its orientation in the TCR-MHC complex. *Science (New York, N.Y.)*, 274(5285), pp.209–19.

Garcia, K.C. et al., 2009. The molecular basis of TCR germline bias for MHC is surprisingly simple. *Nature immunology*, 10(2), pp.143–7.

Garcia, K.C. & Wilson, I.A., 1999. Structural Basis of T cell Recognition. *Annual review of immunology*, 17, pp.369–397.

Germain, R.N., 2002. T-cell development and the CD4-CD8 lineage decision. *Nature reviews. Immunology*, 2(5), pp.309–322.

Glassman, P.M. & Balthasar, J.P., 2014. Mechanistic considerations for the use of monoclonal antibodies for cancer therapy. *Cancer biology & medicine*, 11(July 2013), pp.20–33.

Godfrey, D.I. et al., 2015. The burgeoning family of unconventional T cells. *Nature Immunology*, 16(11), pp.1114–1123.

Godkin, A.J.A.A.J. et al., 2001. Naturally Processed HLA Class II Peptides Reveal Highly Conserved Immunogenic Flanking Region Sequence Preferences That Reflect Antigen Processing Rather Than Peptide-MHC Interactions. *The Journal of Immunology* , 166(11), pp.6720–6727.

Gol-Ara, M. et al., 2012. The role of different subsets of regulatory T cells in immunopathogenesis of rheumatoid arthritis. *Arthritis*, 2012, p.805875.

Goldberg, M. & Drake, C., 2011. LAG3 in tumour immunology.pdf. In G. Dranoff, ed. *Cancer Immunology and Immunotherapy SE - 114*. Current Topics in Microbiology and Immunology. Springer Berlin Heidelberg, pp. 269–278.

Griffin, T. a et al., 1998. Immunoproteasome assembly: cooperative incorporation of interferon gamma (IFN-gamma)-inducible subunits. *The Journal of experimental medicine*, 187(1), pp.97–104.

Guilliams, M. et al., 2014. The function of Fcγ receptors in dendritic cells and macrophages. *Nature Reviews Immunology*, 14(2), pp.94–108.

Gunther, S. et al., 2010. Bidirectional binding of invariant chain peptides to an MHC class II molecule. *Proceedings of the National Academy of Sciences*, 107(51), pp.22219–22224.

Haggar, F.A. & Boushey, R.P., 2009. Colorectal cancer epidemiology: incidence, mortality, survival, and

risk factors. *Clinics in colon and rectal surgery*, 22(4), pp.191–7.

Hanahan, D. & Weinberg, R.A., 2011. Hallmarks of cancer: the next generation. *Cell*, 144(5), pp.646–674.

Hancock, D.C. & OReilly, N.J., 2005. Synthetic Peptides as Antigens for Antibody Production. In *Immunochemical Protocols*. Totowa, NJ: Humana Press, pp. 13–25.

Hannier, S. et al., 1998. CD3/TCR Complex-Associated Lymphocyte Activation Gene-3 Molecules Inhibit CD3/TCR Signaling. *The Journal of Immunology* , 161(8), pp.4058–4065.

Harding, C. V. & Geuze, H.J., 1992. Class II MHC molecules are present in macrophage lysosomes and phagolysosomes that function in the phagocytic processing of listeria monocytogenes for presentation to T cells. *Journal of Cell Biology*, 119(3), pp.531–542.

Harding, F.A. et al., 2010. The immunogenicity of humanized and fully human antibodies. *Landes Bioscience*, 2(3), pp.256–265.

Harrop, R., Ryan, M.G., et al., 2006. Active treatment of murine tumors with a highly attenuated vaccinia virus expressing the tumor associated antigen 5T4 (TroVax) is CD4+ T cell dependent and antibody mediated. *Cancer Immunology, Immunotherapy*, 55(9), pp.1081–1090.

Harrop, R. et al., 2013. Vaccination of castration-resistant prostate cancer patients with TroVax (MVA-5T4) in combination with docetaxel: A randomized phase II trial. *Cancer Immunology, Immunotherapy*, 62(9), pp.1511–1520.

Harrop, R., Connolly, N., et al., 2006. Vaccination of colorectal cancer patients with modified vaccinia Ankara delivering the tumor antigen 5T4 (TroVax) induces immune responses which correlate with disease control: A phase I/II trial. *Clinical Cancer Research*, 12(11 I), pp.3416–3424.

Harrop, R. et al., 2007. Vaccination of colorectal cancer patients with modified vaccinia ankara encoding the tumor antigen 5T4 (TroVax) given alongside chemotherapy induces potent immune responses. *Clinical Cancer Research*, 13(15), pp.4487–4494.

Hedrick, S.M. et al., 1984. Isolation of cDNA clones encoding T cell-specific membrane-associated proteins. *Nature*, 308(5955), pp.149–153.

Hegazy, A.N. et al., 2010. Interferons Direct Th2 Cell Reprogramming to Generate a Stable GATA-3+T-bet+ Cell Subset with Combined Th2 and Th1 Cell Functions. *Immunity*, 32(1), pp.116–128.

Hennecke, J., Car, A. & Wiley, D.C., 2000. Structure of a covalently stabilized complex of a human ab T-cell receptor , in ˉuenza HA peptide and MHC class II molecule , HLA-DR1. , 19(21), pp.5611–5624.

Hennecke, J., Carfi, A. & Wiley, D.C., 2000. Structure of a covalently stabilized complex of a human alphabeta T-cell receptor, influenza HA peptide and MHC class II molecule, HLA-DR1. *The EMBO journal*, 19(21), pp.5611–5624.

Hennecke, J. & Wiley, D.C., 2002. Structure of a Complex of the Human α/β T Cell Receptor (TCR) HA1.7, Influenza Hemagglutinin Peptide, and Major Histocompatibility Complex Class II Molecule, HLA-DR4 (DRA*0101 and DRB1*0401). *Journal of Experimental Medicine*, 195(5), pp.571–581.

Hertz, C.J. et al., 2001. Microbial lipopeptides stimulate dendritic cell maturation via Toll-like receptor 2. *Journal of immunology (Baltimore, Md : 1950)*, 166(4), pp.2444–2450.

Hindley, J.P. et al., 2011. Analysis of the T-cell receptor repertoires of tumor-infiltrating conventional and regulatory T cells reveals no evidence for conversion in carcinogen-induced tumors. *Cancer research*, 71(3), pp.736–46.

Hirahara, K. et al., 2013. Mechanisms underlying helper T-cell plasticity: implications for immune-mediated disease. *The Journal of allergy and clinical immunology*, 131(5), pp.1276–87.

Hodi, F.S. et al., 2010. Improved Survival with Ipilimumab in Patients with Metastatic Melanoma. *New England Journal of Medicine*, 368(26), pp.2455–66.

Hoerter, J.A.H. et al., 2013. Coreceptor affinity for MHC defines peptide specificity requirements for TCR interaction with coagonist peptide–MHC. *The Journal of Experimental Medicine*, 210(9), pp.1807–1821.

Hogquist, K. a et al., 1992. T Cell Receptor Antagonist Peptides Induce Positive Selection. *Cell*, 76, pp.17–27.

Hole, N. & Stern, P.L., 1990. Isolation and characterization of 5T4, a tumour-associated antigen. *International Journal of Cancer*, 45(1), pp.179–184.

Holland, C.J. et al., 2012. Minimal conformational plasticity enables TCR cross-reactivity to different MHC class II heterodimers. *Scientific reports*, 2, p.629.

Holland, C.J., Cole, D.K. & Godkin, A., 2013. Re-Directing CD4(+) T Cell Responses with the Flanking Residues of MHC Class II-Bound Peptides: The Core is Not Enough. *Frontiers in immunology*, 4, p.172.

Houghton, A.N. & Guevara-Patiño, J.A., 2004. Immune recognition of self in immunity against cancer. *Journal of Clinical Investigation*, 114(4), pp.468–471.

Hsieh, C.-S., Lee, H.-M. & Lio, C.-W.J., 2012. Selection of regulatory T cells in the thymus. *Nature Reviews Immunology*, 12(3), p.157.

Huang, C.-T. et al., 2004. Role of LAG-3 in Regulatory T Cells. *Immunity*, 21(4), pp.503–513.

Huard, B. et al., 1995. CD4/major histocompatibility complex class II interaction analyzed with CD4- and lymphocyte activation gene-3 (LAG-3)-Ig fusion proteins. *European Journal of Immunology*, 25(9), pp.2718–2721.

Huard, B., Gaulard, P., et al., 1994. Cellular expression and tissue distribution of the human LAG-3-encoded protein, an MHC class II ligand. *Immunogenetics*, 39(3), pp.213–7.

Huard, B. et al., 1997. Characterization of the major histocompatibility complex class II binding site on LAG-3 protein. *Proceedings of the National Academy of Sciences of the United States of America*, 94(11), pp.5744–9.

Huard, B., Tournier, M., et al., 1994. Lymphocyte-activation gene 3/major histocompatibility complex class II interaction modulates the antigenic response of CD4+ T lymphocytes. *European Journal of Immunology*, 24(12), pp.3216–3221.

Huard, B. et al., 1996. T cell major histocompatibility complex class II molecules down-regulate CD4+ T cell clone responses following LAG-3 binding. *European Journal of Immunology*, 26(5), pp.1180–1186.

Hubackova, S. et al., 2015. IFNγ induces oxidative stress, DNA damage and tumor cell senescence via TGFβ/SMAD signaling-dependent induction of Nox4 and suppression of ANT2. *Oncogene*,

35(March), pp.1–14.

Idusogie, E.E. et al., 2000. Mapping of the C1q Binding Site on Rituxan, a Chimeric Antibody with a Human IgG1 Fc. *The Journal of Immunology*, 164(8), pp.4178–4184.

Iouzalen, N. et al., 2001. LAP, a lymphocyte activation gene-3 (LAG-3)-associated protein that binds to a repeated EP motif in the intracellular region of LAG-3, may participate in the down-regulation of the CD3/TCR activation pathway. *European Journal of …*, 3(10), pp.2885–2891.

Irvine, D. et al., 2002. Direct observation of ligand recognition by T cells. *Nature*, 419(6909), pp.845–849.

Isaacs, J.D., Greenwood, J. & Waldmann, H., 1998. Therapy with monoclonal antibodies. II. The contribution of Fc gamma receptor binding and the influence of C(H)1 and C(H)3 domains on in vivo effector function. *Journal of immunology (Baltimore, Md. : 1950)*, 161(8), pp.3862–9.

Isobe, M. et al., 1986. The gene encoding the T-cell surface protein T4 is located on human chromosome 12. *Proceedings of the National Academy of Sciences of the United States of America*, 83(June), pp.4399–4402.

Itakura, E. et al., 2011. IL-10 expression by primary tumor cells correlates with melanoma progression from radial to vertical growth phase and development of metastatic competence. *Modern pathology : an official journal of the United States and Canadian Academy of Pathology, Inc*, 24(6), pp.801–9.

Itano, A.A. & Jenkins, M.K., 2003. Antigen presentation to naive CD4 T cells in the lymph node. *Nat Immunol*, 4(8), pp.733–739.

James, J.R. & Vale, R.D., 2012. Biophysical mechanism of T-cell receptor triggering in a reconstituted system. *Nature*, 487(7405), p.64.

Janeway, C.A. & Medzhitov, R., 2002. Innate Immune Recognition. *Annual Review of Immunology*, 20(1), pp.197–216.

Jespers, L.S. et al., 1994. Guiding the selection of human antibodies from phage display repertoires to a single epitope of an antigen. *Biotechnology (Nature Publishing Company)*, 12(9), pp.899–903.

Jones, E.Y. et al., 2006. MHC class II proteins and disease: a structural perspective. *Nature reviews. Immunology*, 6(4), pp.271–82.

Jönsson, P. et al., 2016. Remarkably low affinity of CD4/peptide-major histocompatibility complex class II protein interactions. *Proceedings of the National Academy of Sciences*, p.201513918.

Jung, D. et al., 2006. Mechanism and Control of V(d)j Recombination at the Immunoglobulin Heavy Chain Locus. *Annual Review of Immunology*, 24(1), pp.541–570.

Kagermeier-Schenk, B. et al., 2011. Waif1/5T4 inhibits Wnt/β-catenin signaling and activates noncanonical Wnt pathways by modifying LRP6 subcellular localization. *Developmental cell*, 21(6), pp.1129–43.

Kaiko, G.E. et al., 2008. Immunological decision-making: How does the immune system decide to mount a helper T-cell response? *Immunology*, 123(3), pp.326–338.

Kambayashi, T. & Laufer, T.M., 2014. Atypical MHC class II-expressing antigen-presenting cells: can anything replace a dendritic cell? *Nature reviews. Immunology*, 14(11), pp.719–30.

Kappler, J.W., Roehm, N. & Marrack, P., 1987. T cell tolerance by clonal elimation in the thymus. *Cell*,

49, pp.273–280.

Kisielow, M. et al., 2005. Expression of lymphocyte activation gene 3 (LAG-3) on B cells is induced by T cells. *European Journal of Immunology*, 35, pp.2081–2088.

Lanzavecchia, A., 1990. Receptor-mediated antigen uptake and its effect on antigen presentation to class II-restricted T lymphocytes. *Annual review of immunology*, 8(c), pp.773–793.

Larkin, J. et al., 2015. Combined Nivolumab and Ipilimumab or Monotherapy in Untreated Melanoma. *New England Journal of Medicine*, p.150531115012002.

Lefranc, M.-P., 2008. IMGT®, the International ImMunoGeneTics Information System® for Immunoinformatics. *Molecular Biotechnology*, 40(1), pp.101–111.

Li, F.-J. et al., 2013. Expression of LAG-3 is coincident with the impaired effector function of HBV-specific CD8+ T cell in HCC patients. *Immunology Letters*, 150(1), pp.116–122.

Li, N. et al., 2004. Biochemical analysis of the regulatory T cell protein lymphocyte activation gene-3 (LAG-3; CD223). *The Journal of ...*, 3(11), pp.6806–6812.

Li, N. et al., 2007. Metalloproteases regulate T-cell proliferation and effector function via LAG-3. *The EMBO journal*, 26(2), pp.494–504.

Li, Y. et al., 2005. Structure of a human autoimmune TCR bound to a myelin basic protein self-peptide and a multiple sclerosis-associated MHC class II molecule. *The EMBO journal*, 24(17), pp.2968–79.

Liang, B. et al., 2008. Regulatory T Cells Inhibit Dendritic Cells by Lymphocyte Activation Gene-3 Engagement of MHC Class II. *The Journal of Immunology*, 180(9), pp.5916–5926.

Liang, S., Zhang, W. & Horuzsko, A., 2006. Human ILT2 receptor associates with murine MHC class I moleculesin vivo and impairs T cell function. *European Journal of Immunology*, 36(9), pp.2457–2471.

Liu, M., Guo, S. & Stiles, J.K., 2011. The emerging role of CXCL10 in cancer. *Oncology Letters*, 2(4), pp.583–589.

Lonberg, N., 2005. Human antibodies from transgenic animals. *Nature biotechnology*, 23(9), pp.1117–1125.

London, C. a., Lodge, M.P. & Abbas, a. K., 2000. Functional responses and costimulator dependence of memory CD4+ T cells. *J Immunol*, 164(1), pp.265–272.

Ma, Y. et al., 2002. Hairpin opening and overhang processing by an Artemis/DNA-dependent protein kinase complex in nonhomologous end joining and V(D)J recombination. *Cell*, 108(6), pp.781–794.

Magnani, C.F. et al., 2011. Killing of myeloid APCs via HLA class I, CD2 and CD226 defines a novel mechanism of suppression by human Tr1 cells. *European Journal of Immunology*, 41(6), pp.1652–1662.

Maloy, K.J. & Powrie, F., 2001. Regulatory T cells in the control of immune pathology. *Nature Immunology*, 2(9), pp.816–822.

Mandapathil, M. et al., 2009. Increased ectonucleotidase expression and activity in regulatory T cells of patients with head and neck cancer. *Clinical Cancer Research*, 15(20), pp.6348–6357.

Mantovani, A. et al., 2004. The chemokine system in diverse forms of macrophage activation and

polarization. *Trends in Immunology*, 25(12), pp.677–686.

Matsuzaki, J. et al., 2015. Direct tumor recognition by a human CD4+ T-cell subset potently mediates tumor growth inhibition and orchestrates anti-tumor immune responses. *Scientific Reports*, 5, p.14896.

Maynard, J. & Georgiou, G., 2000. Antibody Engineering. *Annual Review of Biomedical Engineering*, 2(1), pp.339–376.

Mazza, C. et al., 2007. How much can a T-cell antigen receptor adapt to structurally distinct antigenic peptides? *The EMBO journal*, 26(7), pp.1972–1983.

McCoy, A.J., 2006. Solving structures of protein complexes by molecular replacement with Phaser. *Acta Crystallographica Section D: Biological Crystallography*, 63(1), pp.32–41.

McLaughlin, P. et al., 1998. Rituximab chimeric anti-CD20 monoclonal antibody therapy for relapsed indolent lymphoma: half of patients respond to a four-dose treatment program. *Journal of clinical oncology : official journal of the American Society of Clinical Oncology*, 16(8), pp.2825–33.

van der Merwe, P.A. & Dushek, O., 2011. Mechanisms for T cell receptor triggering. *Nature Reviews Immunology*, 11(1), pp.47–55.

Miyamoto, M. et al., 2003. Endogenous IL-17 as a mediator of neutrophil recruitment caused by endotoxin exposure in mouse airways. *Journal of immunology (Baltimore, Md. : 1950)*, 170(9), pp.4665–4672.

Mosmann, T.R. & Coffman, R.L., 1989. TH1 and TH2 cells: different patterns of lymphokine secretion lead to different functional properties. *Annual review of immunology*, 7, pp.145–73.

Moysey, R.K. et al., 2010. High affinity soluble ILT2 receptor: a potent inhibitor of CD8 + T cell activation. *Protein & cell*, 1(12), pp.1118–27.

Mulryan, K. et al., 2002. Attenuated recombinant vaccinia virus expressing oncofetal antigen (tumor-associated antigen) 5T4 induces active therapy of established tumors. *Molecular cancer therapeutics*, 1(October), pp.1129–1137.

Murshudov, G.N. et al., 2011. REFMAC5 for the refinement of macromolecular crystal structures. *Acta Crystallographica Section D: Biological Crystallography*, 67(4), pp.355–367.

Nathan, C.F. et al., 1983. Identification of interferon-gamma as the lymphokine that activates human macrophage oxidative metabolism and antimicrobial activity. *The Journal of experimental medicine*, 158(3), pp.670–89.

Nelson, C.A. et al., 1992. Identification of the naturally processed form of hen egg white lysozyme bound to the murine major histocompatibility complex class II molecule I-Ak. *Proceedings of the National Academy of Sciences of the United States of America*, 89(16), pp.7380–3.

Nelson, C.A., Petzold, S.J. & Unanue, E.R., 1994. Peptides determine the lifespan of MHC class II molecules in the antigen-presenting cell. *Nature*, 371(6494), pp.250–252.

Neuberger, M.S. & Rajewsky, K., 1981. Activation of mouse complement by monoclonal mouse antibodies. *European Journal of Immunology*, 11(12), pp.1012–1016.

Nielsen, M. & Lund, O., 2009. NN-align. An artificial neural network-based alignment algorithm for MHC class II peptide binding prediction. *BMC bioinformatics*, 10(1), p.296.

Nimmerjahn, F. & Ravetch, J. V., 2008. Fcγ receptors as regulators of immune responses. *Nature Reviews*

Immunology, 8(1), pp.34–47.

O'Brien, C., Flower, D.R. & Feighery, C., 2008. Peptide length significantly influences in vitro affinity for MHC class II molecules. *Immunome research*, 4, p.6.

Okazaki, T. et al., 2011. PD-1 and LAG-3 inhibitory co-receptors act synergistically to prevent autoimmunity in mice. *J Exp Med*, 208(2), pp.395–407.

Onishi, Y. et al., 2008. Foxp3+ natural regulatory T cells preferentially form aggregates on dendritic cells in vitro and actively inhibit their maturation. *Proceedings of the National Academy of Sciences of the United States of America*, 105(29), pp.10113–8.

Painter, C.A. & Stern, L.J., 2012. Conformational variation in structures of classical and non-classical MHCII proteins and functional implications. *Immunological reviews*, 250(1), pp.144–57.

Pandiyan, P. et al., 2007. CD4+CD25+Foxp3+ regulatory T cells induce cytokine deprivation-mediated apoptosis of effector CD4+ T cells. *Nature immunology*, 8(12), pp.1353–1362.

Parkhurst, M.R. et al., 1996. Improved induction of melanoma-reactive CTL with peptides from the melanoma antigen gp100 modified at HLA-A*0201-binding residues. *Journal of immunology (Baltimore, Md. : 1950)*, 157(6), pp.2539–2548.

Pedroza-Gonzalez, A. et al., 2015. Tumor-infiltrating plasmacytoid dendritic cells promote immunosuppression by Tr1 cells in human liver tumors. *Oncoimmunology*, 4(6), p.e1008355.

Peggs, K.S. et al., 2009. Blockade of CTLA-4 on both effector and regulatory T cell compartments contributes to the antitumor activity of anti-CTLA-4 antibodies. *The Journal of experimental medicine*, 206(8), pp.1717–1725.

Peled, J.U. et al., 2008. The biochemistry of somatic hypermutation. *Annual Review of Immunology*, 26(1), pp.481–511.

Pettersen, E.F. et al., 2004. UCSF Chimera - A visualization system for exploratory research and analysis. *Journal of Computational Chemistry*, 25(13), pp.1605–1612.

Poirier, N. et al., 2011. Antibody-mediated depletion of lymphocyte-activation gene-3 (LAG-3(+))-activated T lymphocytes prevents delayed-type hypersensitivity in non-human primates. *Clinical and experimental immunology*, 164(2), pp.265–74.

Pollizzi, K.N. & Powell, J.D., 2014. Integrating canonical and metabolic signalling programmes in the regulation of T cell responses. *Nature reviews. Immunology*, 14(7), pp.435–46.

Ponz de Leon, M. & Di Gregorio, C., 2001. Pathology of colorectal cancer. *Digestive and liver disease : official journal of the Italian Society of Gastroenterology and the Italian Association for the Study of the Liver*, 33(4), pp.372–88.

Poons, P.H., Phillips, M.L. & Schumaker, N., 1985. Immunoglobulin M Possesses Two Binding Sites for Complement Subcomponent C1q , and Soluble and Soluble 1:1 and 2:1 Complexes Are Formed in Solution at Reduced Ionic Strength. *Journal of Biological Chemistry*, 260(84), pp.9357–9365.

Potts, W.K. & Slev, P.R., 1995. Pathogen-based models favoring MHC genetic diversity. *Immunological reviews*, 143(143), pp.181–197.

Powell, S.M. et al., 1992. APC mutations occur early during colorectal tumorigenesis. *Nature*, 359(6392), pp.235–237.

Propper, D.J. et al., 2003. Low-dose IFN-gamma induces tumor MHC expression in metastatic malignant

melanoma. *Clinical Cancer Research*, 9(1), pp.84–92.

Qureshi, O.S. et al., 2011. Trans-endocytosis of CD80 and CD86 : a molecular basis for the cell extrinsic function of CTLA-4. *Science*, 332(6029), pp.600–603.

Rames, M., Yu, Y. & Ren, G., 2014. Optimized negative staining: a high-throughput protocol for examining small and asymmetric protein structure by electron microscopy. *Journal of visualized experiments : JoVE*, (90), p.e51087.

Rammensee, H.-G., Friede, T. & Stevanovid, S., 1995. MHC ligands and peptide motifs: first listing. *Immunogenetics*, 41, pp.178–228.

Rammensee, H.G., 1995. Chemistry of peptides associated with MHC class I and class II molecules. *Current opinion in immunology*, 7(1), pp.85–96.

Redchenko, I. et al., 2006. Identification of a major histocompatibility complex class I-restricted T-cell epitope in the tumour-associated antigen, 5T4. *Immunology*, 118(1), pp.50–57.

Relf, M. et al., 1997. Expression of the Angiogenic Factors Vascular Endothelial Cell Growth Factor, Acidic and Basic Fibroblast Growth Factor, Tumor Growth Factor β-1, Platelet-derived Endothelial Cell Growth Factor, Placenta Growth Factor, and Pleiotrophin in Human Primary Br. *Cancer Research*, 57(5), pp.963–969.

Robinson, J. et al., 2015. The IPD and IMGT/HLA database: Allele variant databases. *Nucleic Acids Research*, 43(D1), pp.D423–D431.

Rossjohn, J. et al., 2015. T cell antigen receptor recognition of antigen-presenting molecules. *Annual review of immunology*, 33, pp.169–200.

Rudolph, M.G., Stanfield, R.L. & Wilson, I. a, 2006. How TCRs bind MHCs, peptides, and coreceptors. *Annual review of immunology*, 24, pp.419–66.

Sakaguchi, S., 2005. Naturally arising Foxp3-expressing CD25+CD4+ regulatory T cells in immunological tolerance to self and non-self. *Nature immunology*, 6(4), pp.345–52.

Sakaguchi, S. et al., 2009. Regulatory T cells: how do they suppress immune responses? *International immunology*, 21(10), pp.1105–11.

Sant'Angelo, D.B. et al., 2002. Recognition of core and flanking amino acids of MHC class II-bound peptides by the T cell receptor. *European Journal of Immunology*, 32(9), pp.2510–2520.

Sato, T. et al., 2011. Interleukin 10 in the tumor microenvironment: A target for anticancer immunotherapy. *Immunologic Research*, 51(2–3), pp.170–182.

Schatz, D.G. & Swanson, P.C., 2011. V(D)J Recombination: Mechanisms of Initiation. *Annual Review of Genetics*, 45(D), pp.167–202.

Scheres, S.H.W. & Chen, S., 2012. Prevention of overfitting in cryo-EM structure determination. *Nature Methods*, 9(9), pp.853–854.

Scurr, M. et al., 2013. Escalating regulation of 5T4-specific IFN-γ(+) CD4(+) T cells distinguishes colorectal cancer patients from healthy controls and provides a target for in vivo therapy. *Cancer immunology research*, 1(6), pp.416–426.

Scurr, M. et al., 2013. Highly prevalent colorectal cancer-infiltrating LAP(+) Foxp3(-) T cells exhibit more potent immunosuppressive activity than Foxp3(+) regulatory T cells. *Mucosal immunology*, 0(July), pp.1–12.

Scurr, M.J. et al., 2015. Assessing the Prognostic Value of Preoperative Carcinoembryonic Antigen-Specific T-Cell Responses in Colorectal Cancer. *JNCI Journal of the National Cancer Institute*, 107, p.djv001-djv001.

Sega, E.I. et al., 2014. Role of lymphocyte activation gene-3 (lag-3) in conventional and regulatory T cell function in allogeneic transplantation. V. A. Boussiotis, ed. *PloS one*, 9(1), p.e86551.

Seidel, U.J.E., Schlegel, P. & Lang, P., 2013. Natural killer cell mediated antibody-dependent cellular cytotoxicity in tumor immunotherapy with therapeutic antibodies. *Frontiers in immunology*, 4, p.76.

Semba, C.P. & Gadek, T.R., 2016. Development of lifitegrast: A novel T-cell inhibitor for the treatment of dry eye disease. *Clinical Ophthalmology*, 10, pp.1083–1094.

Shankaran, V. et al., 2001. IFNγ and lymphocytes prevent primary tumour development and shape tumour immunogenicity. *Nature*, 410(6832), pp.1107–1111.

Sharma, P. & Allison, J.P., 2015. The future of immune checkpoint therapy. *Science*, 348(6230), pp.56–61.

Shiao, S.L. et al., 2007. Human Effector Memory CD4+ T Cells Directly Recognize Allogeneic Endothelial Cells In Vitro and In Vivo. *The Journal of Immunology*, 179(7), pp.4397–4404.

Shih, K., Arkenau, H.-T. & Infante, J.R., 2014. Clinical Impact of Checkpoint Inhibitors as Novel Cancer Therapies. *Drugs*.

Shimoda, K. et al., 1996. Lack of IL-4-induced Th2 response and IgE class switching in mice with disrupted Stat6 gene. *Nature*, 380, pp.630–633.

Shingler, W.H. et al., 2008. Identification and functional validation of MHC class I epitopes in the tumor-associated antigen 5T4. *International immunology*, 20(8), pp.1057–66.

Shires, J., Theodoridis, E. & Hayday, A.C., 2001. Biological insights into TCRalphabeta+ and TCRgammadelta+ intraepithelial lymphocytes provided by serial analysis of gene expression (SAGE). *Immunity*, 15(3), pp.419–434.

Sierro, S., Romero, P. & Speiser, D.E., 2011. The CD4-like molecule LAG-3, biology and therapeutic applications. *Expert opinion on therapeutic targets*, 15(1), pp.91–101.

Simpson, T.R. et al., 2013. Fc-dependent depletion of tumor-infiltrating regulatory T cells co-defines the efficacy of anti–CTLA-4 therapy against melanoma. *The Journal of Experimental Medicine*, 210(9), pp.1695–1710.

Singh, P.P. et al., 2015. Immune checkpoints and immunotherapy for colorectal cancer. *Gastroenterology report*, 3(October), p.gov053.

Southall, P.J. et al., 1990. Immunohistological distribution of 5T4 antigen in normal and malignant tissues. *British journal of cancer*, 61(1), pp.89–95.

Starzynska, T. et al., 1994. Prognostic significance of 5T4 oncofetal antigen expression in colorectal carcinoma. *British journal of cancer*, 69(5), pp.899–902.

Starzynska, T., Rahi, V. & Stern, P.L., 1992. The expression of 5T4 antigen in colorectal and gastric carcinoma. *British journal of cancer*, 66(5), pp.867–9.

Stern, L.J. et al., 1994. Crystal structure of the human class II MHC protein HLA-DR1 complexed with an influenza virus peptide. *Nature*, 368(6468), pp.215–221.

Stern, L.J. & Wiley, D.C., 1994. Antigenic peptide binding by class I and class II histocompatibility

proteins. *Structure (London, England : 1993)*, 2, pp.245–251.

Stern, L.J. & Wiley, D.C., 1992. The human class II MHC protein HLA-DR1 assembles as empty αβ heterodimers in the absence of antigenic peptide. *Cell*, 68(3), pp.465–477.

Stern, P.L. et al., 2014. Understanding and exploiting 5T4 oncofoetal glycoprotein expression. *Seminars in Cancer Biology*, 29(C), pp.13–20.

Stritesky, G.L. et al., 2013. Murine thymic selection quantified using a unique method to capture deleted T cells. *Proceedings of the National Academy of Sciences of the United States of America*, 110, pp.4679–84.

Tang, G. et al., 2007. EMAN2: An extensible image processing suite for electron microscopy. *Journal of Structural Biology*, 157(1), pp.38–46.

Tegla, C.A. et al., 2011. Membrane attack by complement: the assembly and biology of terminal complement complexes. *Immunologic research*, 51(1), pp.45–60.

The Cancer Gene Atlas et al., 2012. Comprehensive molecular characterization of human colon and rectal cancer. *Nature*, 487(7407), pp.330–7.

Theaker, S.M. et al., 2016. T-cell libraries allow simple parallel generation of multiple peptide-specific human T-cell clones. *Journal of immunological methods*, 430, pp.43–50.

Thibodeau, J., Bourgeois-Daigneault, M.-C. & Lapointe, R., 2012. Targeting the MHC Class II antigen presentation pathway in cancer immunotherapy. *Oncoimmunology*, 1(6), pp.908–916.

Thommen, D.S. et al., 2015. Progression of Lung Cancer Is Associated with Increased Dysfunction of T Cells Defined by Coexpression of Multiple Inhibitory Receptors. *Cancer Immunology Research*, 3(12), pp.1344–1355.

Tian, X. et al., 2015. The Upregulation of LAG-3 on T Cells Defines a Subpopulation with Functional Exhaustion and Correlates with Disease Progression in HIV-Infected Subjects. *The Journal of Immunology*, 194(8), pp.3873–3882.

Topalian, S.L. et al., 2014. Survival, durable tumor remission, and long-term safety in patients with advanced melanoma receiving nivolumab. *Journal of Clinical Oncology*, 32(10), pp.1020–1030.

Tosolini, M. et al., 2011. Clinical impact of different classes of infiltrating T cytotoxic and helper cells (Th1, Th2, Treg, Th17) in patients with colorectal cancer. *Cancer Research*, 71(4), pp.1263–1271.

Triebel, F. et al., 1990. LAG-3, a novel lymphocyte activation gene closely related to CD4. *The Journal of Experimental Medicine* , 171(5), pp.1393–1405.

Triebel, F., 2003. LAG-3: a regulator of T-cell and DC responses and its use in therapeutic vaccination. *Trends in Immunology*, 24(12), pp.619–622.

Triebel, F., Hacene, K. & Pichon, M.-F., 2006. A soluble lymphocyte activation gene-3 (sLAG-3) protein as a prognostic factor in human breast cancer expressing estrogen or progesterone receptors. *Cancer letters*, 235(1), pp.147–53.

Tungatt, K. et al., 2015. Antibody Stabilization of Peptide-MHC Multimers Reveals Functional T Cells Bearing Extremely Low-Affinity TCRs. *The Journal of Immunology*, 194(1), pp.463–474.

Turner, S.J. et al., 2006. Structural determinants of T-cell receptor bias in immunity. *Nature Reviews Immunology*, 6(12), pp.883–894.

Turnis, M.E., Andrews, L.P. & Vignali, D. a. a., 2015. Inhibitory receptors as targets for cancer

immunotherapy. *European Journal of Immunology*, 45(7), pp.1892–1905.

Tykodi, S.S. et al., 2012. CD8+ T-cell clones specific for the 5T4 antigen target renal cell carcinoma tumor-initiating cells in a murine xenograft model. *Journal of immunotherapy (Hagerstown, Md. : 1997)*, 35(7), pp.523–33.

Valitutti, S. et al., 1995. Serial triggering of many T-cell receptors by a few peptide-MHC complexes. *Nature*, 375(6527), pp.148–151.

Vantourout, P. & Hayday, A., 2013. Six‑of‑the-best : unique contributions of γδ T cells to immunology. *Nature Reviews Immunology*, 13(2), pp.88–100.

Vieira, P.L. et al., 2004. IL-10-Secreting Regulatory T Cells Do Not Express Foxp3 but Have Comparable Regulatory Function to Naturally Occurring CD4 + CD25 + Regulatory T Cells. *Journal of immunology (Baltimore, Md. : 1950)*, 172(10), pp.5986–93.

Wang-Gillam, A. et al., 2013. A phase I study of IMP321 and gemcitabine as the front-line therapy in patients with advanced pancreatic adenocarcinoma. *Investigational New Drugs*, 31(3), pp.707–713.

Watts, C., 1997. Capture and processing of exogenous antigens for presentation on MHC molecules. *Annual review of immunology*, 15, pp.821–850.

Wedemayer, G.J. et al., 1997. Structural insights into the evolution of an antibody combining site. *Science (New York, N.Y.)*, 276(5319), pp.1665–9.

Wei, T. et al., 2015. Increased expression of immunosuppressive molecules on intratumoral and circulating regulatory T cells in non-small-cell lung cancer patients. *American journal of cancer research*, 5(7), pp.2190–201.

Weiner, G.J., 2015. Building better monoclonal antibody-based therapeutics. *Nature Reviews Cancer*, 15(6), pp.361–370.

Weiner, G.J., 2010. Rituximab: mechanism of action. *Seminars in hematology*, 47(2), pp.115–23.

Willimsky, G. & Blankenstein, T., 2005. Sporadic immunogenic tumours avoid destruction by inducing T-cell tolerance. *Nature*, 437(7055), pp.141–146.

Winn, M.D. et al., 2011. Overview of the CCP4 suite and current developments. *Acta Crystallographica Section D: Biological Crystallography*, 67(4), pp.235–242.

Wojciech, L. et al., 2014. The same self-peptide selects conventional and regulatory CD4(+) T cells with identical antigen receptors. *Nature communications*, 5, p.5061.

Wolf, a M. et al., 2003. Increase of regulatory T cells in the peripheral blood of cancer patients. *Clin Cancer Res*, 9(2), pp.606–612.

Woo, S.-R. et al., 2012. Immune inhibitory molecules LAG-3 and PD-1 synergistically regulate T-cell function to promote tumoral immune escape. *Cancer research*, 72(4), pp.917–27.

Woods, A.M. et al., 2002. Characterization of the murine 5T4 oncofoetal antigen: a target for immunotherapy in cancer. *The Biochemical journal*, 366(Pt 1), pp.353–365.

Wooldridge, L. et al., 2012. A single autoimmune T cell receptor recognizes more than a million different peptides. *Journal of Biological Chemistry*, 287(2), pp.1168–1177.

Workman, C.C.J., Dugger, K.J. & Vignali, D.A.A., 2002. Cutting Edge: Molecular Analysis of the Negative Regulatory Function of Lymphocyte Activation Gene-3. *The Journal of Immunology*, 169(10), pp.5392–5395.

Workman, C.C.J. & Vignali, D.A.A.D., 2003. The CD4-related molecule, LAG-3 (CD223), regulates the expansion of activated T cells. *European journal of immunology*, 3(4), pp.970–979.

Workman, C.J. et al., 2009. LAG-3 regulates plasmacytoid dendritic cell homeostasis. *Journal of immunology (Baltimore, Md. : 1950)*, 182(4), pp.1885–91.

Workman, C.J. et al., 2002. Phenotypic analysis of the murine CD4-related glycoprotein, CD223 (LAG-3). *European Journal of Immunology*, 32(8), pp.2255–2263.

Wucherpfennig, K.W., 2010. The first structures of T cell receptors bound to peptide-MHC. *Journal of immunology (Baltimore, Md. : 1950)*, 185(11), pp.6391–3.

Xu, F. et al., 2014. LSECtin expressed on melanoma cells promotes tumor progression by inhibiting antitumor T-cell responses. *Cancer research*, 74(13), pp.3418–28.

Yin, Y., Wang, X.X. & Mariuzza, R.A., 2012. Crystal structure of a complete ternary complex of T-cell receptor, peptide-MHC, and CD4. *Proceedings of the National Academy of Sciences of the United States of America*, 109(14), pp.5405–10.

Zavala-Ruiz, Z. et al., 2004. A hairpin turn in a class II MHC-bound peptide orients residues outside the binding groove for T cell recognition. *Proceedings of the National Academy of Sciences of the United States of America*, 101(36), pp.13279–84.

Zhang, X. et al., 2008. Near-atomic resolution using electron cryomicroscopy and single-particle reconstruction. *Proceedings of the National Academy of Sciences*, 105(6), pp.1867–1872.

Zhao, Y. et al., 2014. Structural Insights into the Inhibition of Wnt Signaling by Cancer Antigen 5T4/Wnt-Activated Inhibitory Factor 1. *Structure (London, England : 1993)*, 1(4), pp.1–9.

Zhou, G., Drake, C.G. & Levitsky, H.I., 2006. Amplification of tumor-specific regulatory T cells following therapeutic cancer vaccines. *Blood*, 107(2), pp.628–36.

APPENDIX

Appendix 1

Lymphoprep™ – Axis-Shield

CD4 MicroBeads, human – Miltenyi Biotec

Human T-Activator CD3/CD28 Dynabeads® – Life Technologies

IFNγ Secretion Assay Cell Enrichment and Detection Kit (PE), human – Miltenyi Biotec

Human IFNγ ELISpot^{BASIC} (ALP) – Mabtech

AP Conjugate Substrate Kit #1706432 – Bio-Rad

Human IFN-gamma DuoSet ELISA kit – R&D Systems

Human TNF-alpha DuoSet ELISA kit – R&D Systems

Human CCL4/MIP-1 beta DuoSet ELISA kit – R&D Systems

HRP Substrate Reagent Pack – R&D Systems

Stop Solution 2N Sulfuric Acid – R&D Systems

Roswell Park Memorial Institute (RPMI) 1640 media – Gibco, Life Technologies

Foetal calf serum (FCS) – Gibco, Life Technologies

L-Glutamine – Gibco, Life Technologies

Penicillin-Streptomycin – Gibco, Life Technologies

4-(2-hydroxyethyl)-1-piperazineethanesulfonic acid (HEPES) – Fisher Scientific

Non-essential amino acids – Gibco, Life Technologies

Sodium pyruvate – Gibco, Life Technologies

Human recombinant IL-2 (Proleukin®) – provided by University Hospital of Wales Pharmacy

LIVE/DEAD® Fixable Violet Dead Cell Stain – Invitrogen

Dimethyl sulfoxide (DMSO) – Sigma-Aldrich

Phytohaemagglutinin (PHA) – Alere Medical Inc.

Rosetta™(DE3) Competent Cells – Novagen

Carbenicillin – Carbenicillin Direct

Tryptone – Fisher Scientific

Yeast Extract – Fisher Scientific

Potassium Phosphate Dibasic (K_2HPO_4) – Acros Organics

Sodium Chloride (NaCl) – Fisher Scientific

Agar Bacteriological – Thermo Scientific

2-Amino-2-hydroxymethyl-propane-1,3-diol (Tris) – Fisher Scientific

Ethylenediaminetetraacetic acid (EDTA) – Sigma Aldrich

Isopropyl β-D-1-thiogalactopyranoside (IPTG) – Generon

5 mL Hi-Trap Q Sepharose HP anion exchange columns – GE Healthcare Life Science

One Shot® TOP10 Chemically Competent E. coli – Life Technologies

FastDigest BamHI - ThermoFisher

FastDigest EcoRI - ThermoFisher

Tris base – Sigma-Aldrich

NaCl – Sigma-Aldrich

Urea – Sigma-Aldrich

Triton X-100 – Sigma-Aldrich

Dithiothreitol (DTT) – Sigma-Aldrich

TOPS crystallization Screen– Custom Formulation by Molecular Dimensions

PACT premier™ MD1-29 crystallization screen – Molecular Dimensions

JBScreen PEG/Salt HTS CS-205L crystallization screen – Jena Bioscience GmbH

ARI INTELLI-PLATE 96-2 Low Volume Reservoir plates – Art Robbins Instruments, LLC.

ClearVue™ Sealing Sheets – Molecular Dimensions

MicroSeed Beads™ kit – Hampton Research

EasyXtal X-Seal crystal supports – Qaigen

EasyXtal 15-well DG plates – Qaigen

20 µm Mounted Round LithoLoops – Molecular Dimensions

40 µm Mounted Round LithoLoops – Molecular Dimensions

Roswell Park Memorial Institute (RPMI) 1640 media – Gibco, Life Technologies

Foetal calf serum (FCS) – Gibco, Life Technologies

Dimethyl sulfoxide (DMSO) – Sigma-Aldrich

L-Glutamine – Gibco, Life Technologies

Penicillin-Streptomycin – Gibco, Life Technologies

XbaI FastDigest restriction endonuclease – Thermo Scientific

XhoI FastDigest restriction endonuclease – Thermo Scientific

FastDigest restriction endonuclease 10x Green buffer - Thermo Scientific

UltraPure™ Agarose – Life Technologies

HyperLadder™ 1kb DNA molecular weight marker – Bioline

QIAquick Gel Extraction Kit – Qiagen

XL10 Gold Ultracompetent cells – Agilent Technologies

T4 DNA ligase – Life Technologies

DNA ligase buffer – Life Technologies

Carbenicillin – Carbenicillin Direct

Tryptone – Fisher Scientific

Yeast Extract – Fisher Scientific

Potassium Phosphate Dibasic (K_2HPO_4) – Acros Organics

Sodium Chloride (NaCl) – Fisher Scientific

Agar Bacteriological – Thermo Scientific

Zippy Plasmid DNA mini-prep kit – Zymo Research

PureLink® HiPure Plasmid Filter Maxiprep Kit – Life Technologies

2-Amino-2-hydroxymethyl-propane-1,3-diol (Tris) – Fisher Scientific

4-(2-hydroxyethyl)-1-piperazineethanesulfonic acid (HEPES) – Fisher Scientific

Ethylenediaminetetraacetic acid (EDTA) – Sigma Aldrich

Hydrogen Chloride (HCl) – Fisher Scientific

Sodium Hydroxide (NaOH) – Fisher Scientific

Calcium chloride dihydrate ($CaCl_2 \cdot 2H_2O$) – Sigma Aldrich

Sodium phosphate dibasic anhydrous (Na_2HPO_4) – Sigma Aldrich

Series S CM5 Sensor Chip – GE Healthcare Life Sciences

N-(3-dimethylaminopropyl)-N3-ethylcarbodiimide (EDC) – GE Healthcare Life Sciences

N-hydroxysuccinimide (NHS) – GE Healthcare Life Sciences

Streptavidin solution in 10 mM acetate pH 4.5 – Sigma-Aldrich

1 M ethanolamine – GE Healthcare Life Sciences

Sodium citrate dihydrate – Sigma-Aldrich

L-Arginine – Sigma-Aldrich

Tween-20 – Sigma-Aldrich

Citric acid – Sigma-Aldrich

2 % Uranyl acetate – Agar Scientific

Carbon Films on 400 Mesh Grids Copper – Agar Scientific

Filter paper (Whatman No.1 filter papers) – GE Heathcare Life Sciences

LAG-3:Fc fusion protein – Adipogen

Freund's Complete Adjuvant (CFA) – Sigma-Aldrich

Freund's incomplete adjuvant (IFA) – Sigma-Aldrich

HRP Substrate Reagent Pack – R&D Systems

Stop Solution 2N Sulfuric Acid – R&D Systems

Bovine Serum Albumin (BSA) – Sigma Aldrich

Roswell Park Memorial Institute (RPMI) 1640 media – Gibco, Life Technologies

Foetal calf serum (FCS) – Gibco, Life Technologies

L-Glutamine – Gibco, Life Technologies

Penicillin-Streptomycin – Gibco, Life Technologies

Ultra-Low IgG Fetal Bovine Serum (Ig⁻ FCS) – ThermoFisher Scientific

INTEGRA CELLine flasks – INTEGRA Biosciences AG

Tween® 20 – Sigma Aldrich

Sodium Chloride (NaCl) – Fisher Scientific

Tris – Sigma Aldrich

Triton X-100 – Sigma Aldrich

Invitrolon™ 0.45 μm Pore PVDF/Filter Paper Sandwich – ThermoFisher Scientific

100 % isopropanol – Fisher Chemicals

Bolt® Transfer Buffer – ThermoFisher Scientific

Marvel Whole Skimmed Milk Powder – Premier Foods Group Ltd

Pierce™ ECL Plus Western Blotting Substrate – ThermoFisher Scientific

Series S CM5 Sensor Chip – GE Healthcare Life Sciences

CM5 Sensor Chip – GE Healthcare Life Sciences

N-(3-dimethylaminopropyl)-N3-ethylcarbodiimide (EDC) – GE Healthcare Life Sciences

N-hydroxysuccinimide (NHS) – GE Healthcare Life Sciences

1 M ethanolamine – GE Healthcare Life Sciences

Appendix 2

Gene	Allele	Allele
HLA-A	*24	*11
HLA-B	*07	*51
HLA-DRB1	*01	*12
HLA-DQB1	*05	*03(7)

Appendix 2 – HLA-type of the HD216 healthy donor from which T cell clones were derived
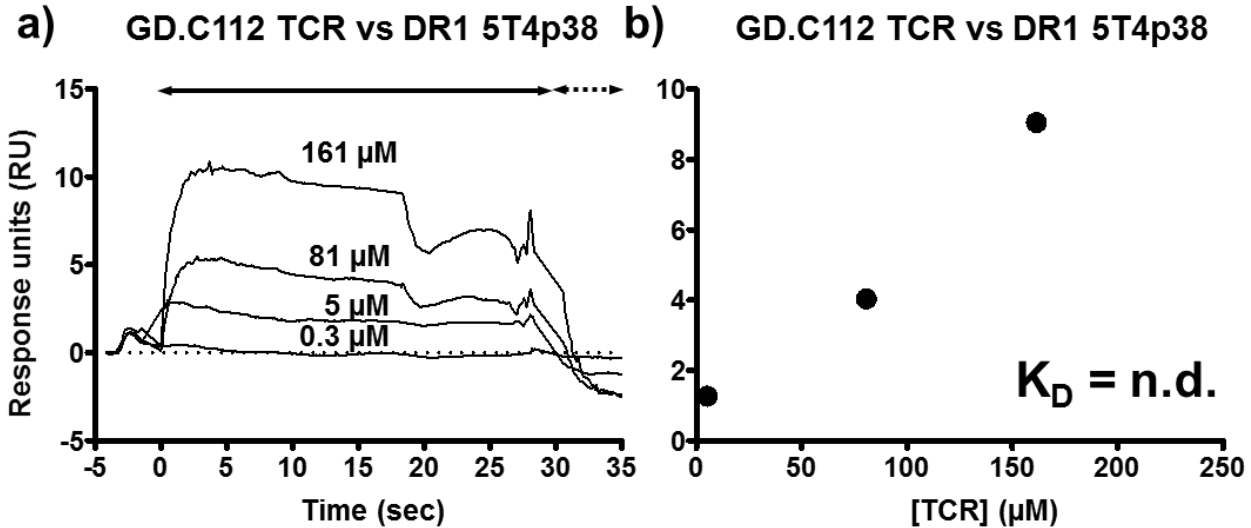
Appendix 3
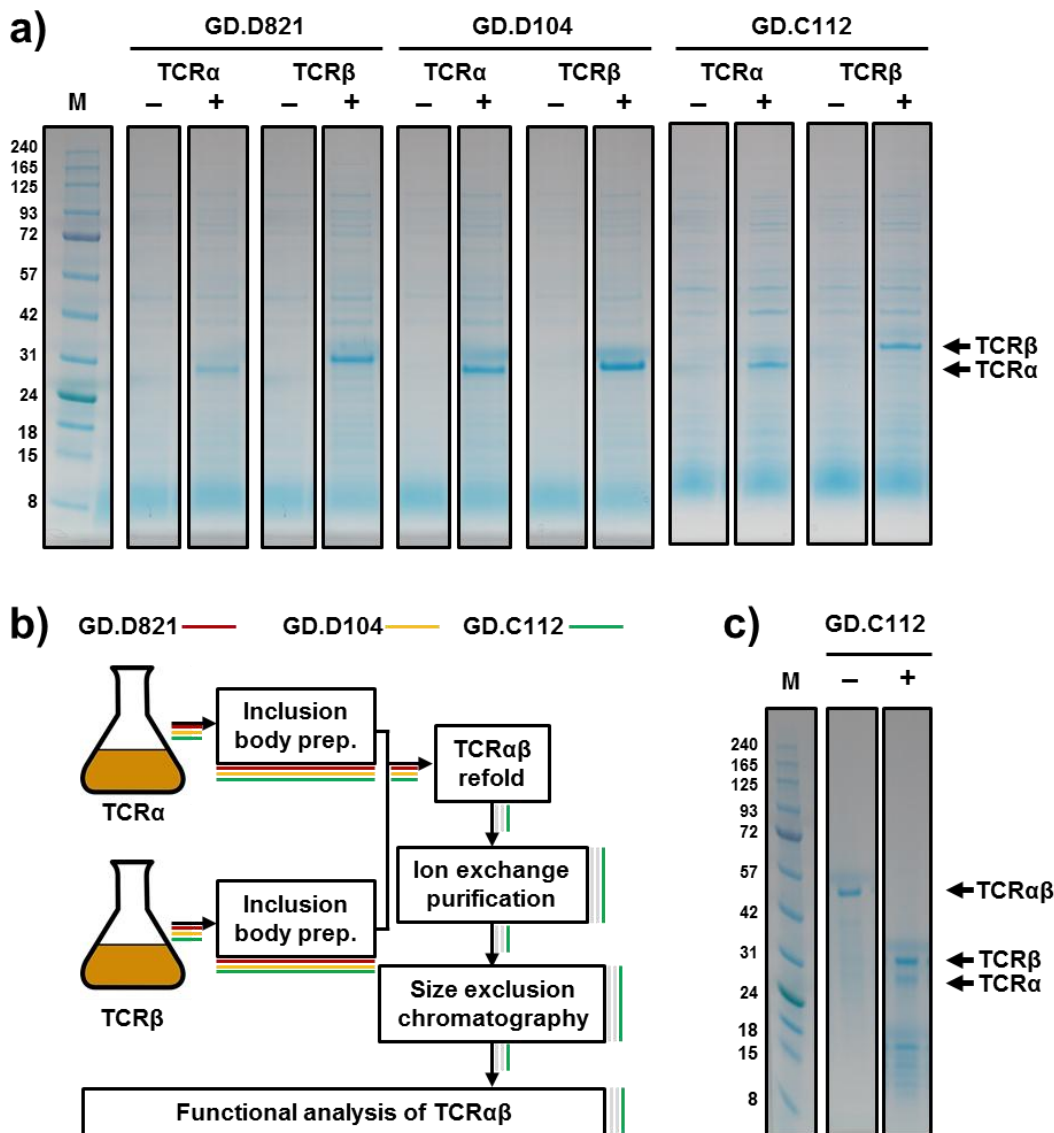
Appendix 3 – Production of 5T4-reactive TCRs for SPR analysis

a) SDS-PAGE analysis of 5T4-TCRα and -TCRβ chain inclusion body preparations produced from transformed *E. coli* cultures. TCR chains from each clone, GD.D821, GD.D104 and GD.C112, was produced as shown by additional protein band indicative of TCRα and TCRβ chains in IPTG induced (+) compared to uninduced (-) bacterial cultures.

b) Summary of the success of the TCRαβ refolding and purification pathway of each of the 5T4-reactive TCRs. GD.D821 and GD.D104 TCRs failed to successfully pass TCRαβ refolding, whilst the GD.C112 TCR was successfully refolded and purified for functional analysis.

c) SDS-PAGE analysis of refolded GD.C112 TCRαβ after processing shown in *b)* highlighting characteristic dimerization of TCRα and TCRβ chains in non-reducing conditions (-), to form TCRαβ, and subsequent dissociation to single chains in the presence of reducing conditions (+) by incubation of sample in 1 M DTT at 95 °C for 5 min.

Appendix 4 – Preliminary binding of the GD.C112 TCR to HLA-DR1 5T4p38:

a) SPR analysis of minimal but detectable binding of the GD.C112 TCR interacting with HLA-DR1 5T4p38 as shown by reference subtracted sensograms performed at 0.3 μM to 161 μM concentrations of analyte TCR. Increase in response units during TCR contact time (black arrow), particularly at highest TCR concentrations (labelled by inset numbers) indicated binding of GD.C112 TCR to 5T4p38 followed by fast dissociation kinetics upon removal of analyte (black dashed arrow)

b) Response unit differences from baseline observed during equilibrium phase of binding (10 seconds) at individual TCR ligand concentration calculated from reference subtracted sensograms shown in *a)*. TCR concentration correlated with observed signal, however, due to inability to reach saturation at high concentrations of TCR and weak signal, TCR binding affinity K_D could not be calculated by a reliable non-linear curve fit.
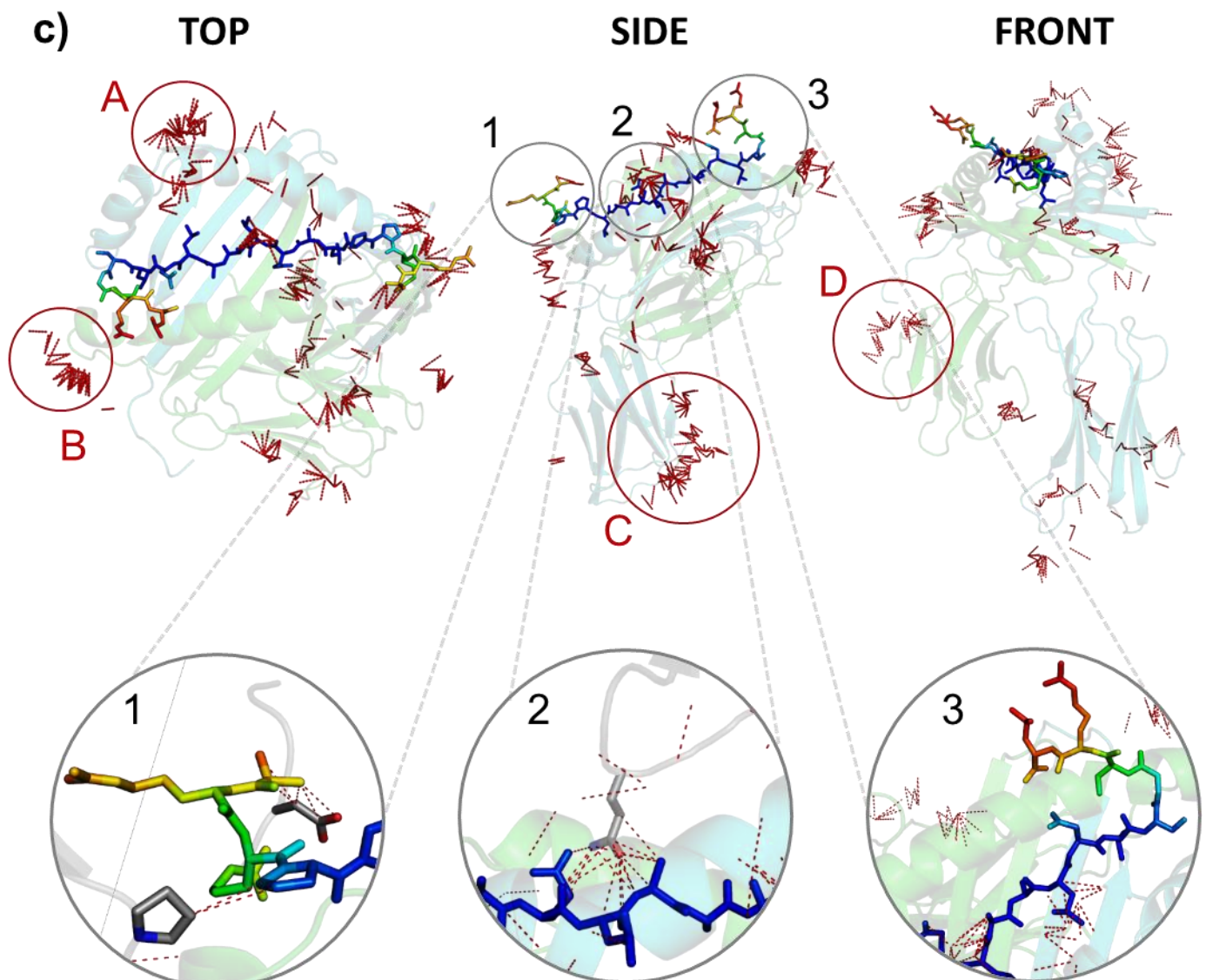
Appendix 5
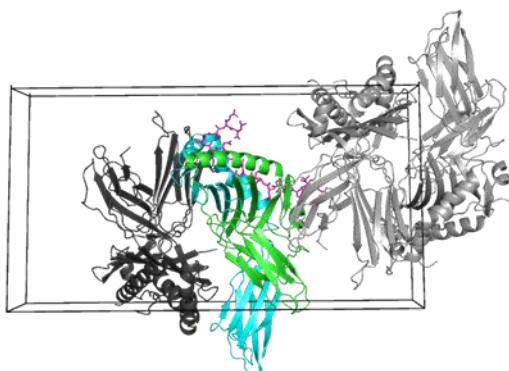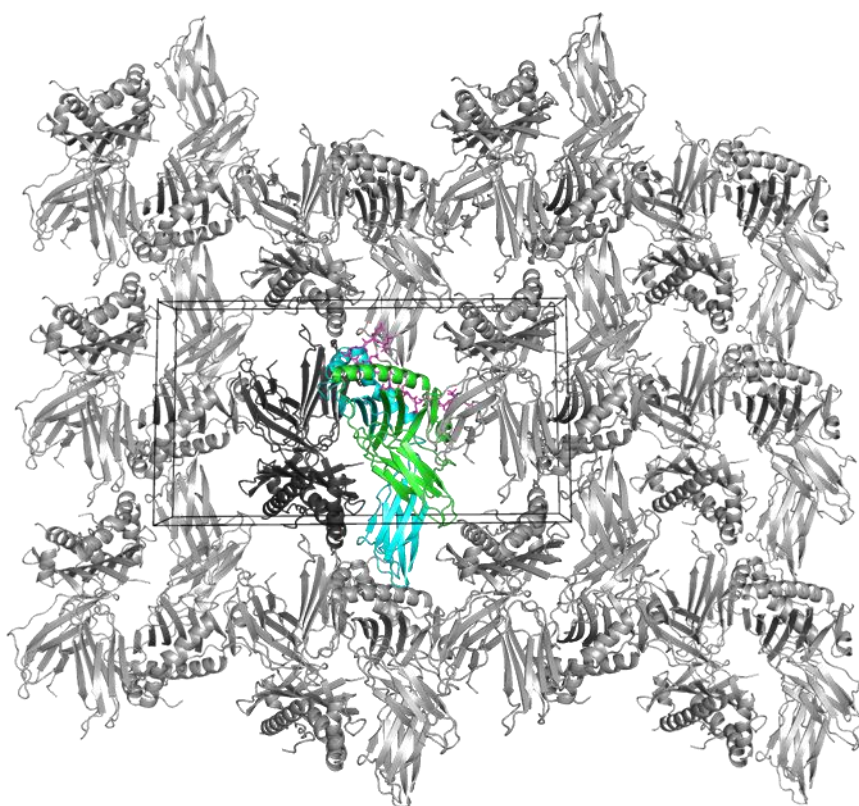
Appendix 5 – Crystal packing and symmetry interactions of the HLA-DR1 5T4p12 structure:
a) Cartoon and stick representation of HLA-DR1 5T4p12 within the unit cell (black box) of the analysed crystal structure. The asymmetric unit consisted of two HLA-DR1 5T4p12 copies: chain A, B & C (green, cyan & pink respectively) from which analyses are calculated, and a second copy D, E & F (dark grey). Symmetry mate within the unit cell is also shown (light grey).
b) Cartoon representation of HLA-DR1 5T4p12 within the observed crystal lattice showing symmetry mates within a single two-dimensional lattice (light grey). Asymmetric unit coloured as in *a)*.
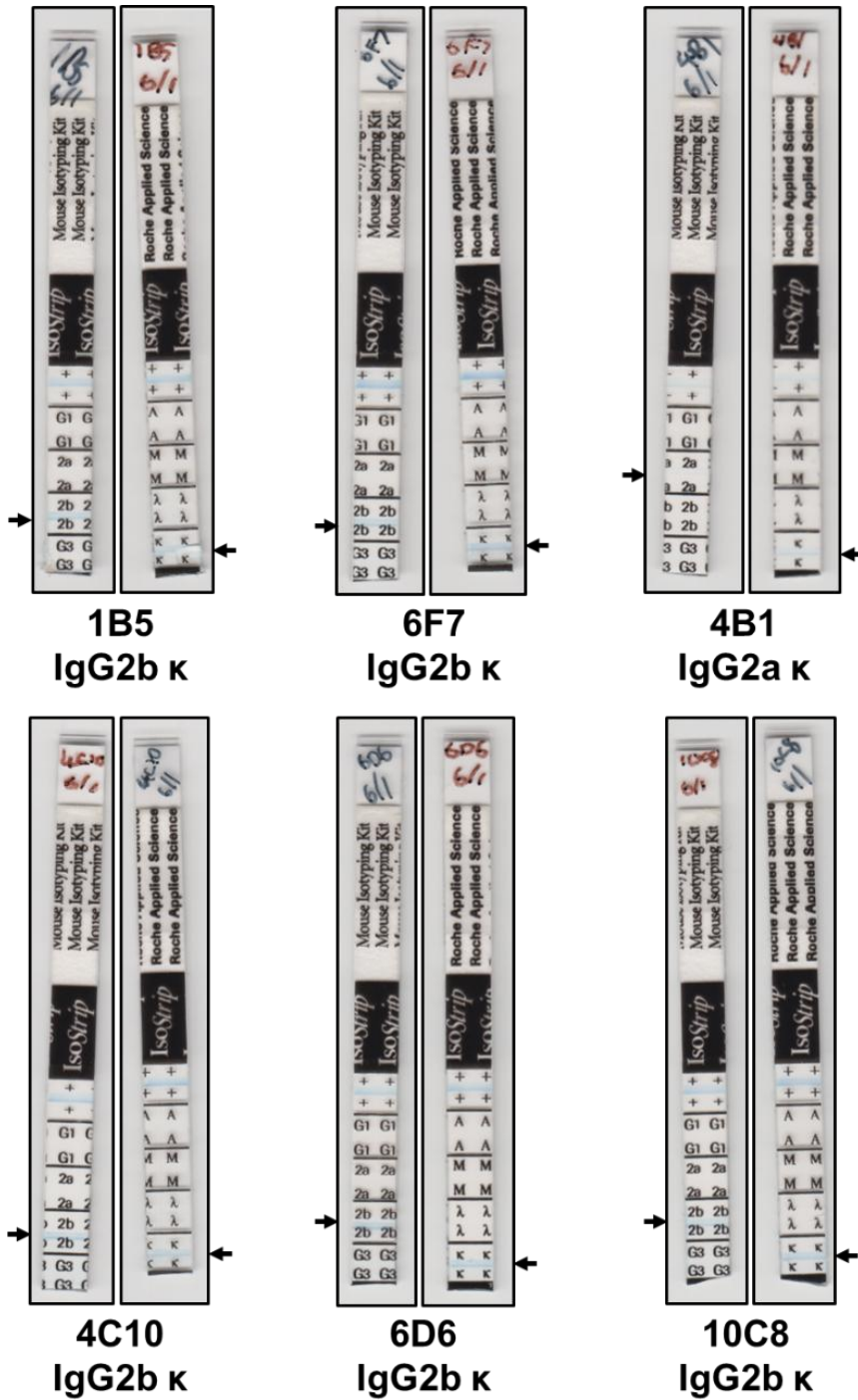
Appendix 5 cont.

c) Cartoon and stick representation of crystal packing interactions. All theoretical crystal contacts (distance $\leq$ 4.0 Å) between the HLA-DR1 5T4p12 (chain A, B & C of asymmetric unit) to the second copy of HLA-DR1 5T4p12 within the asymmetric unit and contacting symmetry mates. Contacts are shown as red dashed lines. Contact hotspots (red circles) included the β1 helix centre (A), the α1 helix C-terminal edge (B), β2 domain back (C) and α2 domain side (D). Some contacts by Pro-2 and Arg-4, to flexible loop regions of symmetry mates, was observed within the peptide N-terminus (grey circle 1). In addition, DR1β-Q110, within a flexible loop of the DR1 β2 domain was stabilised by the rigid central peptide core residues Glu3, Leu4 & Ala5 (grey circle 2). No crystal contacts were made by the C-terminal hairpin loop (grey circle 3). HLA-DR1 represented as cartoon (green & cyan; symmetry mates grey) with contacting side chains represented as sticks. Peptide is represented as sticks coloured by B-factor (blue to red; B-factor range = 21 to 130).

Appendix 6

mAb	Protein yield (mg)
6F7	75.4
4B1	52.0
6D6	37.7
10C8	33.3
1B5	25.8
4C10	5.5

Appendix 6 – Yields of affinity purified anti-LAG-3 monoclonal antibodies stratified by yield

Appendix 7

1B5
IgG2b κ
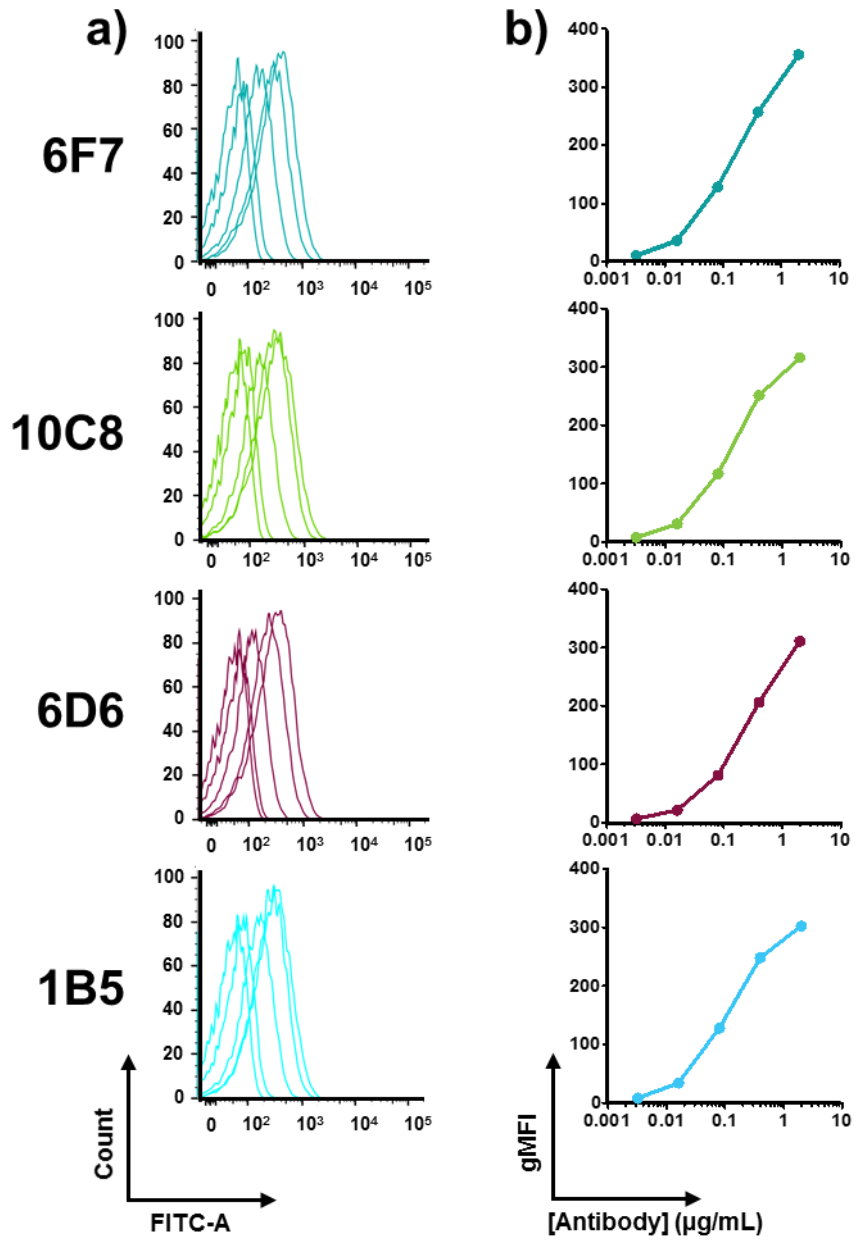
6F7
IgG2b κ

4B1
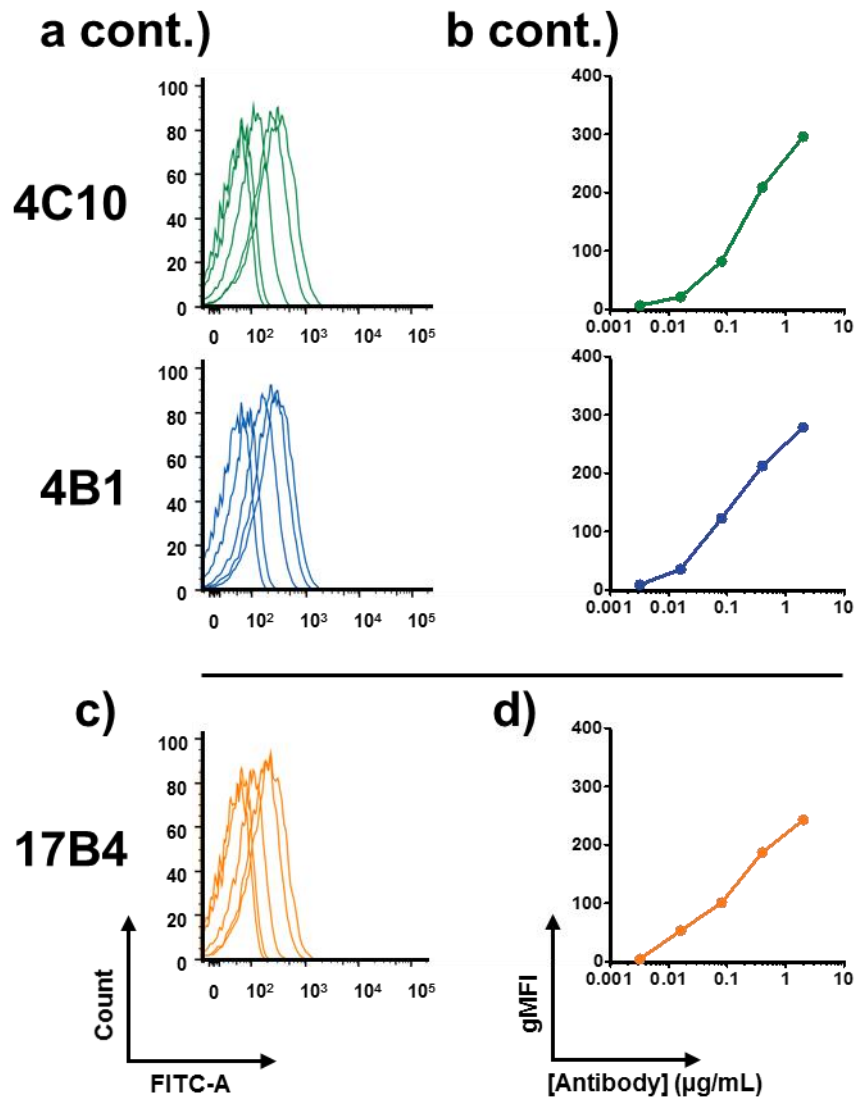IgG2a κ

4C10
IgG2b κ

6D6
IgG2b κ

10C8
IgG2b κ

Appendix 7 – Isotype characterisation of generated anti-LAG-3 antibodies:
Isotype immunoassay shift stick tests defining the isotype characterised by C_H and Ig light chain usage of the six candidate mAbs.

Appendix 8

(Figure continued overleaf)

Appendix 8 – Titratable binding of anti-LAG-3 antibodies to LAG-3+ cells:

a) Fluorescence histograms from flow cytometry analysis showing titratable staining profile of each anti-LAG-3 mAb clone at (2, 0.4, 0.08, 0.016, 0.0032 µg/mL) on JRT LAG-3+ C8 cells detected by secondary staining with FITC-conjugated anti-mouse antibody.

b) Background subtracted (IgG2a or IgG2b isotype control) geometric mean fluorescence intensity values at varying concentrations (as in *a)*) as a function of $\log_{10}$ antibody concentration. Log(dose) response curves are shown for each mAb clone.

c) Fluorescence histograms showing titratable staining profile of commercial 17B4 as described in *a)*.

d) Background subtracted (secondary only) log(dose) response curve of 17B4 binding as described in *b)*.